

Quarterly
OF THE
COLORADO SCHOOL OF MINES

Electrical Prospecting for Oil

George V. Keller

VOLUME 63, NUMBER 2

APRIL 1968



QUARTERLY OF THE COLORADO SCHOOL OF MINES

Volume 63

April 1968

Number 2

ELECTRICAL PROSPECTING FOR OIL

by

GEORGE V. KELLER
Professor of Geophysics
Colorado School of Mines

Price \$8.00

NORTHWEST MISSOURI
STATE COLLEGE LIBRARY
MARYVILLE, MISSOURI

WITHDRAWN
OWENS LIBRARY
N.W.M.S.U.

Published quarterly at Golden, Colorado 80101
Second-class postage paid at Golden
Colorado

Copyright © 1968 by the Colorado School
of Mines. Printed in the United States
of America. Sherman W. Spear, Director of
Publications.



Orlo E. Childs
President

21062

FOREWORD

This monograph is a collection of notes on the topics covered in a graduate course, "Special Problems in Electrical Prospecting Methods," which has been offered at the Colorado School of Mines each spring semester for the past six years (1961-1966). Generally, the problems chosen for consideration have been related to the use of electrical prospecting methods in a layered environment, such as one visualizes in a sedimentary basin. Our interest has been directed toward the possibility of applying electrical prospecting methods in the search for oil, inasmuch as discovery of new fields, particularly in the United States, is becoming more difficult and more costly using the methods which have been in use for several decades. Inasmuch as the consideration of each phase was terminated abruptly at the end of a semester, the material covered tends to be inconclusive and disjointed. However, this monograph is being offered to stimulate interest in the possibility of using electrical prospecting methods in the search for oil, and to point out a number of possible avenues for research.

Three areas are covered: the matter of electrical properties of rocks in and around oil fields, the basic electromagnetic theory for current flow in the ground, and practical design considerations for a variety of electrical methods that might be used in prospecting. In no case, is the discussion complete. Rather, for more complete coverage, we refer the reader to one of a number of texts which have been published on electrical prospecting during the past few years. For a general discussion of electrical prospecting methods, we refer you to "Electrical Methods in Geophysical Prospecting," by G. V. Keller and F. C. Frischknecht, published by Pergamon Press, Oxford. For more detailed coverage of the direct current methods, I recommend three books published during 1966: "Interpretation of Resistivity Data" by Robert G. Van Nostrand and Kenneth L. Cook, published by the U. S. Geological Survey as Professional Paper 499; "Dipole Methods for Measuring Earth Conductivity" by L. M. Alpin and others, published by Consultants Bureau, New York; and "Principles of Direct Current Resistivity Prospecting" by Geza Kunetz, published by Gebrüder Borntraeger, Berlin. Coverage of electromagnetic prospecting methods is more sparse, but I recommend Part III of "Interpretation Theory in Applied Geophysics" by F. S. Grant and G. F. West, published by McGraw-Hill in 1965, "Electromagnetic Depth Soundings" by L. L. Vanyan and others, published by Consultants Bureau in 1967, and volume 2 of "Mining Geophysics" published by the

Society of Exploration Geophysicists in 1967. Additional references to the journal literature are included in the body of this monograph.

The topics covered here represent an interchange of ideas with the members of the class, and especially from ideas nurtured by my colleagues J. I. Pritchard, Hans A. Meinardus, R. L. Gray, J. J. Jacobson, and N. Harthill. I am also grateful to the Colorado School of Mines Foundation, which provided financial support for some of the digitized electric log studies and a field program during the summer of 1966 when some of the design ideas described here were tested, and to Mrs. Ona Steinke, who typed the manuscript.

TABLE OF CONTENTS

Foreword	iii
Introduction	1
Part I: The Properties of Oil Fields and Their Environment	11
Electrical properties of sedimentary rocks	11
Electrical properties of the Mesozoic-Cenozoic sedimentary sequence of the east Gulf Coast area	36
Electrical properties of the Paleozoic to Cenozoic section of the Colorado Plateaus	46
Electrical properties of the Paleozoic to Cenozoic section of the Denver Basin and High Plains area	52
Electrical properties of other rock sequences	72
Electrical properties of the weathered layer	73
Properties of oil fields	79
Part II: Theory of Electrical Sounding	89
Solution of the boundary value problem	93
Solution of Maxwell's equations for a short grounded wire source	95
Solution of Maxwell's equations for a vertical axis dipole source	117
A uniform earth and the problem of defining apparent resistivity	122
Behavior of the \tilde{R} and R^* functions	140
Asymptotic behavior for small m	144
Asymptotic behavior for small ω	145
The Q and K functions	146
The K and Q functions for thin layers	152
The Hankel transform	156
General properties of the Hankel transform	161
Evaluation by series expansion	162

Evaluation using orthogonal polynomial approximation	169
Evaluation using numerical quadrature	170
An alternate approach to the zero frequency case	173
Part III: Design Criteria for Electrical Surveying	189
Comparison of arrays used in direct-current resistivity surveys	189
Depth of probing with electromagnetic methods	211
Noise considerations and power requirements	218
Noise above 1 cps	220
Noise below 1 cps	223
Current requirements for zero-frequency methods	230
Current requirements in AC methods	247
Geologic noise and precision of measurements	252
Summary and Conclusions—Strategy	263

INTRODUCTION

The concept of using electrical prospecting methods in the search for oil is by no means novel. Consideration has been given to the use of electrical methods from the late 20's to the present, with the intensity of interest varying markedly from time to time. To place the present work in proper perspective, it is perhaps wise to quote some of the early contributions to the topic of electrical oil finding. Peters and Bardeen (1932) reviewed early attempts to use electrical prospecting methods, concluding that they might best be used in mapping structural relief of electrical marker horizons. They also say:

The depth which can be obtained reliably in electrical prospecting is a much debated question. Up to the present time (1932), the depth at which structures have been reliably mapped by electrical surveys has not exceeded 1,500 feet.

And in their final paragraph:

At the present time electrical methods of prospecting for oil seem to be in disrepute. This is partly due to cost of electrical surveys as compared with other geophysical methods and partly due to the failure of the extravagant claims made for the process to materialize. However, the electrical method of prospecting for oil cannot be forgotten because it is one of two prominent geophysical methods in which it is possible to control the field being employed. Improvements in methods of interpretation and in field techniques should give electrical methods a definite field of usefulness in prospecting for oil.

Heiland (1932) believed that structure might be mapped effectively, but also considered that it might be possible to detect the resistivity anomaly associated directly with oil saturation. In his abstract, he states:

—the interest in the possibilities of electrical prospecting has been aroused again of late, due to the perfection of the resistivity and PDR method—. The object of the writer is to give a summary of the whole field of the resistivity methods, with particular reference to the recent developments—.

And later in the paper:

As far as the use of resistivity methods in oil work is concerned, the Schlumberger Company has proved the practicability of the method in structural studies since 1921. Work was then begun in the Pechelbron oil region and continued until 1926. In Roumania, commercial work was carried out, among others, for the Steaua Romana in 1923-26. Salt domes were located in the Alsace region in 1926-1927.

Resistivity prospecting for oil structures was begun in the United States in 1925, when the Schlumberger Company was engaged to work for the Roxana Petroleum

Corporation and the Shell Company of California. The work for the latter continued to about 1929.

Gish also surveyed the use of electrical methods for oil exploration in 1932, and made the following comments.

One in whom statistical sense is lacking is likely to extol or condemn a method after too brief a trial.

The quack and the shyster seem to have a strong predilection for electrical vestments.

An attitude of disfavor toward geoelectric methods has perhaps sprung in considerable part from subjective rather than objective sources.

Although some geoelectric methods may under favorable conditions detect oil directly because of its high insulating property, geoelectric as well as other methods are efficacious in the location of oil only to the extent that they disclose subsurface structural features which in turn may indicate oil-bearing structure.

It should be remembered that these comments concerning less-than-intelligent applications of electrical methods and the distrust of advocates of such methods were made on the basis of direct-current resistivity surveys used during the 1920's, prior to the period when electrical transient and radio wave methods were widely ballyhooped.

During the 1930's, considerable interest was developed in the "Eltran method," an electromagnetic approach to studying a layered earth, based on a patent by L. W. Blau (U. S. Patent 1,911,137, issued in 1933). The Eltran method consisted in the generation of an electromagnetic field with a current dipole excited with a current pulse, and detected with an electric dipole situated in line with the source dipole. It was hoped that energy reflected from boundaries between layers with different conductivities would be detected on the recorded transient at the receiver in much the same way that acoustic reflections were detected in the seismic reflection techniques. The method aroused considerable interest among oil companies for about 10 years, with a series of papers appearing which described results of field trials (Karcher and McDermott, 1935; Statham, 1936; West, 1938; Hawley, 1938; White, 1939; Klipsch, 1939; Rust, 1940; and Evjen, 1948). With all this experimentation, there was remarkably little theoretical consideration of the method reported in the literature. A careful theoretical evaluation of the Eltran method was not reported until the work of the Socony Mobil laboratory was published (Yost, 1952; Yost and others, 1952; Orsinger and Van Nostrand, 1954). It was then apparent that for the conductive rocks normally found in sedimentary basins, the transient response to impulse excitation contained such low frequencies that it would be difficult to obtain the resolution needed to identify individual reflected events.

During the late 1940's and early 1950's, interest in the Eltran method was displaced by an intense interest in radio-wave methods. For several years, many of the major oil companies experimented with the use of radio-waves in the 1 to 2 megacycle-per-second frequency range. The most common approach was to make use of a horizontal antenna laid on the ground, with the field-strength decay curve being measured along a inline radial. Presumably, an oil field at depth would lead to a characteristic pattern being superimposed on the decay curve (Barret, 1949). However, simple computations of radio waves in a normal oil-field environment showed that skin depths at radio frequencies were tens of feet at most, and that radio signals reflected from depth would be attenuated so severely that there would be no possibility of the formation of an interference pattern on the decay curve (Haycock, Madsen and Hurst, 1949). Advocates of the use of radio-wave methods put forth the argument that at radio frequencies there might be "windows" where, because of some peculiar behavior of the electrical properties of rocks, attenuation might be much less.

Inasmuch as the electrical properties of rocks were relatively unknown over the radio frequency range at that time (and are still known only rather poorly), this argument could not be answered simply. However, several carefully controlled experiments were carried out using transmission paths between surface antennas and antennas in mines or caves (Pritchett, 1952; McGehee, 1954), which showed that high attenuation rates do in fact apply for radio transmission through wet rocks. The intensity of feeling over the matter of radio transmission through rocks is demonstrated by the lengthy and severe discussion of Pritchett's paper (following Pritchett, 1952).

Despite the fact that an impressive success ratio has been claimed for the use of radio-wave methods, the extent of use has declined markedly in the past 10 years. The present-day explanation of why the technique may work on occasions is that in some cases, oil-fields may coincide with near-surface anomalies in electrical properties, coincidental or not, which give rise to the characteristic pattern observed on the intensity decay curve. According to Barret (1949), 80.6 percent of the observed patterns interpreted as indicating oil were proved to be correct by drilling, while all condemned prospects which were later drilled proved to be nonproductive. Professor Harold M. Mooney (1954), in a study carried out for the U. S. Atomic Energy Commission, concluded that the success ratio for the method is about one to ten, or about the same as would be expected from a completely random drilling pattern carried out in a petroliferous province. On the other hand, the high degree of success reported for condemning prospects is a natural consequence of the fact that seven out of eight randomly located wells will be dry.

Since the mid-fifties, there has been some indication of interest in the use of the magnetotelluric method in oil prospecting. The basis for the magnetotelluric method, which consists of determining resistivity from simultaneous observations of variations in the natural electric and magnetic fields of the earth, was first described by Cagniard (1953). The frequencies used are as low as a thousandth of a cycle per second, assuring penetration even in the most conductive sedimentary basin. The advantage seen for the magnetotelluric method is the supposed simplicity of measurement, which would allow determinations of basin character and configuration, even in remote areas not easily accessible with seismic equipment. A disadvantage appears to be that the resistivity profile with depth cannot be determined with a high degree of accuracy.

The experience with electrical prospecting methods in other countries, where less exotic applications have been developed, has not been as disappointing as the experience in the United States. The telluric current method has been used quite effectively since it was first employed by the Schlumbergers in the 1930's, first in the French community and later in the Soviet Union. According to d'Erceville and Kunetz (1962), the French firm *Compagnie Generale de Geophysique*, carried out some 565 crew months of activity telluric prospecting over the period from 1941 to 1955. According to Berdichevskiy (1965) the number of crews engaged in telluric current surveys in the Soviet Union grew from a few experimental crews in 1955 to 79 crews in 1960. At present, a variety of electrical prospecting methods are being used in the Soviet Union in the search for oil, including the telluric method, the magnetotelluric method, the magnetotelluric profiling method and the electromagnetic sounding method (Alexeyev and others, 1967). In 1965, use had grown to the point where 139 crews were engaged in these three forms of electrical surveying, in addition to crews engaged in the more conventional direct-current surveying techniques. According to Smith (1962), some 200 crews were engaged in electrical prospecting in the Soviet Union in 1961, with about two-thirds using the direct current methods. Apparently, the amount of direct-current exploration has been sharply reduced with the introduction of the new electromagnetic techniques, which provide much more accurate information. According to Berdichevskiy and Fomina (1966), the use of various combinations of the new electrical exploration techniques to study basin structure and locate areas most likely to be profitable prospects for subsequent detailing with seismic methods has reduced the cost of exploration by a factor of ten.

Exploration costs are a significant factor in determining the ultimate cost of produced petroleum. The money spent on geophysical surveys has

increased at a yearly rate of about 7 percent since the late 1940's, and now stands at 0.6 to 0.7 billion dollars per year in the Free World (the level of exploration activity in the Soviet bloc is about the same). According to Newfarmer (1962), in 1959 geophysics accounted for about 20 percent of the exploration budget, with geology, land acquisition and "wildcat" drilling accounting for the rest of the exploration costs:

Type of action	Percent of effort	Cost
Geology	33	\$753 millions
Geophysics	20	\$457 millions
Land acquisition	17	\$388 millions
Wildcat drilling	30	\$685 millions

These costs may be divided into two parts—those involved in exploration to the point of finding a drilling location, which are the costs for geology and geophysics; and those involved in testing these locations, which are costs of land acquisition and wildcat drilling. It is interesting to note that approximately equal amounts are spent on the two parts. This reflects the fact that after a certain point, it is cheaper to drill uncertain prospects than to continue exploration to a more definitive conclusion.

The high cost of exploration and wildcat drilling reflects the inherent difficulty (one might say impossibility) in locating oil. All exploration techniques in use today are indirect: they are not designed to detect oil directly, but only to locate areas which are most favorable for oil occurrence. These areas are tested by drilling, and if enough areas are tested, enough oil fields are found to make money. The factors to be considered in assessing favorability seem to be well known, after a century of experience. It is known, for example, that marine sedimentary rocks are most favorable, particularly those laid down in a platform area (a shallow-water basin) rich in marine life. Under these favorable circumstances, the basin would be tectonically quiet, so that great thickness of organic-rich rock may accumulate without interruption over geologic time, without loss of organic material by sub-aerial erosion. Better yet, the basin should rise and fall gently by a few feet, so that sediment varies in texture from place to place, sometimes being sand, sometimes being mud. This then will allow oil to be separated from water by capillary pressure differences between fine-grained and coarse-grained rocks. Deposition of sediment must go on for a prolonged period of time, to provide at least 6,000 feet of sediment thickness, which seems to be the minimum overburden to provide the pressure needed to start converting organic matter to oil. Oil is found at shallower depths, but as a result of later uplift and erosion of overlying materials. Later tectonic activity, such as folding and faulting, may assist in moving oil into reservoirs, but severe tectonic activity may destroy oil.

Thus, a sedimentary basin is considered a candidate for exploration only if it has adequate thickness of sedimentary rock, and only if these rocks have not been too severely folded. The bulk of the effort in exploration is the search for reservoirs in which oil may accumulate, within these basically favorable basins. Many types of "traps" may be recognized, but they may be grouped in two general classes—structural and capillary. In a structural trap, oil is localized as it migrates upward under the influence of gravity through heavier water until it collects against an impermeable barrier. The classic structural trap is one in which a permeable sandstone has been folded into a gentle arch, or anticline, so that oil can accumulate at the top of the structure. Other examples are fault traps, where a dipping, permeable bed has been broken by a fault which brings the truncated permeable bed up against an impermeable bed. Oil may then migrate up the bed until it is trapped against the fault. The same sort of truncation occurs in stratigraphic traps where a bed may be truncated by erosion and then sealed by later deposition of impermeable sediments, followed by emplacement of oil. Almost all exploration is based on the search for such structures in hopes that when they are found they will be oil bearing. The principal exploration method in use today is the seismic method, which uses travel times for reflected acoustic waves to map relief of marker horizons—those which are characterized by an acoustic impedance contrast so that they reflect a detectable portion of the incident acoustic energy. Usually, these marker horizons are not the beds in which oil accumulates, but are nearby beds which are probably concordant with reservoir beds. Gravity and magnetic methods are also used to some extent in mapping relief of the surface of the denser and more magnetic rocks which form the basement beneath the sediments. These structures may then be continued into the sediments, where oil is found. In the Free World, more than 90 percent of the geophysical effort is devoted to seismic surveys; less than 10 percent is devoted to gravity and magnetic surveys.

In many cases, capillary pressure drive has been observed to be more important than gravity forces in separating oil from water. Rocks usually are preferentially water-wet, so oil will move to coarser rocks, being displaced from finer openings where water is held more strongly. Oil will then accumulate in zones of porous, permeable rock, independently of structure. Many oil fields of this type have been discovered accidentally in drilling for supposed structures. Many combined reservoirs are known—those in which both structural elevation and capillary pressure segregation cause oil accumulation. The abundance of dual-force reservoirs may represent only the fact that exploration is done for structures, and that there is currently no exploration method available for reservoirs with only capillary drive.

Thus, at present, exploration is highly indirect; only structures in potential-

ly petroliferous basins are sought, and then these are drilled to find the ones which have oil. This requires careful weighing of risk against possible return, a subject which has been treated by Kaufman (1963). The best prospects are tested first; then as more confidence is built up, the less likely prospects are drilled. This leads to an exploration history for an oil province which behaves as follows:

1. In the early stages of development, the success ratio for wildcat drilling will increase, as additional information provided by drilling is used to improve the interpretation of geophysical surveys to reduce risk on drilling.
2. After a period ranging from a few years to 10 years, the wildcat drilling success ratio will begin to decline, as the more promising prospects are exhausted and less promising prospects must be tested.

As a result, overall statistics on the success of wildcat drilling are not particularly meaningful. For a province at its peak, the success ratio may be as high as 1 in 2, as reported by V. V. Fedinskiy (personal communication, 1967) for the Siberian lowlands. Similar high success ratios were enjoyed during early oil booms in Pennsylvania, Oklahoma, and Texas. On the other hand, success in wildcat drilling in mature oil provinces is much lower, perhaps as low as 1 in 150, as speculated by J. C. Griffiths (personal communication, 1967). According to a survey by the American Association of Petroleum Geologists, during 1966, one wildcat well in ten was successful.

Even these success ratios tend to be optimistic. Griffiths (1962) has made a statistical analysis of the sizes of oil fields and found that half of the oil fields in several major oil provinces in the USA have values less than a million dollars each, while 1 percent have values in excess of a billion dollars each. Obviously, the cost of developing the less valuable fields is borne by the few large fields. The success ratio in finding large fields is very much less than the overall success ratio of 1 in 10. According to M. T. Halbouty, president of the American Association of Petroleum Geologists in 1966, "—the number of new-field wildcats drilled for each discovery of a new field of sufficient size to return a profit on the operator's investment has ranged between 36 and 59 wildcats. Prior to 1950, the ratio was between 25 and 33." Thus, the exploration problem is severe and becoming more so each year.

In view of the increasing difficulty with which new reserves of oil are being found, it seems appropriate at this time to reconsider the possible role of electrical exploration in a petroleum exploration program. However, to avoid the pitfalls associated with the fascination with exotic applications which promise much but produce little, it would be wise to review the entire theory on which electrical prospecting is based, with particular reference to practical

exploration for oil. Considering the present structure of exploration geophysics, electrical methods might conceivably be applied in three ways:

1. **In the search for structures.** Such an application would be in direct competition with presently used methods, and to be successful, structures would need to be found more economically than with present methods, or the methods would have to be applicable in areas where present methods are ineffective. This is the type of application which is being done successfully in the Soviet Union.

2. **In the search for fine lithologic changes associated with lithologic oil traps.** Oil which is localized by changes in the texture of rock independently of structure may occur in a thick sequence of rocks whose properties differ to some extent from those laterally away from the oil field. Such an environment can be postulated for oil trapped in strand-line or bar sands which represent the boundary between shallow water and deep water in the depositional basin. If the shoreline remains relatively fixed through long periods of deposition, a thick column of rock may have properties diagnostic of the shoreline environment. This thick sequence may then present a reasonable target even for electrical methods which have poor resolution.

3. **In the recognition of resistivity anomalies associated directly with the presence of oil.** The presence of oil in the pore structure of a rock, displacing water, may increase the resistivity of that rock markedly. Detection of resistive zones caused by oil saturation would provide a powerful technique in oil exploration if it is possible. A direct oil-finding method could be considerably more expensive than present seismic methods and still provide more economical overall finding by reducing waste drilling.

In the following three sections, various aspects of electrical prospecting are considered. First the electrical properties of oil-bearing rocks and the sedimentary sequence in which they are found are treated, primarily to provide a basis for estimating the feasibility of recognizing structures, lithologic trends or the resistivity anomaly associated with oil saturation, using the theory developed in the second section. Finally, the requirements for instrumentation are discussed in the last section.

REFERENCES

- Alexeyev, A. M., Berdichevskiy, M. N., Bezruck, I. A., Fomina, V. I., Nickitenko, K. I., Polshkov, M. K., and Vanyan, L. L., 1967. Application of electromagnetic methods in oil and gas exploration in the USSR: World Petroleum Cong. 7th, Trans., Mexico City 1967, Elsevier.
- Al'pin, L. M., and others, 1966. Dipole methods for measuring earth conductivity: New York: Plenum Press, 302 p.
- Barret, W. M. 1949A. Exploring the earth with radio waves: World Oil, April.
- 1949B. Advertising brochure entitled "The Radioil Method," 33 p.

INTRODUCTION

————— 1952. Note on the radio-transmission demonstration at Grand Saline, Texas: Geophysics, v. 17, no. 3, p. 544-549.

Berdichevskiy, M. N., 1965. Electrical prospecting with the telluric current method: Colorado School Mines Quart., v. 60, no. 1, 216 p.

Berdichevskiy, M. N., and Fomina, V. I., 1966. Routine application of new methods for structural electrical prospecting: Exploration Geophysics, v. 47 (English trans., Prikladnaya Geofizika, New York, Plenum Press.)

Cagniard, L., 1953. Basic theory of the magnetotelluric method of geophysical prospecting: Geophysics, v. 18, no. 3, p. 605-635.

d'Erceville, L., and Kunetz, G., 1962. The effect of a fault on the earth's electromagnetic field: Geophysics, v. 27, no. 5, p. 627-650.

Evjén, H. M., 1948. Theory and practice of low-frequency electromagnetic prospecting: Geophysics, v. 13, no. 4, p. 584-594.

Gish, O. H., 1932. Use of geoelectric methods in search for oil: Am. Assoc. Petroleum Geologists Bull., v. 16, no. 12, p. 1337-1348.

Grant, F. S., and West, G. F., 1965. Interpretation theory in applied geophysics: New York, McGraw-Hill, 583 p.

Griffiths, J. C., 1962. Frequency distributions of some natural resource materials: Tech. Conf. on Petroleum Products, 23rd, Sept. 26-28, Pennsylvania State Univ. Min. Ind. Exp. Sta. Circ. 63, p. 174-198.

Hawley, P. F., 1938. Transients in electrical prospecting: Geophysics, v. 3, no. 3, p. 247-257.

Haycock, O. C., Madsen, E. C., and Hurst, S. R., 1949. Propagation of electromagnetic waves in earth: Geophysics, v. 14, no. 2, p. 162-171.

Heiland, C. A., 1932. Advances in technique and application of resistivity and potential-drop-ratio methods in oil prospecting: Am. Assoc. Petroleum Geologists Bull., v. 16, no. 12, p. 1260-1336.

Karcher, J. C., and McDermott, E., 1935. Deep electrical prospecting: Geophysics, v. 19, no. 1, p. 64-77.

Kaufman, G. M., 1963. Statistical decision and related techniques in oil and gas exploration: Englewood Cliffs, N.J., Prentice-Hall, 307 p.

Keller, G. V., and Frischknecht, F. C., 1966. Electrical methods in geophysical prospecting: Oxford, Pergamon Press, 526 p.

Klipsch, P. W., 1939. Recent developments in Eltran prospecting: Geophysics, v. 4, no. 4, p. 283-291.

Kunetz, Geza, 1966. Principles of direct-current resistivity prospecting: Berlin, Gebrüder Borntraeger, 103 p.

McCeech, F. M., Jr., 1954. Propagation of radio frequency energy through the earth: Geophysics, v. 19, no. 3, p. 459-477.

Mooney, H. M., 1954. The status of (non-direct-current) electrical exploration with special reference to uranium prospecting: Final report to U.S. Atomic Energy Comm., Contract AT-(49-1)-900.

Newfarmer, L. R., 1962. Geophysic's share of the exploration dollar in the USA and Canada: Geophysics, v. 27, no. 1, p. 113-120.

Orsinger, A., and Van Nostrand, R., 1954. A field evaluation of the electromagnetic reflection method: Geophysics, v. 19, no. 3, p. 478-489.

Peters, L. J., and Bardeen, John, 1932. Some aspects of electrical prospecting applied in locating oil structures: Soc. Petroleum Geophysics Trans. v. 2, March, p. 1-20.

Pritchett, W. C., 1952. Attenuation of radio frequency waves through the earth: Geophysics, v. 17, no. 2, p. 193-217.

- Rust, W. M., Jr., 1940. Typical electrical prospecting methods: *Geophysics*, v. 5, no. 3, p. 243-249.
- Smith, N. J., 1962. Geophysical activity in 1961: *Geophysics*, v. 27, no. 6, p. 859-886.
- Statham, L., 1936. Electric earth transients in geophysical prospecting: *Geophysics*, v. 1, no. 2, p. 271-277.
- Van Nostrand, R. C., and Cook, K. L., 1966. Interpretation of resistivity data: U. S. Geol. Survey Prof. Paper 499, Washington, D.C., U. S. Gov. Printing Office, 310 p.
- Vanyan, L. L., and others, 1967. Electromagnetic depth soundings: New York, Plenum Press, 312 p.
- West, S. S., 1938. Electrical prospecting with non-sinusoidal alternating currents: *Geophysics*, v. 3, no. 2, p. 157-164.
- White, G. E., 1939. A note on the relations of suddenly applied DC earth transients to pulse response transients: *Geophysics*, v. 4, no. 4, p. 279-282.
- Yost, W. J., 1952. The interpretation of electromagnetic reflection data in geophysical exploration—Part I. General theory: *Geophysics*, v. 17, no. 1, p. 89-108.
- Yost, W. J., Caldwell, R. L., Beard, C. L., McClure, C. D., and Skomal, E. N., 1952. The interpretation of electromagnetic reflection data in geophysical exploration Part II. Metallic model experiments: *Geophysics*, v. 17, no. 4, p. 806-826.

PART I

THE PROPERTIES OF OIL FIELDS AND THEIR ENVIRONMENT

In discussing the feasibility of locating oil fields using electrical exploration methods, we need to describe the properties not only of oil fields, which are the target, but also of their environment, which constitutes the background against which this target must be seen.

ELECTRICAL PROPERTIES OF SEDIMENTARY ROCKS

The relationship between rock resistivity, water content, and texture has been studied in great detail over the past quarter century by well-log analysts, with the result that the probable resistivity of a rock in a marine sedimentary sequence can be estimated with a high degree of reliability. It is generally accepted that Archie's law (Archie, 1942) may be used to describe this relationship:

$$\rho_{\text{rock}} = a \rho_w S^{-n} \phi^{-m} \quad (1)$$

where ρ_{rock} is the bulk resistivity of a rock, usually measured in MKS units, ohmmeters; ρ_w is the resistivity of the water filling in the pore spaces of that rock; ϕ is the volume fraction of pore space in a rock; S is the fraction of that pore space occupied by water; and a , n , and m are empirically determined parameters which seem to depend on the texture of the rock.

Archie's equation indicates that the bulk resistivity of a rock is proportional to the resistivity of the water contained in it; this has led to the use of the ratio of rock resistivity to water resistivity, termed the *formation factor*, as a measure of porosity:

$$F = \rho_{\text{rock}} / \rho_w = a S^{-n} \phi^{-m} \quad (2)$$

The variation of formation factor with porosity, for complete water saturation, is shown graphically in figure 1.

Typical expressions of Archie's law for various lithologies are summarized in table 1.

All rocks have appreciable ion exchange capacity—that is, a supply of ions adsorbed more or less loosely on mineral surfaces or within mineral structures. In the presence of water, these minerals electrolyze, adding their ad-

FRACTIONAL POROSITY

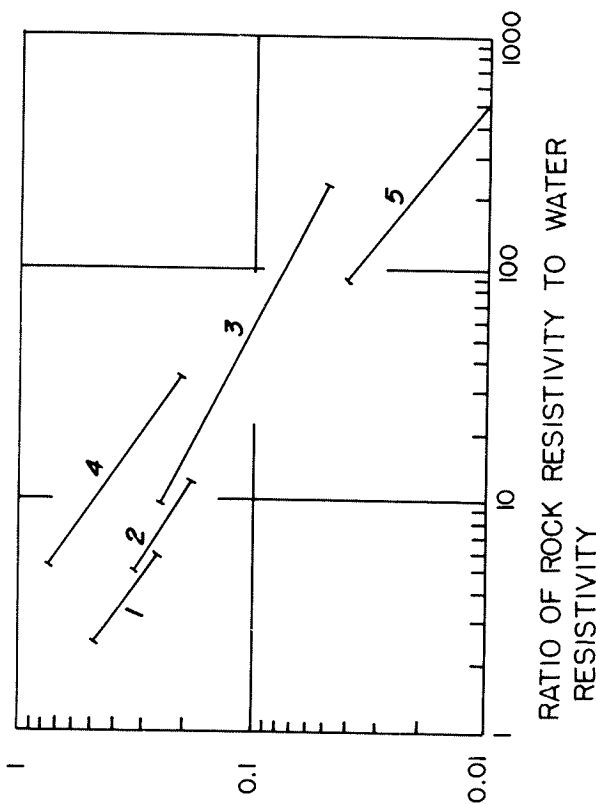


FIGURE 1.—The relationship between rock resistivity, water resistivity and water content given by Archie's law for various types of rocks. Curves 1, 2 and 3 represent clastic detrital rocks of progressively older ages, as indicated in table 1; curve 4 represents porous volcanic rocks, and curve 5 represents low-porosity rocks in which fractures play an important role in the conduction of electricity.

sorbed ions to solution, though with reduced mobility. These ions do not move with the water when a sample is extracted for analysis, and so are not seen as part of the salinity of an extracted sample. They may add significantly to the conductivity of the pore water if the free salinity of that water is low, but if the normal salinity is high, the added salinity may have only a negligible effect on the water conductivity.

The usual connate water in a petroliferous sequence of sedimentary rocks is quite saline. However, in many places, the section over an oil field may have continental sedimentary rocks which are saturated by much less saline waters, and in such rocks, salinity added by desorption from minerals may be significant. The added salinity from adsorbed salts will limit the maximum resistivity a rock may assume, as the free salinity is decreased. The change in resistivity of pore water with change in free salinity is indicated by the curves in figure 2, for various assumed cation exchange capacities in a rock.

These curves stress the idea that fresh-water saturated rocks need not be nearly so resistant as would be predicted by Archie's law, if values for water resistivity are determined from extracted water samples.

TABLE 1.—Archie's law expressions for various rock types

1. Weakly cemented detrital rocks, such as sand, sandstone, and some lime sands, with a porosity range from 25 to 45 percent, usually Tertiary in age:

$$\rho_t/\rho_w = 0.88 \phi^{-1.37}$$

2. Moderately well cemented sedimentary rocks, including sandstones and limestones, with a porosity range from 18 to 35 percent, usually Mesozoic in age:

$$\rho_t/\rho_w = 0.62 \phi^{-1.72}$$

3. Well cemented sedimentary rocks with a porosity range from 5 to 25 percent, usually Paleozoic in age:

$$\rho_t/\rho_w = 0.62 \phi^{-1.95}$$

4. Highly porous volcanic rocks, with a porosity in the range from 20 to 80 percent:

$$\rho_t/\rho_w = 3.5 \phi^{-1.45}$$

5. Rocks with less than 4 percent porosity, such as igneous and metamorphic rocks, where joint porosity is important:

$$\rho_t/\rho_w = 1.4 \phi^{-1.58}$$

Our primary concern here, however, is not with the detailed variation of rock resistivity as a function of water salinity and content, inasmuch as such information is not easily available in sufficient quantity to permit a valid description of the whole sedimentary section. We wish to know reliable average values for the resistivity of thick portions of the sedimentary column, so that we may evaluate the effectiveness of various surface-based electrical measuring techniques. A wealth of information about electrical properties of oil-bearing sequences of rock is available from electrical well logs, with hundreds of thousands of logs being available in well log libraries and oil company files.

Utilization of data contained on electrical well logs has been hindered by the volume of data which exists, even on a single log. The usual method used in interpreting well logs has been a detailed analysis of zones of potential interest, with the rest of the log being ignored, except for noting the depths to formation tops. With the availability of high-speed computers, such deter-

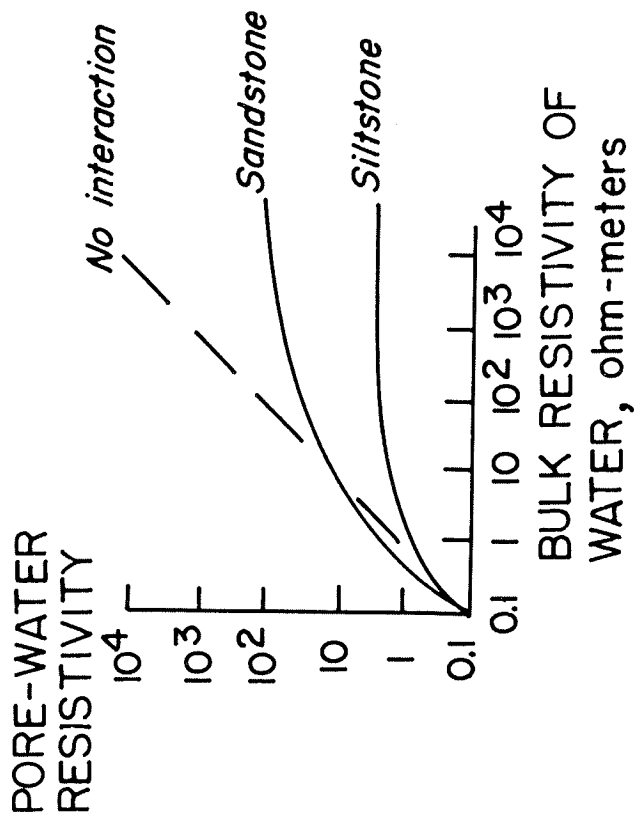


FIGURE 2.—Relationship between the resistivity of water in place in the pore structure of a rock, and the resistivity of the same water measured in bulk. Interaction between the pore water and the solids of the rock cause the two values to differ, with the departure being greatest at low water salinities, and for the finest rocks.

minations have been extended to larger portions of the well section, but only rarely have interpreters been interested in the resistivity recorded on such logs per se.

The large number of individual layers apparent on an electric log cannot be resolved with any of the surface-based electrical prospecting methods, and so, it is necessary to devise a realistic way of defining the average resistivity of an assemblage of relatively thin beds. It has been shown (Schlumberger and others, 1934) that the average electrical properties for a finely layered sequence may be described with a set of 5 parameters, these parameters being defined in terms of a column of rock one meter square cut from the sequence of layers. This column consists of m horizontal beds, each with its own characteristic resistivity, ρ_i , and thickness, t_i , as shown schematically in figure 3.

These parameters are defined by considering the resistance to current flowing either vertically or horizontally through the column. For current flowing vertically through the length of the column, the *transverse resistance*,



FIGURE 3.—Column from a layered sequence of rocks, used in defining average longitudinal resistivity, average transverse resistivity and anisotropy arising from layering.

T , is the sum of the resistances met in each of the individual layers:

$$T = \sum_{i=1}^m \rho_i t_i \quad (3)$$

If the bed resistivities and thickness are given in ohm-meters and meters, respectively, the transverse resistance is expressed in ohms.

By assuming that the transverse resistance applies to a column which is macroscopically uniform, we can calculate the average *transverse resistivity*, ρ_{tr} , which is seen by current flowing vertically through the column:

$$\rho_{tr} = \frac{T}{H} = \frac{\sum \rho_i t_i}{\sum t_i} \quad (4)$$

(H being the total thickness of the assemblage of fine layers).

For current flowing laterally through the column, the *longitudinal resistance* is that of each of the layers considered to be connected in parallel. With parallel circuits, it is more convenient to talk about the conductance, which is the reciprocal of the resistance:

$$S = \sum_{i=1}^m \frac{t_i}{\rho_i} \quad (5)$$

Again by assuming the longitudinal conductance, S , applies to a column which is macroscopically uniform, we can calculate an average *longitudinal resistivity*, ρ_l :

$$\rho_l = \frac{H}{S} = \frac{\sum t_i}{\sum t_i / \rho_i} \quad (6)$$

Unless the resistivities of the individual layers are all exactly the same, the longitudinal resistivity is smaller than the transverse resistivity. This dependence of resistivity on the direction of current flow constitutes anisotropy. The *coefficient of anisotropy* for a layered sequence of rocks is defined as:

$$\lambda = \sqrt{\frac{\rho_{tr}}{\rho_l}} = \sqrt{\frac{ST}{H^2}} \quad (7)$$

Thus, an assemblage of thin layers, each of which is isotropic, will appear to be anisotropic when considered as a macroscopically uniform medium. This type of anisotropy might be termed *macro-anisotropy*. It is also conceivable that the individual layers might be anisotropic on a microscopic scale as a result of some preferential orientation of grains. If the direction of maximum conduction is parallel to the bedding planes, as would normally be the case, it can be seen from the defining equations for the average electric

properties that the total or general anisotropy will be the product of the macro-anisotropy and the average micro-anisotropy.

The primary source of data for evaluating these average electrical properties is an electric log. Electric logs have a limited resolution, and may fail to distinguish between layers which have appreciable thickness. Therefore, the distinction made between macro-anisotropy and micro-anisotropy is usually a practical one—macro-anisotropy arises from layering coarse enough to be distinguished on electric logs, while micro-anisotropy may be used to describe both the microscopic anisotropy inherent in a rock and layering anisotropy from layers too fine to be distinguished on an electric log.

Evaluation of the average defined in equations 3-7 by scaling the thickness and resistivity of each layer apparent on an electric log is a more tedious procedure than is actually necessary. It should be noted that the summations are not ordered—all beds with the same resistivity may be grouped together in the summations and treated as a single layer with the cumulative thickness of the individual layers. Thus, one approach to synthesizing the highly detailed information contained on an electric log is the use of a probability density curve for values of resistivity sampled randomly from the log. Such probability density curves are histograms for the frequency of occurrence for resistivity values within a series of ranges, as shown in the examples of values of resistivity read from an induction log from a section of Pleistocene sediments penetrated by a well in Adams County, Mississippi (fig. 4).

Experience has shown that it is preferable to compile such histograms with logarithmically incremented class intervals, so that the tapering off of probability densities as higher resistivity classes are considered may be reduced. Also, the data may be used to compile a cumulative frequency of occurrence curve for resistivity values, as shown in figure 5 (for the same well from Adams County, Mississippi). The points on a cumulative frequency of occurrence curve may then be fitted with a smooth curve, and this curve may be differentiated to provide a continuous probability density curve such as the one shown in figure 6. The resulting curve is less sensitive in appearance to the sampling than is the histogram presentation.

A probability density curve is a generalized form of a histogram; it is a plot of the ratio of the number of samples per class to class width, as the class width is reduced to zero in the limit. A very large number of samples may be required to establish the shape of the curve in detail. Less than infinite numbers of samples provide an estimate of the probability density curve subject to statistical uncertainty.

A well known example of a probability density curve is the bell-shaped Gaussian distribution curve shown in figure 7, defined by the expression:

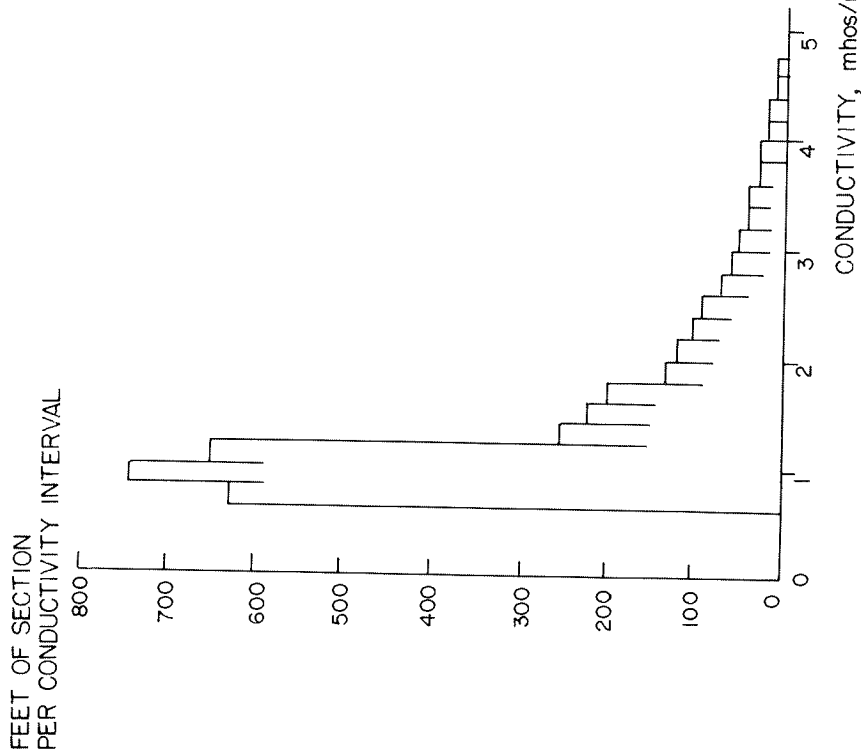


FIGURE 4.— Linear histogram for values of conductivity sampled from a 6FF40 induction log from a well in Mississippi.

$$f(\log \rho) = \frac{1}{(2\pi\sigma^2)^{1/2}} e^{-\log^2 \rho / 2\sigma^2} \quad (8)$$

where σ is the standard deviation of the values for $\log \rho$. A cumulative frequency of occurrence curve for a Gaussian distribution, also shown in figure 7, is obtained by integrating the probability density curve from the left:

$$F(\log \rho') = \int_{-\infty}^{\log \rho'} f(\log \rho) d(\log \rho) \quad (9)$$

When the resistivity samples from an electric log are compiled into probability density curves, designated as functions $G(\log \rho)$, the average electrical

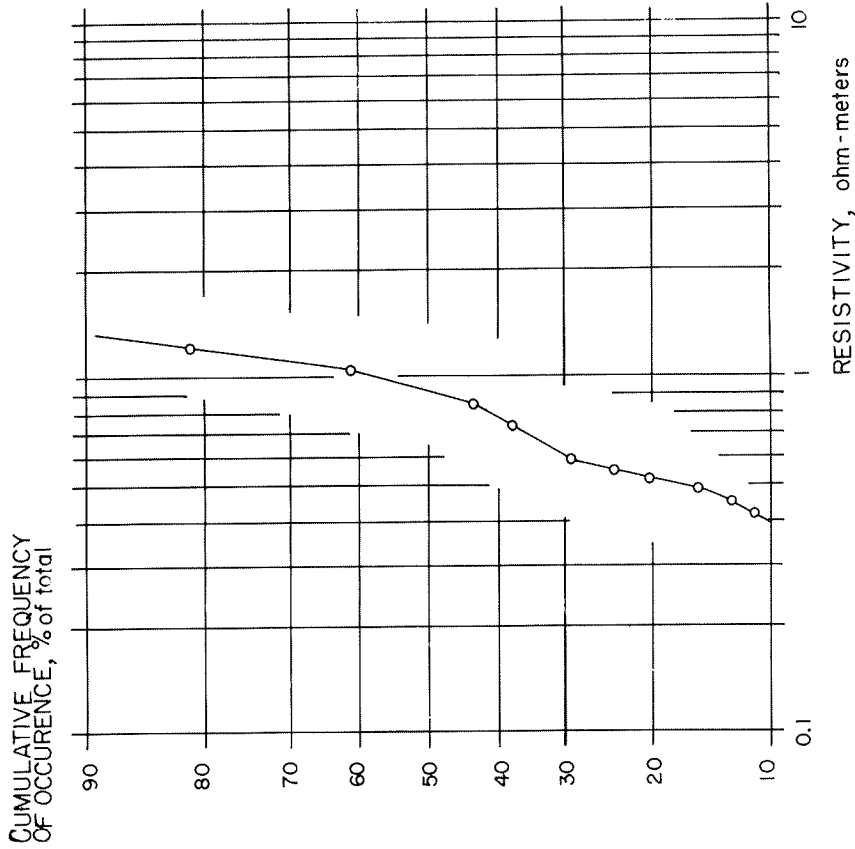


FIGURE 5.— Cumulative frequency of occurrence curve for the resistivity values tabulated in the histogram of figure 4.

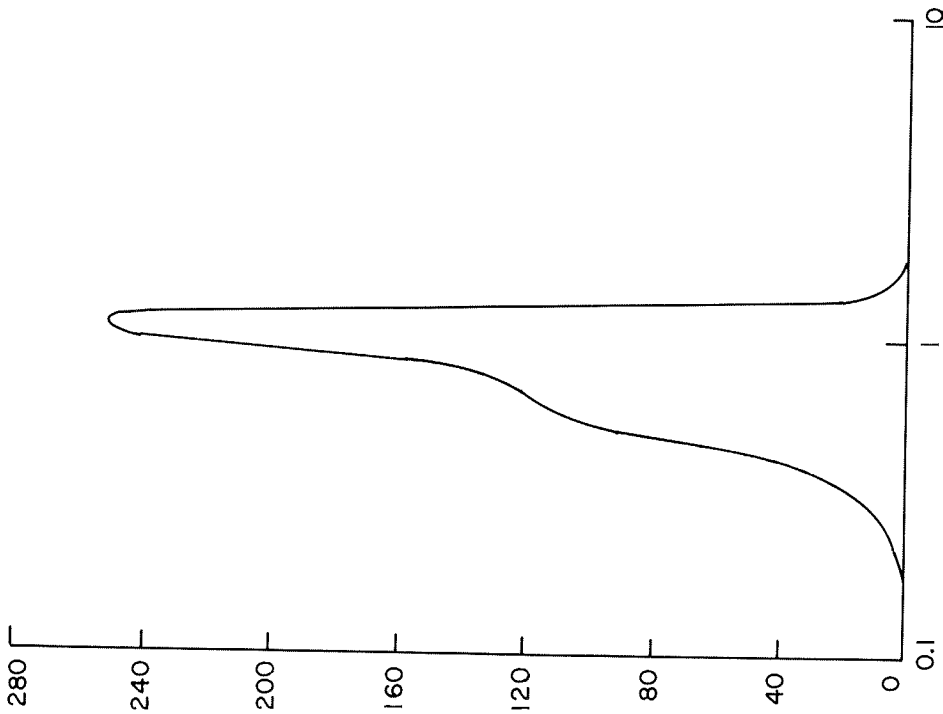
properties for the sequence from which the resistivities were sampled may be evaluated using the expressions:
for transverse resistivity:

$$A_r = \int_0^{\infty} \rho G(\log \rho) d\rho \quad (10)$$

for longitudinal conductivity:

$$\sigma_z = \int_0^{\infty} \frac{G(\log \rho)}{\rho} d\rho \quad (11)$$

RESISTIVITY PROBABILITY DENSITY, percent per decade



RESISTIVITY, ohm-meters

FIGURE 6.—Generalized histogram or resistivity probability density curve compiled for the same log as the data in figure 4. The data were sorted into class intervals with widths increasing exponentially, rather than linearly, as in figure 4.

The resistivity density function was first used as a computational convenience (Keller, 1964), but they are of interest in their own right. The resistivity density curves have properties of two types: shape and position on the resistivity axis. The shape of a resistivity probability density curve is usually

not that of a normal or log-normal distribution. More commonly, the curve appears to represent a multimodal type of log-normal distribution. Several values for resistivity appear to occur more frequently in a particular sequence of rocks than other values, and the sampled resistivities tend to group about these several central values.

Examples of clearly multimodal distributions are shown in figure 8, a probability density curve for the Pierre shale from eastern Colorado, and figure 9, a distribution curve for a sequence of Paleocene and Eocene limestone and dolomite beds from the Sirte Basin in Libya. In these density curves, the probability densities are expressed as the fraction of the total footage per decade of class width:

$$G(\log \rho) = \frac{N}{\log_{10} \frac{\text{upper bound of class}}{\text{lower bound of class}}} \quad (12)$$

where N is the fraction of the total number of sample resistivities which fall within the class bounds under consideration.

The multimodal nature of the probability density results from the presence of several preferred lithologic types in the section, such as shale and siltstone, for example. The multimodal form is characteristic not only of sedimentary rocks, but also of other layered sequences of rocks, including

GAUSSIAN DISTRIBUTION:

$$f(x) = (2\pi\sigma^2)^{-1/2} \exp(-x^2/\sigma^2)$$

$$F(a) = \int_{-\infty}^a f(x) dx$$

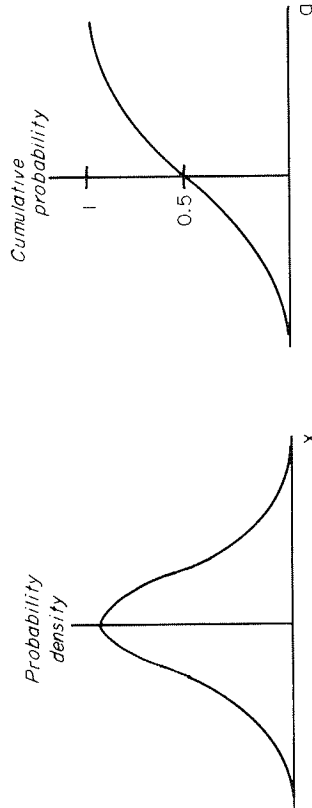


FIGURE 7.—Examples of the probability density curve and the cumulative probability curve for the well-known Gaussian distribution.

Resistivity density function, percent per 0.05 range in log ρ

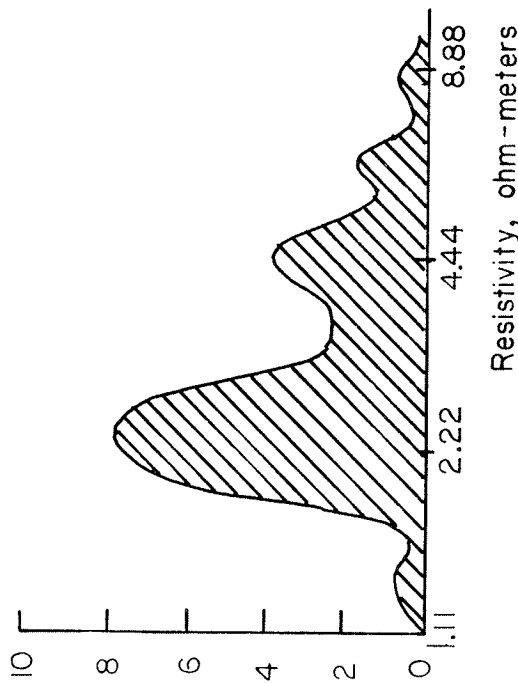


FIGURE 8.—Resistivity probability density curve for values of apparent resistivity measured with a short normal electric log in a 4300 foot section of Pierre Shale in eastern Colorado.

RESISTIVITY PROBABILITY DENSITY, percent per decade

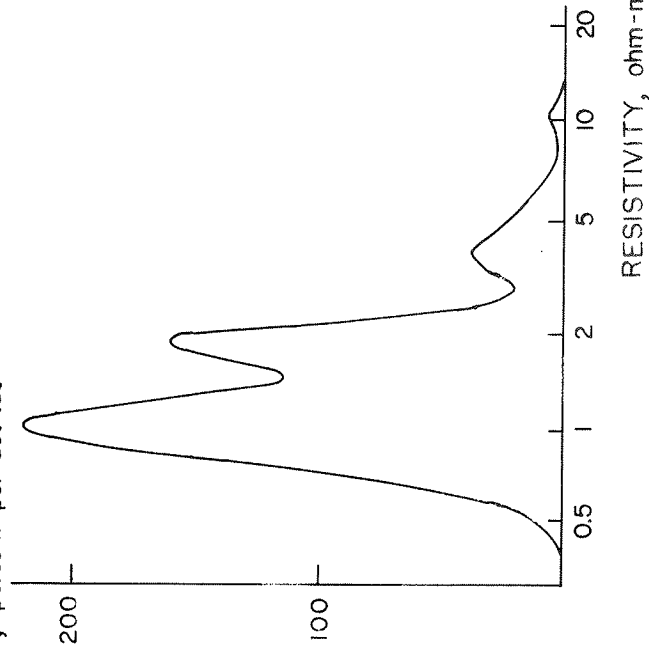


FIGURE 9.—Resistivity probability density curve for values of resistivity sampled from an electric log in a 1900 foot section of Eocene limestone from the Sirte Basin, Libya.

volcanic rocks. An example of a probability density curve for a sequence of volcanic rocks has been given by Jackson (1967), as shown in figure 10. This curve was compiled from an electric log run in Rattlesnake No. 1, drilled to about 10,000 feet in basalt and tuff in the Columbia River Plateau area, near Yakima, Washington. The petrographic significance of the curve shape is not clear, but indicates that there were preferred textures involved in the formation of these basalt layers.

Resistivity density curves might be of some use in determining the ratios of lithologic components which give rise to the various modal peaks. However, before considering the meaning of curve shapes, we must consider the degree of reliability of values for resistivity taken from well logs. The accuracy of a resistivity probability density curve depends on the sizes of errors of two types: those involved in the original measurement of resistivity during logging, and those associated with the sampling procedure. In logging, the recorded resistivity (apparent resistivity) depends not only on the resistivity

PERCENTAGE OF SAMPLES IN EACH RESISTIVITY CLASS

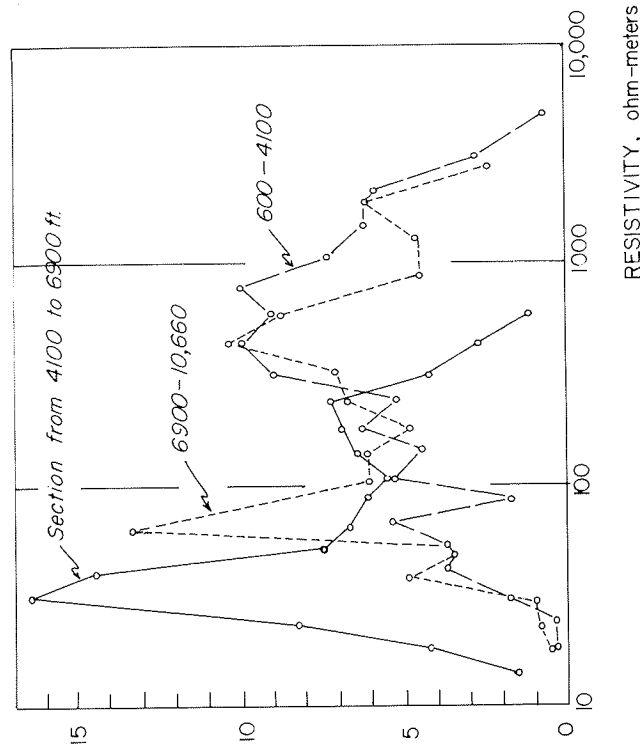


FIGURE 10.—Frequency of occurrence histogram for values of resistivity sampled from an electric log run in a well in basalt on the Columbia River Plateau (from Jackson, 1968).

of the rock around the well, but also on the resistivity of the mud in the well bore, the well diameter, bed thickness, the degree of flushing of the rock by drilling fluid and the type of logging device used. Corrections may be made for each of these effects which are more or less satisfactory, but the work involved in correction procedures is prohibitive if a very large volume of data is to be handled. It appears to be more reasonable to make use only of those types of logs which have minimum corrections for a given set of conditions than to attempt to determine the exact resistivity of each zone penetrated by a well. The resistivity density curve obtained without making corrections will be far from exact, but if the errors are consistent, comparison between sets of resistivity density curves may be made with some confidence.

It is therefore necessary insofar as possible to choose the electric logging curves which come closest to recording the actual resistivity of the rock around the well. In the examples which follow, three types of electric log were used; 16-inch normal spacing logs, 6FF-10 induction logs and laterologs. The latter two types are considered to require virtually no corrections for the shunting effect of the mud column, and to provide essentially the correct resistivity for beds more than a few well diameters thick. However, reliable induction and laterolog systems have been available only for the past decade, and in many areas, these types of logs may not be available except from recently drilled wells. In such areas, spacing logs must be used, and these are subject to large errors resulting from current shunting through the mud column, and the effect of bed thickness is appreciable even for beds tens of feet thick.

In sections where invasion is negligible, the short normal spacing is preferred to the long normal or lateral spacings, because the effect of bed thickness on the log is simpler. An example of the correction procedure which may be used with the spacing logs is given in table 2. The left-hand columns are the distributions of resistivity values taken at 10-foot intervals in the Pierre shale in a well from Morgan County, Colorado, at depths between 120 and 4,470 feet. These values were grouped in class intervals with the upper bound of each interval being larger than the lower bound by the ratio 1.08. The class mark is the geometric average of the upper and lower bounds. On the right-hand side of the table, the class marks have been corrected for the effect of the mud column (for a mud resistivity of 1.2 ohm-meters), using the departure curve shown in figure 11. The longitudinal conductivity and transverse resistivity are then computed for the corrected distribution curve, and are found to differ only slightly from the uncorrected values. See page 25.

It is apparent that if the mud resistivity is not greatly different than the rock resistivity, the correction for mud resistivity is not particularly important. The effect is greater on the value determined for transverse resistivity than on

TABLE 2. — Example of the correction of a resistivity density curve for the effects of mud resistivity (depth interval from 120 to 4,470 feet in the Pierre shale, Fort Morgan County, Colorado)

Uncorrected class mark, ρ_M , ohm-m	N (fraction of samples)	$\rho_M N$	N/ρ_M	Corrected class mark, M'	$\rho_M N$	N/ρ_M'
1.45	.036	.052	.025	1.43	.051	.025
1.57	0					
1.70	.037	.063	.022	1.67	.062	.022
1.83	0					
1.98	.036	.071	.018	1.93	.069	.019
2.13	.080	.170	.037	2.04	.163	.039
2.30	.076	.175	.033	2.20	.167	.034
2.49	.115	.286	.046	2.38	.274	.048
2.69	.136	.365	.051	2.55	.347	.053
2.90	.069	.200	.024	2.72	.187	.025
3.13	.148	.463	.047	2.89	.427	.051
3.38	.005	.017	.002	3.12	.015	.002
3.65	.037	.140	.010	3.31	.122	.011
3.95	.036	.140	.009	3.52	.126	.010
4.26	0					
4.59	0					
4.96	.074	.367	.015	4.32	.319	.017
5.35	.037	.197	.007	4.63	.171	.008
5.78	.037	.197	.007	4.63	.171	.008
6.24	.004	.025	.001	5.38	.021	.001
6.74	.001	.007		5.83	.006	
7.27	.036	.262	.005	6.30	.227	.006
7.85	.036	.282	.005	6.75	.243	.005
Sum	1.000	3.288	.357	3.002	3.002	.374
		(ρ_{tr})	(σ_1)		(ρ_{tr}')	(σ_1')
		$\lambda = 1.08$			$\lambda = 1.06$	

	Uncorrected	Corrected	Percentage difference
Transverse resistivity	3.288 ohm-m	3.002 ohm-m	9.5%
Longitudinal conductivity	0.357 mhos/m	0.374 mhos/m	4.5%
Coefficient of anisotropy	1.03	1.06	1.9%

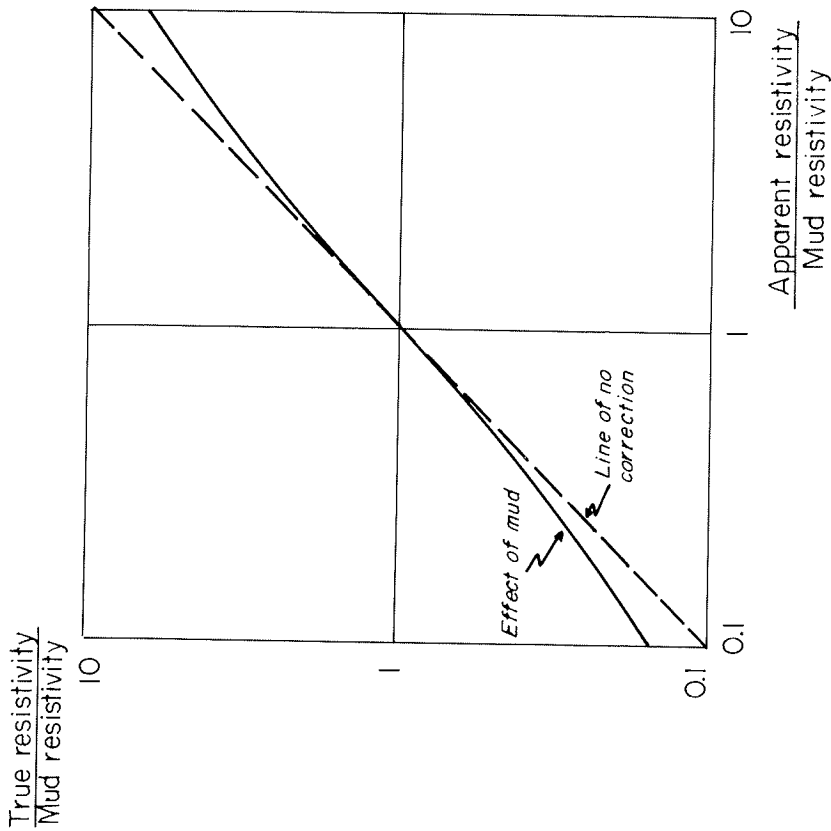


FIGURE 11.— Resistivity departure curve for correcting resistivity measured with the short normal array for the effect of the mud column in the example given in the text.

the values determined for longitudinal resistivity or the coefficient of anisotropy.

It is not so simple to correct for the effect of limited bed thickness when a spacing log is used. In an attempt to estimate the errors caused by departure of resistivity values in thin layers, the curves shown in figure 12 were prepared. A hypothetical section consisting of layers with two resistivities, 1 and 100 ohm-meters, was considered, with the mud resistivity being 1 ohm-meter also. Only the 16-inch normal spacing curve and an 8-inch well diameter were considered. High resistivity beds, with a thickness of 4 well diameters (32 inches) in one case, and 16 well diameters (128 inches) in another case, were assumed to be distributed uniformly through the low re-

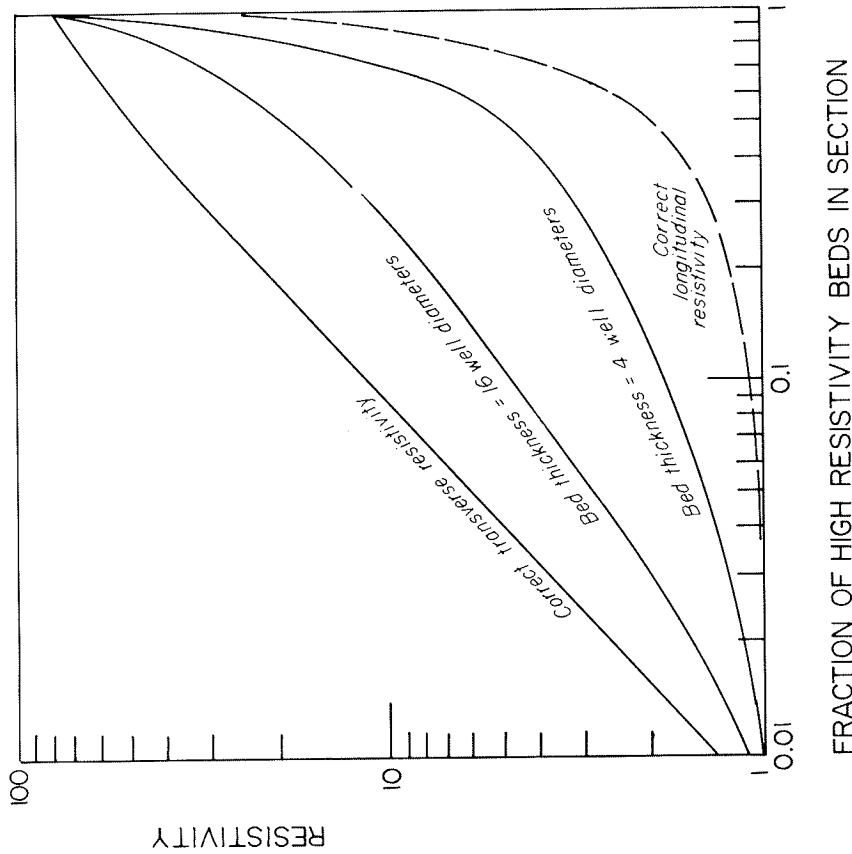


FIGURE 12.— Transverse and longitudinal resistivities which would be obtained using apparent resistivity values recorded for a sequence of layers with alternating resistivities of 1 and 100 ohm-meters.

sistivity rock. The fraction of high resistivity beds in the section was varied by changing the interval between them.

For this section, the correct values of longitudinal and transverse resistivity would lie between 1 and 100 ohm-meters, depending on the ratio of the two components. The value for longitudinal resistivity is close to 1 ohm-meter until the fraction of high resistivity beds is quite large—the value for longitudinal resistivity is dominated by the more conductive beds in the sequence. On the other hand, the transverse resistivity increases rapidly with the addition of even a small fraction of high resistivity beds—the value for transverse resistivity is dominated by the presence of high resistivity beds in the section.

FRACTION OF HIGH RESISTIVITY BEDS IN SECTION

The departure of apparent resistivity as recorded on the log from true resistivity is most significant in the high resistivity beds. As a result, the value for longitudinal resistivity is little affected by considering this departure. On the other hand, the departure in resistant beds contributes a large error to the determination of transverse resistivity from the log, with the error being greater with thinner beds. The error also is larger when the high and low resistivity beds are present in equal portions than when the section is made up mostly of one or the other.

It is reasonable to expect that the error caused by limited bed thickness will be more serious if the contrast in resistivities is large. In order to determine the nature of such a dependence, the curves in figure 13 were prepared. Here, a fixed ratio of high resistivity and low resistivity beds was considered, with each being equally abundant, a condition assumed to insure a maximum

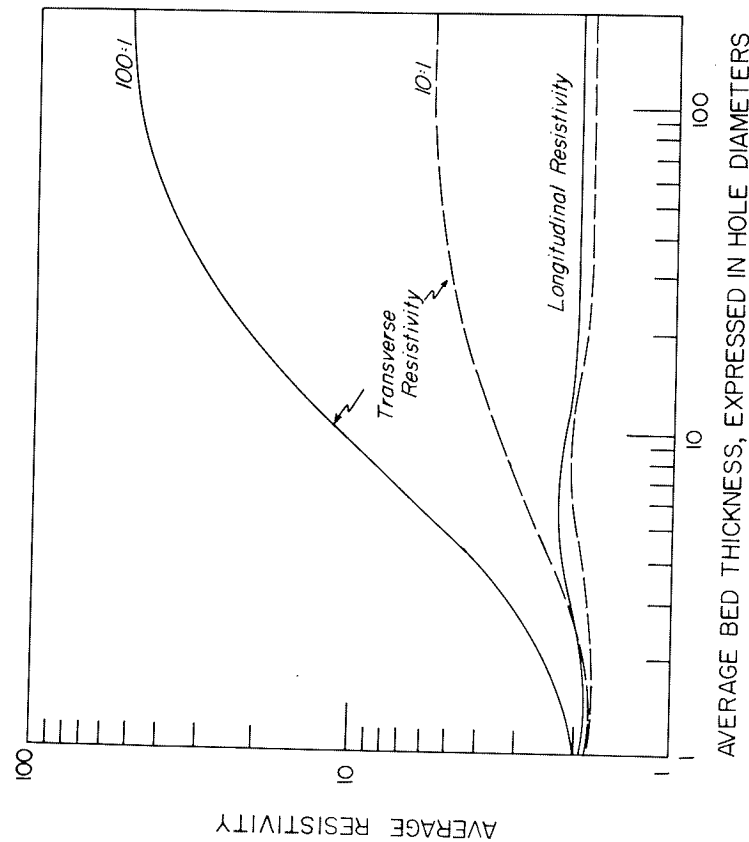


FIGURE 13.—Average transverse and longitudinal resistivities which would be computed from apparent resistivities measured in a section containing equal numbers of beds with two resistivities, the contrast being either 100:1 or 10:1.

effect from the departure of measured rock resistivity from true resistivity. As in the previous case, the resistivity of the mud column and of the conductive beds was taken as 1 ohm-meter, but the resistivity of the resistant beds was varied, as well as the thickness of the layers. Again, the error in longitudinal resistivity is generally negligible, but the transverse resistivity departs seriously from the correct value for bed thickness less than 30 to 50 well diameters. The error is considerably greater for a contrast of 100 to 1 between the resistivities of the two types of beds than for a contrast of 10:1, while the error in longitudinal resistivity does not vary much with resistivity contrast.

The error caused by limited bed thickness is more serious with the spacing logs of greater dimensions than with the short-normal spacing log. However, if there is significant invasion of the rock around the well by mud filtrate, the short-normal log may give an erroneous value for both the longitudinal resistivity and the transverse resistivity. In some areas, the overall permeability of the section is low so that invasion is not a serious problem; in other areas, as for example the Gulf Coast, the entire section may be so permeable that invasion will seriously affect the resistivity density curves taken from a short normal log. Typical of the errors which may develop are the effects shown by the data in figure 14, which consists of two cumulative frequency of occurrence curves for resistivities sampled from a log run in a Cretaceous section in Mississippi. The two logs used here were the 16-inch normal and the 6FF40 induction log. The resistivities taken from the induction log are lower than those from the short normal log generally by a factor of 3. This difference may be attributed to the effect of invasion, inasmuch as the drilling-mud filtrate resistivity in this well was approximately 1.30 ohm-meters, considerably higher than the connate water resistivity.

Considering these various errors in compiled resistivities, some generalizations may be made:

1. Of the spacing logs, the short-normal spacing is preferable, but may be used with confidence only when none of the recorded resistivities differ from the mud resistivity by a factor of more than 10, and when the section is sufficiently tight that invasion is not a problem.
2. Induction and laterologs provide better compiled resistivities, though the induction log is limited to use in sections where the maximum resistivity is less than 50 or 100 ohm-meters, and the laterolog is limited to use in areas where there is no significant invasion. These two limitations tend to be complementary, inasmuch as tight rocks not subject to invasion tend to have higher resistivities.
3. The value for longitudinal resistivity is less subject to error than is the value for transverse resistivity. The coefficient of anisotropy may be intermediate in sensitivity to errors, inasmuch as it is the square root of the ratio

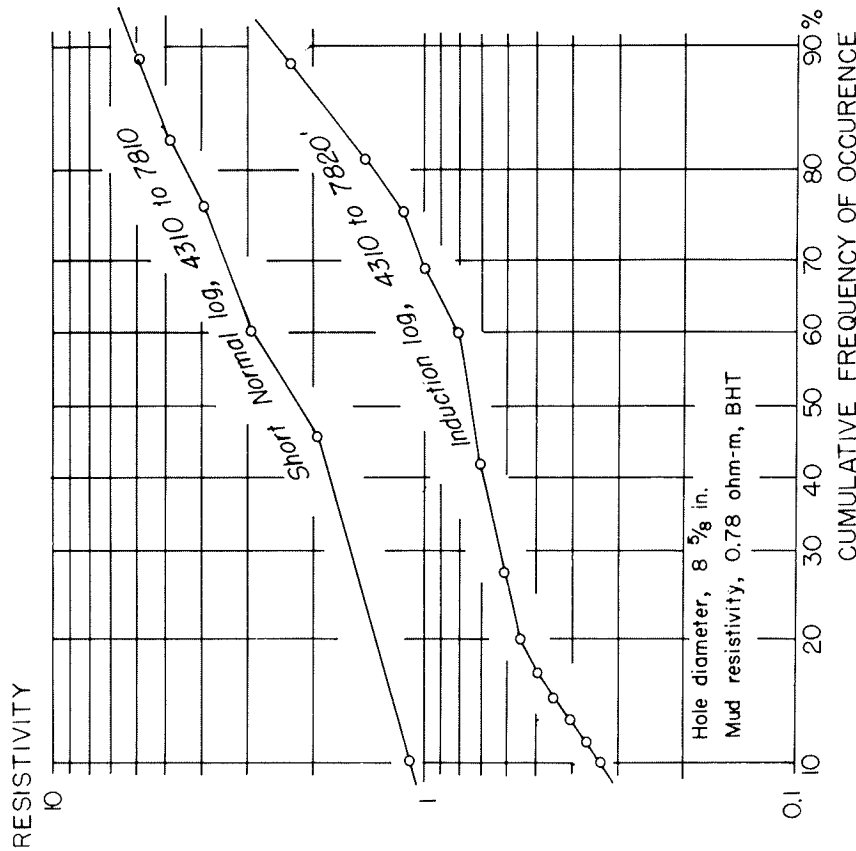


FIGURE 14.— Cumulative frequency of occurrence curves for values of resistivity sampled from a 6FF40 induction log and a short normal electric log for a common interval in a well in Mississippi. The difference between the two sets of values may be attributed to overall invasion of the section by drilling mud filtrate.

of the transverse and longitudinal resistivities.

Having considered how the compiled resistivity parameters depend on the errors involved in logging, we may now turn to the relationship between the compiled parameters and the geological nature of the section for which they are compiled. If a sequence of rocks consists of layers of only two kinds, each characterized by a single resistivity value, the coefficient of macroanisotropy is a simple function of the ratio of one component to the other, and of the resistivity contrast between the two components:

$$\lambda = \left\{ \frac{1}{\rho} \left[\beta \alpha^2 + \beta (1-\alpha)^2 + \alpha (1-\alpha) + \beta^2 \alpha (1-\alpha) \right] \right\}^{1/2} \quad (13)$$

where α is the fraction of the section made up of beds with a resistivity ρ_1 , and β is the ratio of resistivities between the two types of rocks, ρ_1/ρ_2 . Figure 15 shows the variation of the coefficient of anisotropy and of the longitudinal resistivity:

$$\rho_2/\rho_1 = \frac{1}{[\alpha + \beta(1-\alpha)]} \quad (14)$$

as the fraction of siltstone beds with a resistivity $\rho_2 = 4.5$ ohm-meters in a shale with resistivity $\rho_1 = 3.0$ ohm-meters is varied. As one would anticipate, the anisotropy is a minimum when one or the other component is the only one present, and the anisotropy is maximum when both components are present in equal abundances. This maximum coefficient of anisotropy is

$$\lambda_{\max} = \frac{1}{2} \left[\beta + 2 + \frac{1}{\beta} \right]^{1/2} \quad (15)$$

COEFFICIENT OF ANISOTROPY

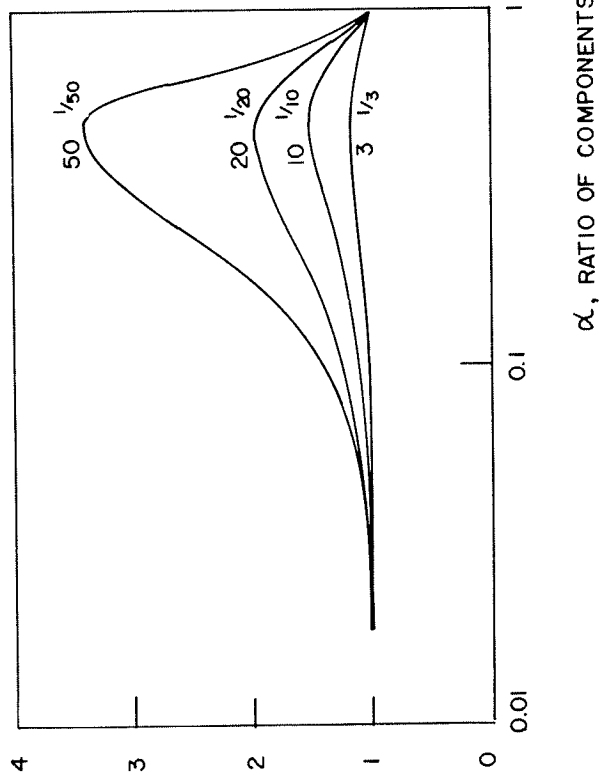


FIGURE 15.— Variation of the coefficient of anisotropy, arising from layering, as a function of the ratio of two components with different resistivities, as indicated on the curves.

or, approximately 1.02 for the assumed case.

It is difficult to see the behavior of the coefficient of anisotropy from the curve in figure 15 because the values are so close to unity. It is more convenient to subtract 1 from the coefficient of anisotropy before plotting it so that the variations are more easily observed. A family of curves for the coefficient of anisotropy plotted in this manner is shown in figure 16a, for various contrasts in resistivity between the two members of a simple sequence. The corresponding curves for the variation in longitudinal resistivity are shown in figure 16b.

A rock sequence might be characterized by a pattern plot of the value for the reduced coefficient of anisotropy, or $\lambda-1$, and the value for longitudinal

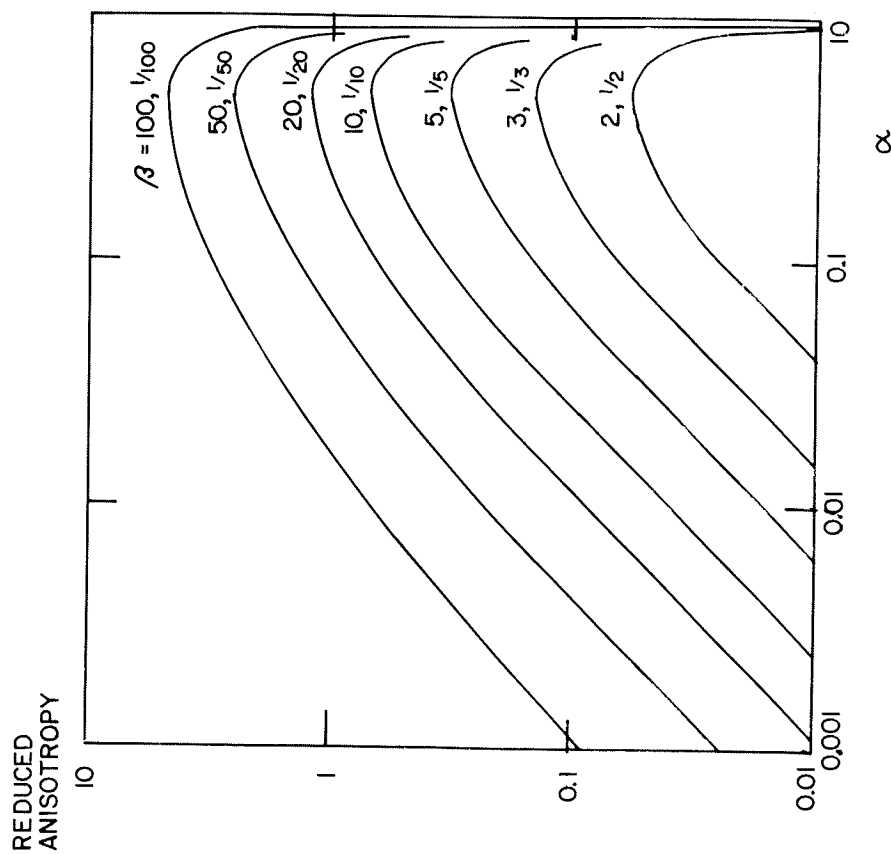


FIGURE 16A.—Variation of the coefficient of anisotropy with the ratio of components, α , in a two-component system of layers having resistivity contrast, $\rho_2/\rho_1 = \beta$.

resistivity. Using such a plot, we might be able to postulate the control exerted by changes in lithology or other factors on the electrical properties of a sequence of rocks. One typical type of marine sequence might consist of essentially mud or shale, in which there are included varying amounts of thin sandstone, limestone or evaporite beds. The properties of such a sequence could change laterally either because the relative portions of shale and other rock types changed, or because the nature of the second rock type, and therefore the resistivity contrast, changed. Three curves relating the reduced coefficient of anisotropy and the longitudinal resistivity are shown in figure 17. The parameter for each curve is the resistivity contrast, β , which

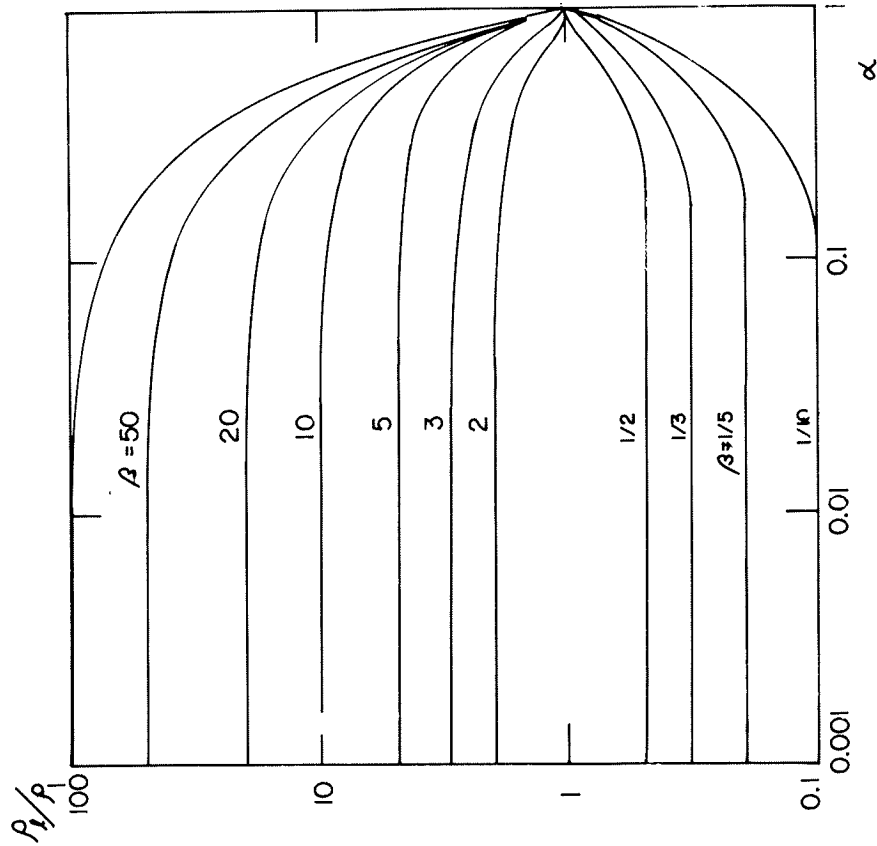


FIGURE 16B.—Variation of longitudinal resistivity with the ratio of components, α , in a two-component system of layers having a resistivity contrast, $\rho_2/\rho_1 = \beta$.

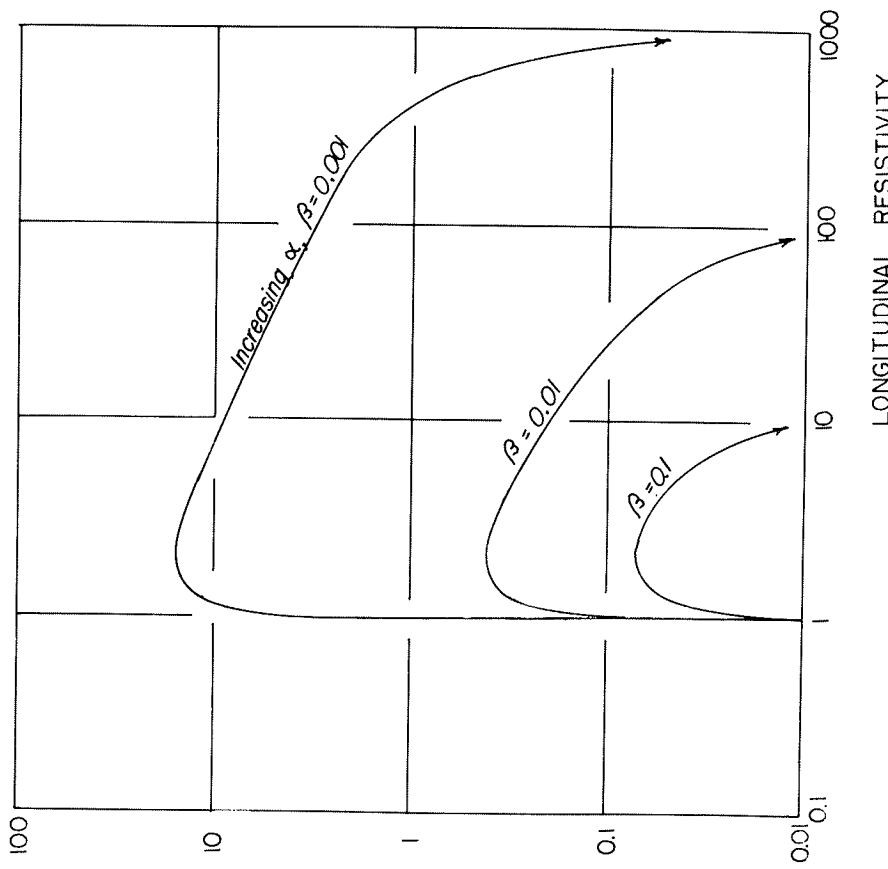
REDUCED
ANISOTROPY

FIGURE 17.— Paths followed by resistivity-anisotropy field plots as the ratio, α , of a high-resistivity component to a low resistivity component is increased. The low-resistivity component has a resistivity of 1 ohm-meter; the high resistivity component has a resistivity of $1/\beta$.

was assumed to be 0.1 (corresponding to a shale-sand sequence), 0.01 (corresponding to a shale limestone sequence) or 0.001 (corresponding to a shale-evaporite sequence). The ratio of non-shale to shale (assumed to have a resistivity of 1 ohm-meter) increases in travelling along these curves from left to right. The maximum point on each of these curves corresponds to a ratio of 1:1 between shale and the other lithologic component. It is apparent

that the coefficient of anisotropy rises with but little change in longitudinal resistivity, so long as the shale remains the dominant lithological constituent of the section. However, when the other component becomes the more abundant, longitudinal resistivity varies quite significantly, while the coefficient of anisotropy drops slowly.

Another set of geological conditions which might affect the electrical characteristics of a sequence in a consistent manner is a change in the salinity of the connate water, perhaps with no change in the lithology or lithologic ratios. Considering Archie's law, it is conceivable that a uniform change in the salinity of the water in both the shale and non-shale facies in a sequence would change the longitudinal resistivity without changing the coefficient of anisotropy—that is, the resistivity of each bed in a sequence would increase in the same proportion as the water salinity decreased. Such a situation would lead to the translation of a field plot of anisotropy vs. resistivity parallel to the resistivity axis, as shown by line A in figure 18. It is more likely, though, that water salinity will not change by the same amount in both the shale and the non-shale beds. If the change in salinity across a basin is the result of depositional environment, the salinity in shale beds may change less rapidly than the salinity in non-shale beds because of the moderating influence of adsorbed salinity in clay minerals. This salinity is essentially a function of the cation exchange capacity of a rock, and not particularly sensitive to the salinity of the water in the pore spaces. Therefore, if the salinity of the water at time of deposition varies across a basin, the variation in salinity for shale members will be less than will be the variation in salinity for non-shale members. As a consequence, the contrast in resistivity between shale and non-shale beds will increase as the connate water salinity decreases, and the coefficient of anisotropy will vary with the resistivity as indicated by line B in figure 18. At high salinities, the change in the coefficient of anisotropy will be small, because the effect of the added salinity from cation exchange capacity will be relatively small. At low salinities, the change in resistivity and the coefficient of anisotropy will be greater.

A similar phenomenon may be observed if the salinity is changed by circulation of fresh water into a marine sequence sometime after deposition. In this case, the water resistivity will be most increased in the layers which are most permeable. The effect will be that of increasing the contrast in resistivity between the shale and non-shale beds. This will result in pronounced changes in the coefficient of anisotropy with lesser changes in the resistivity (if the shale is the dominant rock type), with a transition of the anisotropy-resistivity field as shown by line C on figure 18.

Let us now consider some examples of the behavior of the gross electrical properties of sedimentary sequences.

COEFFICIENT OF ANISOTROPY

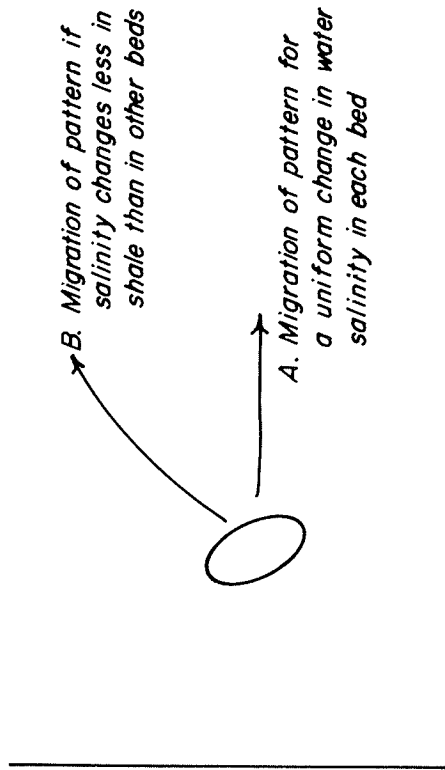


FIGURE 18. — Hypothetical shifts in the resistivity-anisotropy pattern for a change in connate water salinity as might be caused by a change in depositional environment (A) or by flooding from surface waters (B).

LONGITUDINAL RESISTIVITY

Electrical properties of the Mesozoic-Cenozoic sedimentary sequence of the east Gulf Coast area

Induction-electric logs were selected from wells in Mississippi, southern Alabama and the Florida panhandle, at locations indicated on the map in figure 19. The contours on this map are the depths to the base of the Mesozoic, taken from the Basement Map of North America (U. S. Geol. Survey, 1967). The sediments in this column are chiefly sand, clay, marl, limestone, and chalk, all rather poorly consolidated. Calcareous sediments tend to be more abundant in the lower part of the column than in the upper part, and increase in importance toward the Gulf Coast (Eardley, 1962; Sloss, Dapples, and Krumbein, 1960). The section varies rapidly in character over short distances, so that correlations in detail are difficult. The sequence in southeastern Mississippi—the center of the area of the log study—has been reviewed in a recent paper by Eargle (1963).

Despite the difficulty in correlating beds in detail, all logs from the area, except those in the far north which penetrate pre-Mesozoic rocks, exhibit a similar overall character: surficial resistivities are high, decreasing gradually to a minimum resistivity at a depth of several thousands of feet, increasing

again slowly at greater depths. In picking depth intervals for averaging the electrical properties, zones which appeared to be consistent in electrical properties were selected without attempting to assign formation boundaries. In this process, four geoelectric units could usually be picked consistently. The units are designated in table 3 with the letters U, M or L, indicating that they are in the upper part of the section, the middle part where resistivity is a minimum, or in the lower part, where the resistivity increases with depth. If one of these sections is further subdivided, the letter designator is subscripted to indicate the sequence from top down, within that section. Thus, if the section above the interval with minimum resistivity has been broken into two parts, the upper part is designated U₁, and the lower part, U₂. Lithologically, the upper sequence, U, consists of formations of Miocene and latter age, while the mid part of the section consists generally of formations of Eocene and Oligocene age, including the Wilcox, Claiborne, Jackson and Vicksburg formations. The lower part of the sequence, L, includes beds of Cretaceous age, though not the whole Cretaceous section in any of the wells included in this study. A summary of formation names and lithology, taken from Eargle (1963) is given in table 4.

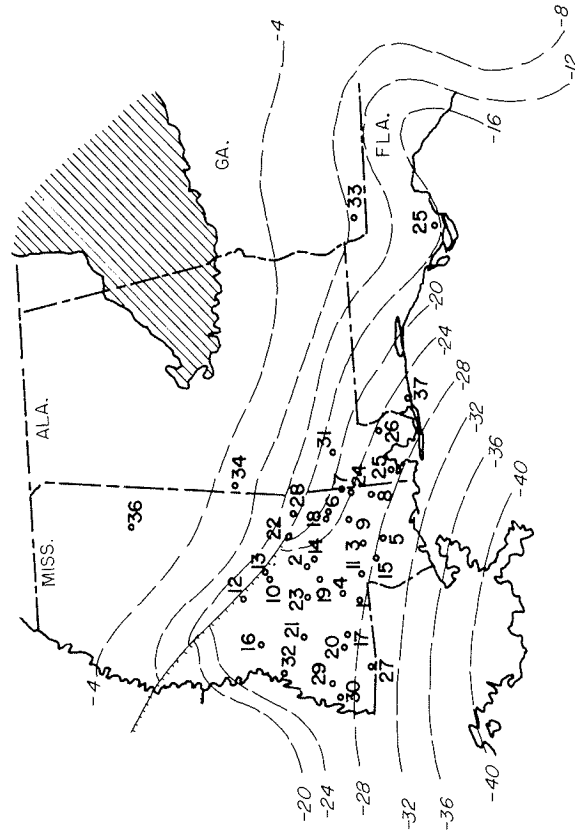


FIGURE 19. — Map of the eastern Gulf Coast area, showing locations of wells for which electric logs were compiled. Contours are the elevation of the pre-Mesozoic surface, in thousands of feet (from Basement Map of the United States).

TABLE 3. — *Electrical resistivities summarized from induction logs of wells penetrating Mesozoic-Cenozoic rocks of the east Gulf Coast*

Index No. of well	Location	Depth interval	Designator	Transverse resistivity	Longitudinal resistivity	Coefficient of anisotropy
1.	Walthall County, Mississippi Sec. 18, 2N, 12E	2,130-3,150 3,160-6,800 6,810-7,650 7,660-11,000	U M L ₁ L ₂	3.19 0.71 1.25 2.28	1.70 0.66 1.21 1.50	1.37 1.04 1.02 1.23
2.	Smith County, Mississippi Sec. 6, 10N, 16W	2,580-5,350 5,350-6,020 6,020-11,080 11,090-14,000	U M L ₁ L ₂	2.40 0.89 2.28 7.44	2.00 0.86 1.73 6.35	1.10 1.02 1.15 1.08
3.	Forrest County, Mississippi Sec. 17, 1S, 13W	2,500-5,330 5,330-5,830 5,830-8,380	M ₁ M ₂ L	0.66 0.93 1.62	0.64 0.80 1.51	1.01 1.08 1.04
4.	Marion County, Mississippi Sec. 3, 4N, 19W	100-1,740 1,750-2,470 2,480-6,350 6,360-7,300	U ₁ U ₂ M ₁ M ₂	10.1 3.48 0.85 0.98	3.59 2.16 0.77 0.93	1.68 1.27 1.05 1.02
5.	Stone County, Mississippi Sec. 1, 3S, 12W	1,550-2,500 2,510-5,770 5,770-8,590	U M L	4.56 0.76 1.66	2.86 0.69 1.42	1.26 1.05 1.08
6.	Wayne County, Mississippi Sec. 16, 7N, 9W	1,720-3,650 3,650-4,140 4,140-8,650 8,650-12,010	U M ₁ L ₁ L ₂	2.25 0.61 1.26 2.06	2.08 0.60 0.93 1.36	1.04 1.01 1.17 1.23
7.	Green County, Mississippi Sec. 10, 4N, 5W	9,870-13,050	L ₂	3.58	3.22	1.05
8.	George County, Mississippi Sec. 15, 3S, 6W	830-2,330 2,340-5,540 5,540-7,950 7,960-8,570	U M ₁ M ₂ M ₃	1.76 0.59 1.04 0.66	1.42 0.57 0.97 0.59	1.11 1.02 1.04 1.06

TABLE 3 (cont.)

Index No. of well	Location	Depth interval	Designator	Transverse resistivity	Longitudinal resistivity	Coefficient of anisotropy
9.	Perry County, Mississippi Sec. 18, 3N, 9W	1,980-2,670 2,680-5,760 5,770-8,650 8,660-12,350	M ₁ M ₂ L ₁ L ₂	0.77 0.67 1.41 2.43	0.76 0.65 1.04 1.68	1.01 1.02 1.17 1.21
10.	Rankin County, Mississippi Sec. 14, 5N, 5E	5,040-8,790 8,800-12,500	L ₁ L ₂	1.33 2.67	0.96 1.76	1.18 1.25
11.	Lamar County, Mississippi Sec. 19, 2N, 16W	1,760-2,480 2,490-5,900 5,910-6,650 6,650-10,820	U M ₁ M ₂ L ₁	3.84 0.66 0.83 2.75	2.24 0.63 0.81 1.91	1.31 1.02 1.01 1.20
12.	Madison County, Mississippi Sec. 1, 8N, 2E	1,450-3,830 3,830-4,600 4,600-7,530 7,540-9,740 9,740-11,000	U M L ₁ L ₂ L ₃	5.02 0.86 1.67 3.11 2.86	3.15 0.84 1.08 1.36 2.23	1.21 1.01 1.24 1.51 1.13
13.	Scott County, Mississippi Sec. 15, 5N, 6E	660-2,260 2,260-4,030 4,030-4,560 4,660-7,500	U ₁ U ₂ M L ₁	4.25 3.34 0.63 1.45	2.75 2.31 0.61 1.19	1.24 1.20 1.02 1.10
14.	Smith County, Mississippi Sec. 6, 10N, 16W	2,500-5,340 5,350-6,020 6,020-11,080 11,090-14,000	U M L ₁ L ₂	2.25 0.57 1.55 5.08	1.08 0.55 0.94 2.82	1.44 1.02 1.28 1.34
15.	Pearl River County, Mississippi Sec. 11, 2S, 15W	1,250-2,070 2,070-2,850 2,850-5,480 5,480-6,340 6,340-8,710 8,710-10,200	U ₁ U ₂ M ₁ M ₂ L ₁ L ₂	7.58 3.20 0.82 1.05 1.84 1.78	6.12 2.61 0.66 1.03 1.63 1.02	1.11 1.12 1.11 1.01 1.06 1.32

TABLE 3 (cont.)

Index No. of well	Location	Depth interval	Designator	Transverse resistivity	Longitudinal resistivity	Coefficient of anisotropy
16. Hinds County, Mississippi Sec. 30, 6N, 4W		3,210-5,900	U	1.20	0.88	1.17
		5,900-6,820	M	0.98	0.96	1.01
		6,830-9,720	L ₁	1.89	1.33	1.19
		9,730-11,100	L ₂	4.03	2.83	1.19
17. Pike County, Mississippi Sec. 1, 4N, 7E		1,500-3,160	U	4.27	2.21	1.39
		3,160-7,350	M	0.80	0.70	1.07
		7,360-8,500	L ₁	1.31	1.23	1.03
18. Jones County, Mississippi Sec. 16, 7N, 10W		8,500-11,100	L ₂	3.15	2.87	1.05
		2,390-5,020	U	1.49	0.85	1.32
19. Covington County, Mississippi Sec. 4, 7N, 17W		5,030-5,660	M	0.68	0.66	1.01
		5,670-10,020	L ₁	1.36	1.04	1.14
		10,030-14,860	L ₂	3.84	2.84	1.16
20. Lincoln County, Mississippi Sec. 32, 5N, 6E		3,050-5,750	U	1.04	0.76	1.17
		5,760-6,740	M	0.82	0.80	1.01
		6,750-10,650	L ₁	2.20	1.68	1.14
		10,660-13,460	L ₂	3.59	3.01	1.09
21. Copiah County, Mississippi Sec. 9, 9N, 7E		1,700-3,400	U	3.13	1.54	1.42
		3,410-7,700	M	0.82	0.73	1.06
		7,710-8,870	L ₁	1.33	1.30	1.01
		8,880-11,250	L ₂	3.05	2.78	1.05
22. Jasper County, Mississippi Sec. 12, 3N, 11E		2,110-3,130	U	4.04	3.74	1.04
		3,140-7,110	M ₁	0.76	0.73	1.02
		7,110-7,970	M ₂	0.80	0.79	1.01
		7,980-10,900	L ₁	2.03	1.49	1.16
23. Simpson County, Mississippi		10,910-12,340	L ₂	3.68	3.55	1.02
		2,520-2,980	U	2.81	2.50	1.06
24. Adams County, Mississippi Sec. 4, 6N, 2W		2,980-3,570	M	0.79	0.77	1.03
		3,580-8,850	L ₁	1.04	0.79	1.15
		8,860-14,330	L ₂	4.51	1.39	1.80
25. Clarke County, Alabama Sec. 11, 10N, 2W		2,410-6,080	U	7.23	6.39	1.06
		6,080-6,780	M	0.63	0.62	1.01

TABLE 3 (cont.)

Index No. of well	Location	Depth interval	Designator	Transverse resistivity	Longitudinal resistivity	Coefficient of anisotropy
26. Baldwin County, Alabama Sec. 16, 2N, 4E		6,790-9,990	L ₁	1.60	1.13	1.18
		9,990-12,980	L ₂	3.80	2.94	1.14
27. Amite County, Mississippi Sec. 28, 1N, 3E		1,990-5,070	M	0.89	0.81	1.05
		5,070-8,270	L ₁	1.33	1.10	1.10
		8,270-9,870	L ₂	1.36	0.89	1.23
28. Clarke County, Mississippi Sec. 6, 2N, 15E		240-1,200	U	3.82	2.13	1.34
		1,210-4,340	M ₁	1.05	0.74	1.18
		4,350-9,620	M ₂	1.12	0.53	1.44
29. Adams County, Mississippi Sec. 36, 7N, 1W		9,630-10,560	L ₁	4.32	2.95	1.19
		1,400-5,200	U	1.02	0.83	1.11
30. Adams County, Mississippi Sec. 4, 6N, 2W		5,210-6,720	M	0.71	0.42	1.30
		1,760-2,430	U	8.52	6.03	1.19
		2,440-6,000	M	1.01	0.59	1.29
31. Clarke County, Alabama Sec. 11, 10N, 2W		6,010-9,510	L ₁	1.40	1.11	1.12
		9,520-10,620	L ₂	2.64	2.49	1.03
29. Adams County, Mississippi Sec. 6, 2N, 15E		520-2,380	U ₁	9.75	6.17	1.25
		2,390-4,120	U ₂	1.57	1.39	1.06
		4,130-6,120	M	1.18	0.46	1.59
30. Adams County, Mississippi Sec. 36, 7N, 1W		1,880-4,100	M	0.54	0.38	1.18
		4,160-6,990	L ₁	1.65	0.86	1.40
31. Clarke County, Alabama Sec. 11, 10N, 2W		6,990-13,000	L ₂	2.30	1.51	1.23
		1,140-4,300	U	1.35	0.74	1.46
32. Adams County, Mississippi Sec. 4, 6N, 2W		4,310-7,820	M ₁	0.89	0.70	1.13
		7,830-9,410	L ₁	1.49	1.18	1.13
		9,410-10,810	L ₂	4.46	3.17	1.19
33. Clarke County, Alabama Sec. 11, 10N, 2W		460-3,000	U	5.72	4.07	1.18
		3,000-3,930	M	0.92	0.62	1.21

TABLE 3 (cont.)

Index No. of well	Location	Depth interval	Designator	Transverse resistivity	Longitudinal resistivity	Coefficient of anisotropy
32.	Claiborne County, Mississippi	2,220-3,760	U	1.23	0.76	1.27
		3,770-6,970	M	0.89	0.52	1.31
Sec. 27, 13N, 2E		6,980-8,050	L ₁	0.98	0.96	1.01
		8,060-10,430	L ₂	3.15	2.06	1.23
33.	Decatur County, Georgia	1,200-6,150	L	2.65	1.45	1.35
		80-3,950	L ₃	33.6	14.4	1.52
34.	Sumpter County, Alabama	3,960-10,020	L ₄	190.	158.	1.10
		1,840-5,300	M	1.05	0.90	1.05
35.	Mobile County, Alabama	5,310-8,720	L ₁	2.09	1.54	1.16
		8,730-13,030	L ₂	10.8	5.35	1.42
36.	Clay County, Mississippi	2,050-8,800	L ₃	80.0	43.3	1.35
		2,350-4,580	M	0.94	0.88	1.03
37.	Escambia County, Florida	1,580-7,590	L ₁	1.57	1.47	1.03
		7,600-10,420	L ₂	3.89	2.52	1.24
		10,430-12,500	L ₃	7.35	4.59	1.26

Note: All resistivities are compiled from the 6FF10 induction log.

All resistivities compiled in table 3 were taken from 6FF10 induction logs. (See Pirson, 1963, for a discussion of induction log characteristics.) The short-normal electric logs were also sampled, but generally gave resistivities several times larger than those on the induction logs. This departure is probably caused by invasion over most of the section, and so, the induction log, having a greater depth of investigation than the short normal log, probably indicates more closely the true formation resistivity.

Anisotropy-resistivity field plots are shown in figures 20-23 for the U, M, L₁ and L₂ portions of the section. The lower three parts of the section exhibit field plots that are elongated vertically, indicative of a sequence that is

quite uniform, except for the addition of a small fraction of resistant beds. The pattern for the uppermost rocks is not elongate, but this probably reflects the non-uniform nature of these rocks. It is interesting to note that there is a tendency for the anisotropy to be greater for the more conductive sections within a single plot. Such behavior is contrary to that postulated earlier in this section for increasing amounts of nonshale members in a shale sequence. It may be explained by a tendency for shale to become more conductive under the same circumstances that lead to the introduction of resistive beds, such as limestone or evaporites, into the section. In a near-shore environment, it is more likely that the section will consist mainly of clastics, so that there is less range in resistivity for the members of a sequence, and the shale will tend to be less conductive. Further from shore, the section may include more conductive shales and carbonates or evaporites, resulting in a section which is more conductive in general, but with a higher anisotropy than near-shore deposits. To summarize, the sedimentary column along the east Gulf Coast is characterized by the presence of thick sections of highly conductive rocks, with thousands of feet of section having a resistivity of less than one ohm-meter, and with the first 2 to 3 miles of section having an average resistivity of less than 5 ohm-meters. This low resistivity is accompanied by values for the coefficient of anisotropy ranging from 1.01 to 2.00.

TABLE 4. — Formation names from the east Gulf Coast

Electrical designator	Formation names	Age	Thickness	Lithology
U	Citronelle, Pascagoula, Hattiesburg, Catahoula	Miocene	1,100-3,700	sand, gravel, clay, marl
M	Vicksburg, Jackson, Claiborne, Wilcox, Midway	Paleocene-Eocene	3,200-6,000	clay, shale, sand, marl, limestone
L	Selma, Eutaw, Tuscaloosa, Dantzer, Andrew, Paluxy, Mooring-sport, Ferry Lake, Sligo, Hosston	Cretaceous	5,000	shale, limestone, anhydrite

ANISOTROPY

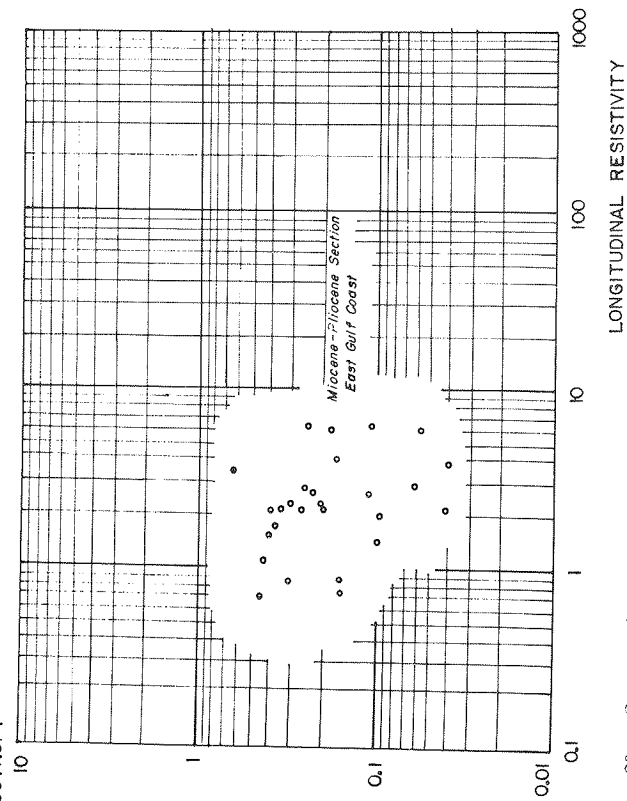


FIGURE 20.—Scatter plot of values for longitudinal resistivity and coefficient of anisotropy for the Miocene section penetrated by wells in the east Gulf Coast area. The values for the coefficient of anisotropy have been reduced by subtracting 1 from them.

REDUCED ANISOTROPY

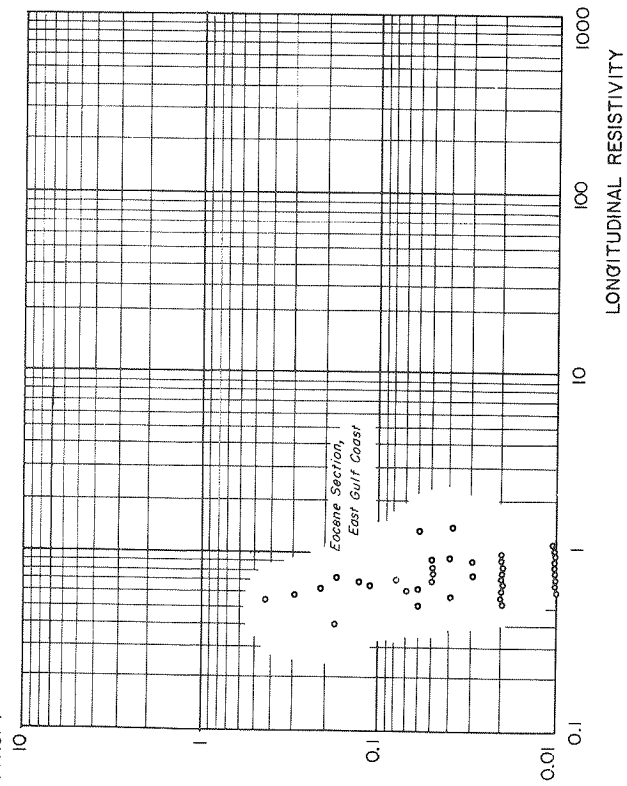


FIGURE 21.—Scatter plot for values of longitudinal resistivity and coefficient of anisotropy for the Paleocene-Eocene section penetrated by wells in the east Gulf Coast area. The values for the coefficient of anisotropy have been reduced by subtracting 1 from them.

ANISOTROPY

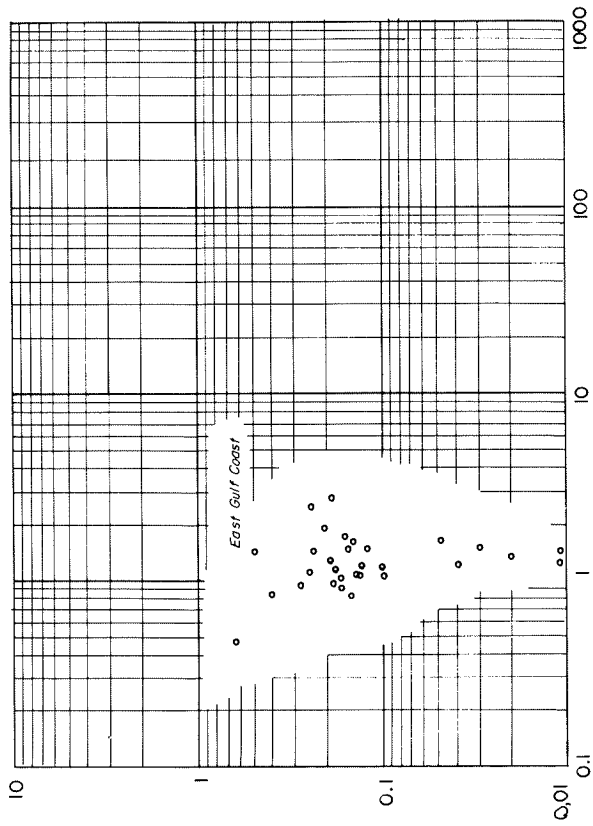


FIGURE 22.—Scatter plot of values for longitudinal resistivity and the coefficient of anisotropy for sections of Paleocene rocks penetrated by wells in the east Gulf Coast area.

REDUCED ANISOTROPY

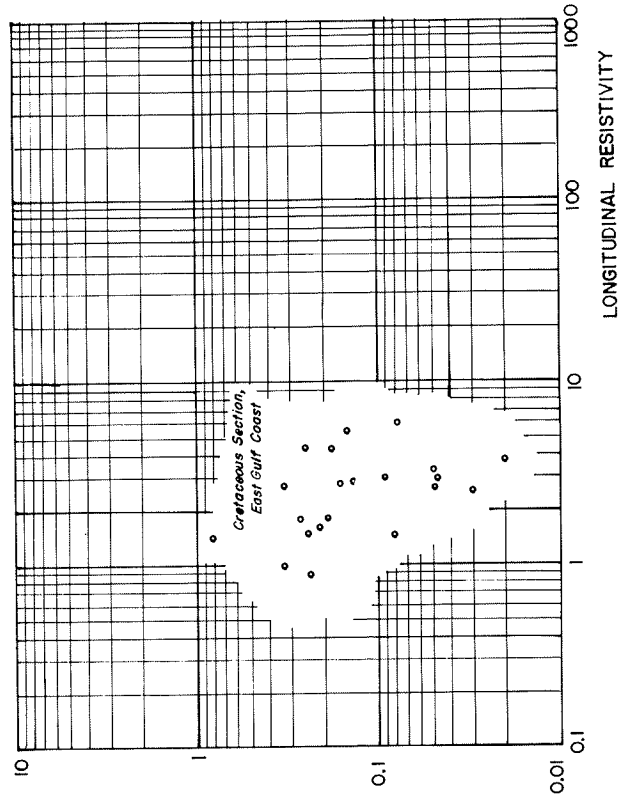


FIGURE 23.—Scatter plot of values for longitudinal resistivity and coefficient of anisotropy for the Cretaceous section penetrated by wells in the east Gulf Coast area. Values for the coefficient of anisotropy have been reduced by subtracting 1 from them.

Jackson (1965, 1967) has described a similar study of electric logs from the Colorado Plateaus area, in the states of Colorado, Utah, New Mexico, and Arizona, with wells at the locations indicated on figure 24. The contours on this map are the elevation of the Precambrian basement, again taken from the Basement Map of North America. As may be seen from these contours, the Colorado Plateaus area is much more complex structurally than the east Gulf Coast area.

According to Jackson (1965), in compiling the average electrical properties for rocks of the sedimentary section on the Colorado Plateaus, it was found that the section could logically be divided into four gross geoelectrical units, though not all four are present over all of the area because of the complex structure. These units are:

1. Sedimentary rocks, predominantly shale and sandstone, of Upper Cretaceous and lower Cenozoic age, which exhibit low resistivity. The most conductive portions of the section are rocks such as the Mancos and Lewis shales. Generally, the sandstone beds in these formations have lower resistivities than sandstone beds in the lower part of the sequence.
2. Sedimentary rocks, primarily sandstones, of Permian to Lower Cretaceous age, which are present nearly everywhere across the Plateaus. These rocks have somewhat higher resistivity than the overlying rocks. Near the southern margin of the Paradox basin, where the evaporite facies of the Cutler Formation is well developed, these rocks may better be grouped with the high resistivity beds just beneath them in the section.
3. In places, the Paradox Formation, of Pennsylvanian age, is sufficiently thick and has such a high resistivity in comparison to beds above and below that it must be considered as a separate electrical unit. Nearly all the evaporite beds in this section have resistivities of a thousand ohm-meters or more.
4. Sedimentary rocks, mainly limestones and dolomites, of Cambrian to Permian age, which have high to very high resistivities. This part of the sedimentary sequence thickens from the east side of the Plateaus towards the west.

The relatively high resistivity of rocks on the Colorado Plateaus makes the determination of average electrical properties less certain than in the case of the east Gulf Coast area. Wherever possible, laterolog or induction electric logs were used in the compilation.

It is interesting to note that the normal sedimentary column on the Colorado Plateaus exhibits the same overall character as that for the east Gulf Coast—the resistivity passes through a minimum with increasing depth from

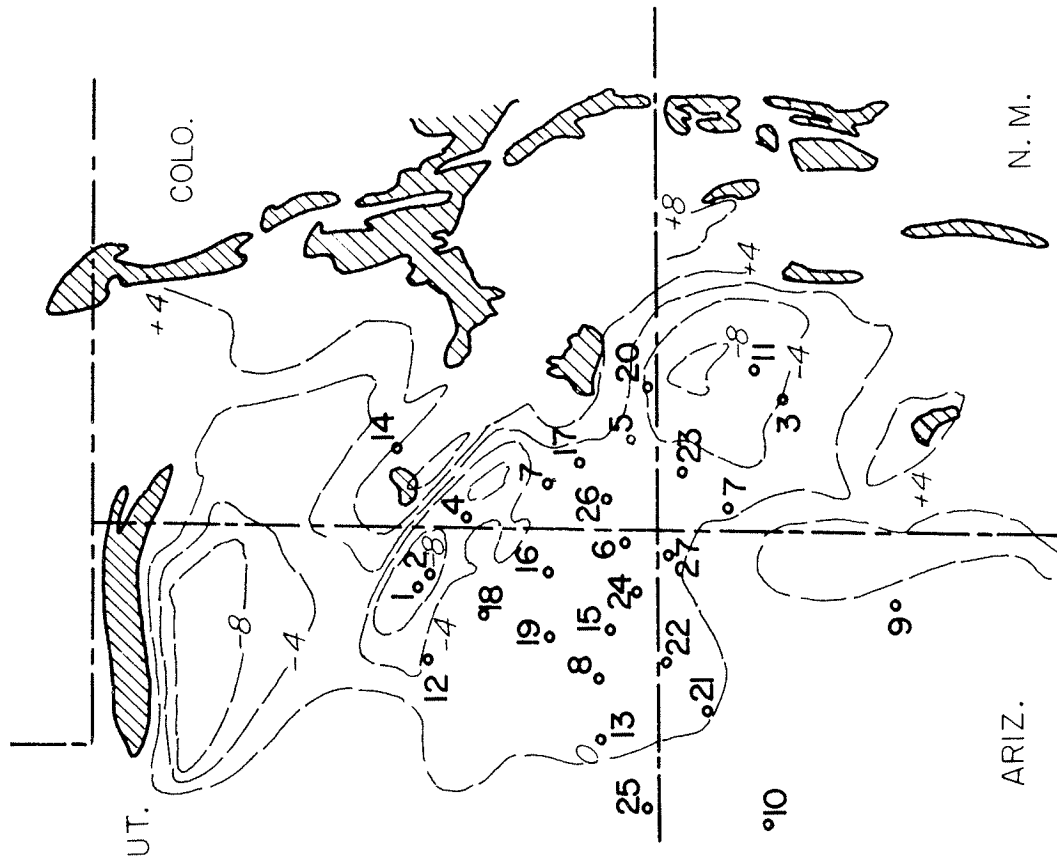


FIGURE 24.—Map of the Four-Corners area in the states of Colorado, Utah, Arizona and New Mexico, with locations of wells for which electric logs were compiled. Contours represent the elevation of the Precambrian basement surface, in thousands of feet from sea-level (taken from USGS Basement Map of the United States). Shaded areas are areas of basement outcrop.

the surface, and then tends to increase continually with depth, if bed to bed variations are ignored. The surface layer of high resistivity is relatively thin on the Colorado Plateaus, and so, the section might be indicated as the sequence of designators M, L₁, L₂ and L₃, defined analogously to those used for the east Gulf Coast area. A summary of formation names and lithology, taken from Eardley (1962), is given in table 5.

TABLE 5. — Formation names from the Colorado Plateaus

Electrical designator	Formation names	Age	Thickness	Lithology
M	Mancos, Mesa Verde, Lewis Shale, Fruitland, Kirtland, Animas	Cretaceous and younger	to 6,000'	shale, sandstone
L ₁	Cutler, Dolores, La Plata, McElmo, Dakota, Monticopi, Shinarump, Clinle, Glen Canyon, San Rafael, Morrison	Permian to Cretaceous	to 4,000'	sandstone, shale, limestone
L ₂	Paradox, Cutler, Kaibab, Coconino	Pennsylvanian to Permian	to 2,000'	limestone, evaporites
L ₃	Hermosa, Cutler, Ignacio, Elbert, Ouray	Cambrian to Permian	to 2,000'	limestones

Compiled resistivities for wells from the Colorado Plateaus province are listed in table 6. Resistivity-anisotropy field plots for these same data are given in figures 25-27 (the L₁ and L₃ data are plotted together on figure 27). It is quite obvious that the sedimentary rocks on the Colorado Plateaus have much higher resistivities and anisotropies than rocks from the east Gulf Coast. This reflects the greater heterogeneity in porosity from bed to bed in the sequence. This heterogeneity may be a consequence of the greater age of the lower part of the section treated for the Colorado Plateaus, with varying degrees of post-depositional cementation resulting in a wide difference in resistivity between the various lithologic elements comprising the section.

TABLE 6. — Average resistivities compiled from electric logs run in wells on the Colorado Plateaus

Index No. of well	Location	Depth interval	Designator	Transverse resistivity	Longitudinal resistivity	Coefficient of anisotropy
1.	Grand County, Utah	310-2,398	M	17.8	11.7	1.10
23.	20S, 21E	2,100-1,123	L ₁	37.9	21.5	1.21
		1,125-1,715	L ₂	1,050.	582.	1.35
2.	Grand County, Utah	310-1,930	M	22.0	13.2	1.29
		1,932-3,370	L ₁	47.1	35.0	1.16
20.	21S, 23E	3,372-3,800	L ₂	1,530.	691.	1.19
3.	McKinley County, N.M.	1,200-2,118	M	14.7	9.10	1.25
		2,150-2,230	—	1,550.	570.	1.65
11.	11N, 8W	2,736-6,206	L ₁	52.5	21.2	1.17
4.	Montrose County, Colo.	1,700-5,100	M	19.7	14.6	1.16
		5,130-11,250	L ₁	112.	81.3	1.32
21.	17N, 19W					
5.	La Plata County, Colo.	980-1,800	M	21.8	15.2	1.20
		6,920-10,025	L ₁	116.	83.2	2.32
17.	31N, 11W					
6.	San Juan County, Utah	255-535		15.2	13.2	1.08
		532-805		51.3	35.2	1.21
7.	40S, 26E	807-3,137	M	25.6	17.9	1.20
		3,127-5,576		25.7	17.9	1.20
		5,528-7,890	L ₂	800.	49.9	4.11
7.	San Juan County, N.M.	420-743		9.7	8.1	1.07
		715-1,330	M	39.8	22.0	1.31
30.	26N, 19W	1,332-3,770		16.2	9.1	1.31
		3,776-7,001	L ₁	135.	41.8	1.80
8.	Garfield County, Utah	1,400-4,505	M	62.3	38.0	1.28
		1,507-6,080		156.	137.	1.07
18.	36S, 10E	6,082-8,360	L ₁	620.	179.	1.86
9.	Navajo County, Ariz.	110-590		25.2	23.6	1.03
		592-1,980	M	35.1	13.9	1.59
6.	19N, 23E	3,022-3,310		39.6	28.4	1.18

TABLE 6 (cont.)

Index No. of well	Location	Depth interval	Designator	Transverse resistivity	Longitudinal resistivity	Coefficient of anisotropy
10.	Coconino County, Ariz.	605-2,370	L ₁	350.	297.	1.09
		2,372-3,090	L ₂	1,100.	610.	1.32
	35, 28N, 1W	3,092-3,522	L ₃	67.	63.	1.03
11.	McKinley County, N.M.	450-1,160		41.3	30.4	1.16
		1,162-2,115	M	21.8	14.2	1.24
	14, 19N, 3W	2,117-7,776		10.6	8.0	1.15
		7,777-8,600	L ₁	43.9	21.2	1.44
		8,602-9,626	L ₂	335.	38.7	2.95
12.	Emery County, Utah	0-1,020	L ₁	145.	120.	1.10
		1,022-3,675	L ₂	1,280.	200.	2.52
	6, 22S, 12E	3,677-4,180	L ₃	89.	68.	1.14
13.	Garfield County, Utah	175-700		6.3	5.7	1.01
		700-1,290		28.1	18.6	1.23
	12, 36S, 1E	1,290-2,350	M	11.6	9.6	1.10
		2,350-4,710		38.3	31.3	1.06
		4,710-5,150		8.1	6.7	1.10
		5,150-5,970		28.6	25.8	1.06
		5,970-6,438		340.	310.	1.01
		6,438-6,828	L ₁	2,850.	2,125.	1.16
		6,828-8,010		95.	68.	1.18
		8,010-8,767		193.	82.	1.55
		8,767-10,098	L ₂	750.	53.	3.76
14.	Delta County, Colo.	100-970		10.0	8.80	1.07
		970-1,202	M	32.0	26.4	1.10
	16, 15S, 95W	1,202-2,025		10.8	9.9	1.12
		2,025-7,841	L ₁	57.3	45.6	1.12
15.	San Juan County, Utah	218-740		50.6	45.4	1.06
		740-1,745	M	414.	382.	1.04
	33, 37S, 15E	1,745-2,195		90.	66.	1.17
		2,195-5,023	L ₁	560.	76.	2.71
16.	San Juan County, Utah	70-835	U	128.	83.	1.24
		835-5,050	M	36.0	18.2	1.41
	8, 31S, 22E	5,050-7,800	L ₂	1,920.	97.	4.50

TABLE 6 (cont.)

Index No. of well	Location	Depth interval	Designator	Transverse resistivity	Longitudinal resistivity	Coefficient of anisotropy
17.	Montezuma County, Colo.	84-1,582		75.8	53.7	1.19
		1,582-4,064	M	54.0	35.2	1.24
	19, 39N, 14W	4,064-5,034		178.	28.0	2.50
		5,034-6,506	L ₁	580.	39.5	3.75
		6,506-8,700	L ₂	3,250.	171.	4.29
18.	San Juan County, Utah	500-2,875	M	21.6	15.7	1.17
		2,875-4,160	L ₁	232.	35.2	2.56
	3, 27S, 19E	4,160-7,000	L ₂	545.	85.5	2.52
		7,000-8,000	L ₃	177.	43.7	2.02
19.	Garfield County, Utah	10-670		78.8	69.6	1.06
		670-1,200	M	245.	199.	1.11
	33, 32S, 15E	1,200-1,770		57.1	49.5	1.07
		1,770-4,955	L ₁	340.	143.	1.54
20.	La Plata County, Colo.	300-1,720		15.2	12.8	1.09
		1,722-2,920	M	49.7	29.2	1.30
	15, 33N, 7W	3,000-6,400		19.2	15.6	1.11
		6,402-13,050	L ₁	163.	31.8	2.27
21.	Coconino County, Ariz.	300-2,935	M	31.4	15.6	1.42
		2,910-5,305	L ₁	98.	64.	1.24
	28, 37N, 11E	5,310-7,210	L ₂	458.	93.	2.22
22.	Navajo County, Ariz.	450-1,310	M	44.2	41.6	1.03
		1,313-2,550	L ₁	200.	81.8	1.57
	12, 41N, 18E	2,553-4,530	L ₂	950.	210.	2.13
23.	San Juan County, N.M.	70-675		6.6	5.2	1.13
		680-930	M	50.1	20.2	1.57
	19, 29N, 16W	935-3,930		8.4	6.4	1.15
		3,935-5,456	L ₁	14.0	11.7	1.09
		5,460-7,456	L ₂	250.	41.6	2.45
24.	San Juan County, Utah	750-3,105	M	14.2	9.8	1.20
		3,170-6,146	L ₁	56.2	30.6	1.36
	36, 41S, 20E	6,150-7,560	L ₃	106.	70.3	1.23

TABLE 6 (cont.)

Index No. of well	Location	Depth interval	Designator	Transverse resistivity	Longitudinal resistivity	Coefficient of anisotropy
25.	Kane County, Utah 2, 43S, 8W	1,820-2,395		40.0	34.7	1.07
		2,400-4,840	M	15.6	8.3	1.37
		4,843-8,500	L ₁	270.	94.	1.69
		8,770-10,060	L ₃	720.	414.	1.32
26.	Montezuma County, Colo. 27, 37N, 17W	1,160-1,470		83.8	77.3	1.04
		1,475-2,650	M	31.8	22.9	1.18
		2,653-4,950	L ₁	88.3	51.5	1.31
		4,953-8,650	L ₂	395.	64.8	2.47
27.	Apache County, Ariz. 12, 40N, 28E	70-1,650		26.2	22.2	1.09
		1,655-2,300	M	6.4	4.5	1.20
		2,305-3,300		22.9	21.0	1.04
		3,303-4,700	L ₁	53.7	13.1	1.29
		4,703-5,750	L ₂	370.	92.5	2.00

Electrical properties of the Paleozoic to Cenozoic section of the Denver basin and High Plains area

The most detailed study to date of averaged electrical resistivities from electric logs is that which has been done for the Denver basin area of eastern Colorado and the surrounding High Plains area of Nebraska and Wyoming. This study consisted of two parts; an initial study in which logs from deep wells, those penetrating the Paleozoic section, were selected from the three-state area, followed by a detailed study of logs from wells in eastern Colorado. The locations for the wells used in the initial study are indicated on the map in figure 28. The contours are elevations of the Precambrian surface, taken from the Basement Map of North America (U.S. Geol. Survey, 1967). The second part of the study was a detailed evaluation of average resistivities from approximately 250 wells located in Townships 1 and 2 North, in eastern Colorado (fig. 29). These wells generally did not penetrate to the Paleozoic section.

Both Jackson (1962) and Harthill (1966, 1967) recognize a series of four units in the section which one might expect to differentiate readily on the basis of average electrical properties:

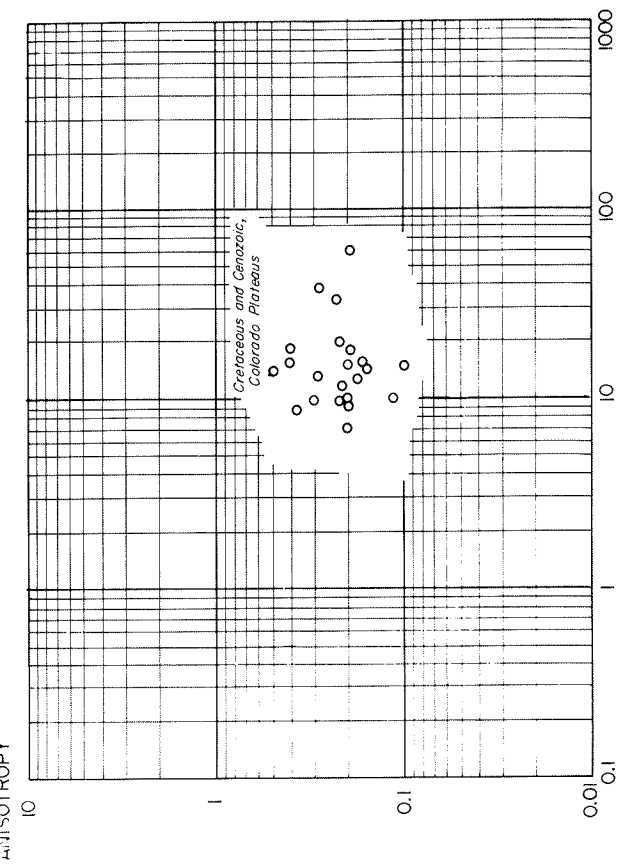


FIGURE 25.—Scatter plot for values of longitudinal resistivity and coefficient of anisotropy for the Cretaceous and Cenozoic sections penetrated by wells on the Colorado Plateaus. The values for the coefficient of anisotropy have had 1 subtracted from them.

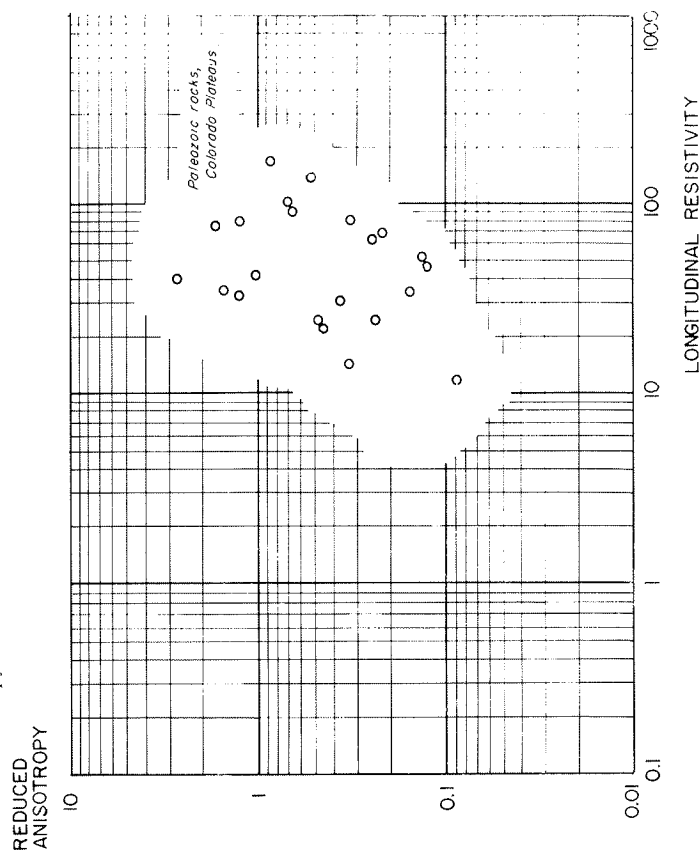


FIGURE 26.—Scatter plot for values of longitudinal resistivity and coefficient of anisotropy for the Paleozoic section (excluding the Paradox Formation) penetrated by wells on the Colorado Plateaus. The values for the coefficient of anisotropy have been reduced by subtracting 1 from them.

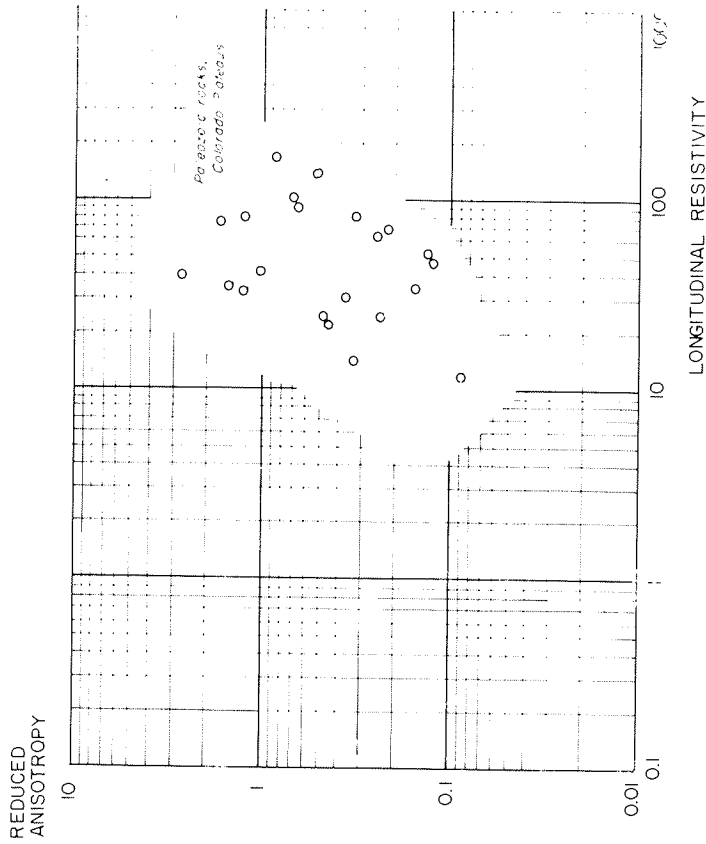


FIGURE 27.—Scatter plot for values of longitudinal resistivity and coefficient of anisotropy for the Paradox Formation where it was penetrated by wells on the Colorado Plateaus. The value for the coefficient of anisotropy has been reduced by subtracting 1.

Layer U (surface layer): The upper rocks are discontinuous and vary significantly in thickness across the area. In the west, along the Front Range in Colorado, this unit consists of the Fox Hills, Laramie, Denver, and Arapahoe formations of Cretaceous age. The Fox Hills and Laramie formations are made up of sandstone beds separated by shales, while the Denver and Arapahoe formations are a heterogeneous mixture of sandstones, claystones, and siltstones. The upper layer is the Ogallala Formation in the eastern part of the region, being an assemblage of continental conglomerates, sandstones, siltstones, claystones, and cementstones. The upper layer varies in thickness from as much as 1,000 feet in the west to as little as 500 feet in the east.

Layer M, the Pierre Shale: This unit is composed mainly of shale and siltstone, the silt being found in the Transition Zone at the top of the formation. The Pierre Formation is remarkably uniform in character over large distances. It thins from about 4,000 feet in the central part of the Denver basin to about 500 feet over the eastern part of the area under consideration.

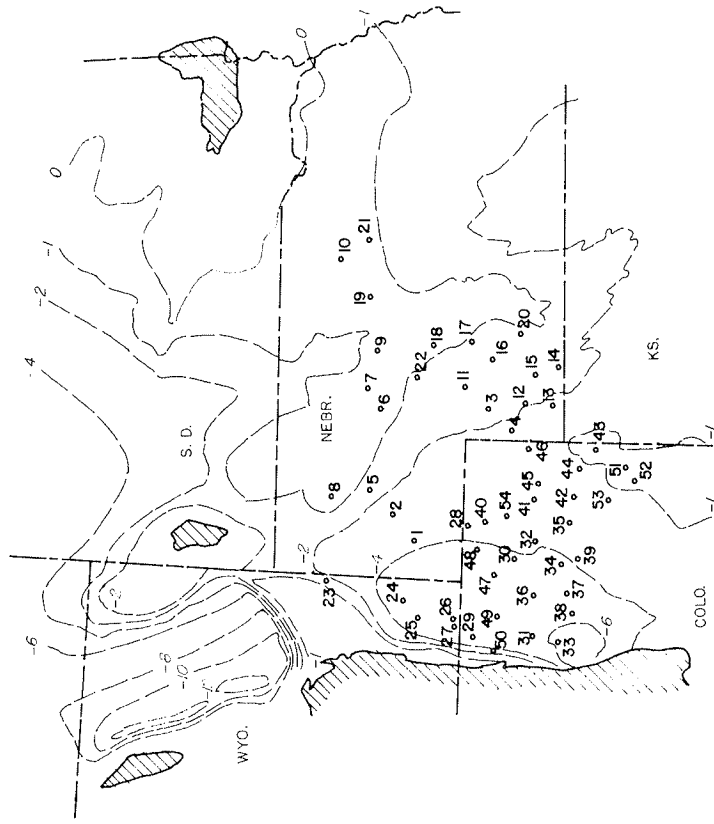


FIGURE 28. Map of the High Plains region showing the locations of wells for which electric logs were compiled. Contours are elevations of the Precambrian surface, in thousands of feet (from the Structural Map of the United States).

The L_1 layer: Beneath the Pierre Formation, the resistivity tends to increase with increasing depth, though this part of the section may generally be divided into an upper and lower part on the basis of resistivity. The layer immediately under the Pierre, the L_1 layer, consists of the Dakota, Benton, and Niobrara formations, of Jurassic to Cretaceous age. The third layer is mixed sandstone, shale and limestone, which despite the heterogeneity of rock types, varies uniformly over the area. The thickness is consistently about 1,100 feet in eastern Colorado but thins to the north and east.

The L_2 layer: The lowermost layer in the sedimentary column includes all beds from the basement surface to the top of the Jurassic Morrison Formation. The beds are mainly of Pennsylvanian, Permian, and Jurassic ages. Relatively few wells have been drilled through the Paleozoic section, but logs from these wells, as well as outcrop information from the edges of the Denver basin in

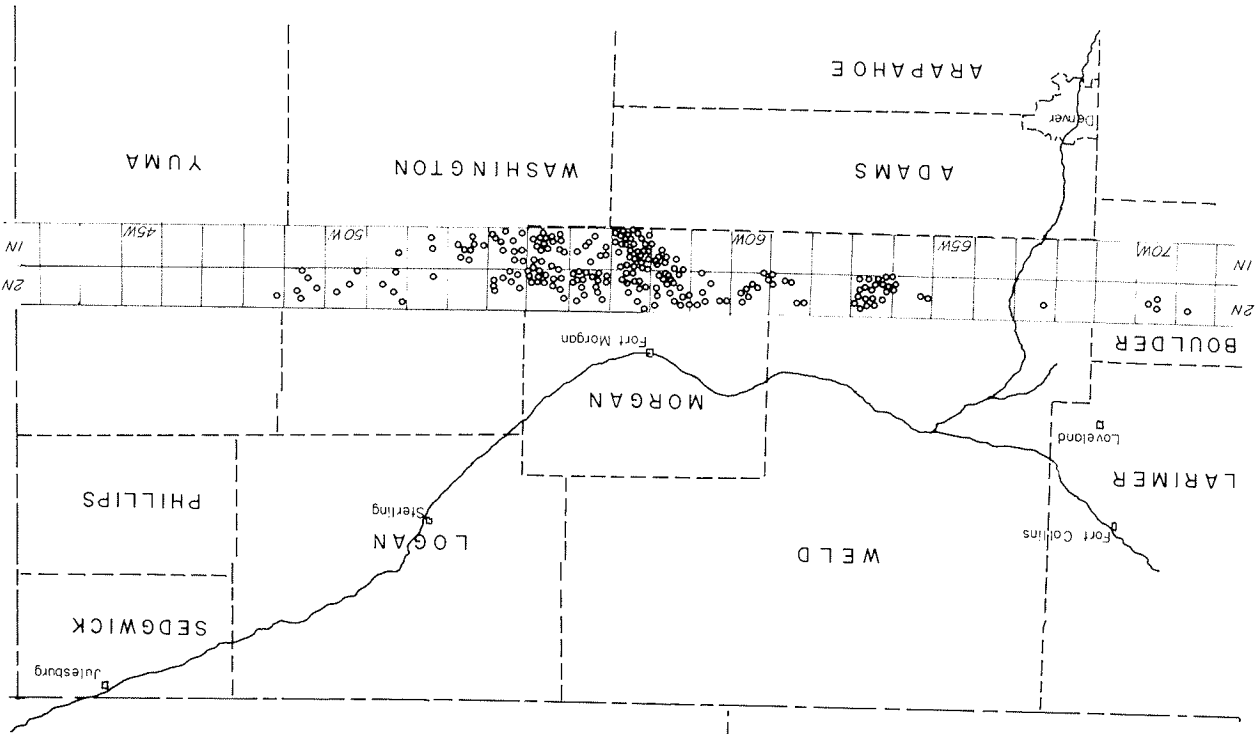


FIGURE 29.—Map of northeastern Colorado, showing the locations of wells in Townships 1 and 2 North, for which electric logs have been compiled.

the west, and outcrops of similar rocks in Kansas and Oklahoma, indicate that the section is mainly composed of claystones and siltstones interbedded with limestones, dolomites, and anhydrites. Wells within the area under consideration indicate that the strata, except for the evaporites, are continuous across the basin. Although the resistivity varies drastically from bed to bed, the layer comprises a uniform electrical unit about 1,000 feet thick.

As in other cases, the section may be divided into a set of geoelectric units in which the resistivity first decreases with depth from the surface, and then increases with depth once a zone of minimum resistivity (the M-layer) is passed. The formation names assigned to the electrical U, M and L layers are summarized in table 7.

TABLE 7.—Formation names from the Denver basin

Electrical designator	Formation names	Age	Thickness	Lithology
U	Fox Hills, Laramie, Denver, Arapahoe, Ogallala	Cretaceous	1,000'	sandstone, shale, siltstone
M	Pierre	Cretaceous	4,000'	shale, siltstone
L ₁	Dakota, Benton, Niobrara	Cretaceous	1,100'	shale, sandstone, limestone
L ₂	Fountain, Lyons, Lykins, Morrison	Carboniferous, Jurassic	1,000'	shale, sandstone, limestone, anhydrite

The average electrical parameters for 51 wells which penetrated at least part of the Paleozoic section are listed in table 8 (from Jackson, 1962). Although the wells are sparsely distributed over the area, and the reliability of individual values for the averaged properties are subject to errors comparable to the change from well to well, it is possible to contour the areal variation in properties for several of the units. The most reliable data are those for the M and L₁ units, primarily because the logs in the U and L₂ units are usually incomplete. Contour maps showing variation in longitudinal resistivity and the coefficient of anisotropy over the High Plains area are given in figures 30 and 31. It is interesting to note that the resistivity tends to increase both to the east and to the west from the center of the area. The minimum resistivities are not found in the center of the Denver basin, however, but considerably to the

east of the center. The change in resistivity away from the center of the area possibly reflects decreases in water salinity near outcrop areas.

TABLE 8. — Resistivities compiled from logs run in wells on the High Plains

Index No. of well	Location	Depth interval	Designator	Transverse resistivity	Longitudinal resistivity of anisotropy
1. Banner County, Nebr. 15, 19N, 53W		675- 895(SN)	U	5.63	5.43
		900- 4,080(SN)	M	2.78	2.62
		4,085- 5,085(SN)	L ₁	6.55	3.81
		5,090- 5,720(LL)	L ₁	6.92	4.27
		5,725- 7,457(LL)	L ₂	94.1	16.3
2. Morrill County, Nebr. 1, 21N, 49W		730- 2,880(SN)		2.05	1.39
		2,885- 4,400(SN)		4.95	2.58
		4,405- 4,590(SN)		4.58	2.47
		4,405- 4,590(LN)		24.5	7.19
3. Perkins County, Nebr. 23, 10N, 39W		4,405- 4,590(LL)		37.5	8.20
		4,590- 6,310(SN)		3.37	2.74
		4,590- 6,310(LL)		3.13	2.68
		450- 2,010(SN)	M	3.30	2.52
		2,015- 3,541(SN)	L ₁	5.72	3.47
4. Chase County, Nebr. 10, 7N, 41W		510- 2,680(LL)	M	2.74	1.83
		2,685- 3,745(LL)	L ₁	4.13	2.75
		3,750- 5,550(LL)	L ₂	56.2	5.04
5. Garden County, Nebr. 12, 22N, 46W		1,220- 2,346(SN)	M	2.05	1.97
		2,350- 3,710(SN)	L ₁	3.41	2.09
		4,112- 5,650(LL)	L ₂	291.	12.3
6. Grant County, Nebr. 1, 23N, 38W		1,160- 1,936(SN)	M	7.15	4.82
		1,940- 3,356(SN)	L ₁	12.1	8.54
		3,360- 4,080(SN)	L ₂	51.2	16.2
7. Cherry County, Nebr. 23, 25N, 35W		640- 1,486(SN)	M	5.50	4.22
		1,490- 3,070(SN)	L ₁	7.86	4.76
		3,075- 3,781(LL)	L ₂	28.7	2.21
		3,785- 4,681(LL)	L ₂	158.	2.56

TABLE 8 (Cont.)

Index No. of well	Location	Depth interval	Designator	Transverse resistivity	Longitudinal resistivity of anisotropy
8. Sheridan County, Nebr. 17, 26N, 46W		1,750- 2,370(SN)	M	6.94	5.14
		2,375- 3,621(SN)	L ₁	10.4	8.04
		3,625- 4,245(SN)	L ₂	61.0	9.15
9. Hooker County, Nebr. 5, 23N, 31 W		1,270- 1,930(SN)	M	6.01	3.30
		1,935- 3,365(SN)	L ₁	10.4	6.15
		3,370- 3,960(LL)	L ₂	57.7	15.1
10. Brown County, Nebr. 13, 26N, 22W		160- 1,141(SN)	M	9.64	4.88
		1,612- 2,110(SN)	L ₁	11.9	6.92
11. Lincoln County, Nebr. 8, 12N, 34W		730- 1,160(SN)	U	5.10	4.95
		1,165- 1,700(SN)	M	2.38	2.22
		1,705- 3,565(SN)	L ₁	5.98	4.23
		3,570- 4,710(SN)	L ₂	16.5	5.14
12. Chase County, Nebr. 9, 6N, 37W		560- 900(SN)	U	5.45	5.29
		905- 2,300(SN)	M	3.09	2.83
		2,305- 3,400(SN)	L ₁	5.15	3.57
		3,402- 5,165(SN)	L ₂	12.5	6.18
13. Dundy County, Nebr. 33, 2N, 37W		150- 1,640(SN)	M	2.85	2.30
		1,645- 2,870(SN)	L ₁	6.82	3.64
		2,875- 5,090(SN)	L ₂	19.3	7.01
14. Hitchcock County, Nebr. 26, 1N, 33W		190- 1,340(SN)	M	3.40	3.18
		1,345- 2,550(SN)	L ₁	4.84	3.13
		2,554- 4,648(SN)	L ₂	14.0	5.84
15. Hitchcock County, Nebr. 23, 4N, 33W		160- 1,330(SN)	M	2.22	1.85
		1,335- 2,530(SN)	L ₁	4.56	3.29
		2,535- 4,420(SN)	L ₂	10.2	3.80
16. Lincoln County, Nebr. 2, 9N, 32W		450- 700(SN)	U	8.89	7.40
		705- 1,875(SN)	M	3.81	3.38
		1,880- 4,396(SN)	L ₁	16.4	5.11

TABLE 8 (Cont.)

Index No. of well	Location	Depth interval	Designator	Transverse resistivity	Longitudinal resistivity	Coefficient of anisotropy
17. Lincoln County, Nebr.		675-1,020(LN)	M	4.59	3.97	1.08
25, 12N, 30W		1,025-3,960(SN)	L ₁	13.0	6.25	1.44
18. Logan County, Nebr.		650-750(SN)	U	16.9	15.4	1.05
36, 18N, 28W		750-1,130(SN)	M	3.95	3.48	1.06
		1,135-1,575(SN)	L ₁	9.74	5.61	1.32
		1,580-3,750(SN)	L ₁	9.90	5.95	1.29
19. Blaine County, Nebr.		146-804(SN)	U	29.5	14.1	1.45
23, 24N, 27W		810-1,265(SN)	M	4.38	3.82	1.07
		1,290-3,510(SN)	L ₁	28.7	10.4	1.66
20. Frontier County, Nebr.		510-994(SN)	U	13.2	13.0	1.01
21, 5N, 29W		1,000-3,874(SN)	M	10.0	4.68	1.46
21. Blaine County, Nebr.		90-740(SN)	U	39.3	25.6	1.24
22, 24N, 21W		745-1,240(SN)	M	4.56	3.88	1.08
		1,260-2,720(SN)	L ₁	17.8	11.2	1.26
		2,722-3,360(SN)	L ₂	53.5	17.9	1.81
22. McPherson County, Nebr.		980-1,450(SN)	M	3.19	2.29	1.18
25, 19N, 33W		1,465-4,350(SN)	L ₁	9.72	4.41	1.48
23. Goshen County, Wyo.		1,000-3,150(SN)	M	2.32	2.11	1.05
32, 30N, 60W		3,155-4,300(SN)	L ₁	6.10	4.78	1.13
		4,305-5,200(SN)	L ₂	20.7	13.0	1.26
		5,205-7,020(SN)	L ₂	129.	50.8	1.60
24. Goshen County, Wyo.		200-2,150(SN)	U	9.40	6.10	1.24
10, 20N, 64W		2,155-7,945(SN)	M	5.04	4.10	1.10
		7,947-9,020(SN)	L ₁	10.3	6.48	1.26
25. Laramie County, Wyo.		500-1,640(SN)	U	8.72	5.21	1.29
15, 19N, 67W		1,645-8,275(SN)	M	5.06	4.01	1.12

TABLE 8 (Cont.)

Index No. of well	Location	Depth interval	Designator	Transverse resistivity	Longitudinal resistivity	Coefficient of anisotropy
26. Laramie County, Wyo.		525-2,515(SN)	U	7.60	6.52	1.08
12, 13N, 68W		2,520-8,660(SN)	M	4.06	2.95	1.17
		8,665-10,300(SN)	L ₁	7.65	5.84	1.14
27. Laramie County, Wyo.		1,900-3,995(SN)	M	4.02	3.72	1.01
13, 13N, 68W		3,952-4,370(SN)	M	16.5	14.3	1.08
		4,375-7,550(SN)	M	3.77	3.16	1.09
		7,552-8,755(SN)	L ₁	10.7	6.07	1.33
28. Logan County, Colo.		620-1,160(SN)	U	6.23	5.99	1.02
26, 11N, 53W		1,165-4,150(SN)	M	2.03	1.82	1.05
		4,155-6,161(SN)	L ₁	7.18	4.33	1.28
		6,165-8,111(LL)	L ₂	301.	8.20	6.05
29. Weld County, Colo.		515-2,191(SN)	U	10.5	8.39	1.11
5, 11N, 66W		2,195-8,731(SN)	M	5.26	3.92	1.16
		8,735-11,067(SN)	L ₁	16.8	10.0	1.30
30. Morgan County, Colo.		400-1,320(SN)	U	6.92	6.58	1.02
10, 6N, 57W		1,325-5,101(SN)	M	2.82	2.30	1.10
		5,105-6,891(SN)	L ₁	10.5	5.74	1.35
		6,895-7,205(SN)	L ₂	14.2	7.24	1.39
31. Weld County, Colo.		960-1,470(SN)	U	6.62	5.79	1.08
20, 5N, 66W		1,475-7,071(SN)	M	4.03	3.43	1.08
		7,075-8,841(SN)	L ₁	20.7	11.4	1.35
		8,845-9,503(SN)	L ₂	68.5	33.8	1.42
32. Morgan County, Colo.		360-4,176(SN)	M	1.84	1.56	1.13
32, 3N, 55W		4,180-5,220(SN)	L ₁	4.61	3.75	1.10
		5,223-5,901(LL)	L ₁	6.77	2.39	1.68
		5,905-8,451(LL)	L ₂	324.	10.0	5.67
33. Weld County, Colo.		980-1,720(SN)	U	7.07	6.51	1.04
8, 2N, 67W		1,725-7,235(SN)	M	5.93	5.30	1.05
		7,240-8,921(SN)	L ₁	17.9	13.2	1.16
		8,912-9,210(SN)	L ₂	30.0	15.8	1.38

TABLE 3 (Cont.)

Index No. of well	Location	Depth interval	Designator	Transverse resistivity	Longitudinal resistivity	Coefficient of anisotropy
34. Morgan County, Colo.	14, 1N, 59W	420-1,600 (SN)	U	4.53	4.22	1.01
		1,605-5,351 (SN)	M	1.45	1.20	1.10
		5,355-7,265 (SN)	L ₁	6.77	4.33	1.25
		7,270-7,866 (SN)	L ₂	20.1	10.3	1.38
35. Washington County, Colo.	7, 2S, 52W	505-1,101 (SN)	U	4.72	4.34	1.04
		1,105-3,585 (SN)	M	2.15	1.96	1.04
		3,590-5,286 (SN)	L ₁	7.88	3.04	1.60
		5,290-8,000 (SN)	L ₂	29.9	2.28	3.60
36. Weld County, Colo.	21, 4N, 63W	450-6,510 (SN)	M	3.89	3.39	1.07
		6,515-8,221 (SN)	L ₁	19.2	10.8	1.33
		8,222-8,600 (SN)	L ₂	38.4	21.4	1.34
		500-960 (SN)	U	6.71	4.75	1.19
37. Adams County, Colo.	14, 2S, 62W	960-6,231 (SN)	M	2.61	2.33	1.06
		6,235-8,141 (SN)	L ₁	8.90	5.55	1.27
		8,142-8,500 (SN)	L ₂	15.8	8.70	1.35
		230-1,720 (SN)	U	5.59	4.21	1.15
38. Adams County, Colo.	17, 2S, 65W	1,725-7,495 (SN)	M	3.30	2.98	1.05
		7,500-9,280 (SN)	L ₁	18.4	11.2	1.27
		9,285-9,475 (SN)	L ₂	50.6	29.0	1.32
		480-5,270 (SN)	M	2.65	2.38	1.06
39. Adams County, Colo.	24, 3S, 59W	5,275-7,135 (SN)	L ₁	7.15	4.43	1.26
		7,142-7,380 (SN)	L ₂	28.8	15.9	1.34
		7,420-7,512 (SN)	L ₂	11.6	9.46	1.11
		400-840 (SN)	U	5.91	5.58	1.03
40. Logan County, Colo.	23, 10N, 53W	845-3,955 (SN)	M	2.11	1.52	1.17
		3,970-6,110 (SN)	L ₁	5.82	2.92	1.40
		6,110-7,636 (LL)	L ₂	561.	11.9	6.85
		1,140-2,970 (SN)	M	1.53	1.34	1.07
41. Yuma County, Colo.	24, 4N, 48W	2,975-3,745 (SN)	L ₁	3.33	2.24	1.22
		3,750-5,036 (LL)	L ₂	40.3	3.01	3.66
		5,040-6,678 (LL)	L ₂	50.3	9.69	2.28
		1,140-2,970 (SN)	M	1.53	1.34	1.07

TABLE 3 (Cont.)

Index No. of well	Location	Depth interval	Designator	Transverse resistivity	Longitudinal resistivity	Coefficient of anisotropy	
42. Yuma County, Colo.		900-2,510 (SN)	M	2.35	2.03	1.06	
		2,515-4,245 (SN)	L ₁	25.5	5.15	2.20	
		4,250-6,550 (LL)	L ₂	180.	14.5	3.52	
		250-1,590 (SN)	M	1.40	1.25	1.06	
43. Yuma County, Colo.	17, 3S, 42W	1,595-3,151 (SN)	L ₁	2.54	1.78	1.20	
		3,155-5,551 (SN)	L ₂	12.3	3.36	1.91	
		505-2,315 (SN)	M	2.10	1.50	1.26	
		2,320-4,300 (SN)	L ₁	10.0	3.32	1.74	
44. Yuma County, Colo.	18, 1S, 45W	1,305-6,007 (SN)	L ₂	35.2	15.3	1.51	
		920-2,576 (SN)	M	2.17	1.89	1.07	
		2,580-6,380 (SN)	L ₁	6.60	3.68	1.34	
		31, 4N, 46W					
46. Yuma County, Colo.	1, 4N, 43W	970-2,105 (SN)	M	2.53	2.11	1.02	
		2,110-2,800 (SN)	L ₁	5.73	4.36	1.15	
		2,900-3,650 (LL)	L ₁	3.19	2.46	1.19	
		3,655-5,751 (LL)	L ₂	33.3	5.71	2.11	
47. Weld County, Colo.	19, 8N, 61W	590-1,886 (SN)	U	5.32	4.42	1.10	
		1,890-6,510 (SN)	M	3.17	2.61	1.15	
		6,515-8,243 (LL)	L ₁	13.9	6.21	1.50	
		8,244-10,228 (LL)	L ₂	268.	19.8	3.68	
48. Weld County, Colo.	18, 10N, 56W	488-1,380 (SN)	U	5.39	5.15	1.02	
		1,385-5,121 (SN)	M	2.10	1.78	1.08	
		5,125-6,001 (SN)	L ₁	9.84	6.17	1.26	
		6,005-8,807 (SN)	L ₂	35.7	12.8	1.67	
49. Weld County, Colo.	27, 8N, 66W	1,015-1,691 (LL)	U	7.22	6.92	1.02	
		1,695-7,101 (LL)	M	5.51	4.88	1.06	
		7,105-8,905 (LL)	L ₁	30.8	15.1	1.42	
		8,910-10,616 (LL)	L ₂	1,480.	38.8	6.18	
50. Larimer County, Colo.		1,015-1,775 (SN)	U	10.2	8.53	1.09	
		1,780-3,610 (SN)	M	5.35	5.05	1.03	

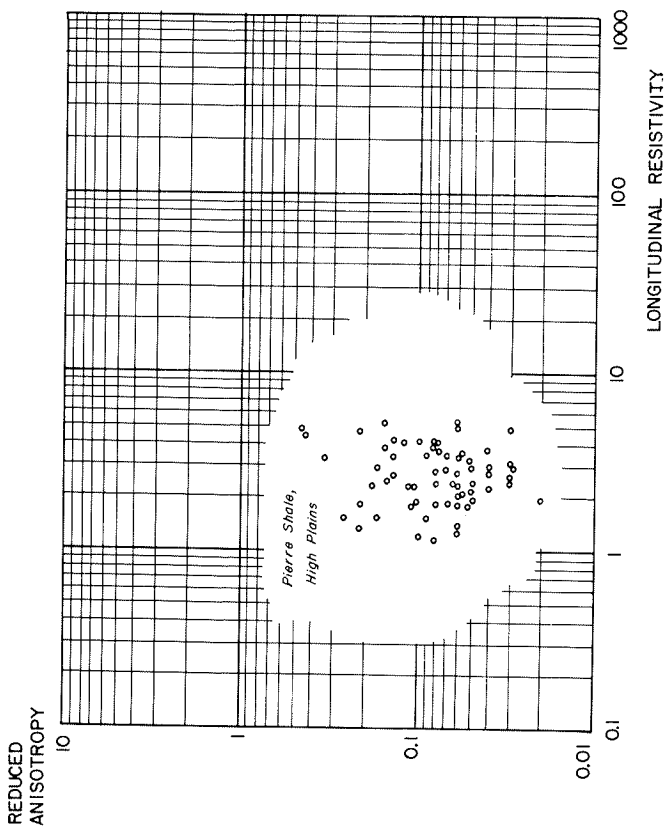


FIGURE 32.—Scatter plot of values for longitudinal resistivity and the coefficient of anisotropy for sections of Pierre Shale penetrated by wells in the High Plains area.

The detailed studies show clearly the trend from higher resistivities along the Front Range to lower resistivities east of the center of the Denver basin, and a reversal in the trend still further east. It is interesting to note that the data for the lower unit, consisting of shale, sandstone and limestone beds, show considerably more scatter than do the data for the overlying Pierre Shale. The average scatter in resistivity values for the Pierre Shale is approximately ± 7 percent about a trend line, while the average scatter in the underlying unit is ± 25 percent, nearly 4 times greater. In part this may be caused by a difference in the number of values sampled from the logs for the two electrical units, inasmuch as samples were read from the logs at intervals of 10 feet, providing 100 to 500 values in the Pierre Shale and 90 to 120 values in the Dakota to Niobrara interval. The statistical reliability of an average computed from a large number of samples varies as the square root of the number of samples. Therefore, if the scatter in the two cases reflected only variations caused by sampling, the averages for the Dakota-to-Niobrara sections would be expected to show about twice the scatter of the averages for the Pierre section. Because the scatter is considerably more than twice as great, the higher degree of

scatter for longitudinal resistivity in the Dakota-to-Niobrara section most probably reflects a greater real variability in resistivity from bed to bed. This in turn should contribute a higher coefficient of anisotropy in the Dakota to Niobrara section than in the Pierre Shale, and this appears to be the case.

Values for the coefficient of anisotropy in the Pierre Shale also show considerably less scatter than do the values for the Dakota to Niobrara section. An interesting feature of these data is the well-defined maximum in values for the Pierre Shale in the area of Ranges 52-53 West. A similar maximum is noted also in the data from Tier 1 North, and possibly may be present in

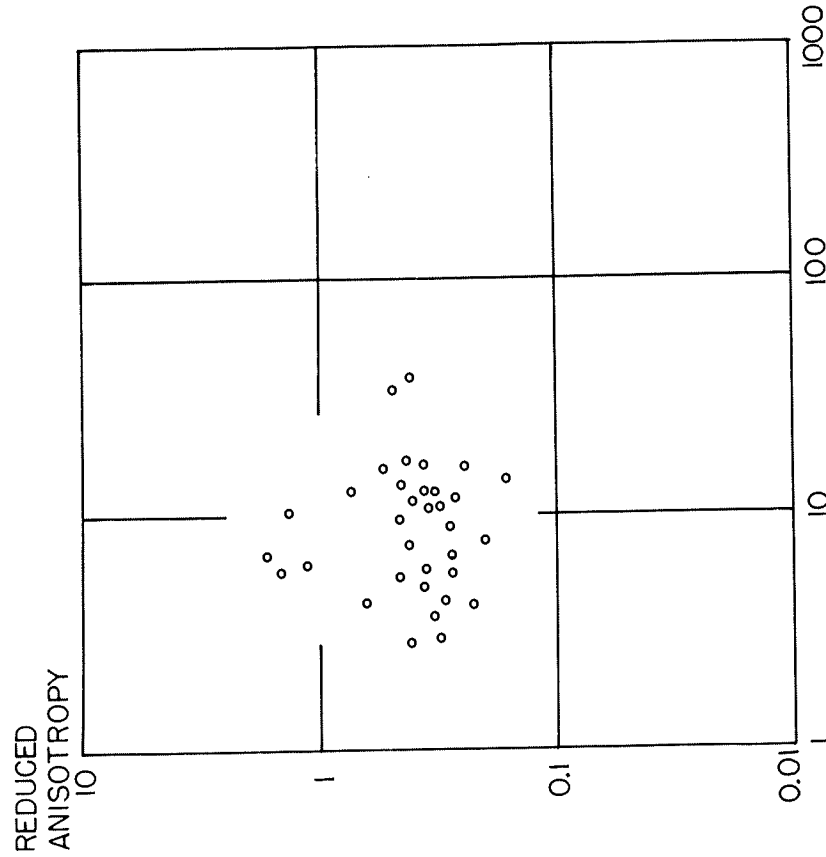


FIGURE 33.—Scatter plot of values for longitudinal resistivity, and coefficient of anisotropy for the Jurassic-Cretaceous section from the Dakota to the Benton formations for wells in the High Plains area.

FIGURE 33.—Scatter plot of values for longitudinal resistivity, and coefficient of anisotropy for the Jurassic-Cretaceous section from the Dakota to the Benton formations for wells in the High Plains area.

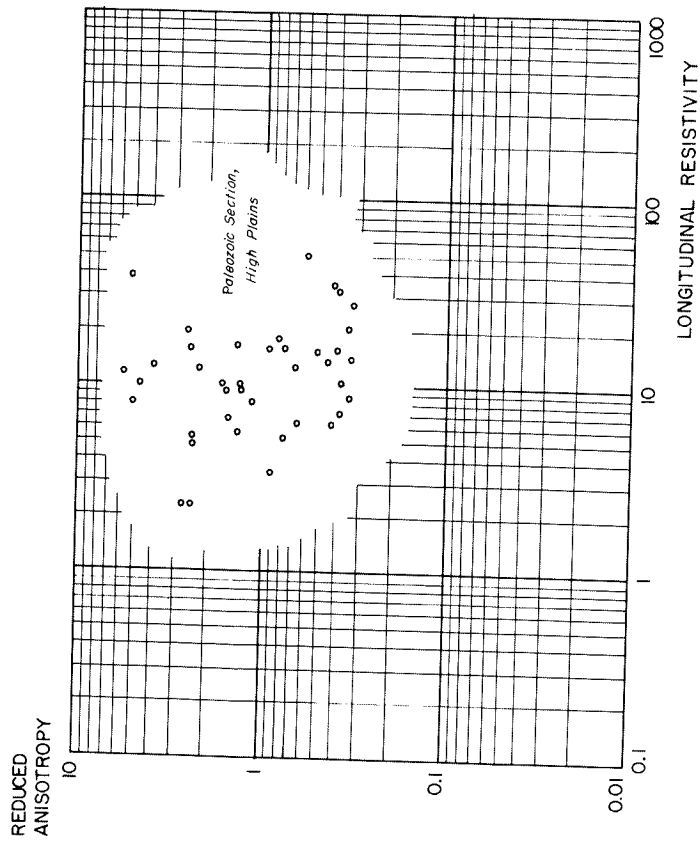


FIGURE 34.—Scatter plot of values for longitudinal resistivity and coefficient of anisotropy for sections of Paleozoic rock penetrated by wells in the High Plains area.

the data for the Dakota to Niobrara sections also. This maximum apparently reflects a trend line along which the Jurassic and Cretaceous beds contain a higher than normal proportion of sandstone beds.

The behavior of the electrical properties for the Pierre Shale may be better understood by considering typical resistivity probability density curves for typical wells along the strip under consideration (fig. 37). As one goes east (towards lower Range numbers), the probability density curves have progressively higher peaks at lower resistivities. The higher the peak of a distribution curve, the lower will be the coefficient of anisotropy. Thus, it appears that the Pierre becomes more uniform and more conductive to the east.

The anisotropy-resistivity field plots for data from Tier 2 North show considerably less scatter than do similar plots for the entire High Plains area (see figs. 38 and 39). This suggests that the large scatter shown by the other such pattern plots represents a real variation of electric properties over large areas and not errors in compilation.

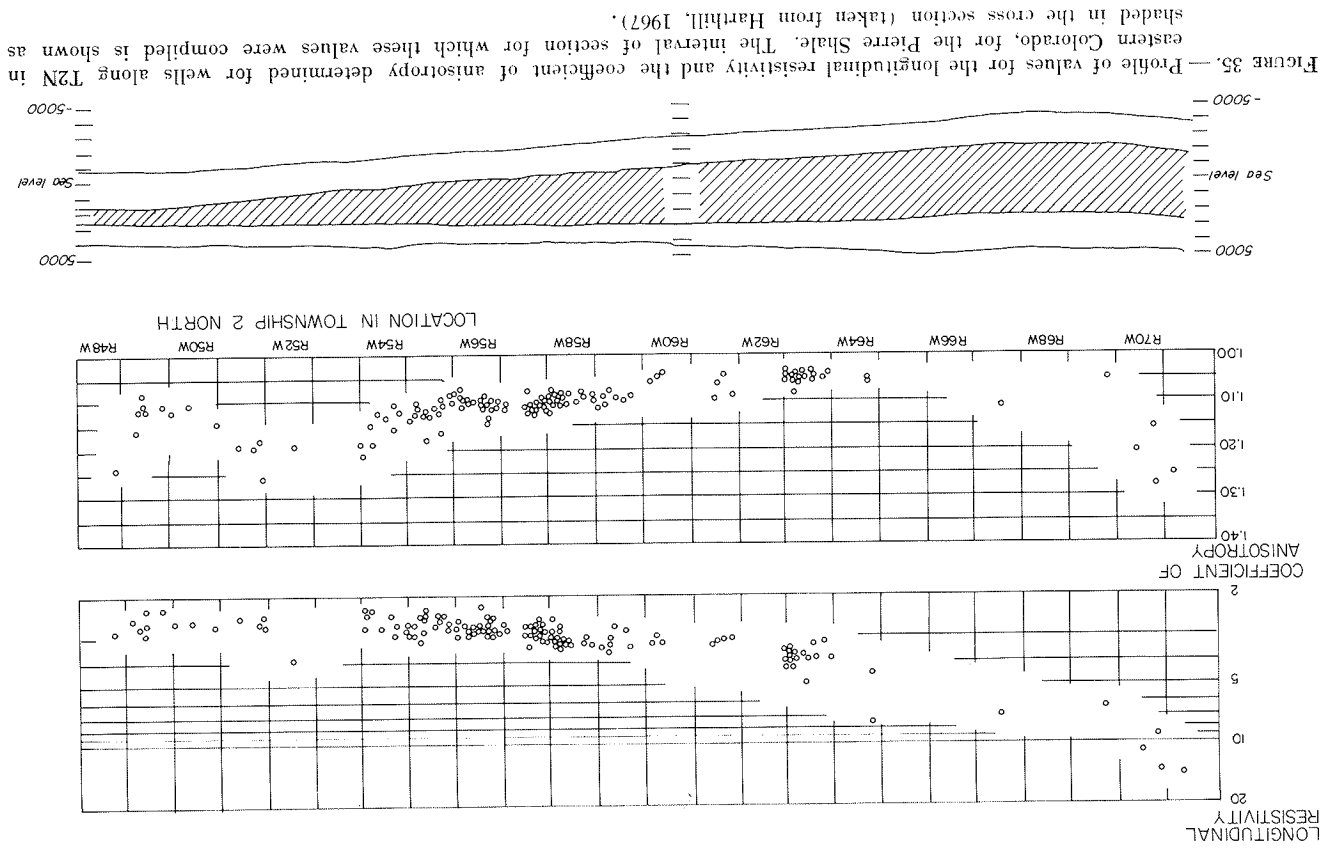


FIGURE 35.—Profile of values for the longitudinal resistivity and the coefficient of anisotropy determined for wells along T2N in eastern Colorado, for the Pierre Shale. The interval of section for which these values were compiled is shown as shaded in the cross section (taken from Hartill, 1967).

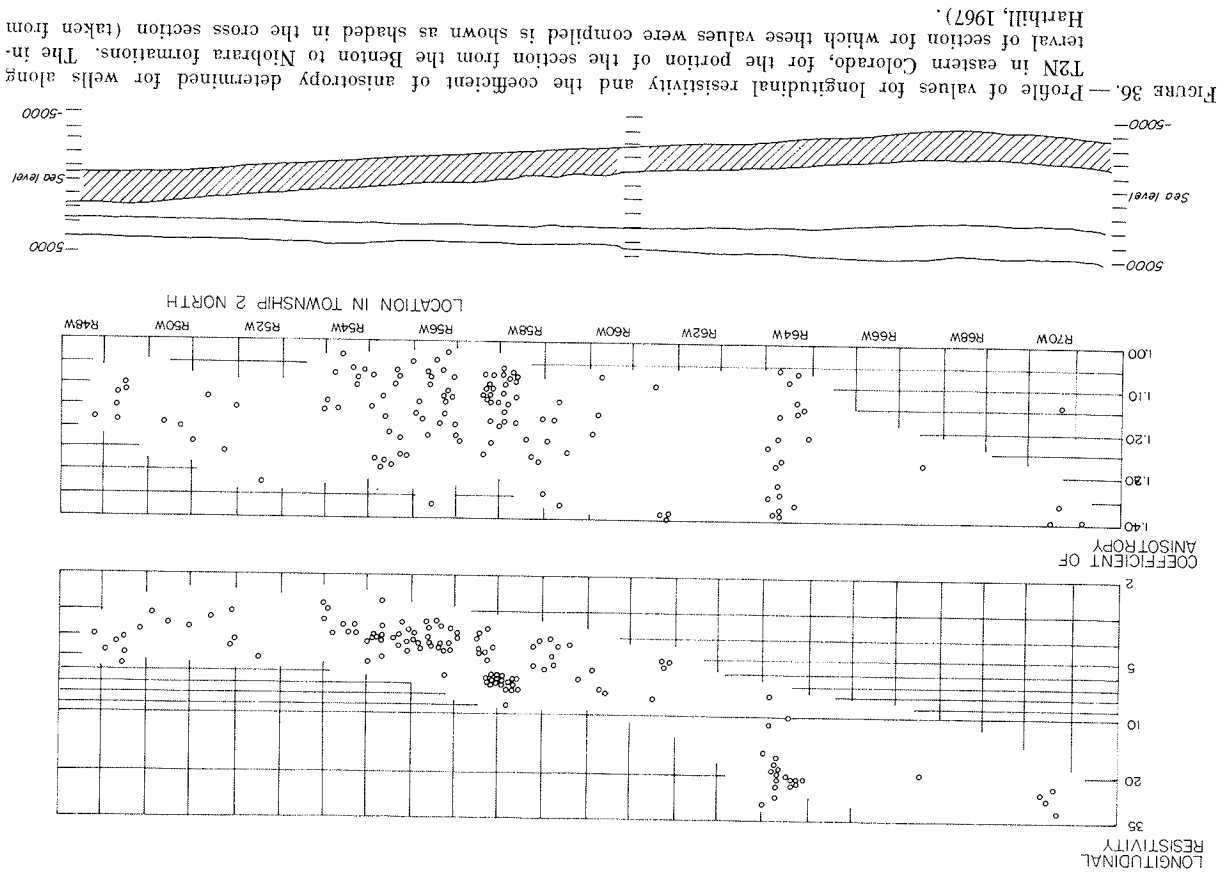


FIGURE 36.—Profile of values for longitudinal resistivity and the coefficient of anisotropy determined for wells along T2N in eastern Colorado, for the portion of the section from the Benton to Niobrara formations. The interval of section for which these values were compiled is shown as shaded in the cross section (taken from Harthill, 1967).

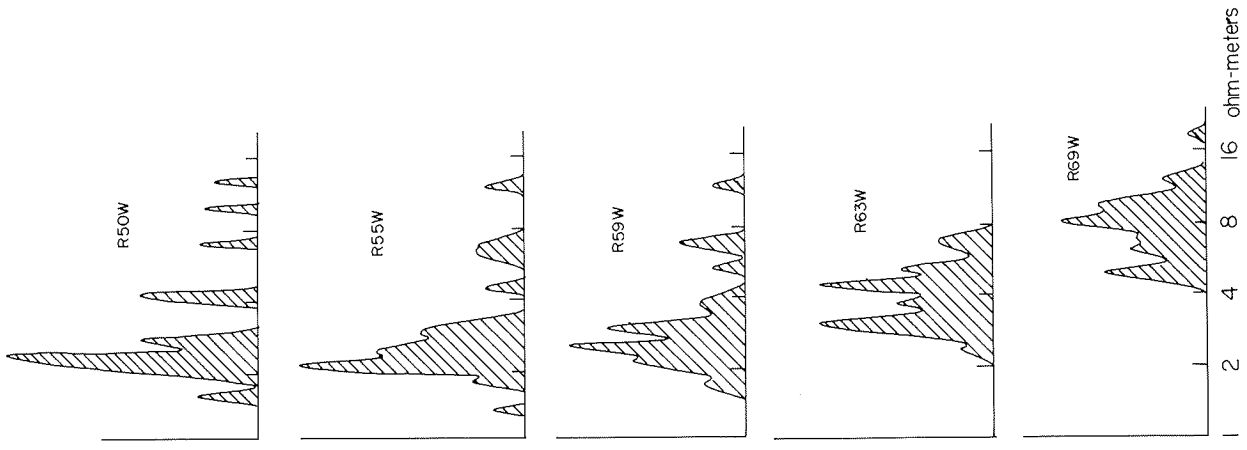


FIGURE 37.—Typical resistivity probability density curves for the Pierre Shale at locations in Township 2 North, in eastern Colorado.

Electrical properties of other rock sequences

In addition to the detailed studies made of electric log resistivities in these three areas—the east Gulf Coast, the Colorado Plateaus, and the High Plains—a few scattered compilations of resistivities have been made, covering other types of rock sequences. Anderson (1965) has compiled average resistivities from logs run in eight deep wells in Pennsylvania, at the locations indicated on the map in figure 40. The sections logged were mainly of Paleozoic age, consisting of Cambrian to Pennsylvanian shale and limestone beds. The compiled resistivities and anisotropies for these eight wells are listed in table 9. It may be noted that, while the resistivities are very high, the coefficients of anisotropy are low to moderate.

TABLE 9. — *Resistivities compiled from logs run in deep wells in Pennsylvania*

Location	Depth interval	Transverse resistivity	Longitudinal resistivity	Coefficient of anisotropy
1. Sullivan County	3,070- 8,050	190.	151.	1.12
	8,100- 8,400	4.41	2.83	1.25
	8,470-12,310	205.	72.3	1.68
2. Indiana County	1,380- 6,460	39.5	32.7	1.12
	6,500- 8,190	72.0	56.8	1.12
3. Indiana County	1,400- 6,570	39.1	31.1	1.12
	6,600- 8,760	44.8	38.5	1.11
4. Indiana County	2,020- 6,620	41.2	31.4	1.14
5. Cameron County	910- 4,620	65.3	50.2	1.14
	4,630- 5,850	204.	154.	1.15
6. Mercer County	4,880- 6,510	170.	139.	1.10
	6,570- 7,360	1,800.	1,490.	1.11
	7,370- 8,200	606.	303.	1.42
7. Fayette County	1,800- 3,570	28.1	22.6	1.11
	3,600- 9,060	73.7	63.6	1.07
8. Fayette County	1,300- 3,090	44.2	37.6	1.09
	3,100- 8,000	79.1	65.7	1.09

Keller (1960) has reported resistivity values from 11 drill holes which penetrate Paleozoic carbonate rocks in the zinc-mining district in eastern Tennessee. The rocks penetrated by the holes were of the Knox group, of Cambrian or Ordovician age, being almost entirely limestone and dolomite beds. The logged section was about 1,000 feet thick, and the 11 holes provided the following average values for electrical properties:

Transverse resistivity	12,700	Longitudinal resistivity	11,300	Coefficient of anisotropy	1.07
------------------------	--------	--------------------------	--------	---------------------------	------

A few data have been reported for non-sedimentary rocks but the data are sparse. It appears reasonable to assume, though, that igneous and metamorphic rocks will have high resistivities, but relatively moderate anisotropies, inasmuch as the conduction in such rocks is controlled largely by joint patterns which tend to be rather uniformly distributed in preferred directions. Volcanic rocks, which tend to be porous and have a layered structure, might be expected to have a moderately high anisotropy.

All of the foregoing plots of anisotropy and longitudinal resistivity might be combined on a common graph to provide a generalized approach to summarizing the electrical properties of layered rocks. Such a plot is shown in figure 41. This generalized plot should provide us with the information we need in discussing the application of surface-based electrical prospecting methods in petroleum exploration.

ELECTRICAL PROPERTIES OF THE WEATHERED LAYER

In the application of surface-based electrical prospecting methods, the electrical properties of the weathered layer at the earth's surface are of particular importance, inasmuch as this is the material closest to the equipment, and it exerts a particularly large effect on the results. No detailed studies of the electrical properties of the weathered layer have been reported, but in 1954, the National Bureau of Standards published a catalog of 7,237 values of earth conductivity determined from radio-wave intensity patterns about 621 broadcast stations in the 540 to 1,600 kilohertz frequency range. Radiowaves in this frequency range penetrate the earth to some tens or hundreds of feet, so that the conductivity seen by the radiowaves is largely that of the surficial weathered zone. The skin depth for radiowaves in the broadcast spectrum is shown as a function of earth conductivity for an assumed uniform earth in figure 41.

The Federal Communications Commission requires that radio broadcasting stations submit measurements of the intensity of their broadcast field as a

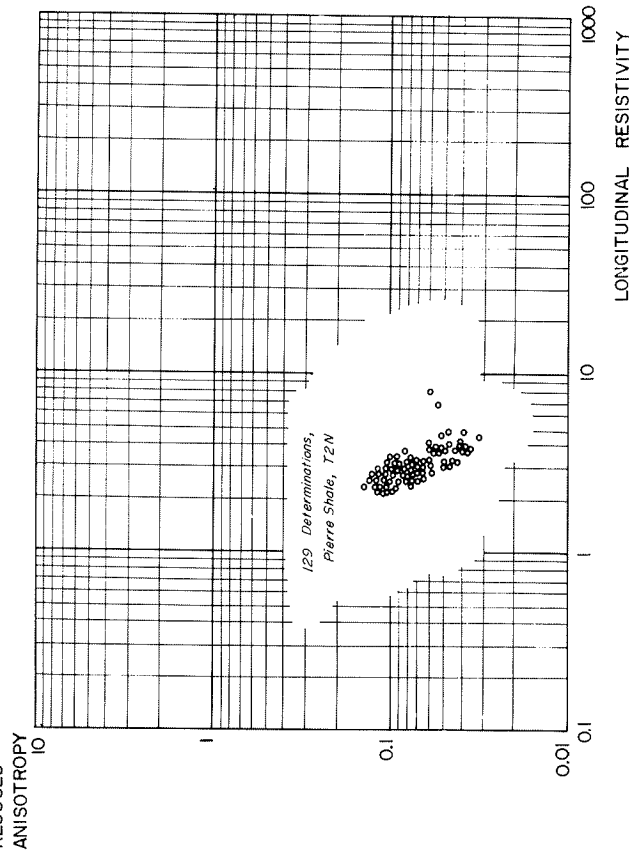


FIGURE 38.—Scatter plot of values for longitudinal resistivity and coefficient of anisotropy for the Pierre Shale, compiled from electric logs from wells in Township 2 North in eastern Colorado.

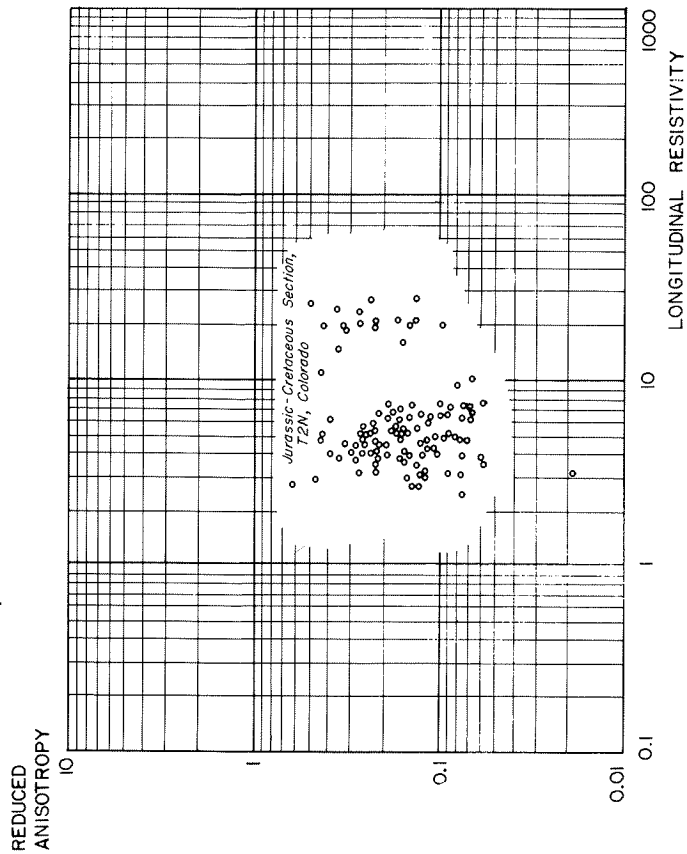


FIGURE 39.—Scatter plot of values for longitudinal resistivity and coefficient of anisotropy for the Jurassic-Cretaceous section from the Dakota to the Benton formations for wells in the strip in Township 2 North, in eastern Colorado.

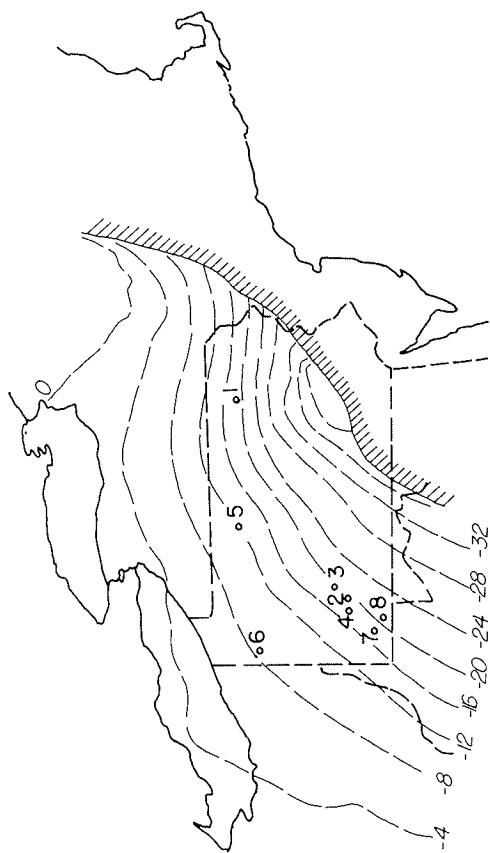


FIGURE 40.—Locations of wells in Pennsylvania for which electric logs were compiled. Contours are elevations of the Precambrian surface in thousands of feet.

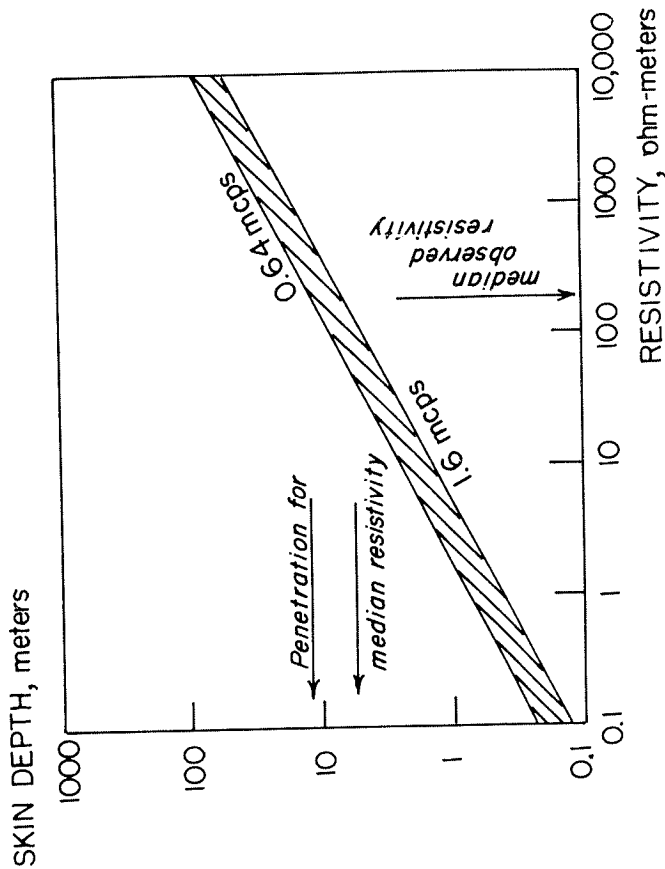


FIGURE 41.—Skin depths at broadcast frequencies as a function of earth resistivity.

part of standard operating practice. Such field strength measurements are usually made along a number of radial traverses about a radio transmitter. At least 18 or 20 point measurements must be made along each radial to establish a decay curve, and generally, measurements are made along eight or more radials about each station. In evaluating these measurements, a transparent overlay consisting of a group of theoretical decay curves for various ground conductivities is placed over an observed decay curve. The theoretical curve which most closely corresponds to the experimental curve is chosen, and so, a value for ground conductivity is assigned. Variations in transmitter power, inhomogeneities in earth conductivity and various experimental errors cause some scatter to the data. Also, the theoretical curves do not vary greatly for different values of earth conductivity. As a result, the value of earth conductivity assigned by the visual comparison of theoretical curves and experimental data points probably has an average error of ± 30 percent.

Between 1947 and 1953, the National Bureau of Standards compiled a catalog of 7,237 ground conductivity determinations made in such a manner about 621 broadcast stations for the purpose of constructing a ground conductivity map of the United States. Such a map was published by Fine (1954). However, the correlation between conductivity and soil type was not impressive, probably for two reasons. First, the Department of Agriculture soil classification system used in this correlation lists 256 soil classes, and is based on a number of factors which might not be expected to relate to soil conductivity. Secondly, the radiowaves penetrate to depths of 10s to 100s of feet, while the soil mapped by the Department of Agriculture may be only a few feet thick. Although surface soil types reflect the properties of rocks at depth in the case of residual soils, this reflection of subsurface properties by surface soil characteristics is not always to be expected. However, radiowave conductivities do appear to correlate reasonably well with bedrock geology as given on the Geological Map of the United States (Stose and Ljungstedt, 1932).

Conductivity values determined along radials about a transmitter represent the average characteristics of the subsurface rocks over a horizontal distance of from 5 to 50 miles. Therefore, the geologic units with which conductivity values are correlated must be chosen large enough in size that any particular radial will be entirely within a single geologic unit. The smallest subdivision which can be used appears to be a geologic period, though in cases where rock type varies radically within a period, further subdivision is necessary. About half the data reported by Kirby and others (1954) were for radials which could be assigned to a single geological environment of this sort.

A comparison of the data with geology was carried out by tracing the radials from National Bureau of Standards Circular 516 (Kirby and others, 1954) onto the Geological Map of the United States, and then compiling the value of conductivity within each geologic unit. Probability density curves for 39 units, grouped in seven groups according to age or lithology, are shown in figures 12-19, and the areas over which the 39 units outcrop are shown on the map of the United States in figure 50.

The size of each geological unit used in this study is so great that the data cannot be used to detect differences between rock types (that is, between sandstone and shale), though it is possible to recognize differences between the sedimentary sequences and the igneous and metamorphic rocks. One may also note a correlation between resistivity and the age of the bedrock, if only the sedimentary sequences are considered. The resistivity is not a monotonous function of time, but exhibits maximum values during the Precambrian and Cenozoic eras and minima during the Mesozoic era and Quaternary time. Similar correlations with age have been noted by Card (1940) using conductivity determinations based on induction from power lines.

The variation in resistivity with age must represent the results of a combination of bedrock lithology and modifications of the normal porosity and water content by weathering processes. It is interesting to note that the soil resistivities may vary considerably from the resistivities in the unweathered rock beneath. The surficial resistivities vary from about 50 ohm-meters over sections of highly conductive sedimentary rock to about 2,000 ohm-meters over highly resistive igneous and metamorphic rocks. The median surficial resistivity for all of the measurements made at radio frequencies is 143 ohm-meters. It appears therefore that the effect of weathering is to increase the resistivity of normally conductive rocks and to decrease the resistivity of normally resistive rocks.

The very low resistivity of some Quaternary alluvial deposits is probably a result of the large amount of water contained in such unconsolidated materials. As a consequence, Quaternary deposits may have a low resistivity even when saturated with brackish or fresh water. Exceptions are Quaternary windblown sand and gravel deposits which are relatively dry and have high resistivities.

Miocene and Pliocene sediments have a greater resistivity than most Quaternary rocks, probably representing the effect of reduction of porosity on compaction, as well as the fact that Miocene and Pliocene rocks are primarily fresh and backish water deposits.

The very low resistivities observed for surficial rocks of late Paleozoic to Mesozoic age reflect the fact that these rocks are largely marine in origin, in

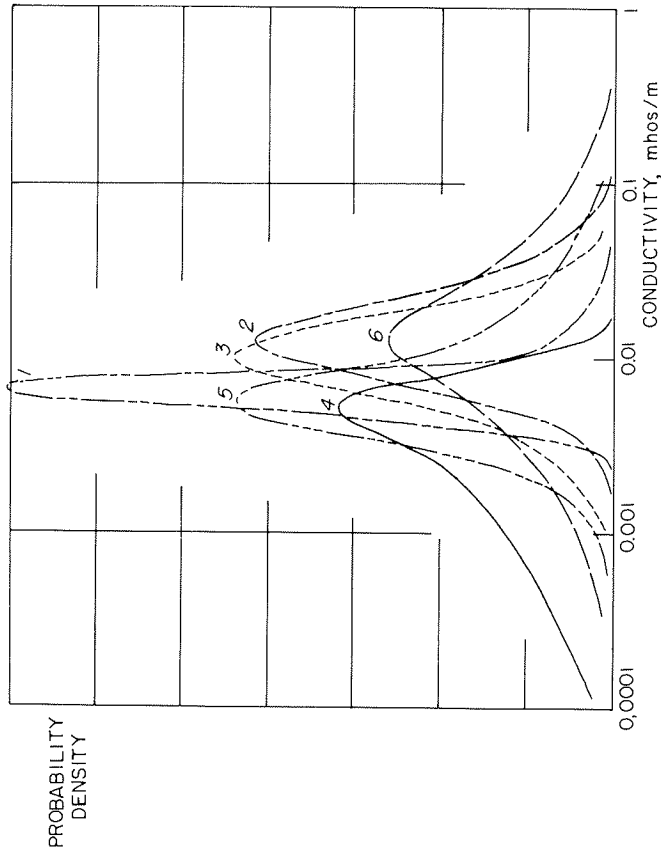


FIGURE 42.—Resistivities determined from decay of radio wave field strength over outcrops of Quaternary deposits in the United States.

Curve 1. Q₁, marine limestones.
 Curve 2. Q_a, Pacific coast
 Curve 3. Q_a, Rocky Mountain area
 Curve 4. Q_a, Atlantic Coast
 Curve 5. Q_a, Mississippi valley
 Curve 6. Q_a, Gulf Coast

contrast to later rocks which are largely continental in origin. While these rocks have less porosity than the later sediments, the salinity of the connate water is much greater, causing the rocks to be quite conductive, even after weathering.

Relatively high resistivities are noted over areas where early Paleozoic rocks form the suboutcrop. This may reflect the fact that these rocks have been well indurated prior to exposure for weathering, and therefore weathering is not nearly so effective in increasing their conductivity.

The information about the weathered-layer resistivity provided by these radiowave evaluations necessarily is averaged over large areas, and so does not provide an essential part of the information needed in designing surface-based electrical sounding methods: the small scale variability in resistivity in the weathered layer. However, these data do provide a feeling for the surficial

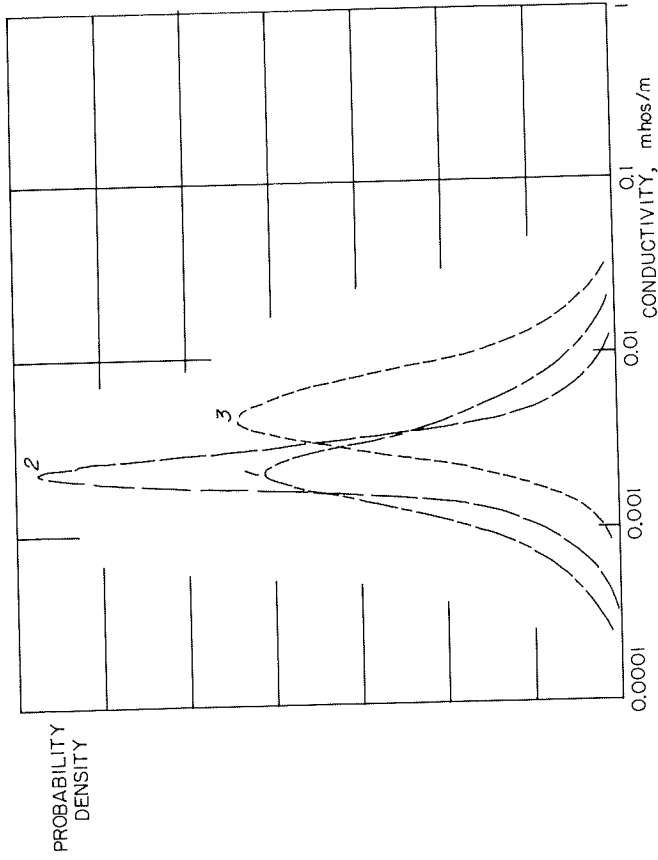


FIGURE 43.—Resistivities determined from decay of radio wave field strengths over outcrops of Miocene sedimentary rocks in the United States.

Curve 1. Mab, Gulf Coast
 Curve 2. My, Atlantic Coast
 Curve 3. Mt, Gulf Coast
 Formation names and abbreviations taken from the Geologic Map of the United States.

resistivity which may be encountered in a particular exploration problem in the United States.

PROPERTIES OF OIL FIELDS

We need not only to know the electrical properties of the environment of oil fields but also the properties of the oil fields themselves, if we are to consider the possibility of locating oil fields directly as a consequence of the anomaly in resistivity associated with them. Most physical properties are modified to some extent when oil is present in place of water in a porous rock, and these changes in physical properties serve as the basis for evaluation techniques used in interpreting a wide variety of geophysical well logs. However, the property which is affected the most is the electrical resistivity. Accepting a simple form of Archie's law, the resistivity of an oil-bearing rock may be written as:

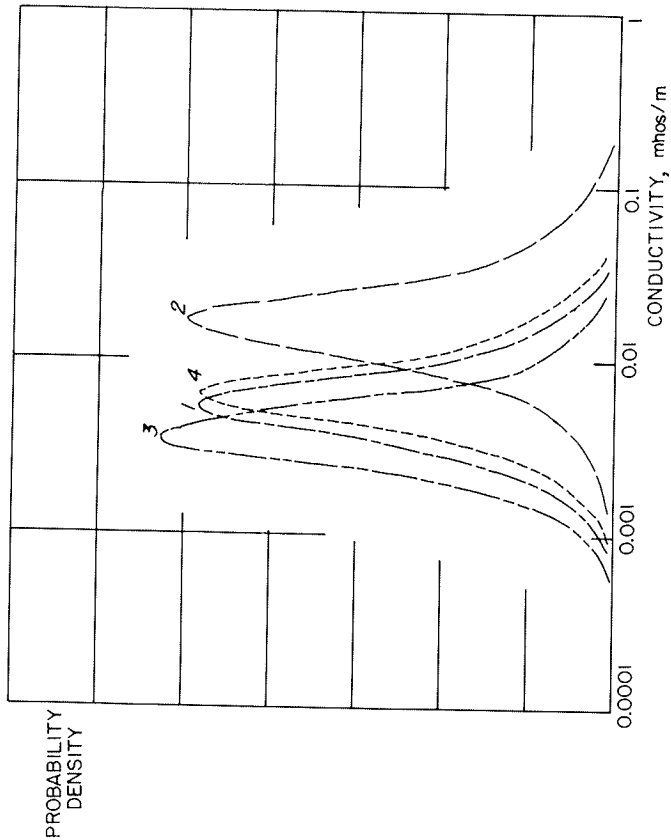


FIGURE 44. — Resistivities determined from decay of radio wave field strength over outcrops of Eocene sedimentary rocks in the United States.
 Curve 1. Eocene formations of the Gulf Coast
 Curve 2. Egr, Efu, Ews formations, Great Plains
 Curve 3. Pacific Coast continental sediments
 Curve 4. Pacific Coast marine sediments
 Formation names and abbreviations taken from Geologic Map of the United States.

$$\rho = \rho_w \phi^{-m} S_w^{-n} = \rho_w \phi^{-m} (1 - S_o)^{-n} \quad (16)$$

where ρ_w is the resistivity of the water in the rock, ϕ is the porosity expressed as a fraction of the pore space filled with water, S_o is the fraction filled with hydrocarbons, and m and n are empirical constants, commonly having values close to 2 in oil reservoir rocks. If the surrounding rock is similar to the rock in which the oil is trapped, differing only in that it is fully saturated with water with the same resistivity, ρ_w , the contrast in resistivity between the oil-saturated rock and the water-saturated rock is:

$$\frac{\rho_{t,o}}{\rho_{t,w}} = (1 - S_o)^{-n} \quad (17)$$

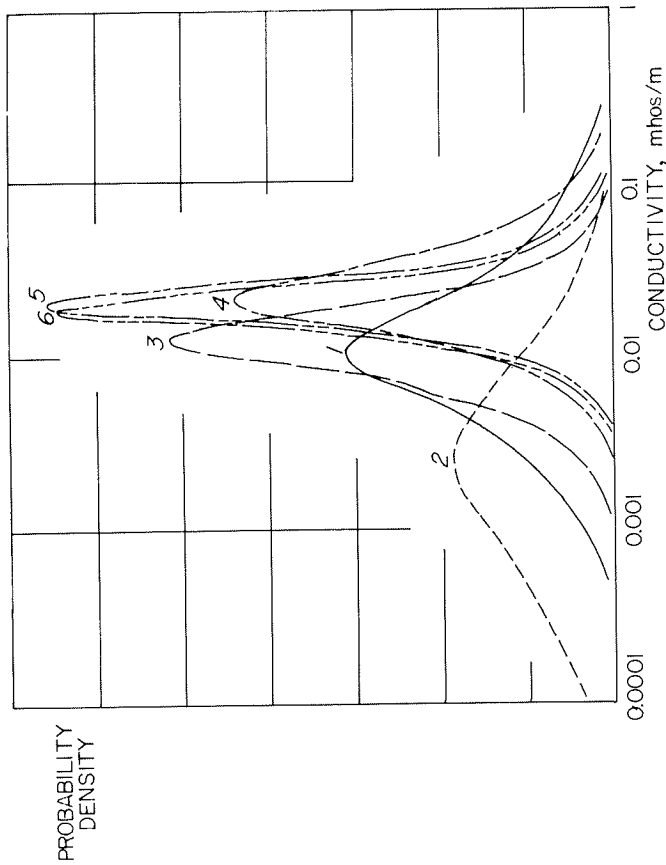


FIGURE 45. — Resistivities determined from decay of radio wave field strength over outcrops of Cretaceous sedimentary rocks in the United States.
 Curve 1. K_{tr} , K_w formations, Texas
 Curve 2. K_1 , K_2 , K_3 formations, southeastern United States
 Curve 3. K_1 , K_2 , K_{mv} formations, Rocky Mountain area
 Curve 4. K_{sw} , K_a , K_{ca} , K_{n1} formations, Texas
 Curve 5. K_{n1} , K_m formations, Great Plains
 Curve 6. K_{n1} , K_q formations, Great Plains
 Formation names and abbreviations taken from Geologic Map of the United States.

where $\rho_{t,o}$ is the true resistivity of the oil-saturated rock and $\rho_{t,w}$ is the true resistivity of the water-saturated rock.

In evaluating the sensitivity of surface-based electrical exploration techniques, we will find that the transverse resistance of a bed, defined as the product of resistivity and thickness, is a descriptive parameter needed in the theoretical development. If we assume an extremely simplified model in which the oil zone is contained in a rock which is completely uniform in resistivity, the resistivity being that which the oil zone would have if it were completely water saturated, the transverse resistance for the rocks above the oil field would be $T_1 = H\rho_{t,w}$, with H being the depth to the oil field, and the

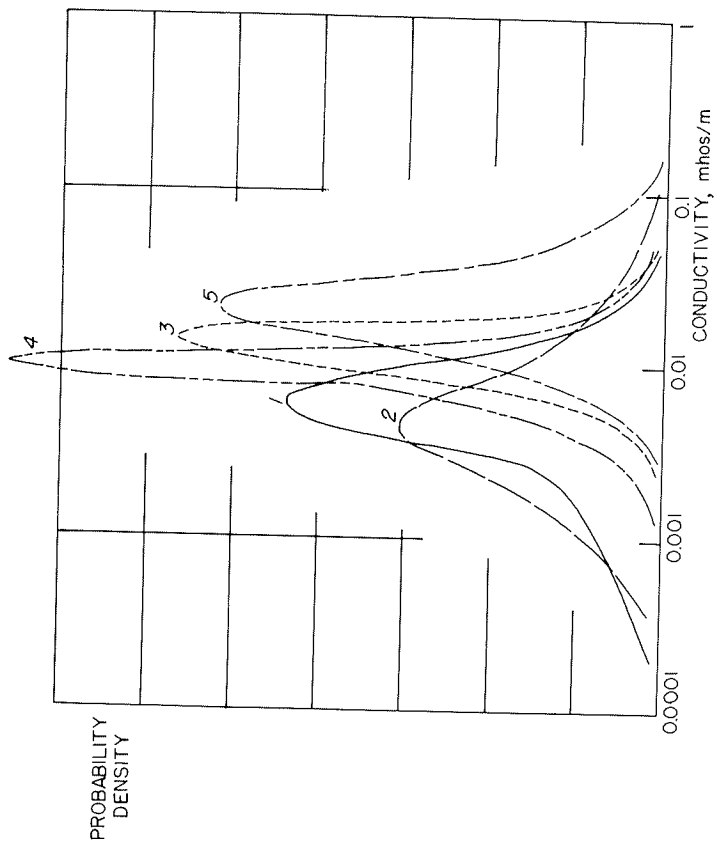


FIGURE 46.— Resistivities determined from decay of radio wave field strength over outcrops of late Paleozoic sedimentary rocks in the United States.
 Curve 1. Ca, Cc, Cpv formations, Great Lakes area
 Curve 2. Cml, Cmm formations, midcontinent area
 Curve 3. Pennsylvanian formations of the midcontinent
 Curve 4. Mississippian formations of the Great Plains
 Curve 5. Permian formations of the midcontinent
 Formation names and abbreviations are taken from the Geologic Map of the United States.

transverse resistance for the oil zone would be $T_2 = t\rho_{t,0}$ with t being the thickness of the pay zone.

The ratio of transverse resistances between the overlying rock and the pay zone is then:

$$\frac{T_2}{T_1} = (1 - S_0)^{-n} \frac{t}{H} \quad (18)$$

The anomaly in transverse resistance indicated in this expression has been plotted in figure 51 as a function of the thickness of the pay zone, expressed as a ratio to the thickness of the overlying rock, and as a function

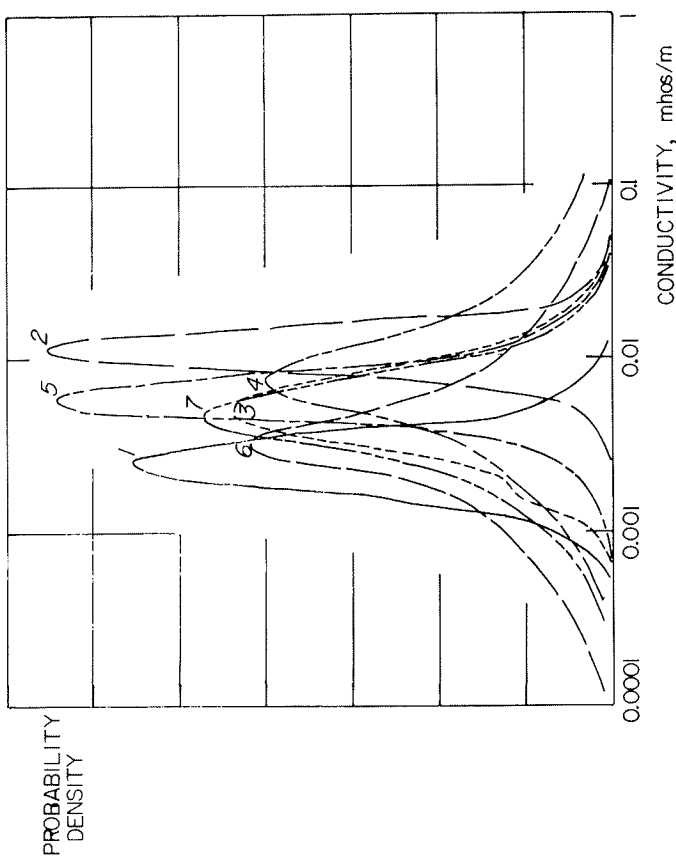


FIGURE 47.— Resistivities determined from decay of radio wave field strength over outcrops of early Paleozoic sedimentary rocks in the United States.
 Curve 1. Cg, Cl, Cu formations, Appalachian area
 Curve 2. Silurian formations of the midcontinent area
 Curve 3. Devonian formations of the Great Lakes area
 Curve 4. Dm, Dml, Dl limestone formations of the Great Lakes area
 Curve 5. Sl, Sm, Su formations, New England
 Curve 6. Ordivician and Cambrian formations, New England
 Curve 7. Osp, Ol, Gu formations, Great Lakes area
 Formation names and abbreviations taken from Geologic Map of the United States.

of oil saturation. Usually an oil field must have an oil saturation in excess of 50 percent to be profitable. Also, even with favorable drilling conditions, the thickness of the pay zone should be at least 10 feet at a depth of 10,000 feet, in order to provide a marginally profitable well. These considerations provide a lower limit to the value for T_2/T_1 which would be associated with an oil zone worth producing, as indicated by the shaded area in figure 51. It appears that the lowest ratio T_2/T_1 which might represent a worthwhile oil field is 1.01 (a one percent contrast). Of course, larger values for T_2/T_1 would be expected for larger oil fields.

A second factor to be considered in constructing an electrical model of an oil field is the areal extent. Some types of oil fields, such as shoestring sand

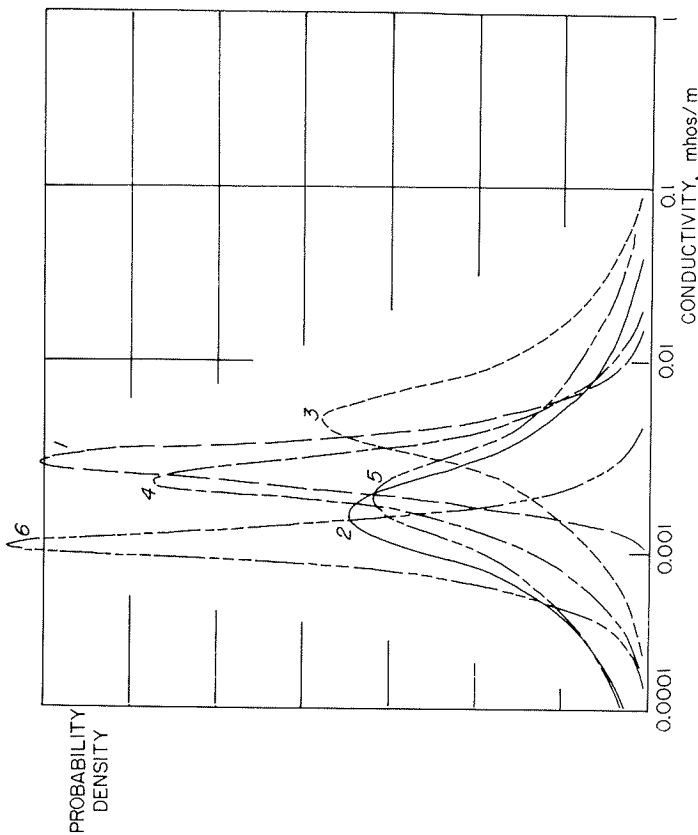


FIGURE 48. — Resistivities determined from decay of radio wave field strength over outcrops of igneous and metamorphic rocks in the United States.

Curve 1. Carboniferous granites, Appalachian area
 Curve 2. Paleozoic intrusives, New England
 Curve 3. Precambrian rocks of the Great Lakes area
 Curve 4. Precambrian rocks of the Appalachian area
 Curve 5. Triassic rocks of New England
 Curve 6. Archean rocks of New England

producers, have very small areal extents, and will not be considered here. According to Griffiths and Drew (1965), who have made statistical analyses of the sizes and shapes of typical oil fields, a field is usually about equant in dimensions, with the long dimension averaging only 50 percent greater than the narrow dimension. A summary of their data for the sizes of oil fields in three U.S. provinces (west Texas, Denver basin and Indiana) is shown in figure 52, plotted as cumulative frequency of occurrence curves for sizes (areas) of oil fields. The west Texas fields are larger on the average (1.7 square miles) than either those in Indiana (average, 0.77 square mile) or those in the Denver basin (0.62 square mile). The average depths at which these oil fields are found range from somewhat less than a mile in Indiana, to about a mile in the Denver basin, and somewhat more than a mile in west

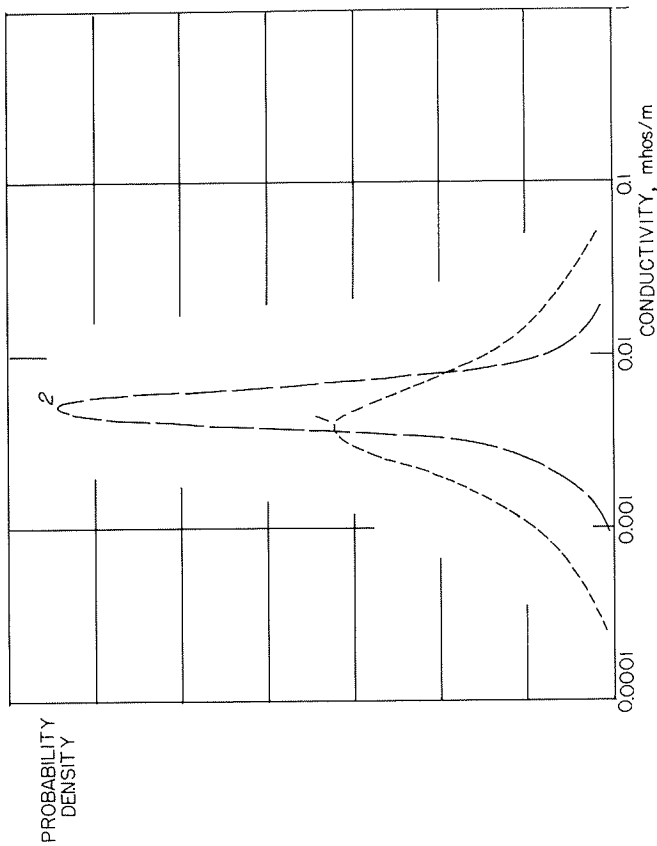


FIGURE 49. — Resistivities determined from decay of radio wave field strength over outcrops of volcanic rock in the United States.

Curve 1. PMv, Columbia River Plateau
 Curve 2. Tv, Ev, Rocky Mountain area
 Formation names and abbreviations taken from the Geologic Map of the United States.

Texas. It is apparent from the statistical summaries that the bulk of oil production must come from the fields bigger than average. Most of the smaller than average oil fields are probably less than profitable. Therefore, we may define the least of oil fields that would be of interest as having an area of about $3/4$ -square mile at a depth of one mile.

Larger fields are required at greater depths in order to provide profitable production, and so, it may be reasonable to express the areal extent of a minimum-size oil field in terms of the solid angle subtended when viewed from the surface directly over the field. Using such a measure of area, the least of oil fields would occupy an area of $3/4$ -steradian. In summary, the least oil field which might be of interest in exploration is characterized by a thickness of at least one foot per 1,000 feet of burial, an areal extent of at least $3/4$ -steradian and a transverse resistance contrast with overlying rocks of at least 1 percent.

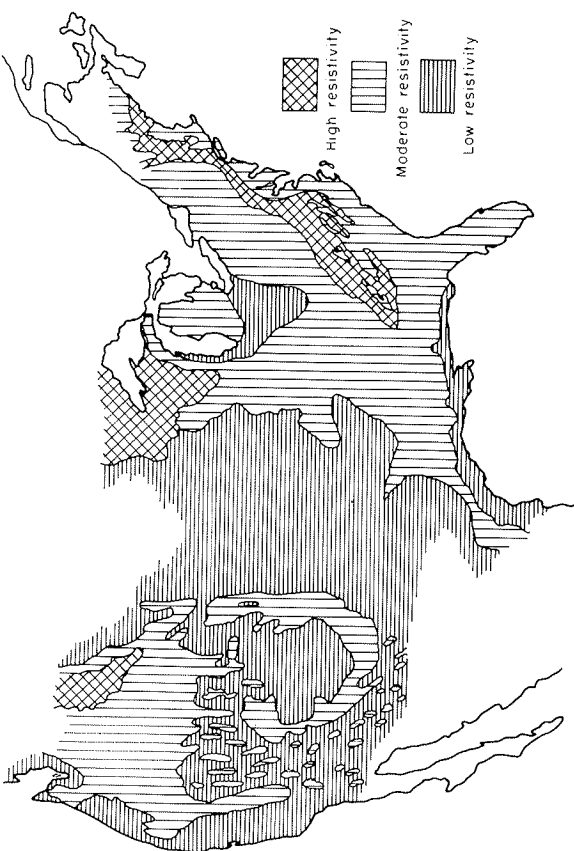


FIGURE 50. — Map showing the locations where resistivities of the surficial rock are higher than average, moderate, and lower than average, based on determinations made at radio frequencies (from Keller, 1966; reprinted by permission from the Society of Exploration Geophysicists).

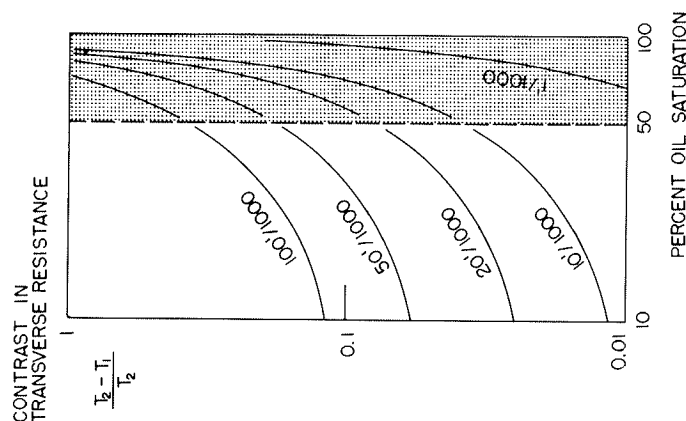


FIGURE 51. — Anomaly in transverse resistance as a function of oil saturation and pay-zone thickness. The pay-zone thickness is expressed as a ratio to the thickness of the overburden.

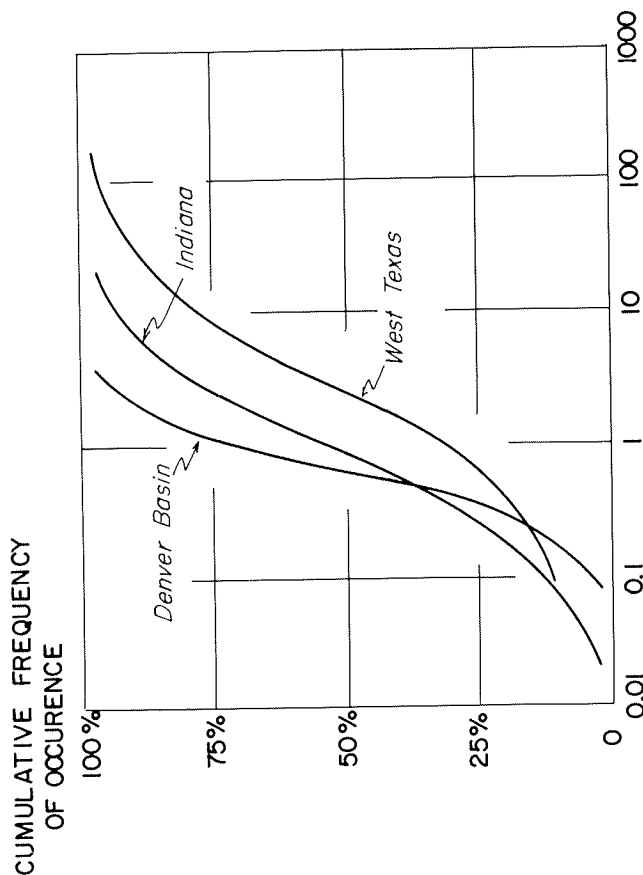


FIGURE 52. — Statistical summary of the sizes of some oil fields in the United States (from Griffiths and Drew).

REFERENCES

Archie, G. E., 1942, The electrical resistivity log as an aid in determining some reservoir characteristics: Am. Inst. Mining, Metall., Petroleum Engineers, Tech. Paper 1422.

Anderson, L. A., 1965, Experimental deep resistivity probes in central and eastern United States: U.S. Geol. Survey Tech. Let. Crustal Studies-31, March 26.

Card, R. H., 1940, Correlation of earth resistivity with geological structure and age: Am. Inst. Mining, Metall. Petroleum Engineers Trans., v. 138, p. 380-398.

Eardley, A. J. 1962, Structural geology of North America, second edition: New York, Harper and Row, 743 p.

Eargle, D. H., 1963, Surface and subsurface stratigraphic sequence in southeastern Mississippi: Short Papers in Geology and Hydrology: U.S. Geol. Survey Prof. Paper 475-D, Washington, U.S. Govt. Printing Office, p. 43-48.

Fine, H., 1954, An effective ground conductivity map for the continental United States: Proc. IRE, v. 42, p. 1405-1408.

Griffiths, J. C., and Drew, L. J., 1965, Size, shape and arrangement of some oilfields in the U.S.A.: Computers and Computer Applications in Mining and Exploration Symposium, Univ. Arizona, March 15-19, v. 3.

- Hartill, N., 1967, An evaluation of the audio-magneto-telluric method: M.Sc. Thesis, Colorado School Mines.
- 1968, The CSM test area for electrical surveying methods: Geophysics, in print.
- Jackson, D. B., 1962, Electrical properties of the sedimentary section in the High Plains area: Denver, Colo., U.S. Geol. Survey Tech. Let. Report. ARPA Order No. 193-61.
- 1965, Deep resistivity probes in the southwestern United States: U.S. Geol. Survey open-file rept., Tech. Let. Crustal Studies-29, March 19, 97 p.
- 1967, Deep resistivity probes in the southwestern United States: Geophysics, v. 32, no. 1, p. 1123-1144.
- 1968, Division of the geologic column in the Rattlesnake Hills, Washington into three major geoelectric sections: Log Analyst, in print.
- Keller, C. V., 1960, Electrical properties of zinc-bearing rocks in Jefferson County, Tennessee: Short Papers in the Geological Sciences: U.S. Geol. Survey Prof. Paper 400B, p. B369-B400.
- 1964, Compilation of electrical properties from electrical well logs: Colorado School Mines Quart., v. 59, no. 4, p. 91-110.
- Kirby, R. S., Harman, J. C., Capps, F. M., and Jones, R. N., 1954, Effective radio ground-conductivity measurements in the United States: Washington, D. C., U.S. Govt. Printing Office, Nat. Bur. Standards Circ. 546.
- Pirson, S. J., 1963, Handbook of well log analysis: Englewood Cliffs, Prentice-Hall, N. J., 326 p.
- Schlumberger, C., Schlumberger, M., and Leonardon, E. G., 1934, Some observations concerning electrical measurements in anisotropic media, and their interpretation: Ann. Inst. Mining, Metall. Petroleum Engineers Trans., v. 110, p. 159-182.
- Sloss, L. L., Dapples, E. C., and Krumbein, W. C., 1960, Lithofacies maps: New York, John Wiley and Sons, 108 p.
- Stose, G. W., and Ljungstedt, O. U., 1932, Geological map of the United States: U.S. Geol. Survey.
- U.S. Geological Survey, 1967, Basement Map of North America.

PART 2. — THEORY OF ELECTRICAL SOUNDING

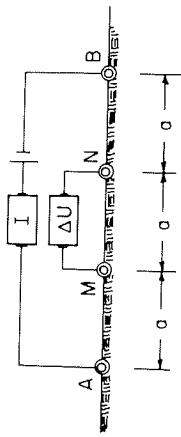
The resistivity of sedimentary sequences appears to vary consistently over large areas, so that the measurement of resistivity from the surface of the earth might conceivably provide information of interest in an exploration program. Moreover, the presence of oil in a rock normally increases the resistivity of that rock. If such resistivity changes could be measured from the earth's surface, it would be of considerable value in petroleum exploration. The purpose of this section, then, is to lay the theoretical foundation for methods to measure resistivity from the earth's surface.

By convention, electrical sounding methods have been classified as "DC" methods or "AC" methods. The DC methods for measuring earth resistivity have been used most widely, and there are a number of texts and monographs devoted to the subject of direct current methods (Kalenov, 1957; Lasfargues, 1957; Tagg, 1964; Van Nostrand and Cook, 1966; Kunetz, 1966, Alpin and others, 1966). Generally, four-terminal arrays are used in order to minimize the effect of material near the current electrodes. Current is driven through one pair of electrodes; the potential established in the earth by this current is measured with the second pair of electrodes. Strictly direct current is not used, but rather a low-frequency alternating current is used so that the voltages developed in the earth by this current can be easily recognized in the presence of the other, miscellaneous voltages (or self-potential) which arise at electrode contacts. However, the frequency of the current is made sufficiently low that the assumption may be made that the flow of current in the earth can be completely described by a solution to Laplace's equation.

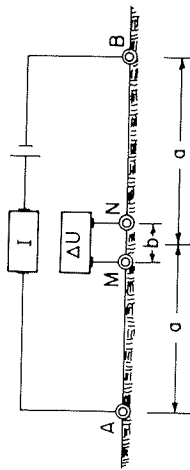
Direct-current sounding methods differ from one another primarily in the way the electrode contacts are arranged on the surface of the earth. Electrode arrangements may be of three types:

1. Arrangements in which the *potential difference* between two widely spaced measuring electrodes is said to be measured. An example is the Wenner array, in which four electrodes are equally spaced along a straight line, as shown in figure 53a.
2. Arrangements in which the *gradient of potential* (or electric field intensity) is said to be measured, using a closely spaced pair of measuring electrodes. An example is the Schlumberger array, in which two closely spaced measuring electrodes are placed midway between two current electrodes, and in line with them, as shown in figure 53b. The measuring electrodes are placed closely enough together that the ratio of voltage observed between them

Wenner array



Schlumberger array



Polar dipole array

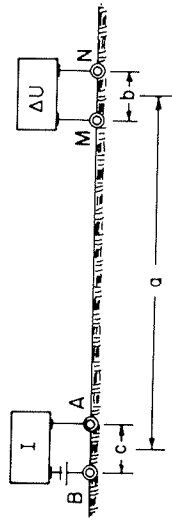


FIGURE 53. — Electrode arrays commonly used in the direct-current resistivity method. A and B are current electrodes, M and N are measuring electrodes, and a, b, and c are array spacing factors (from Keller, 1966; reprinted by permission from the Society of Exploration Geophysicists).

to their separation approximately equals the potential gradient at the midpoint of the current spread.

3. Arrangements in which a *second spatial derivative of the potential* is said to be measured, using a closely spaced current electrode pair as well as a closely spaced measuring electrode pair. An example is the polar dipole array, shown in figure 53c. The voltage measured this way is approximately equal to the second derivative of the potential, after it has been divided by the distances AB and MN, provided these distances are small compared to the separation between dipole centers.

Any one of these arrays may be used to study horizontal and vertical variations in resistivity. In studying the variation of resistivity with depth, as in the case of a horizontally layered medium, the spacings between the various

electrodes are gradually increased. Larger spacings accentuate the effect on the measurements of material at depth. Although it is difficult to specify how deeply the resistivity is being sampled with a particular electrode array, it is generally accepted that the depth of sampling is less than half the total electrode span, for most of the arrays. We will consider the sampling depth of all the electrical methods in a later section.

In the AC methods for measuring earth resistivity, a time-varying magnetic field is generated by driving an alternating current through an ungrounded loop of wire or a grounded length of wire. If conductive material is present within the magnetic field so generated, *induced or eddy currents* will flow in closed loops along paths normal to the direction of the magnetic field. These eddy currents, in turn, generate their own magnetic fields so that at any point in space, the total magnetic field may be thought of as consisting of two parts: a *primary*, or normal field due to the source current and a *secondary* or disturbing field due to eddy currents induced in conductors. The electromagnetic field may be detected either by measuring the voltage drop between a pair of electrodes or by measuring the magnetic induction using a coil of wire as a magnetometer. The AC or electromagnetic methods have been used most commonly in mining exploration, where the objective is to detect an anomaly in electromagnetic field strength caused by a conductive ore body, rather than in quantitative studies of earth-resistivity. As a consequence, there is less literature on the use of the AC methods than of the DC methods for electrical sounding (Vanyan, 1967).

In measuring earth conductivity, one must first generate an electromagnetic field and then measure or detect the distortion in this field caused by the presence of a conductive earth. This may be done in many ways, and the variety of ways of using an electromagnetic field in studying earth conductivity has actually hindered the application of the methods.

The three common controlled sources for electromagnetic fields used in geophysical exploration are loops of wire, short grounded lengths of wire and long grounded lengths of wire. A current flowing in a small loop of wire generates a magnetic field which cannot be distinguished from that caused by a dipole magnet, when the field is observed at moderate distances (a moderate distance being greater than about five times the diameter of the loop). The magnetic field generated by such a current-carrying loop has a strength equivalent to a dipole magnet with a moment equal to the product of the number of turns of wire in the loop, the area of the loop and the current flowing in the wire. If the current is oscillatory, such a source is called a *harmonic*, or *oscillating magnetic dipole* source. A steady current provides a magnetic field which is constant in time. An abrupt termination or initiation of current flow in such a loop leads to a *transient magnetic field*.

A loop may be oriented arbitrarily with respect to the surface of the earth, but normally, the plane of the loop is placed either parallel to the surface of the earth, in which case it is called a *vertical magnetic dipole*, or perpendicular to the surface of the earth, in which case it is called a *horizontal magnetic dipole*. The axis of the equivalent magnetic dipole coincides with the loop axis.

For a vertical magnetic dipole source located at the earth's surface, there are only three electromagnetic field components which may be observed at the surface of a uniform earth: a vertical component of the magnetic field, H_z , a radial component of the magnetic field H_r , and a tangential component of the electric field, E_ϕ . With a horizontal dipole source, five of the six orthogonal field components may be observed over a uniform earth. The vertical component of the electric field is the only field component not observed. The vertical magnetic field from a horizontal loop is the same as the radial magnetic field from a vertical magnetic dipole, as follows from reciprocity.

A grounded wire may serve as the source of an electromagnetic field as well as a current-carrying loop. In this case, if the length of the grounded wire is short compared to the distance at which the field is observed, the source may be termed a *current dipole* or an *electric dipole*. If observations are made at distances greater than about ten times the wire length, it is found that the product of wire length and current is the only parameter describing the source strength which is significant. This product, Ids , is called the dipole moment.

With a horizontal current dipole, all six components of the electromagnetic field may be observed at the surface of a homogeneous earth.

A third idealized type of source for an electromagnetic field which is used in geophysical exploration is a long grounded wire. Field components are measured close enough to the wire so that it may be considered to be infinitely long. Only two components of the electromagnetic field from a long wire may be observed at the surface of a uniform earth—the parallel component of the electric field and the vertical component of the magnetic field.

In recent years, a fourth source of energy has come into use for making electromagnetic depth soundings—the natural electromagnetic energy contained in rapid variations of the earth's magnetic field. When such energy is considered to be a plane wave traveling downward into the earth, the conductivity of the earth, if it is homogeneous, can be computed from the ratio of magnetic field strength to electric field strength (Cagniard, 1953).

In measuring the electric field in the earth, normally a short grounded wire is used. Magnetic field components may be measured with a magnetometer, though this is rarely done except in the case of the magnetotelluric method. More commonly, the magnetic field components are measured with induction coils, which detect the time-rate of change of the magnetic induction:

$$\text{EMF} = -nA \frac{dB}{dt}$$

If the source is harmonic—that is, if the current to the source is a sinusoid at a specific frequency, ω —in the steady state, the derivative may be replaced by a multiplying term, $i\omega$:

$$\text{EMF} = -i\omega n A \mu_0 H \quad (19)$$

Thus, a voltage is measured, rather than a magnetic field component. In all cases, this voltage is proportional to the strength of the source, or the current in the source, and must be normalized for this strength.

It is apparent that there are a great variety of techniques which might be used in electromagnetic sounding. Four types of source have been listed, and with various source-receiver component combinations, 16 different combinations of source and receiver could be used in electromagnetic depth sounding.

Depth soundings may be made either by varying the spacing between the source and the receiver, or by varying the frequency content of the source current. The first is termed a *geometric sounding*, and the second, a *parametric sounding*. There are operating advantages to both approaches, and both are used in practice. However, control of frequency is used more commonly than variation of source-receiver separation.

With a fixed separation, measurements may be made either in the *frequency domain* (one frequency at a time, through a range of frequencies) or in the *time domain* (use of transients containing a wide spectrum of frequencies). Although it is readily shown that time-domain measurements and frequency-domain measurements are uniquely related through the Fourier transform, the operating procedures and interpretation involved in the two approaches are quite different.

As a result, there are 45 variants which might be used in the controlled source methods, plus the magnetotelluric method, making a total of 46. Each of the 46 methods requires somewhat different instrumentation and quite different interpretation procedures and theoretical curves. Commonly, in the literature, a single method is considered at a time so that comparison between methods is difficult. The variety of methods has led to confusion in understanding the basic principles of depth sounding, and so, a unified approach to the theory of electromagnetic depth soundings is essential.

SOLUTION OF THE BOUNDARY VALUE PROBLEM

The first thing we must accomplish is a solution of Maxwell's equations for an earth made up of a sequence of horizontal layers. In fact, as it turns

out, we must do this twice in order to have expressions which we can use with each type of source—a short grounded wire or a vertical-axis-coil—which is of interest in oil prospecting. In so doing, I will follow closely the development used by Vanyan (1967), and so far as convenient, use his notation.

Let us first establish precisely the earth model we wish to use. The essential features of the model are shown in figure 54. The earth is assumed to consist of a sequence of layers, each designated with an index p , which runs from 0 to N going downward through the sequence. The $p=0$ layer in reality will be taken as a half-space representing the air above the earth, inasmuch as we are not planning to discuss layering in the ionosphere. We will allow each layer to be anisotropic in two dimensions—that is, each layer is represented by two values of resistivity, ρ_l in a horizontal direction and ρ_t in the vertical direction. Each value of resistivity also carries the index p to indicate the layer to which it is assigned. Each layer is also characterized by a dielectric constant ϵ_p and a magnetic permeability μ_p , though we shall ignore displacement currents and we will assume that all values of magnetic permeability are equal to the value in free space, $4\pi \times 10^{-7}$ H/M.

In all cases, the behavior of an electromagnetic field is described by Maxwell's equations. The first of these:

$$\nabla \times \vec{H} = \vec{J} + \epsilon \mu \frac{\partial \vec{E}}{\partial t} \tag{20}$$

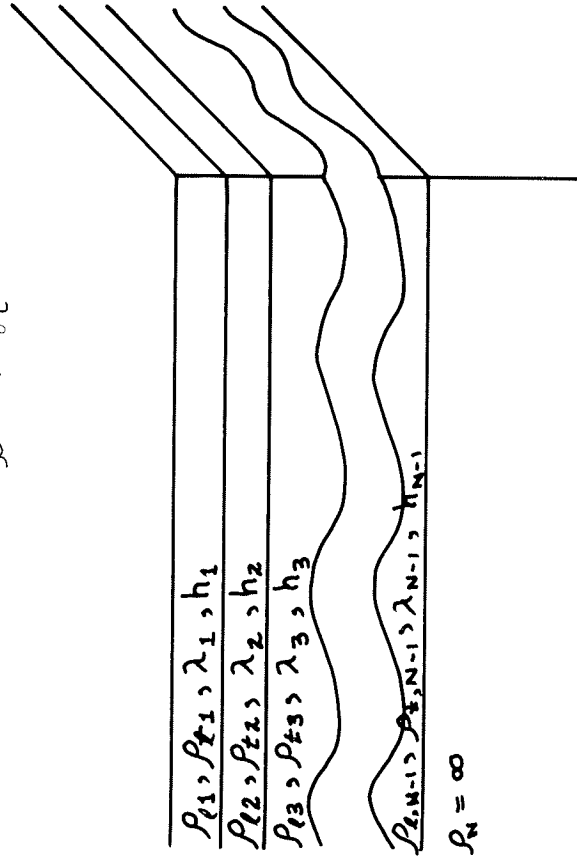


FIGURE 54. — Definition of an anisotropic layered medium.

describes the fact that the observed magnetic field is generated either by current flowing in the medium or displacement currents. Maxwell's second equation relates the induced electric field to the rate of change of magnetic induction:

$$\nabla \times \vec{E} = - \frac{\partial \vec{B}}{\partial t} \tag{21}$$

Two additional equations which express the continuity of magnetic and electric lines of force in the absence of free magnetic poles and electric charges, respectively, are sometimes also considered to be part of Maxwell's equations, though there are many problems in which they must be expressed differently:

$$\text{div } \vec{B} = 0 \tag{22}$$

$$\text{div } \vec{E} = 0 \tag{23}$$

Application of these divergence conditions means that we are going to consider only solutions to Maxwell's equations for a uniform space. In fact, inasmuch as we wish to consider a layered space, we will actually obtain a number of solutions, each of which is valid for a full space with the properties of one of the layers, and then match the solutions at boundaries between layers, using auxiliary boundary conditions. These boundary conditions consist of requiring that the tangential components of the electric and magnetic fields be continuous at the boundaries, that the electromagnetic field approach zero at large distances, and that the expression for the electromagnetic field approaches the value for a uniform medium close to the source.

We can simplify matters somewhat by seeking a solution only for the steady-state harmonic case, in which each of the field components is assumed to vary with time as

$$- i \omega t$$

This means that each time derivative can be represented as a multiplication by the coefficient $- i \omega$:

Maxwell's equations are:

$$\nabla \times \vec{B} = \left(\frac{\mu_0}{\rho} - i \omega \mu_0 \epsilon \right) \vec{E} \tag{24}$$

$$\nabla \times \vec{E} = i \omega \vec{B} \tag{25}$$

a. *Solution of Maxwell's equations for a short grounded wire source*

As is usually the case, it is convenient to seek a solution to Maxwell's equations in terms of a vector potential, which is allowed by the fact that the two

divergences are zero. On the basis that $\text{div } \vec{B} = 0$, we may always define a vector potential, \vec{A} , which satisfies the condition:

$$\vec{B} = \nabla \times \vec{A} \tag{26}$$

The nature of this vector potential can best be seen by considering the fundamental law of force between elements of current:

$$d\vec{F} = \frac{\mu_0}{4\pi} \frac{I I'}{R^3} d\vec{l} \times (d\vec{l}' \times \vec{R}) \tag{27}$$

which gives the force on the element $d\vec{l}$ due to the presence of $d\vec{l}'$. The two elements are thin wires that carry currents I and I' , respectively. The radius vector R is directed from $d\vec{l}'$ to $d\vec{l}$. The force on a single wire element in a field of magnetic induction, B , is given by the fundamental law:

$$d\vec{F} = I d\vec{l} \times \vec{B} \tag{28}$$

The dF in this equation differs from the one in equation 27 in that it represents the total force on the element $d\vec{l}$ due to the presence of all other existing currents, while the dF in equation 27 represents only the force due to the current element $d\vec{l}'$. Comparing equations 27 and 28, we see that the field of magnetic induction is:

$$\vec{B} = \frac{\mu_0}{4\pi} \int \frac{I'}{R^3} d\vec{l}' \times \vec{R} \tag{29}$$

where the integration is carried out over all the elements of current $d\vec{l}'$ which exert a force on an element placed at the point for which B is being evaluated. Recognizing that

$$\frac{\vec{R}}{R^3} = -\nabla \left(\frac{1}{R} \right) \tag{30}$$

we can expand equation 29 as:

$$\vec{B} = \frac{\mu_0}{4\pi} \int I' \left[\hat{i} \frac{\partial}{\partial x} \left(\frac{1}{R} \right) + \hat{j} \frac{\partial}{\partial y} \left(\frac{1}{R} \right) + \hat{k} \frac{\partial}{\partial z} \left(\frac{1}{R} \right) \right] \times d\vec{l}' \tag{31}$$

Expanding the cross product indicated in this last equation, we may recognize the expression for a curl:

$$\begin{aligned} \vec{B} &= \frac{\mu_0}{4\pi} \int I' \left[\hat{i} \left(\frac{\partial}{\partial y} \frac{d\vec{l}'_z}{R} - \frac{\partial}{\partial z} \frac{d\vec{l}'_y}{R} \right) + \hat{j} \left(\frac{\partial}{\partial z} \frac{d\vec{l}'_x}{R} - \frac{\partial}{\partial x} \frac{d\vec{l}'_z}{R} \right) + \hat{k} \left(\frac{\partial}{\partial x} \frac{d\vec{l}'_y}{R} - \frac{\partial}{\partial y} \frac{d\vec{l}'_x}{R} \right) \right] \\ &= \nabla \times \frac{\mu_0}{4\pi} \int I' d\vec{l}' \end{aligned} \tag{32}$$

Thus, the vector potential, \vec{A} , has the significance of being the integral of effects of current elements, and so, \vec{A} will have only those components that current flow in the medium has. This is of assistance in recognizing from symmetry that certain components of the vector potential may be zero in certain cases.

As an example, consider the vector potential for a source which is a wire carrying current in the x direction. If there is no other current flowing in the system, the vector potential will have only an x -component. Now, if we let current flow from the wire into a laterally symmetric earth, the vector potential must also represent the effects of this current. Because the current is symmetrical in the y direction, there can be no net contribution to the integral, and so, for this case, the vector potential has no y component. The current flow is not symmetrical in the z direction inasmuch as the resistivity distribution is not symmetrical in the plus and minus z directions. The vector potential must be allowed to have a z component.

Substituting curl \vec{A} in place of \vec{B} in Maxwell's second equation (25), we have

$$\nabla \times \vec{E} = i\omega \nabla \times \vec{A} \tag{33}$$

$$\text{or} \quad \nabla \times (\vec{E} - i\omega \vec{A}) = 0$$

If the curl of a vector quantity is zero, that vector can be represented as the gradient of some function U called the scalar potential. Thus:

$$\vec{E} - i\omega \vec{A} = \nabla U \tag{34}$$

Expanding equation 33 into three scalar equations in Cartesian coordinates, we have (with $A_y = 0$, as explained above):

$$\begin{aligned} \frac{\partial}{\partial y} \left(-\frac{\partial A_x}{\partial y} \right) - \frac{\partial}{\partial z} \left(\frac{\partial A_x}{\partial z} - \frac{\partial A_z}{\partial x} \right) &= \left(\frac{\mu_0}{\rho_1} - i\omega \epsilon \mu_0 \right) (i\omega A_x - \frac{\partial U}{\partial x}) \\ \frac{\partial}{\partial z} \left(\frac{\partial A_x}{\partial y} \right) - \frac{\partial}{\partial x} \left(-\frac{\partial A_x}{\partial z} \right) &= \left(\frac{\mu_0}{\rho_1} - i\omega \epsilon \mu_0 \right) \left(-\frac{\partial U}{\partial y} \right) \\ \frac{\partial}{\partial x} \left(\frac{\partial A_x}{\partial z} - \frac{\partial A_z}{\partial x} \right) - \frac{\partial}{\partial y} \left(\frac{\partial A_z}{\partial y} \right) &= \left(\frac{\mu_0}{\rho_1} - i\omega \mu_0 \epsilon \right) \left(i\omega A_z - \frac{\partial U}{\partial z} \right) \end{aligned} \tag{35}$$

Integrating the second of these equations with respect to y , we obtain a relationship between the vector and scalar potentials which is valid for this particular problem (an x -directed wire element source over a laterally homogeneous earth):

$$\frac{\partial A_x}{\partial x} + \frac{\partial A_z}{\partial z} = (i\omega \epsilon \mu_0 - \frac{\mu_0}{\rho_1}) U \tag{36}$$

$$\text{Using the designations} \quad \frac{\partial A_x}{\partial x} + \frac{\partial A_z}{\partial z} \equiv \text{div } \vec{A} \tag{37}$$

and

$$-\frac{i\omega\mu_0}{\rho_\ell} - \omega^2\epsilon\mu_0 = \gamma_\ell^2 \quad (38)$$

we can rewrite equation 36 as:

$$\mathcal{U} = \frac{i\omega}{\gamma_\ell^2} \operatorname{div} \vec{A} \quad (39)$$

It might be pointed out that the parameter γ_ℓ which has been defined here is the "longitudinal radian wave number" at the frequency ω . The actual wave length, L , of the electromagnetic wave is related to the radian wave number as:

$$L = 2\pi/\gamma_\ell \quad (40)$$

We will see later that the first term in equation 38 represents the contribution from conduction currents, while the second term represents the contribution from displacement currents. Normally, displacement currents can be neglected in comparison with conduction currents in geophysical applications of electromagnetic sounding methods, and if this is the case, the wave number is written as:

$$\begin{aligned} \gamma_\ell &= \left(-\frac{i\omega\mu_0}{\rho} - \omega^2\epsilon\mu_0\right)^{1/2} \\ &\approx \left(-\frac{i\omega\mu_0}{\rho}\right)^{1/2} = \left(\frac{\omega\mu_0}{2\rho}\right)^{1/2} - i\left(\frac{\omega\mu_0}{2\rho}\right)^{1/2} \end{aligned} \quad (41)$$

The second expression is useful in numerical evaluations, inasmuch as the wave number is separated into real and imaginary parts.

We now return to the first of the scalar representations of Maxwell's first equation in (35), and rearrange terms to obtain the following:

$$-\frac{\partial^2 A_x}{\partial x^2} - \frac{\partial^2 A_x}{\partial z^2} + \frac{\partial^2 A_x}{\partial x \partial z} = -\frac{\gamma_\ell^2}{i\omega} \left[i\omega A_x - \frac{i\omega}{\gamma_\ell^2} \left(\frac{\partial^2 A_x}{\partial z^2} + \frac{\partial^2 A_x}{\partial x \partial z} \right) \right] \quad (42)$$

which simplifies to:

$$\frac{\partial^2 A_x}{\partial x^2} + \frac{\partial^2 A_x}{\partial y^2} + \frac{\partial^2 A_x}{\partial z^2} - \gamma_\ell^2 A_x = 0 \quad (43)$$

Introducing the Laplacian operator notation, we have the basic equation used in finding the x-component of the vector potential, A_x :

$$(\nabla^2 - \gamma_\ell^2) A_x = 0 \quad (44)$$

The third scalar representation of Maxwell's first equation (in 35) can be

rearranged in a somewhat similar manner:

$$-\frac{\partial^2 A_z}{\partial x^2} - \frac{\partial^2 A_z}{\partial y^2} + \frac{\partial^2 A_z}{\partial x \partial z} = \left(\frac{i\omega\mu_0}{\rho_{tr}} + \omega^2\epsilon\mu_0 \right) A_z - \frac{i\omega}{\gamma_{tr}^2} \left(\frac{\mu_0}{\rho_{tr}} - i\omega\epsilon\mu_0 \right) \left(\frac{\partial^2 A_x}{\partial x^2} + \frac{\partial^2 A_x}{\partial x \partial z} \right) \quad (45)$$

We can define another wave number, γ_{tr} , in which ρ_{tr} replaces ρ , and a coefficient of anisotropy as follows:

$$\gamma_{tr}^2 = -\frac{i\omega\mu_0}{\rho_{tr}} - \omega^2\epsilon\mu_0 \quad (46)$$

$$\lambda = \gamma_\ell / \gamma_{tr} \quad (47)$$

At low frequencies, the coefficient of anisotropy assumes its usual form, which is valid so long as displacement currents can be neglected:

$$\lambda_{\omega \rightarrow 0} = (\rho_{tr}/\rho_\ell)^{1/2} \quad (48)$$

With these definitions, equation 45 can be rewritten as:

$$\frac{\partial^2 A_z}{\partial x^2} + \frac{\partial^2 A_z}{\partial y^2} + \frac{1}{\lambda^2} \frac{\partial^2 A_z}{\partial z^2} - \gamma_{tr}^2 A_z = \left(1 - \frac{1}{\lambda^2}\right) \frac{\partial^2 A_x}{\partial x \partial z} \quad (49)$$

Unlike the first of the scalar equations, the third does not reduce to a homogeneous form, with A_x and A_z separating. This will make the solution of the differential equation for A_z more difficult than the solution of the differential equation for A_x . It is interesting to notice that if there is no anisotropy, equation 49 reduces to the same form of wave equation as given in equation 44.

So far we have not done anything except rearrange Maxwell's equations into a more convenient form for solution. We may now proceed to this solution, seeking first an expression for A_x in the form of functions with cylindrical symmetry—that is, depending only on the vertical coordinate and the distance from the source.

In cylindrical coordinates, equations 44 and 49 for A_x and A_z take the form:

$$\frac{\partial^2 A_x}{\partial r^2} + \frac{1}{r} \frac{\partial A_x}{\partial r} + \frac{\partial^2 A_x}{\partial z^2} - \gamma_\ell^2 A_x = 0 \quad (50)$$

$$\frac{\partial^2 A_z}{\partial r^2} + \frac{1}{r} \frac{\partial A_z}{\partial r} + \frac{1}{\lambda^2} \frac{\partial^2 A_z}{\partial z^2} - \gamma_{tr}^2 A_z = \left(1 - \frac{1}{\lambda^2}\right) \frac{\partial^2 A_x}{\partial x \partial z} \quad (51)$$

As noted above, the second equation is inhomogeneous, but the degree of inhomogeneity may be reduced with the following device. We write the vertical component A_z as the derivative of a function W , which has cylindrical symmetry, with respect to x :

$$A_z = \frac{\partial W}{\partial x} \tag{52}$$

With this definition of W , equation 39 which relates U and \bar{A} may be re-written as:

$$U = \frac{i\omega}{\gamma^2} \frac{\partial}{\partial x} \left(A_z + \frac{\partial W}{\partial z} \right) \tag{53}$$

Substituting the appropriate form of the function W in the inhomogeneous wave equation 61, we get:

$$\frac{\partial^3 W}{\partial r^2 \partial x} + \frac{1}{r} \frac{\partial^2 W}{\partial r \partial x} + \frac{1}{\lambda^2} \frac{\partial^3 W}{\partial z^2 \partial x} - \gamma_{tr}^2 \frac{\partial W}{\partial x} = \left(1 - \frac{1}{\lambda^2}\right) \frac{\partial^2 A_x}{\partial z \partial x} \tag{54}$$

Integrating this expression with respect to x we get:

$$\frac{\partial^2 W}{\partial r^2} + \frac{1}{r} \frac{\partial W}{\partial r} + \frac{1}{\lambda^2} \frac{\partial^2 W}{\partial z^2} - \gamma_{tr}^2 W = \left(1 - \frac{1}{\lambda^2}\right) \frac{\partial A_x}{\partial z} \tag{55}$$

Notice that the inhomogeneous term has been reduced from a second-order derivative to a first-order derivative.

Equations 50 and 55 are the manipulated forms of Maxwell's equations for which we seek a solution. One of the commonest methods used in solving equations of this type consists of "separation of variables." We assume that there are solutions, a_x to equation 50 and w to equation 55, which may be written in the forms:

$$a_x = X(z) \cdot \psi_1(r) \tag{56}$$

$$w = Z(z) \cdot \psi_2(r) \tag{57}$$

where ψ_1 and ψ_2 are functions of r but not of z , and where X and Z are functions of z but not of r . Substituting the assumed solution 56 into equation 50, we find:

$$X \psi_1'' + \frac{1}{r} X \psi_1' + X'' \psi_1 - \gamma_{tr}^2 X \psi_1 = 0 \tag{58}$$

Dividing both sides of the equation by $X \psi_1$, we find that the variables truly separate. The terms to the left of the equality sign are a function of r alone, and not of z , while the terms on the right of the equality sign are a function of z alone, and not of r . Therefore, the expression to the right of the equality sign cannot vary with the expression to the left of the equality sign, and therefore,

each expression must be a constant, which we will choose to call $-m^2$, for later convenience:

$$\frac{\psi_1''}{\psi_1} + \frac{1}{r} \frac{\psi_1'}{\psi_1} = \gamma_{tr}^2 - \frac{X''}{X} = -m^2 \tag{59}$$

The constant m is called the "separation constant," and it has the same dimensions as γ , or inverse distance. Writing the two separated equations, we have the following two complete differential equations:

$$\psi_1'' + \frac{1}{r} \psi_1' + m^2 \psi_1 = 0 \tag{60}$$

$$X'' - (\gamma_{tr}^2 + m^2) X = 0 \tag{61}$$

The well known solution to equation 61 is an exponential term with either positive or negative power, but we will not bother to express this solution immediately. The solution to equation 60 is the Bessel functions of the first and second kinds of order 0, $J_0(mr)$ and $H_0(mr)$.

Substituting the assumed solution 57 into equation 55, we have:

$$\psi_2'' Z + \frac{1}{r} \psi_2' Z + \frac{\psi_2}{\lambda^2} Z'' - \gamma_{tr}^2 \psi_2 Z = \left(1 - \frac{1}{\lambda^2}\right) \psi_1 X' \tag{62}$$

Again, dividing by the product $\psi_2 Z$ to obtain separation of the variables, we have:

$$\frac{\psi_2''}{\psi_2} + \frac{1}{r} \frac{\psi_2'}{\psi_2} = \gamma_{tr}^2 - \frac{1}{\lambda^2} \frac{Z''}{Z} + \left(1 - \frac{1}{\lambda^2}\right) \frac{\psi_1}{\psi_2} \frac{X'}{Z} \tag{63}$$

Inasmuch as the equation we have here for ψ_2 is precisely the same as the equation for ψ_1 in 59, we may take ψ_1 and ψ_2 as being the same function of r , and the separation constant in the two cases will be the same. The two separated differential equations are:

$$\psi_2'' + \frac{1}{r} \psi_2' + m^2 \psi_2 = 0 \tag{64}$$

$$Z'' - \lambda^2 (m^2 + \gamma_{tr}^2) Z = (\lambda^2 - 1) X' \tag{65}$$

It appears that the quantities $(m^2 + \gamma_{tr}^2)^{1/2}$ and $(m^2 + \gamma_{tr}^2)^{1/2}$ will occur frequently, so it will be convenient to use the shorter notation, n and \bar{n} for these, respectively.

We now have three ordinary differential equations to solve:

$$\psi'' + \frac{1}{r} \psi' + m^2 \psi = 0 \tag{66}$$

$$X'' - n^2 X = 0 \quad (67)$$

$$Z'' - (\lambda \bar{n})^2 Z = (\lambda^2 - 1) X' \quad (68)$$

The general solution to the inhomogeneous equation for Z (68) is made up of the general solution, say V , for the corresponding homogeneous differential equation (equation 68 with the term to the right of the equality sign set to zero) and the particular solution to the inhomogeneous equation. We can readily see that the function

$$-\frac{1}{m^2} X'$$

is the particular solution to the inhomogeneous equation by substituting this solution in the left-hand side of equation 68:

$$\frac{d^2}{dz^2} \left(-\frac{1}{m^2} X' \right) - (\lambda \bar{n})^2 \left(-\frac{1}{m^2} X' \right) = -\frac{1}{m^2} X''' + \left(\frac{\lambda \bar{n}}{m} \right)^2 X' \quad (69)$$

However, by differentiating equation 67 once with respect to z , we have

$$\begin{aligned} X''' &= n^2 X' \\ -\frac{1}{m^2} X''' + \left(\frac{\lambda \bar{n}}{m} \right)^2 X' &= \frac{-n^2 + (\lambda \bar{n})^2}{m^2} X' \\ &= \frac{-m^2 - \lambda^2 + \lambda^2 \bar{n}^2 + \lambda^2 \bar{n}^2}{m^2} X' \end{aligned} \quad (70)$$

and so

$$= (\lambda^2 - 1) X'$$

which provides the correct term for the right-hand side of the equality to satisfy equation 68. Therefore, we can write the general solution to the inhomogeneous equation in the form:

$$Z = V - \frac{1}{m^2} X' \quad (71)$$

This form would be of little value if we did not have a homogeneous equation in X that we can solve first. Now, we really have only two homogeneous solutions to get, X and V , and then we have the inhomogeneous solution by a linear combination of V and X' .

Let us now recall that the assumed solutions to the two original partial differential equations, (equations 56 and 57) are functions of the separation parameter m^2 . Any single value of m will generate a solution. However, in order to match boundary conditions, we want to express the solutions in a

more general form. This can be done by taking a linear combination (sum) of individual solutions for individual values of m^2 with arbitrary weighting factors. The parameter m^2 can assume any positive value or zero. The most general sum of such solutions will then be an integral of the Stefanescu type taken over a distribution of m from zero to infinity. Thus, the solution we are seeking for the x -component of the vector potential, A_x , is:

$$A_x = \frac{I \mu_0}{4\pi} \int_0^\infty X \cdot \int_0^\infty (mr) \, d\lambda m \quad (72)$$

(Note that the multiplying factor $I \mu_0 / 4\pi$ has been used only for later convenience.) The solution for the z -component of vector potential, A_z , is:

$$A_z = \frac{I \mu_0}{4\pi} \frac{\partial W}{\partial x} = \frac{I \mu_0}{4\pi} \frac{\partial}{\partial x} \int_0^\infty \int_0^\infty \mathcal{J}_0(mr) \, d\lambda m \quad (73)$$

Now we need only the forms of the functions, X , V and X' for a given set of layer parameters to complete our solution.

The two independent solutions to an equation of the type of 67 or 68 are of the form

$$e^{-apz} \quad \text{and} \quad e^{+apz}$$

So, for each layer, we may write a solution for X and V which is a linear combination of these two types of solutions, and then seek to find values for the arbitrary constants which suit boundary conditions.

a. Solution of equation 67:

$$X_p = d_p e^{-n_p z} + c_p e^{n_p z} \quad (74)$$

b. Solution to the homogeneous part of equation 68:

$$V_p = d_p e^{-n_p z} + c_p e^{n_p z} \quad (75)$$

(Note that the two sets of constants, d_p and C_p , are not necessarily the same for the two equations).

In order to evaluate the constants in these solutions, we must apply reasonable boundary conditions, which are best defined in terms of the original field components rather than the modified vector potential functions X and V .

Continuity of the tangential components of the electric and magnetic fields at the boundaries between layers requires continuity of A_x , A_z , $\partial A_x / \partial z$ and U . Equations (67) and (68) must be solved with consideration of continuity of X , Z , $\partial X / \partial z$, and $\rho_t (X + \partial Z / \partial z)$ at boundaries, as a consequence of continuity in A_x , A_z , $\partial A_x / \partial z$, and U , along with the conditions that both X and Z become vanishingly small as z is made large.

An addition condition is engendered for the function X by the presence of the dipole current source at the boundary $z = 0$. Tikhonov (1950) has shown that while X is continuous across the boundary $z = 0$, the vertical derivative X' has a discontinuity given by:

$$X'_0 - X'_1 = 2m \tag{76}$$

at $z = 0$. Inasmuch as the solution for X in the upper halfspace can contain only the exponential term which tends to zero upward along the z axis, we have:

$$X_0(z) = X_0(0) e^{mz} \tag{77}$$

This means that a derivative of X may be taken merely by multiplication by the factor m , and equation 76 might be written as

$$m X_1 - X'_1 = X_0(0) e^{mz} \tag{78}$$

$$X_1 = \frac{2m}{m - X'_1} X_0 \tag{79}$$

Tikhonov and Shakhshvarov (1956), as well as Zhogolev and others (1962) have suggested an approach to the solution of the problem which involves operations with ratio X/X' which arises in the last equation, rather than by a solution for X .

The ratio X/X' is then:

$$\frac{X_p}{X'_p} = -\frac{1}{n_p} \frac{d_p e^{-n_p z} + c_p e^{n_p z}}{d_p e^{-n_p z} - c_p e^{n_p z}} \equiv \frac{\tilde{R}_p}{n_p} \tag{79}$$

and the ratio V/V' is:

$$\frac{V_p}{V'_p} = \frac{1}{\lambda n_p} \frac{d_p e^{-\lambda n_p z} + c_p e^{\lambda n_p z}}{d_p e^{-\lambda n_p z} - c_p e^{\lambda n_p z}} \equiv \frac{R_p^*}{\lambda n_p} \tag{80}$$

The ratio, \tilde{R}_{np} , may be expressed as a hyperbolic function after some algebraic manipulation. First, we divide both the numerator and denominator of the ratio by the quantity $(d_p/c_p)^{1/2}$:

$$\tilde{R}_p = \frac{(d_p/c_p)^{1/2} e^{-n_p z} + (c_p/d_p)^{1/2} e^{n_p z}}{(d_p/c_p)^{1/2} e^{-n_p z} - (c_p/d_p)^{1/2} e^{n_p z}} \tag{81}$$

Then, using the identity $(d_p/c_p)^{1/2} = e^{\ln(d_p/c_p)^{1/2}}$, we have the form for the hyperbolic cotangent:

$$\tilde{R}_p = \frac{\exp[\ln(d_p/c_p)^{1/2} - n_p z] + \exp[-\ln(d_p/c_p)^{1/2} + n_p z]}{\exp[\ln(d_p/c_p)^{1/2} - n_p z] - \exp[-\ln(d_p/c_p)^{1/2} + n_p z]} \tag{82}$$

$$= \coth[n_p z - \ln(d_p/c_p)^{1/2}]$$

The constant $(d_p/c_p)^{1/2}$ may be eliminated by considering values for the ratio at two different depths, z_1 and z_2 , within a layer. At depth z_1 equation 82 is solved for $\ln(d_p/c_p)^{1/2}$:

$$-\ln(d_p/c_p)^{1/2} = \coth^{-1} \tilde{R}_{p1} - n_p z_1 \tag{83}$$

Then, the ratio at depth z_2 can be rewritten with expression 83 used in place of the constants:

$$\tilde{R}_{p2} = \coth[n_p z_2 - \ln(d_p/c_p)^{1/2}] \tag{84}$$

$$= \coth[n_p(z_2 - z_1) + \coth^{-1} \tilde{R}_{p1}]$$

This relation is, of course, valid only if the two points, z_1 and z_2 , are in the same layer. The utility of equation 84 is that we may compare values for the ratio \tilde{R}_p at the top and bottom of the p th layer. Normally, we will be concerned with field quantities at the surface of the earth, so we would like to express the values for \tilde{R}_1 at $z_2 = 0$ in terms of \tilde{R}_1 at the bottom of the first layer, at $z_1 = h_1$:

$$\tilde{R}_{1,z=0} = \coth[n_1 h_1 + \coth^{-1} \tilde{R}_{1,z=h_1}] \tag{85}$$

Inasmuch as X and X' are continuous across the boundary between the first and second layers, we have the continuity condition

$$\left. \frac{\tilde{R}_1}{n_1} \right|_{z=h_1} = \left. \frac{\tilde{R}_2}{n_2} \right|_{z=h_2} \tag{86}$$

We may now replace \tilde{R}_1 in equation 85 with its equivalent in terms of \tilde{R}_2 at $z = h_1$ from equation 86:

$$\tilde{R}_{1,z=0} = \coth[n_1 h_1 + \coth^{-1}(\frac{n_2}{n_1} \tilde{R}_{2,h_1})] \tag{87}$$

And again, \tilde{R}_2 at the top of the second layer can be written in terms of \tilde{R}_2 at the bottom of the second layer:

$$\tilde{R}_{2,h_1} = \coth [n_2 h_2 + \coth^{-1} (\tilde{R}_{2,z=h_1+h_2})] \quad (88)$$

\tilde{R}_2 at $z = h_1 + h_2$ then can be written in terms of \tilde{R}_3 at the top of the third layer. This process can be continued to the top of the last layer, layer N . Then, the ratio at the top of the last layer, expressed in terms of \tilde{R} at the bottom of the layer, which is infinitely thick, is:

$$\tilde{R}_{N,H} = \coth [n_N h_N + \coth^{-1} \tilde{R}_{N,z=\infty}]; \quad H = \sum_{p=1}^N h_p; \quad h_N = \infty \quad (89)$$

Thus, we have a sequential expression for $\tilde{R}_{1,z=0}$ which can be extended to any number of layers, and which involves only the repetition of the expression for two layers:

$$\begin{aligned} \tilde{R}_{1,z=0} &= \coth [n_1 h_1 + \coth^{-1} \frac{n_1}{n_2} \tilde{R}_2] \\ \tilde{R}_2 &= \coth [n_2 h_2 + \coth^{-1} \frac{n_2}{n_3} \tilde{R}_3] \\ \tilde{R}_3 &= \coth [n_3 h_3 + \coth^{-1} \frac{n_3}{n_4} \tilde{R}_4] \\ &\vdots \\ \tilde{R}_{N-1} &= \coth [n_{N-1} h_{N-1} + \coth^{-1} \frac{n_{N-1}}{n_N} \tilde{R}_N] \\ \tilde{R}_N &= 1 \end{aligned} \quad (90)$$

In effect, a multi-layer sequence can be built up by adding layers to the top of the sequence, one at a time.

This concept is important at this stage, because of a difficulty in the evaluation of the formula as it stands. This difficulty is apparent on considering the behavior of the inverse hyperbolic cotangent, which is shown graphically in figure 55. The inverse hyperbolic cotangent does not exist for arguments between zero and one. If such arguments are generated in evaluation of the chain in equation (90), it would indicate that not all conditions were considered when the expression was written in the form of a hyperbolic cotangent (equations 81 and 82). The argument of the inverse hyperbolic cotangent can easily be less than unity—this would happen in the last equation of the chain (90) if the wave number in the n th layer, n_N , were greater than the

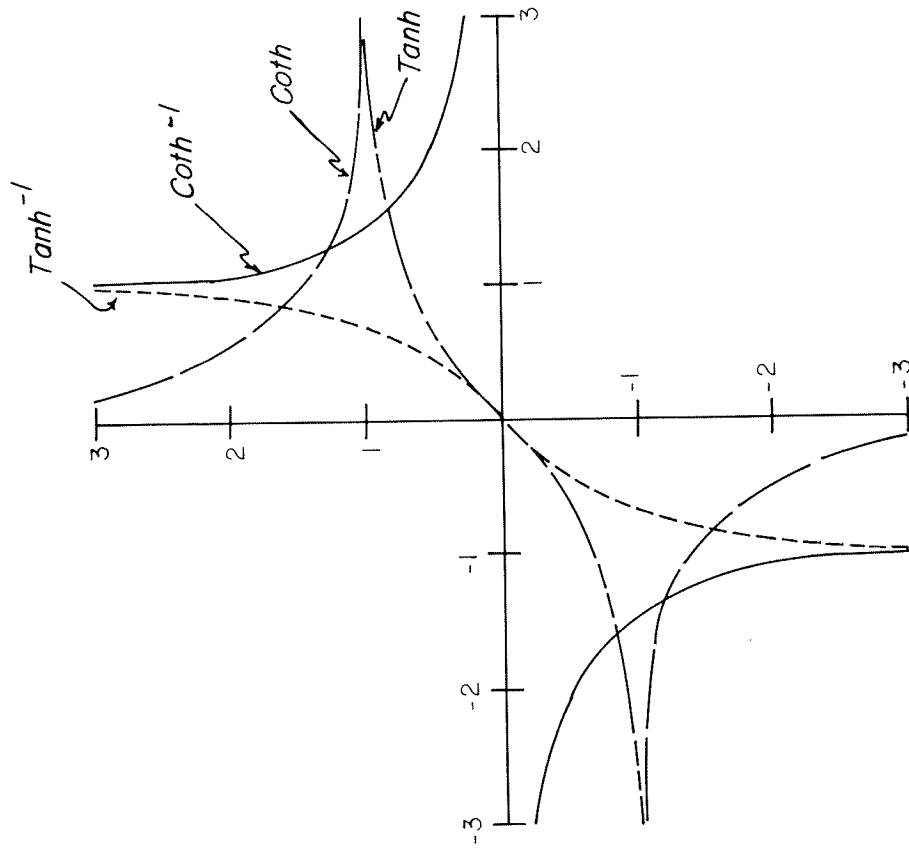


FIGURE 55.—Behavior of the hyperbolic functions.

wave number in the overlying layer, n_{N-1} . Then the ratio n_{N-1}/n_N would be less than unity.

However, it is well known that if the reciprocals of the electrical contrasts are considered, the values found for the R functions will be the reciprocals of those given in equation 90. This can be readily seen by considering two different two-layer sequences, one of which has an electrical contrast, $n_1/n_2 = k$ and the other of which has the reciprocal contrast, $n_1/n_2 = 1/k$. The two R functions will be

$$\tilde{R}(k) = \coth [n_1 h_1 + \coth^{-1} k] = \frac{k \coth n_1 h_1 + 1}{k + \coth n_1 h_1}$$

$$\tilde{R}\left(\frac{1}{k}\right) = \coth [n_1 h_1 + \coth^{-1} \frac{1}{k}] = \frac{\frac{1}{k} \coth n_1 h_1 + 1}{\frac{1}{k} + \coth n_1 h_1}$$

so

$$\tilde{R}(k) - \frac{1}{\tilde{R}(k)} = \frac{k \coth n_1 h_1 + 1}{k + \coth n_1 h_1} - \frac{\frac{1}{k} + \coth n_1 h_1}{\frac{1}{k} \coth n_1 h_1 + 1} = 0$$

This means that equation 90 might better be written as

$$\begin{aligned} \tilde{R}_{1,z=0} &= \coth [n_1 h_1 + \coth^{-1} \frac{n_1}{n_2} \tilde{R}_2] \text{ or } \tanh [n_1 h_1 + \tanh^{-1} \frac{n_1}{n_2} \tilde{R}_2] \\ \tilde{R}_2 &= \coth [n_2 h_2 + \coth^{-1} \frac{n_2}{n_3} \tilde{R}_3] \text{ or } \tanh [n_2 h_2 + \tanh^{-1} \frac{n_2}{n_3} \tilde{R}_3] \\ &\vdots \\ \tilde{R}_{N-1} &= \coth [n_{N-1} h_{N-1} + \coth^{-1} \frac{n_{N-1}}{n_N} \tilde{R}_N] \text{ or } \tanh [n_{N-1} h_{N-1} + \tanh^{-1} \frac{n_{N-1}}{n_N} \tilde{R}_N] \\ \tilde{R}_N &= 1 \end{aligned} \tag{90'}$$

(Note that instead of writing the reciprocals, the equivalent step of using the tangent instead of the cotangent has been employed.)

The same procedure can be followed with the V-function. If we designate the ratio for the V function as R^* , the analog to equation 82 may be written as:

$$R_p^* = \coth [\lambda \bar{n}_p z - \epsilon_n (\lambda/c_p)^{1/2}] \tag{91}$$

and to equation 83 as

$$-\epsilon_n (\lambda/c_p)^{1/2} = \coth^{-1} R_{p1}^* - \lambda \bar{n}_p z_1 \tag{92}$$

and to equation 84 as

$$R_{p2}^* = \coth [\lambda \bar{n}_p (z_2 - z_1) + \coth^{-1} R_{p1}^*] \tag{93}$$

and finally, to equation 85 as

$$R_{1,z=0}^* = \coth [\lambda \bar{n}_1 h_1 + \coth^{-1} R_{1,z=h_1}^*] \tag{94}$$

The expression for the R^* and \tilde{R} functions in terms of hyperbolic functions may sometimes be awkward to evaluate because of the necessity to interchange hyperbolic tangents and cotangents as the arguments move to either side from unity. An alternate expression for the R functions similar to that given by Sunde (1949) may be preferable in such cases. The development of the Sunde algorithm may be seen by starting with the first equation in 90. The inverse hyperbolic cotangent (or tangent, as the case may be) in this expression may be rewritten in terms of a natural logarithm (Abramowitz and Stegun, 1965, p. 87):

$$\begin{aligned} \tilde{R}_{1,z=0} &= \coth [n_1 h_1 + \frac{1}{2} \epsilon_n \frac{\frac{n_1}{n_2} \tilde{R}_2 + 1}{\frac{n_1}{n_2} \tilde{R}_2 - 1}] \text{ if } \frac{n_1}{n_2} \tilde{R}_2 > 1 \\ &= \tanh [n_1 h_1 + \frac{1}{2} \epsilon_n \frac{1 + \frac{n_1}{n_2} \tilde{R}_2}{1 - \frac{n_1}{n_2} \tilde{R}_2}] \text{ if } \frac{n_1}{n_2} \tilde{R}_2 < 1 \end{aligned} \tag{95}$$

For convenience, we can designate the argument of the natural logarithm as I/k :

$$\begin{aligned} k_a &= \frac{\frac{n_1}{n_2} \tilde{R}_2 - 1}{\frac{n_1}{n_2} \tilde{R}_2 + 1} \text{ if } \frac{n_1}{n_2} \tilde{R}_2 > 1 \\ k_b &= \frac{1 - \frac{n_1}{n_2} \tilde{R}_2}{1 + \frac{n_1}{n_2} \tilde{R}_2} \text{ if } \frac{n_1}{n_2} \tilde{R}_2 < 1 \end{aligned} \tag{96}$$

Next, the hyperbolic tangent or cotangent can be expanded in its exponential form:

$$\begin{aligned} \tilde{R}_{1,z=0} &= \frac{e^{n_1 h_1 - \frac{1}{2} \epsilon_n k_a} + e^{-(n_1 h_1 - \frac{1}{2} \epsilon_n k_a)}}{e^{n_1 h_1 - \frac{1}{2} \epsilon_n k_a} - e^{-(n_1 h_1 - \frac{1}{2} \epsilon_n k_a)}} \text{ if } \frac{n_1}{n_2} \tilde{R}_2 > 1 \\ \tilde{R}_{1,z=0} &= \frac{e^{n_1 h_1 - \frac{1}{2} \epsilon_n k_b} + e^{-(n_1 h_1 - \frac{1}{2} \epsilon_n k_b)}}{e^{n_1 h_1 - \frac{1}{2} \epsilon_n k_b} - e^{-(n_1 h_1 - \frac{1}{2} \epsilon_n k_b)}} \text{ if } \frac{n_1}{n_2} \tilde{R}_2 < 1 \end{aligned} \tag{97}$$

This may also be written as:

$$\tilde{R}_{1,z=0} = \frac{\frac{1}{\sqrt{k_a}} e^{\eta_1 h_1} + \sqrt{k_a} e^{-\eta_1 h_1}}{\frac{1}{\sqrt{k_b}} e^{\eta_1 h_1} - \sqrt{k_b} e^{-\eta_1 h_1}}$$

$$\tilde{R}_{1,z=0} = \frac{\frac{1}{\sqrt{k_b}} e^{\eta_1 h_1} + \sqrt{k_b} e^{-\eta_1 h_1}}{\frac{1}{\sqrt{k_a}} e^{\eta_1 h_1} - \sqrt{k_a} e^{-\eta_1 h_1}}$$

(98)

We now divide both the numerator and denominator by the first term in each:

$$\tilde{R}_{1,z=0} = \frac{1 + k_a e^{-2\eta_1 h_1}}{1 - k_a e^{-2\eta_1 h_1}} \quad \text{if } \frac{\eta_1}{\tilde{r}_2} \tilde{R}_2 > 1$$

$$\tilde{R}_{1,z=0} = \frac{1 - k_b e^{-2\eta_1 h_1}}{1 + k_b e^{-2\eta_1 h_1}} \quad \text{if } \frac{\eta_1}{\tilde{r}_2} \tilde{R}_2 < 1$$

However, $k_a = -k_b$, and so, these two expressions are the same. By convention,

if we define k as
$$k = \frac{1 - \frac{\eta_1}{\tilde{r}_2} \tilde{R}_2}{1 + \frac{\eta_1}{\tilde{r}_2} \tilde{R}_2} \quad \text{for all } \frac{\eta_1}{\tilde{r}_2} \tilde{R}_2$$
 (100)

we need only a single expression for $\tilde{R}_{1,z=0}$:

$$\tilde{R}_{1,z=0} = \frac{1 - k e^{-2\eta_1 h_1}}{1 + k e^{2\eta_1 h_1}} \quad \text{for all } \frac{\eta_1}{\tilde{r}_2} \tilde{R}_2 \quad (101)$$

The same process can be extended to the second equation in 90', as well as the following expressions. This leads to the development of a recursive formula for the \tilde{R} function similar to Sunde's resistivity kernel expression:

$$\tilde{R}_{1,2,3 \dots N} = \frac{1 - k_{1,2,3 \dots N} e^{-2\eta_1 h_1}}{1 + k_{1,2,3 \dots N} e^{2\eta_1 h_1}}$$

$$k_{1,2,3 \dots N} = \frac{\eta_2 - \eta_1 \tilde{R}_{2,3,4 \dots N}}{\eta_2 + \eta_1 \tilde{R}_{2,3,4 \dots N}}$$

$$\tilde{R}_{2,3,4 \dots N} = \frac{1 - k_{2,3,4 \dots N} e^{-2\eta_2 h_2}}{1 + k_{2,3,4 \dots N} e^{2\eta_2 h_2}}$$

$$k_{2,3,4 \dots N} = \frac{\eta_3 - \eta_2 \tilde{R}_{3,4,5 \dots N}}{\eta_3 + \eta_2 \tilde{R}_{3,4,5 \dots N}}$$

$$\vdots$$

$$\tilde{R}_{(N-1)N} = \frac{1 - k_{(N-1)N} e^{-2\eta_{N-1} h_{N-1}}}{1 + k_{(N-1)N} e^{-2\eta_{N-1} h_{N-1}}}$$

$$k_{(N-1)N} = \frac{\eta_N - \eta_{N-1}}{\eta_N + \eta_{N-1}} \quad (102)$$

The boundary condition at $z=h_1$ for V is written as:

$$\frac{\delta_{t,z=1}}{\lambda \bar{r}_1} R_1^* \Big|_{z=h_1} = \frac{\delta_{t,z=2}}{\lambda \bar{r}_2} R_2^* \Big|_{z=h_1} \quad (103)$$

We now see that the general N -layer expression for the R^* function equivalent to 90 is written as:

$$R_{1,z=0}^* = \coth [\lambda_1 \bar{r}_1 h_1 + \coth^{-1} \frac{\lambda_1 \bar{r}_1 \rho_1 R_2^*}{\lambda_2 \bar{r}_2 \rho_2}] \text{ or } \tanh [\lambda_1 \bar{r}_1 h_1 + \tanh^{-1} \frac{\lambda_1 \bar{r}_1 \rho_1 R_2^*}{\lambda_2 \bar{r}_2 \rho_2}]$$

$$R_{2,z=0}^* = \coth [\lambda_2 \bar{r}_2 h_2 + \coth^{-1} \frac{\lambda_2 \bar{r}_2 \rho_2 R_3^*}{\lambda_3 \bar{r}_3 \rho_3}] \text{ or } \tanh [\lambda_2 \bar{r}_2 h_2 + \tanh^{-1} \frac{\lambda_2 \bar{r}_2 \rho_2 R_3^*}{\lambda_3 \bar{r}_3 \rho_3}]$$

$$\vdots$$

$$R_{N-1}^* = \coth [\lambda_{N-1} \bar{r}_{N-1} h_{N-1} + \coth^{-1} \frac{\lambda_{N-1} \bar{r}_{N-1} \rho_{N-1} R_N^*}{\lambda_N \bar{r}_N \rho_N}]$$

$$\text{or } \tanh [\lambda_{N-1} \bar{r}_{N-1} h_{N-1} + \tanh^{-1} \frac{\lambda_{N-1} \bar{r}_{N-1} \rho_{N-1} R_N^*}{\lambda_N \bar{r}_N \rho_N}] \quad (104)$$

$$R_N^* = 1$$

This expression may also be rewritten in a Sunde-type algorithm, as follows:

$$R_{1,2,3 \dots N}^* = \frac{1 - k_{1,2,3 \dots N} e^{-2\lambda_1 \bar{r}_1 h_1}}{1 + k_{1,2,3 \dots N} e^{-2\lambda_1 \bar{r}_1 h_1}}$$

$$k_{1,2,3 \dots N} = \frac{\lambda_2 \bar{r}_2 \rho_2 - \lambda_1 \bar{r}_1 \rho_1 R_{2,3,4 \dots N}^*}{\lambda_2 \bar{r}_2 \rho_2 + \lambda_1 \bar{r}_1 \rho_1 R_{2,3,4 \dots N}^*}$$

$$\begin{aligned}
 R_{234 \dots N}^* &= \frac{1 - k_{234 \dots N}}{1 + k_{234 \dots N}} e^{-2\lambda_2 \bar{\rho}_2 h_2} \\
 K_{234 \dots N} &= \frac{\lambda_3 \bar{\rho}_3 \rho_{23} - \lambda_2 \bar{\rho}_2 \rho_{22}}{\lambda_3 \bar{\rho}_3 \rho_{23} + \lambda_2 \bar{\rho}_2 \rho_{22}} R_{345 \dots N}^* \\
 \vdots \\
 R_{(N-1)N}^* &= \frac{1 - k_{(N-1)N}}{1 + k_{(N-1)N}} e^{-2\lambda_{N-1} \bar{\rho}_{N-1} h_{N-1}} \\
 K_{(N-1)N} &= \frac{\lambda_N \bar{\rho}_N \rho_{N-1} - \lambda_{N-1} \bar{\rho}_{N-1} \rho_{N-1}}{\lambda_N \bar{\rho}_N \rho_{N-1} + \lambda_{N-1} \bar{\rho}_{N-1} \rho_{N-1}}
 \end{aligned}
 \tag{105}$$

Equations 90 and 104 are not sufficient to determine the functions X and V completely, inasmuch as there are only N-1 boundaries to be used with each of the two continuity conditions. Tikhonov (1950) has noted that while X is continuous across every layer boundary, including the surface of the earth, there is a discontinuity in X' at the earth's surface which has the size:

$$X'_0 - X'_1 = 2m \text{ at } z = 0$$

The reason for this may be seen by assuming that the current dipole is situated at a height h_0 above the earth's surface, and by expressing the electromagnetic field in the upper halfspace as the sum of a primary field, which increases without limit near the source, and a secondary field:

$$A_{x,0} = A_{x,0}^{(0)} + A_{x,0}^{(1)} \tag{106}$$

where $A_{x,0}^{(0)}$ is the vector potential for a homogeneous medium, and $A_{x,0}^{(1)}$ is the vector potential for the induction field.

In view of the symmetry of the problem, the electromagnetic field for an electric dipole in a homogeneous medium may be written in terms of a vector potential having only the single component, $A_x^{(0)}$. Symmetry also indicates that the differential equation for A_x (equation 54) should be solved in spherical coordinates. With the spherical symmetry, the vector potential does not depend on θ or ϕ , but only on the radius vector, R, so that:

$$\nabla^2 A_x^{(0)} = \frac{1}{R} \frac{\partial^2 (R A_x^{(0)})}{\partial R^2} = \frac{1}{R^2} A_x^{(0)} \tag{107}$$

The solution to this equation is:

$$A_x^{(0)} = \frac{C}{R} e^{-\gamma_0 R} \tag{108}$$

The constant of integration, C, may be evaluated by considering the application of the Biot-Savart law at zero-frequency:

$$B_z = \frac{I dl \mu_0 \sin \theta}{4\pi r^2} = -\frac{\partial A_x}{\partial y} = \frac{C \sin \theta}{r^2} \quad \omega \rightarrow 0 \tag{109}$$

We can make use of Sommerfeld's integral:

$$\frac{e^{-\gamma_0 \sqrt{r^2 + z^2}}}{(r^2 + z^2)^{3/2}} = \int_0^\infty \frac{e^{-m^2 \gamma_0^2}}{m^2 + \gamma_0^2} m J_0(mr) dm \tag{110}$$

to convert the solution in equation 109 to the same form as our solution for the secondary fields: (equations 83 and 84).

$$A_{x,0}^{(0)} = \frac{I dl \mu_0}{4\pi} \int_0^\infty \frac{m}{\eta_0} e^{-\eta_0 |z + h_0|} J_0(mr) dm \tag{111}$$

where h_0 is the height of the source.

In the upper half space, the coefficient d_0 in the solution for X (equation 74) must be zero for an axis which is z-positive downwards. Otherwise, since the 0-halfspace extends to infinity in the minus direction, the vector potential would increase without limit. Therefore, the expression for the vector potential for the secondary field in the upper halfspace is:

$$A_{x,0}^{(1)} = \frac{I dl \mu_0}{4\pi} \int_0^\infty c_0 e^{-\eta_0 z} J_0(mr) dm \tag{112}$$

Combining the two contributions to vector potential, we have for the upper halfspace:

$$A_{x,0} = \frac{I dl \mu_0}{4\pi} \int_0^\infty \left(\frac{m}{\eta_0} e^{-\eta_0 |z + h_0|} + c_0 e^{\eta_0 z} \right) J_0(mr) dm \tag{113}$$

The vector potential, A_x , in the first layer is:

$$A_{x,1} = \frac{I dl \mu_0}{4\pi} \int_0^\infty (c_1 e^{-\eta_1 z} + d_1 e^{-\eta_1 z}) J_0(mr) dm \tag{114}$$

Both A_x and $\partial A_x / \partial z$ are continuous across the surface of the earth ($z=0$), so we can write the boundary conditions as:

$$\begin{aligned} \frac{m}{n_0} e^{-n_0 h_0} + C_0 &= c_1 + d_1 = X_1 \\ -m e^{-n_0 h_0} + n_0 C_0 &= n_1 (c_1 - d_1) = X_1' \end{aligned}$$

Solving for the constant C_0 , we have:

$$C_0 = \frac{\frac{m}{n_0} \frac{X_1'}{X_1} + m}{n_0 - \frac{X_1'}{X_1}} e^{-n_0 h_0} \quad (115)$$

Thus the function X at the earth's surface can be expressed in terms of the ratio X_1/X_1' , which in turn is expressed in terms of the ratio function, \bar{R} :

$$X = \frac{2 m e^{-n_0 h_0}}{n_0 - \frac{X_1'}{X_1}} = \frac{2 m e^{-n_0 h_0}}{n_0 + \frac{n_1}{\bar{R}}} \quad (116)$$

and

$$X' = -\frac{n_1}{\bar{R}} X = -\frac{n_1}{\bar{R}} \frac{2 m e^{-n_0 h_0}}{n_0 + \frac{n_1}{\bar{R}}} \quad (117)$$

for x at $z = 0$, we have:

$$X' = n_0 C_0 - m e^{-n_0 h_0}$$

and

$$X = c_0 + \frac{m}{n_0} e^{-n_0 h_0}$$

or

$$X' = n_0 X - 2 m e^{-n_0 h_0} \quad (118)$$

Thus, at the earth's surface, there is discontinuity of X' of size $-2m e^{-n_0 h_0}$.

The other needed boundary condition at the earth's surface may be found in V' , the vertical derivative of the general solution to the inhomogeneous equation in Z . This solution consisted of a particular and a general part:

$$Z = V - \frac{X'}{m^2}$$

Continuity of scalar potential requires continuity in:

$$\rho_2 (X + Z') \quad (119)$$

but this is

$$\begin{aligned} \rho_2 (X + Z') &= \rho_2 (X + V' - \frac{X''}{m^2}) \\ &= \rho_2 V' + (\rho_2 - \frac{n^2}{m^2}) X \end{aligned}$$

Inasmuch as X is continuous across all boundaries, this indicates that the product $\rho_1 V'$ is continuous. Thus

$$\begin{aligned} \rho_{20} V_0' &= \rho_{21} V_1' \\ V_0' &= \frac{\rho_{21}}{\rho_{20}} V_1' = \frac{Y_0^2}{Y_0^2} V_1' \end{aligned} \quad (120)$$

Also, because the function V must remain finite for large negative values of z in the upper halfspace, only the positive exponential may be retained in the solution for the upper halfspace, and so:

$$V_0' = n_0 V_0 \quad (121)$$

$$\begin{aligned} \text{But } V_0 - V_1 &= (Z_0 + \frac{X_0'}{m^2}) - (Z_1 + \frac{X_1'}{m^2}) \\ &= \frac{1}{m^2} (X_0' - X_1') \\ &= \frac{2}{m} e^{-n_0 h_0} \end{aligned} \quad (122)$$

Combining equations 120, 121 and 122, we have

$$\frac{Y_0^2}{Y_1^2} \frac{V_0'}{V_1} - V_1 = \frac{2}{m} e^{-n_0 h_0} \quad (123)$$

Solving these equations for V_1 and V_1' at $z=0$, we have

$$V_1 = -\frac{R^*}{\lambda_1 n_1} \frac{2 e^{-n_0 h_0}}{m \left(\frac{Y_0^2}{Y_1^2} n_0 + \frac{R^*}{\lambda_1 n_1} \right)} \quad (124)$$

and

$$V_1' = \frac{2 e^{-n_0 h_0}}{m \left(\frac{Y_0^2}{Y_1^2} n_0 + \frac{R^*}{\lambda_1 n_1} \right)} \quad (125)$$

Now that we have the solution functions X_1, X_1', V_1 and V_1' , we can write expressions for the vertical and horizontal components of vector potential, the vertical derivatives of the vector potential and for the scalar potential at the earth's surface:

$$A_x = \frac{I dl \mu_0}{2\pi} \int_0^\infty \left[\frac{m e^{-n_0 h_0}}{n_0 + \frac{n_1}{R}} - \frac{R^*}{\lambda_1 \bar{n}_1} J_0(mr) \right] J_0(mr) dm \quad (126)$$

$$A_z = \frac{I dl \mu_0}{2\pi} \frac{\partial}{\partial x} \int_0^\infty \left[\frac{e^{-n_0 h_0}}{m} \frac{\frac{n_1}{R}}{n_0 + \frac{n_1}{R}} - \frac{R^*}{\lambda_1 \bar{n}_1} \frac{e^{-n_0 h_0}}{m \left(\frac{\gamma_0^2}{\gamma_1^2 n_0} + \frac{R^*}{\lambda_1 \bar{n}_1} \right)} \right] J_0(mr) dm \quad (127)$$

$$\frac{\partial A_x}{\partial z} = - \frac{I dl \mu_0}{2\pi} \int_0^\infty \frac{\frac{n_1}{R}}{n_0 + \frac{n_1}{R}} \frac{m e^{-n_0 h_0}}{n_0 + \frac{n_1}{R}} - \frac{R^*}{\lambda_1 \bar{n}_1} J_0(mr) dm \quad (128)$$

$$\begin{aligned} \mathcal{U} &= \frac{I dl \mu_0}{4\pi} \frac{\partial}{\partial x} \frac{\partial}{\partial x} \int_0^\infty (X_1 + Z_1') J_0(mr) dm \\ &= - \frac{I dl \mu_0}{2\pi} \frac{i\omega}{\gamma_0^2} \cos \theta \int_0^\infty \left[\frac{1}{\frac{\gamma_0^2}{\gamma_1^2 n_0} + \frac{R^*}{\lambda_1 \bar{n}_1}} - \frac{\gamma_{e1}^2}{n_0 + \frac{n_1}{R}} \right] e^{-n_0 h_0} J_1(mr) dm \end{aligned} \quad (129)$$

For a dipole at the earth's surface ($h_0=0$), these equations become:

$$A_x = \frac{I dl \mu_0}{2\pi} \int_0^\infty \frac{m}{n_0 + \frac{n_1}{R}} J_0(mr) dm \quad (130)$$

$$A_z = \frac{I dl \mu_0}{2\pi} \frac{\partial}{\partial x} \int_0^\infty \left[\frac{\frac{n_1}{R}}{m \left(n_0 + \frac{n_1}{R} \right)} - \frac{R^*}{m \lambda_1 \bar{n}_1} \frac{1}{\frac{\gamma_0^2}{\gamma_1^2 n_0} + \frac{R^*}{\lambda_1 \bar{n}_1}} \right] J_0(mr) dm \quad (131)$$

$$\frac{\partial A_x}{\partial z} = - \frac{I dl \mu_0}{2\pi} \int_0^\infty \frac{\frac{n_1}{R}}{n_0 + \frac{n_1}{R}} J_0(mr) dm \quad (132)$$

$$\mathcal{U} = - \frac{I dl \mu_0}{2\pi} \frac{i\omega}{\gamma_0^2} \cos \theta \int_0^\infty \left[\frac{1}{\frac{\gamma_0^2}{\gamma_1^2 n_0} + \frac{R^*}{\lambda_1 \bar{n}_1}} - \frac{\gamma_{e1}^2}{n_0 + \frac{n_1}{R}} \right] J_1(mr) dm \quad (133)$$

We are now in a position to write integrals for electromagnetic field components about an electric dipole at the surface of a stratified earth:

$$B_z = - \frac{I dl \mu_0}{2\pi} \frac{\partial}{\partial y} \int_0^\infty \frac{m}{n_0 + \frac{n_1}{R}} J_0(mr) dm \quad (134)$$

$$B_x = \frac{I dl \mu_0}{2\pi} \frac{\partial^2}{\partial x \partial y} \int_0^\infty \left[\frac{\frac{n_1}{R}}{m \left(n_0 + \frac{n_1}{R} \right)} - \frac{R^*}{m \lambda_1 \bar{n}_1} \frac{1}{\frac{\gamma_0^2}{\gamma_1^2 n_0} + \frac{R^*}{\lambda_1 \bar{n}_1}} \right] J_0(mr) dm \quad (135)$$

$$\begin{aligned} E_x &= \frac{I dl i\omega}{2\pi} \int_0^\infty \frac{m}{n_0 + \frac{n_1}{R}} J_0(mr) \\ &+ \frac{I dl \mu_0 i\omega}{2\pi \gamma_{e1}^2} \frac{\partial}{\partial x} \int_0^\infty \left[\frac{1}{\frac{\gamma_0^2}{\gamma_1^2 n_0} + \frac{R^*}{\lambda_1 \bar{n}_1}} - \frac{\gamma_{e1}^2}{n_0 + \frac{n_1}{R}} \right] J_1(mr) dm \end{aligned} \quad (136)$$

and so on. These equations are the solution to our problem of determining how to measure resistivity with an electric dipole as a source!

Solution of Maxwell's equations for a vertical-axis magnetic dipole source

Now let us pursue the solution to the same problem but with a vertical-axis magnetic dipole serving as a source. Fortunately, many of the steps in solution of the problem are the same, so we do not have such a mass of analysis to go through. Taking advantage of the condition that $\text{div } \vec{E}^* = 0$ (for a uniform medium with no sources), we find it is convenient to define a new vector potential, \vec{A}^* , such that:

$$\vec{E}^* = i\omega \nabla \times \vec{A}^* \quad (137)$$

(note that the asterisk is used to distinguish fields due to a magnetic dipole source from fields due to an electric dipole source).

As was the argument in the case of the electric vector potential, \vec{A}^* , we would expect the magnetic vector potential, \vec{A}^* , to have components parallel to the flow of magnetic flux lines from the source and in the medium. A coil of wire energized with current behaves exactly as a magnetic dipole directed along the coil axis. Thus, the current flowing in the loop contributes only a vertical component to the vector potential. Current flow induced in the earth, provided the earth is laterally uniform, forms loops in horizontal planes, with axes coincident with the axis of the source loop. Each of these induced current loops also acts as a magnetic dipole, and contributes only a vertical component to the vector potential. The magnetic flux lines outside the dipole sources have other than vertical components, as indicated in figure 56, but inasmuch as we have assumed that all of space has the same magnetic permeability, μ_0 , these lines exhibit perfect radial symmetry, and their contributions to other than vertical components of the vector potential cancel. Therefore, for a vertical-axis magnetic dipole source over a laterally uniform medium with no contrasts in magnetic permeability, the magnetic vector potential, \vec{A}^* , has only a vertical component, A_z^* .

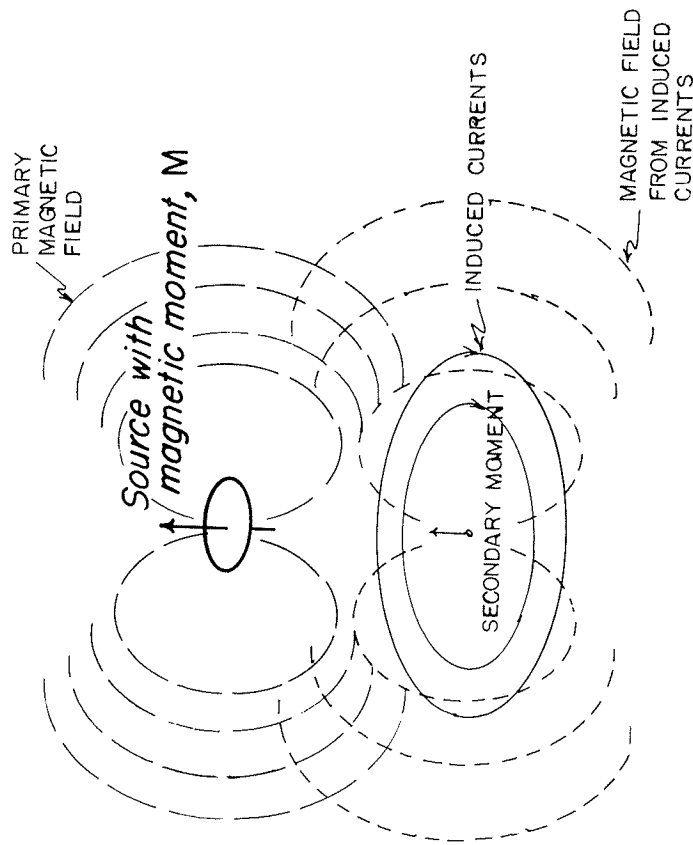


FIGURE 56. — Primary magnetic flux from a magnetic dipole source and secondary magnetic flux from currents induced in the earth.

Substituting \vec{A}^* in Maxwell's first equation, we have the following result for the field about a vertical magnetic dipole:

$$\begin{aligned} \nabla \wedge \vec{B}^* &= \left(\frac{i\omega H_0}{R_0} + \omega^2 \epsilon \mu_0 \right) \nabla \wedge \vec{A}^* \\ &= -\gamma_e^2 \nabla \times \vec{A}^* \end{aligned} \tag{138}$$

Doing the inverse curl operation, this equation becomes:

$$\vec{B}^* = -\gamma_e^2 \vec{A}^* - \nabla \mathcal{U}^* \tag{139}$$

(The grad \mathcal{U}^* term is the most general constant of integration term which can be introduced as a result of the inverse curl operation).

Replacing \vec{E}^* by $i\omega \text{curl } \vec{A}^*$ in Maxwell's second equation, we have

$$\begin{aligned} \nabla \wedge (\nabla \wedge \vec{A}^*) &= \vec{B}^* \\ \Delta \vec{A}^* - \nabla (\nabla \cdot \vec{A}^*) &= \vec{B}^* \end{aligned} \tag{140}$$

or

Selecting as our arbitrary gauge condition the relation

$$\mathcal{U}^* = -\nabla \cdot \vec{A}^* \tag{141}$$

we have:

$$\begin{aligned} \Delta \vec{A}^* + \nabla \mathcal{U}^* &= -\vec{B}^* \\ &= \gamma_e^2 \vec{A}^* + \nabla \mathcal{U}^* \end{aligned} \tag{142}$$

or

$$(\Delta - \gamma_e^2) \vec{A}^* = 0$$

This is precisely the same equation as the one for A_z in the development of the vector potential for an electric dipole source. Therefore, the solution is also the same:

$$A_z^* = \frac{M \mu_0}{4\pi r} \int_0^\infty X J_0(mr) dm \tag{143}$$

Let us now consider the continuity conditions which may be applied to further define the solution X^* . Inasmuch as the vector potential has only one component, we have only three field components to be concerned with:

a. The azimuthal electric field,

$$E_\phi^* = -i\omega \frac{\partial A_z^*}{\partial r} \tag{144}$$

b. The vertical magnetic field.

$$\begin{aligned} B_z^* &= -\gamma_\rho^2 A_z^* + \frac{\partial^2 A_z^*}{\partial z^2} \\ &= -\frac{1}{r} \frac{\partial}{\partial r} \left(r \frac{\partial A_z^*}{\partial r} \right) \end{aligned} \quad (145)$$

c. The radial magnetic field,

$$B_r^* = \frac{\partial^2 A_z^*}{\partial r \partial z} \quad (146)$$

We require continuity of tangential components of electric field and magnetic induction at the boundaries, so the sole component of vector potential, A_z^* , as well as its vertical derivative, $\partial A_z^*/\partial z$ is continuous.

These are the same two boundary conditions we had for A_x in the case of an electric dipole source, so we may follow the same reasoning in evaluating the boundary conditions and write an expression for the ratio X_p^*/X_p' as in the equation (79), leading to the following result for an N-layered anisotropic earth:

$$\frac{X_p^*}{X_p'} = \frac{R_p}{n_p}$$

where

$$R_p = \coth \left\{ n_1 h_1 + \coth^{-1} \frac{n_1}{n_2} \left[\coth (n_2 h_2 + \coth^{-1} \dots \coth^{-1} \frac{n_N}{n_{N-1}}) \dots \right] \right\} \quad (147)$$

For the upper halfspace (the atmosphere) we can separate the vector potential into primary and secondary parts:

$$A_{z_0}^* = A_{z_0}^{*(0)} + A_{z_0}^{*(1)} \quad (148)$$

where $A_{z_0}^{*(0)}$ is the vector potential for a homogeneous medium and $A_{z_0}^{*(1)}$ is the vector potential for the induction field (analogous to equation 106).

The vector potential for the magnetic dipole source in a homogeneous medium can be derived in exactly the same manner as was done for the electric dipole (equations 107-109) with the results:

$$A_{z_0}^{*(0)} = \frac{M \mu_0}{4\pi} \frac{e^{-\gamma_0 R}}{R} \quad (149)$$

where M is the magnetic moment of the source, the product of the area, number of turns and current.

Using the Sommerfeld integral, this can be expressed as a Hankel transform:

$$A_{z_0}^{*(0)} = \frac{M \mu_0}{4\pi} \int_0^\infty \frac{m}{n_0} e^{-n_0 |z+h_0|} J_0(mr) dm \quad (150)$$

In the upper halfspace, the solution for X_0^* can contain only a positive exponential term if the secondary field is to disappear at great distances in the $-z$ direction:

$$X_0^* = C_0^* e^{n_0 z} \quad (151)$$

so that the vector potential in the upper halfspace is:

$$A_{z_0}^* = \frac{M \mu_0}{4\pi} \int_0^\infty \left(C_0^* e^{n_0 z} + \frac{m}{n_0} e^{-n_0 |z+h_0|} \right) J_0(mr) dm \quad (152)$$

Applying the conditions of continuity in A_z^* and $\partial A_z^*/\partial z$ at the ground surface, as in equation 115, we can evaluate the constant C_0^* :

$$C_0^* = \frac{\frac{m}{n_0} \frac{X_p^*}{X_p'} + m}{n_0 - \frac{X_p^*}{X_p'}} e^{-n_0 h_0} \quad (153)$$

Thus, the functions X^* and $X^{*'}$ at the earth's surface are the same as those given in equations 116 and 117. The vector potential solutions we are seeking for the magnetic dipole source are therefore:

$$A_z^* = \frac{M \mu_0}{2\pi} \int_0^\infty \frac{m}{n_0 + \frac{n_0}{R}} J_0(mr) dm \quad (154)$$

$$\frac{\partial A_z^*}{\partial z} = -\frac{M \mu_0}{2\pi} \int_0^\infty \frac{n_0}{R} \frac{m}{n_0 + \frac{n_0}{R}} J_0(mr) dm \quad (155)$$

and the electromagnetic field components are therefore:

$$E_\varphi^* = -\frac{M \mu_0}{2\pi} i \omega \frac{\partial}{\partial r} \int_0^\infty \frac{m}{n_0 + \frac{n_0}{R}} J_0(mr) dm \quad (156)$$

$$B_z^* = -\frac{M \mu_0}{2\pi} \frac{1}{r} \frac{\partial}{\partial r} \left\{ r \frac{\partial}{\partial r} \int_0^\infty \frac{m}{n_0 + \frac{n_0}{R}} J_0(mr) dm \right\} \quad (157)$$

$$B_r^* = -\frac{M \mu_0}{2\pi} \frac{\partial}{\partial r} \int_0^\infty \frac{n_0}{R} \frac{m}{n_0 + \frac{n_0}{R}} J_0(mr) dm \quad (158)$$

A UNIFORM EARTH AND THE PROBLEM OF DEFINING APPARENT RESISTIVITY

It has become a convention in electrical geophysics to define "apparent resistivity" as the resistivity one would compute from measured mutual inductance and receiver-transmitter geometry, assuming the earth is uniform. Let us first consider equations 156-158 which give the field components for a vertical-axis magnetic dipole source. For a uniform earth, \bar{R} becomes unity and the expressions for these field components are:

$$E_{\phi}^* = -i\omega \frac{M\mu_0}{2\pi} \frac{\partial}{\partial r} \int_0^{\infty} \frac{m}{n_0 + n_1} J_0(mr) dm \quad (159)$$

$$B_z^* = -\frac{M\mu_0}{2\pi} \frac{1}{r} \frac{\partial}{\partial r} \left[r \frac{\partial}{\partial r} \int_0^{\infty} \frac{m}{n_0 + n_1} J_0(mr) dm \right] \quad (160)$$

$$B_r^* = -\frac{M\mu_0}{2\pi} \frac{\partial}{\partial r} \int_0^{\infty} \frac{mn_1}{n_0 + n_1} J_0(mr) dm \quad (161)$$

The integral in the first two equations can be converted to a known form by multiplying numerator and denominator by the quantity $(n_0 - n_1)$:

$$E_{\phi}^* = -i\omega \frac{M\mu_0}{2\pi} \frac{\partial}{\partial r} \int_0^{\infty} \frac{mn_0 - mn_1}{\gamma_0^2 - \gamma_1^2} J_0(mr) dm \quad (162)$$

This is now the sum of two integrals, each of the Sommerfeld form:

$$\int_0^{\infty} m \epsilon^{-n_1 z} J_0(mr) dm = \frac{e^{-\gamma(r^2+z^2)^{1/2}}}{(r^2+z^2)^{1/2}}$$

Differentiating both sides of this identity with respect to z and setting $z=0$, we have:

$$\int_0^{\infty} mn J_0(mr) dm = -\frac{e^{-\gamma r}}{r^3} (1 + \gamma r) \quad (163)$$

Using this identity to integrate equation 162, we have:

$$E_{\phi}^* = -i\omega \frac{M\mu_0}{2\pi(\gamma_0^2 + \gamma_1^2)} \left\{ \frac{\partial}{\partial r} \left[\frac{1}{r^3} e^{-\gamma_0 r} (1 + \gamma_0 r) + e^{-\gamma_1 r} (1 + \gamma_1 r) \right] \right\} \quad (164)$$

Carrying out the differentiation indicated in equation 164, we have the following result:

$$E_{\phi}^* = -i\omega \frac{M\mu_0}{2\pi(\gamma_0^2 - \gamma_1^2)} \left\{ \frac{1}{r^3} \left[-\gamma_0 e^{-\gamma_0 r} (1 + \gamma_0 r) + \gamma_0 e^{-\gamma_0 r} - \gamma_1 e^{-\gamma_1 r} (1 + \gamma_1 r) + \gamma_1 e^{-\gamma_1 r} \right] - \frac{3}{r^4} \left[e^{-\gamma_0 r} (1 + \gamma_0 r) + e^{-\gamma_1 r} (1 + \gamma_1 r) \right] \right\}$$

$$= -i\omega \frac{M\mu_0}{2\pi(\gamma_0^2 - \gamma_1^2)} \frac{1}{r^4} \left\{ e^{-\gamma_0 r} [3 + 3\gamma_0 r + (\gamma_0 r)^2] - e^{-\gamma_1 r} [3 + 3\gamma_1 r + (\gamma_1 r)^2] \right\} \quad (165)$$

Here, it is assumed that a single value for wave number, γ_0 , describes the properties of the 0-th layer. If the 0-th layer is the atmosphere, the conductivity may be taken as zero and the wave number reduces to a single value for both the longitudinal and transverse directions:

$$\gamma_0 = i\omega (\epsilon_0/\mu_0)^{1/2} \quad (166)$$

Inasmuch as $\epsilon_0 = 3.85 \times 10^{-12}$ F/m and $\mu_0 = 4\pi \times 10^{-7}$ H/m, the wave number in the atmosphere has a magnitude of 3.3×10^{-9} per meter.

It is not necessary at this point to assume that the 0-th layer is the atmosphere. Rather it might be assumed that the 0-th layer is sea water, as would be the case for measurements made on the sea bottom. In this case also, the wave number reduces to a single value for both the longitudinal and transverse directions. However, inasmuch as sea water is an excellent conductor, with $\sigma = 3$ to 5 mhos per meter, the displacement current term in the expression for wave number could be neglected in comparison with the conduction current term:

$$\gamma_0 = \left(\frac{\omega\mu_0\sigma}{2} \right)^{1/2} + i \left(\frac{\omega\mu_0\sigma}{2} \right)^{1/2} \quad (167)$$

For sea water, the magnitude of the inphase and quadrature components of wave number would be about 2.5×10^{-3} per meter.

In the first case, the wave number at any reasonable frequency for use in electromagnetic sounding would be very small in the atmosphere in comparison with that in the earth, and we should consider the possibility of dropping small terms from equation 165. Let us consider the ratio of the sum of terms containing γ_0 to the sum in terms containing γ_{11} :

$$\frac{3 + 3\gamma_0 r + (\gamma_0 r)^2}{3 + 3\gamma_{11} r + (\gamma_{11} r)^2} e^{-(\gamma_0 + \gamma_{11})r} \quad (168)$$

We know for a certainty that $\gamma_0 r \ll \gamma_{11} r$. Therefore, for small values of $\gamma_{11} r$ (say less than unity), only the exponential multiplier in 168 need be considered. Here γ_0 may be neglected in comparison with γ_{11} and it is readily

apparent that we do not need to consider that γ_0 has any value other than zero. In the term $(3 + 3\gamma_0 r + \gamma_0^2 r^2)$, the second two terms can usually be neglected, inasmuch as $\gamma_0 r \ll 1$ in most cases. Taking $\gamma_0 \approx 0$, equation 165 simplifies to:

$$E_\varphi^* = \frac{M\mu_0}{2\pi\sigma} \cdot \frac{1}{r^2} \left\{ 3 - e^{-\lambda_1 r} \left[3 + 3\lambda_1 r + (\lambda_1 r)^2 \right] \right\} \quad (169)$$

This equation is not really so simple as it looks, inasmuch as the wave number is a complex quantity. For frequencies below about 10 kilohertz, the displacement current term can be neglected for most rocks, and we can write the complex wave number as:

$$\lambda_1 = G_1 + iG_2 \quad (170)$$

$$G_1 = (\omega\mu\sigma/2)^{1/2}$$

Thus, for the purpose of numerical evaluation, equation 169 can be rewritten as two equations, one with only the real terms and one with only the imaginary terms:

$$\begin{aligned} \text{Real}\{E_\varphi^*\} &= 3 - e^{-G_1 r} \left[(3 + 3G_1 r) \cos G_2 r - (3G_1 r + 2G_2^2 r^2) \sin G_2 r \right] \\ \text{Imag}\{E_\varphi^*\} &= i \left[(3 + 3G_1 r) \sin G_2 r - (3G_1 r + 2G_2^2 r^2) \cos G_2 r \right] e^{-G_1 r} \end{aligned} \quad (171)$$

These two expressions can be evaluated numerically without any great difficulty. It is interesting to note that the only parameter to which values need be assigned is the product $G_1 r$, which is a dimensionless spacing factor. Numerical values for the real and imaginary parts of E_φ computed from these expressions (equations 171 and 172) are given in table 10, while a single curve for each equation is shown in figure 57.

TABLE 10. — Tangential electric field about a vertical-axis magnetic dipole

Gr	Real component, multiplied by $\frac{4\pi r^3 \sigma}{\mu_0 M}$	Imaginary component, multiplied by $\frac{4\pi r^3 \sigma}{\mu_0 M}$
0.1	.99975	.004734
0.2	.99812	.017878
0.3	.99406	.037883
0.4	.96681	.063270
0.5	.97591	.092657

TABLE 10 (Cont.)

Gr	Real component, multiplied by $\frac{4\pi r^3 \sigma}{\mu_0 M}$	Imaginary component, multiplied by $\frac{4\pi r^3 \sigma}{\mu_0 M}$
0.6	.96109	.12177
0.7	.94229	.15817
0.8	.91961	.19274
0.9	.89325	.22670
1.0	.86353	.25960
1.2	.79552	.31985
1.4	.71901	.36989
1.6	.63774	.40782
1.8	.55505	.43305
2.0	.47400	.44601
2.2	.39702	.44784
2.4	.32592	.44014
2.6	.26189	.42471
2.8	.20560	.40340
3.0	.15723	.37797
3.2	.11661	.35003
3.4	-.08326	.32094
3.6	.05655	.29183
3.8	.03571	.26358
4.0	.01993	.23684
4.2	.00940	.21204
4.4	.00034	.18945
4.6	-.00494	.16916
4.8	-.00808	.15118
5.0	-.00962	.13542
5.5	-.00923	.10465
6.0	-.00635	.08368
6.5	-.00341	.06943
7.0	-.00138	.05943
7.5	-.00022	.05200

where M is the moment of the source.

NORMALIZED ELECTRIC FIELD

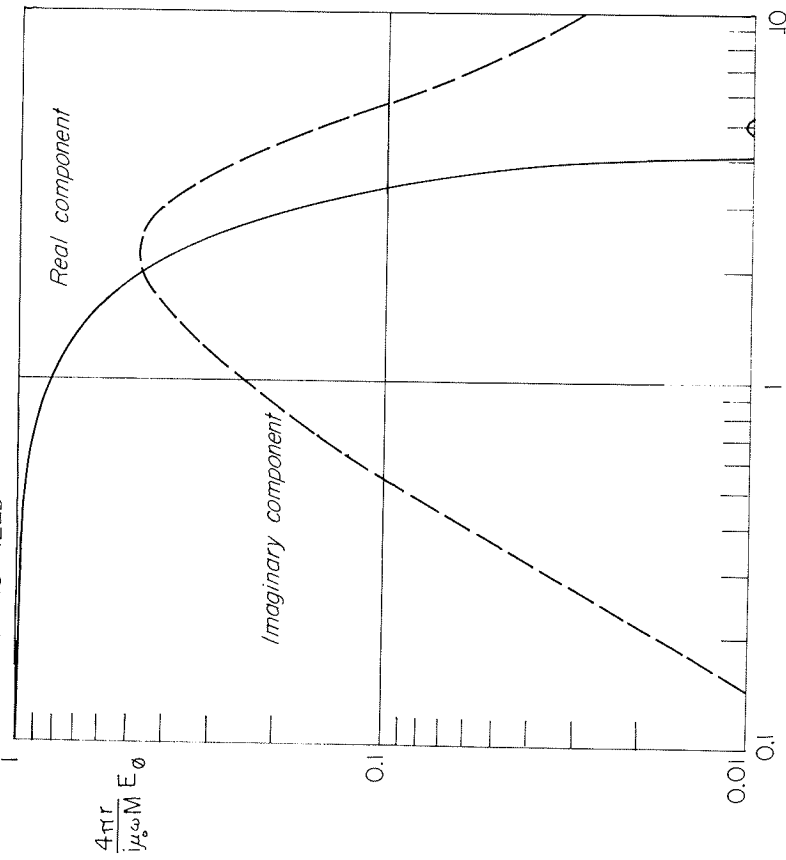


FIGURE 57.—Components of tangential electric field generated by a vertical-axis magnetic dipole source located on the surface of a homogeneous earth. G is the real part of the wave number in the earth, and r is the separation from source to receiver.

It is difficult to visualize the behavior of $E\phi^*$ from the equations (171 and 172), and so it is worthwhile to examine the asymptotic behavior both for large values of the dimensionless spacing, $\gamma_1 r$, and for small values. For small values of $\gamma_1 r$, which would be equivalent to a small source-receiver separation, r , or to a low frequency or conductivity in the wave number expression, making, γ_1 small, we have:

$$E_\phi^* \Big|_{\gamma_1 r \rightarrow 0} \approx \frac{M\mu_0}{2\pi\sigma} \cdot \frac{1}{r^4} \left\{ 3 - \left[1 - \gamma_1 r + \frac{\gamma_1^2 r^2}{2} \right] \cdot \left[3 + 3\gamma_1 r + \gamma_1^2 r^2 \right] \right\}$$

$$= \frac{M\mu_0}{2\pi\sigma} \cdot \frac{1}{2} \cdot \frac{\gamma_1^2 r^2}{r^4}$$

$$= i \frac{M\mu_0}{4\pi r^2} \omega\mu_0 \tag{173}$$

That is, the tangential electric field for $\gamma_1 r = 0$ is zero, and increases as $(\gamma_1 r)^2$ for small values of the dimensionless spacing.

Of primary concern is the fact that for small values of $\gamma_1 r$, the observed electric field is independent of the conductivity of the earth, and so, is of no value in attempting to measure that conductivity. We should also note that for small $\gamma_1 r$, the response is entirely out-of-phase.

Next, let us consider what happens at large values of the dimensionless spacing. Here, the exponential becomes vanishingly small and we are left with:

$$E_\phi^* \Big|_{\gamma_1 r \rightarrow \infty} = \frac{3M\mu_0}{2\pi\sigma r^4} \tag{174}$$

In this case, the response does depend on conductivity and is entirely real. We can solve this last expression explicitly for conductivity, and so define apparent conductivity for the case in which $\gamma_1 r$ is sufficiently large. In comparing the curve for the approximate expression in equation 174 with the curve for the true expression for the real part of the tangential voltage in equation 171, as shown on figure 57, it is apparent that $\gamma_1 r$ is sufficiently large when it exceeds about 6, or about one real wave length in the earth.

The definition of apparent conductivity for $\gamma r > 6$ is:

$$\sigma_a = \frac{3\mu_0}{2\pi r^4} \frac{M}{E_\phi^*} \tag{175}$$

This is not entirely satisfactory, inasmuch as some knowledge of the actual conductivity of the earth is required to assure that the inequality is satisfied. Furthermore, quite commonly it is difficult to use such large spacings, r , that $\gamma r > 6$, inasmuch as the signal strength decreases as the fourth power of the spacing.

For small values of $\gamma_1 r$, it is possible to obtain an alternate expression for apparent resistivity by including the next higher order terms in $\gamma_1 r$, those to the third power, in the expansion of the exponential in equation 173:

$$E_\phi^* \Big|_{\gamma_1 r \rightarrow 0} = i\omega\mu_0 \frac{M\mu_0}{4\pi r^2} \left\{ 1 + 3\gamma_1 r \right\} \tag{176}$$

If we were to measure only the in-phase component of voltage for small spacing, we would have a quantity which depends on the square root of conductivity, and which could be solved to provide an expression for apparent conductivity as follows:

Let us next consider the vertical component of magnetic induction from a vertical-axis magnetic dipole source for a uniform earth, as given in equation 160. The integral is the same as the one in equation 159 so the same result may be taken. The magnetic induction is then:

$$B_z^* = -\frac{M\mu_0}{2\pi} \cdot \frac{1}{r} \frac{\partial}{\partial r} \left\{ r \frac{\partial}{\partial r} f(r) \right\} \quad (179)$$

where

$$f(r) = \frac{1}{\gamma^2 r^4} \left\{ 3 - e^{-\gamma r} [3 + 3\gamma r + (\gamma r)^2] \right\}$$

Carrying out the differentiation, we have:

$$B_z^* = -\frac{M\mu_0}{2\pi\gamma^2} \cdot \frac{1}{r^5} \left\{ q - e^{-\gamma r} [q + 9\gamma r + 5(\gamma r)^2 + (\gamma r)^3] \right\} \quad (180)$$

For small values of γr , the exponential may be replaced with a short series. Retaining only first order terms, equation 180 reduces to:

$$B_z^* = -\frac{M\mu_0}{2\pi\omega\sigma} \cdot \frac{1}{r^5} \left\{ q - \left[1 - \gamma r + \frac{(\gamma r)^2}{2} - \frac{(\gamma r)^3}{6} + \dots \right] \cdot [q + 9\gamma r + 5(\gamma r)^2 + (\gamma r)^3] \right\} \\ \approx -\frac{\mu_0 M}{4\pi r^3} \quad (181)$$

It should be noted that the magnetic induction (the vertical component) is independent of the conductivity of the earth in this first approximation, and that the received field is completely imaginary. If first and second order terms are retained in the approximation for small γr , we have:

$$B_z^* \approx -i \frac{\mu_0 M}{4\pi r^3} (1 + 2\gamma r) = -i \frac{\mu_0 M}{4\pi r^3} (1 + 2Gr + 2iGr) \quad (182)$$

The real part of this second approximation contains a term which is proportional to the square root of conductivity, and so can be used to define an apparent conductivity:

$$\sigma_a \Big|_{\gamma r \rightarrow 0} = \frac{8\pi^2 r^4}{\mu_0^2 \omega^2} \left(\frac{B_z^{real}}{M} \right)^2; \quad |\gamma r| \ll 1 \quad (183)$$

At the other extreme, for large values of γr , the term multiplied by the exponential may be neglected, with the result:

$$B_z^* = -\frac{M}{2\pi\omega\sigma} \cdot \frac{q}{r^5}; \quad |\gamma r| \gg 1 \quad (184)$$

The apparent conductivity defined from this expression is:

$$\sigma_a \Big|_{\gamma r \rightarrow \infty} = -\frac{q}{2\pi\omega r^5} \left(\frac{M}{B_z^*} \right); \quad |\gamma r| \gg 1 \quad (185)$$

In this case, the vertical component of magnetic induction is entirely real. In numerical evaluation of the exact expression, given in equation 180, it is necessary to divide the real and imaginary parts. These are:

$$B_z^{*real} = -\frac{M}{2\pi\omega\sigma} \cdot \frac{1}{r^5} \left\{ q + e^{-Gr} [(q + 9Gr + 2G^3r^3) \cos Gr + (9Gr - 10G^2r^2 - 2G^3r^3) \sin Gr] \right\} \quad (186)$$

$$B_z^{*imag} = -\frac{iM}{2\pi\omega\sigma} \cdot \frac{1}{r^5} \left\{ e^{-Gr} [(9Gr - 10G^2r^2 - 2G^3r^3) \cos Gr - (q + 9Gr + 2G^3r^3) \sin Gr] \right\} \quad (187)$$

The numerical values for the real and imaginary parts of the vertical magnetic induction from a vertical-axis magnetic dipole source are listed in table II, and are given graphically in figure 59.

The expression for the radial component of the magnetic induction field about a vertical-axis magnetic dipole source, given in equation 161, presents a more difficult problem in that the integral cannot be reduced to a simple closed form. However, we can get asymptotic expressions for the radial magnetic field using an approach similar to that used in evaluating the other two integrals. We first multiply the integrand by $(n_0 - n_1)/(n_0 - n_1)$, thus dividing the integral into three simpler integrals:

$$B_r^* = \frac{M\mu_0}{2\pi(\gamma_0^2 - \gamma_1^2)} \frac{\partial}{\partial r} \int_0^\infty \eta_1 m (n_1 - n_0) J_0(mr) dm \\ = \frac{M\mu_0}{2\pi} \frac{\partial}{\partial r} \int_0^\infty (m^2 \eta_1 - m^3 - m\gamma_1^2) J_0(mr) dm \quad (188)$$

A very useful integral identity for Bessel functions is

$$\lim_{r \rightarrow \infty} \int_0^\infty m^{2q+1} J_0(mr) dm = 0; \quad q = 1, 2, 3, \dots$$

(The J_0 function when weighted by an odd power of the dummy m integrates to zero over the infinite range. If we are dealing with J_1 , the same is true when the weighting factor is an even power of m). In view of this identity, only the first of the three integrals in 188 has a value other than zero:

TABLE II.—Vertical induction about a vertical-axis magnetic dipole

Gr	Real-component, multiplied by $\frac{4\pi r^3}{\mu_0 M}$	Imaginary component, multiplied by $\frac{4\pi r^3}{\mu_0 M}$
0.1	1.0002	0.0022
0.2	1.0013	0.0085
0.3	1.0041	0.0175
0.4	1.0091	0.0282
0.5	1.0166	0.0396
0.6	1.0266	1.0510
0.7	1.0391	0.0614
0.8	1.0540	0.0702
0.9	1.0709	0.0769
1.0	1.0896	0.0808
1.2	1.1306	0.0792
1.4	1.1734	0.0636
1.6	1.2144	0.0334
1.8	1.2502	-0.0106
2.0	1.2779	-0.0667
2.2	1.2951	-0.1328
2.4	1.3003	-0.2062
2.6	1.2925	-0.2839
2.8	1.2717	-0.3632
3.0	1.2381	-0.4412
3.2	1.1927	-0.5157
3.4	1.1367	-0.5846
3.6	1.0718	-0.6461
3.8	0.9997	-0.6990
4.0	0.9223	-0.7425
4.2	0.8414	-0.7761
4.4	0.7588	-0.7998
4.6	0.6762	-0.8137
4.8	0.5950	-0.8185
5.0	0.5166	-0.8147
5.5	0.3393	-0.7737
6.0	0.1962	-0.7003
6.5	0.0906	-0.6100
7.0	0.0203	-0.5160
7.5	-0.0208	-0.4277

NORMALIZED VERTICAL MAGNETIC INDUCTION

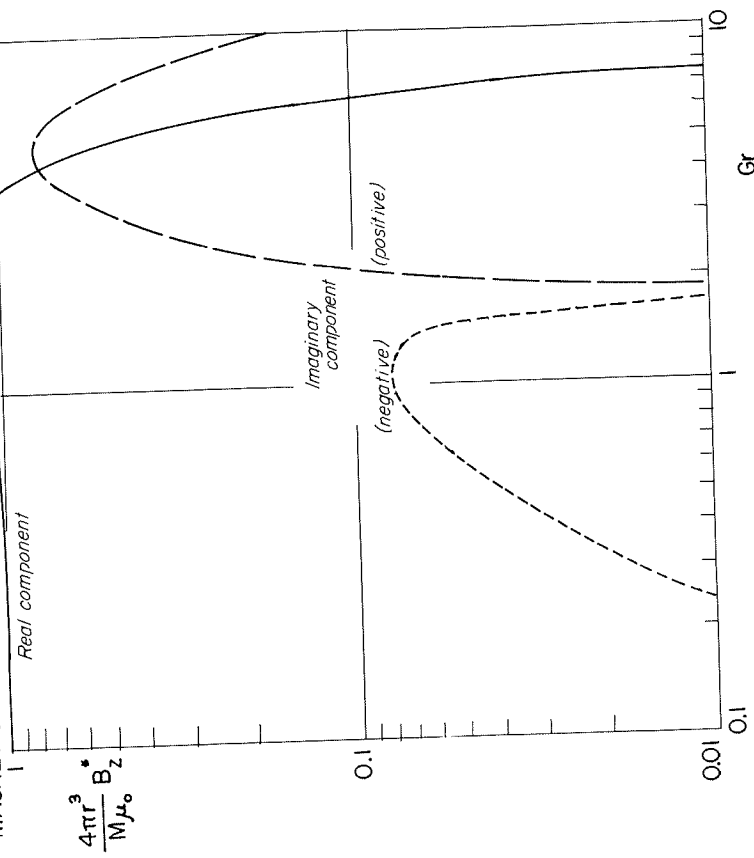


FIGURE 59.—Vertical magnetic induction about a vertical-axis magnetic dipole source. G is the wave number in a uniform medium, and r is the spacing from source to receiver.

$$B_r^* = \frac{M\mu_0}{2\pi\lambda_i^2} \frac{\partial}{\partial r_i} \int_0^\infty m^2 \eta J_0(mr) dm \quad (189)$$

This last integral may be evaluated using the identity

$$\int_0^\infty \frac{e^{-\eta z}}{\eta} J_0(mr) dm = I_0 \left\{ \frac{\lambda_i}{2} (\sqrt{r^2 - z^2} - z) \right\} \cdot K_0 \left\{ \frac{\lambda_i}{2} (\sqrt{r^2 - z^2} + z) \right\} \quad (190)$$

where I_0 and K_0 are the modified Bessel functions. In order to convert this integral to the same form as the one in equation 189 that we wish to evaluate, it is necessary to differentiate twice with respect to z , set z equal to

zero and then differentiate twice with respect to r . The differentiations are somewhat tedious but lead to the result:

$$B_r^* = -\frac{M\mu_0}{4\pi r^3} \left[(\delta r)^2 (I_1 K_1 - I_0 K_0) + 4\delta r (I_1 K_0 - I_0 K_1) + 16 I_1 K_1 \right] \quad (191)$$

For large values of the argument γr , the modified Bessel functions have the asymptotic expressions:

$$\begin{aligned} I_0(mr) &= \frac{e^{-mr}}{\sqrt{2\pi mr}} \left\{ 1 + \frac{1}{8mr} + \dots \right\} \\ K_0(mr) &= \left(\frac{\pi}{2mr}\right)^{1/2} e^{-mr} \left\{ 1 - \frac{1}{8mr} + \dots \right\} \\ I_1(mr) &= \frac{e^{-mr}}{\sqrt{2\pi mr}} \left\{ 1 + \frac{1}{8mr} + \dots \right\} \\ K_1(mr) &= \left(\frac{\pi}{2mr}\right)^{1/2} e^{-mr} \left\{ 1 - \frac{1}{8mr} + \dots \right\} \end{aligned}$$

so that the equation 191 may be written approximately as:

$$B_r^* = -\frac{4\delta M\mu_0}{\pi r^4} \quad (192)$$

This equation may be solved for apparent conductivity:

$$\sigma_a = \frac{\pi^2 r^8 B_r^{*2}}{16 i \omega \mu_0^3 M^2} \quad (193)$$

In order to determine the behavior at small values or γr , we return to the integral in equation 189 and expand the quantity η_1 as follows:

$$\eta_1 = \frac{mr}{r} \left(1 + \frac{\delta^2 r^2}{m^2 r^2} \right)^{1/2} = m \left[1 + \frac{1}{2} \left(\frac{\delta r}{mr} \right)^2 + \frac{1}{8} \left(\frac{\delta r}{mr} \right)^4 + \dots \right] \quad (194)$$

Substituting the first three terms into the expression for the integral, we have:

$$B_r^* = -\frac{M\mu_0}{2\pi r^2} \frac{\partial}{\partial r} \left\{ \int_0^\infty m J_0(mr) dm + \frac{\delta^2}{2} \int_0^\infty m J_0(mr) dm + \frac{\delta^4}{8} \int_0^\infty \frac{1}{m} J_0(mr) dm \right\} \quad (195)$$

The first two integrals are of the type weighted by m raised to an odd integer power, and so, are zero. The third integral is of the type listed by Eredlyi (Higher Transcendental Functions, v. 2, p. 49, equation 19) and has the value:

$$\int_0^\infty \frac{1}{m} J_0(mr) dm = \frac{1}{2r} \frac{\Gamma(0)}{\Gamma(1)} = \frac{1}{2r} \quad (196)$$

Differentiating this expression, we have the simplified expression for radial magnetic induction for small γr :

$$B_r^* = \frac{M\mu_0}{32\pi r^2} \cdot i\omega\mu_0\sigma \quad (197)$$

Let us now turn to the definition of apparent conductivity for field components measured about an electric dipole source.

The principal of reciprocity states that if the role of transmitter and receiver are interchanged, there will be no difference in the measured field. This can be used to evaluate the vertical magnetic induction from an electric dipole source in terms of the results we have already obtained for the tangential electric field about a vertical-axis magnetic dipole source. The complete expression for B_z is obtained from equation 169 by substituting B_z for E_ϕ^* and $|dl|$ for $M\mu_0$:

$$B_z = \frac{I dl}{2\pi\sigma} \cdot \frac{1}{r^4} \left\{ 3 - e^{-\delta r} \left[3 + 3\delta r + (\delta r)^2 \right] \right\} \quad (198)$$

Likewise we have the expression for B_z at small values of γr from equation 173:

$$B_z \Big|_{\delta r \rightarrow 0} = i \frac{I dl}{4\pi r^2} \omega\mu_0 \quad (199)$$

and the expression for large γr from equation 176

$$B_z \Big|_{\delta r \rightarrow \infty} = \frac{3 I dl}{2\pi\sigma r^4} \quad (200)$$

The two forms for apparent conductivity are:

$$\sigma_a \Big|_{\delta r \rightarrow 0} = \frac{32\pi^2 r^4}{9\omega^3 \mu_0^3} \left(\frac{B_z \Big|_{\delta r \rightarrow 0}}{I dl} \right)^2 \quad (201)$$

and

$$\sigma_a \Big|_{\delta r \rightarrow \infty} = \frac{3\mu_0}{2\pi r^4} \frac{I dl}{B_z} \quad (202)$$

The other field components about an electric dipole are somewhat more difficult to evaluate. From equations 134-136, taking $R=1$ for a uniform earth and $\gamma_0=0$ for practicality, we have the following integral expressions to evaluate:

a. Parallel electric field:

$$E_x = i\omega \frac{I dl \mu_0}{2\pi} \int_0^\infty \frac{m}{m+n_1} J_0(mr) dm - \frac{I dl \rho_1}{2\pi} \frac{\partial}{\partial x} \frac{x}{r} \int_0^\infty (\lambda \bar{n}_1 - \frac{\gamma_{e1}^2}{m+n_1}) J_1(mr) dm \quad (203)$$

b. Perpendicular electric field:

$$E_z = i\omega \frac{I dl \mu_0}{2\pi} \frac{\partial}{\partial x} \int_0^{n_1} \left[\frac{n_1}{m(m+n_1)} - \frac{1}{m} \right] J_0(mr) dm - \frac{I dl \rho_1}{2\pi} \frac{x}{r} \frac{\partial}{\partial z} \int_0^\infty (\lambda \bar{n}_1 - \frac{\gamma_{e1}^2}{m+n_1}) J_1(mr) dm \quad (204)$$

c. Parallel magnetic induction:

$$B_x = \frac{I dl \mu_0}{2\pi} \frac{\partial^2}{\partial x \partial y} \int_0^{n_1} \left[\frac{n_1}{m(m+n_1)} - \frac{1}{m} \right] J_0(mr) dm \quad (205)$$

In the expression for E_x , the first integral is precisely the same as the integral for E_ϕ^* which was evaluated earlier. The second term in the second integrand is multiplied by $(m-n_1)/(m+n_1)$ to make it more tractable:

$$\int_0^\infty (\lambda \bar{n}_1 - \frac{\gamma_{e1}^2}{m+n_1}) J_1(mr) dm = \int_0^\infty (\lambda \bar{n}_1 + m - n_1) J_1(mr) dm \quad (206)$$

Consider the following integral, which may be integrated by parts:

$$\begin{aligned} \int_0^\infty e^{-n_1 z} J_1(mr) dm &= -\frac{1}{r} \int_0^\infty e^{-n_1 z} d\{J_0(mr)\} \\ &= -\frac{1}{r} \{ [e^{-n_1 z} J_0(mr)]_0^\infty - \int_0^\infty J_0(mr) d(e^{-n_1 z}) \} \\ &= -\frac{1}{r} [-e^{-\gamma_{e1} z} + z \int_0^\infty \frac{m}{n_1} e^{-n_1 z} J_0(mr) dm] \\ &= \frac{e^{-\gamma_{e1} z}}{r} - \frac{z e^{-\gamma_{e1} \sqrt{r^2+z^2}}}{\sqrt{r^2+z^2}} \end{aligned} \quad (207)$$

Differentiating the left- and right-hand sides of this equation with respect to z and setting $z=0$, we have:

$$\int_0^\infty n_1 J_1(mr) dm = \frac{\gamma_{e1} r + e^{-\gamma_{e1} r}}{r^2} \quad (208)$$

We obtain the other integral in 206 by considering the case with $\gamma_1=0$:

$$\int_0^\infty m J_1(mr) dm = \frac{1}{r^2} \quad (209)$$

Replacing all the integrals in equation 205 by their closed-form expressions, we have:

$$\begin{aligned} E_x &= i\omega \frac{I dl \mu_0}{2\pi} \frac{1}{r^4} \left\{ 3 - e^{-\gamma_{e1} r} \left[3 + 3\gamma_{e1} r + (\gamma_{e1} r)^2 \right] \right\} \\ &\quad - \frac{I dl \rho_1}{2\pi} \frac{x}{r} \left[\lambda \frac{\gamma_{e1} + e^{-\gamma_{e1} r}}{r^2} - \frac{\gamma_{e1} r + e^{-\gamma_{e1} r}}{r^2} + \frac{1}{r^2} \right] \\ &= i\omega \frac{I dl \mu_0}{2\pi} \frac{1}{r^4} \left\{ 3 - e^{-\gamma_{e1} r} \left[3 + 3\gamma_{e1} r + (\gamma_{e1} r)^2 \right] \right\} \\ &\quad - \frac{I dl \rho_1}{2\pi} \frac{x}{r^3} \left[(\lambda \gamma_{e1} - \gamma_{e1} r) + (\lambda - 1) e^{-\gamma_{e1} r} + 1 \right] \end{aligned} \quad (210)$$

Carrying out the indicated differentiation, and collecting terms of the same forms, we have

$$\begin{aligned} E_x &= \frac{I dl \rho_1}{2\pi r^3} \left\{ \left[3 \left(\frac{x}{r} \right)^2 - 2 \right] + e^{-\gamma_{e1} r} (1 + \gamma_{e1} r) + e^{-\gamma_{e1} r} \left[1 + 3 \left(\frac{x}{r} \right)^2 - (\gamma_{e1} r)^2 \right] \right. \\ &\quad \left. - e^{-\gamma_{e1} r / \lambda} \left[\lambda - 3\lambda \left(\frac{x}{r} \right)^2 - \gamma_{e1} r \left(\frac{x}{r} \right)^2 \right] \right\} \end{aligned} \quad (211)$$

Normally, the electric field about a current dipole source is measured along the polar axis of the source dipole (as in the *polar* or *inline* dipole array) or along the equatorial axis of the source dipole (as in the *equatorial* or *broadside* dipole array). In the first case, the ratio x/r is unity, and equation 211 simplifies to:

$$E_x = \frac{I dl \rho_1}{2\pi r^3} \left[1 - e^{-\gamma_{e1} r} + e^{-\gamma_{e1} r / \lambda} (2\lambda + \gamma_{e1} r) \right] \quad (\text{Polar dipole array}) \quad (212)$$

In the second case, the ratio x/r is zero, and equation 211 simplifies to:

$$E_x = -\frac{I dl \rho_1}{\pi r^3} \left[1 - \left(1 + \frac{\gamma_{e1} r}{2} \right) e^{-\gamma_{e1} r} + \frac{\lambda}{2} e^{-\gamma_{e1} r / \lambda} \right] \quad (\text{Equatorial dipole array}) \quad (213)$$

For very low frequencies, or for direct current, the parameter γr becomes essentially zero, and these two equations reduce to:

$$E_x \approx \frac{I dl}{2\pi r^3} \lambda \rho_1 \quad (\text{Polar dipole array}) \quad (214)$$

and

$$E_x \approx -\frac{I dl}{\pi r^3} \lambda \rho_0 \quad (\text{Equatorial dipole array}) \quad (215)$$

These, of course, are the standard equations derivable from Laplace's equation for the direct-current resistivity problem, and can be solved for resistivity to provide the usual definition of apparent resistivity for the polar and equatorial dipole arrays. It should be noted that the resistivity which is measured at DC is the quadratic average resistivity in a homogeneous anisotropic medium, $\rho_Q = (\rho_t \cdot \rho_l)^{1/2} = \lambda \rho_l$.

For low frequencies, we can replace the exponential in equations 212 and 213 with the first three terms of its series expansion, and so arrive at the following expressions valid at small γr :

$$E_x \approx \frac{I dl \rho_0}{2 \pi r^3} \left[2 \lambda + \frac{i \omega \mu_0}{\rho_0} r^2 \right] \quad (\text{Polar dipole array}) \quad (216)$$

and

$$E_x \approx \frac{I dl \rho_0}{\pi r^3} \left[\frac{\lambda}{2} - \frac{i \omega \mu_0}{\rho_0} r^2 \right] \quad (\text{Equatorial dipole array}) \quad (217)$$

From these expressions, we may say that the zero-frequency behavior is valid so long as

$$\gamma^2 r^2 \ll 2$$

Thus, direct-current behavior should be expected with a good degree of accuracy for source-receiver separations up to half a radian wave length. The imaginary component of electric field in the two cases is:

$$E_{x, \text{imag}} = i \frac{I dl \omega \mu_0}{2 \pi r} \quad (\text{Polar dipole array}) \quad (218)$$

$$E_{x, \text{imag}} = -i \frac{I dl \omega \mu_0}{2 \pi r} \quad (\text{Equatorial dipole array}) \quad (219)$$

The variation of resistivity computed from equation 214 and 215 as a function of γr is shown graphically in figure 60.

For high frequencies, where γr is large, equation 211 reduces to the following approximation:

$$E_x \Big|_{\gamma r \rightarrow \infty} \approx \frac{I dl \rho_0}{2 \pi r^3} \left(3 \frac{x^2}{r^2} - 2 \right) \quad (220)$$

For the equatorial and polar dipole arrays, the corresponding expressions are:

AC FIELD STRENGTH
DC FIELD STRENGTH

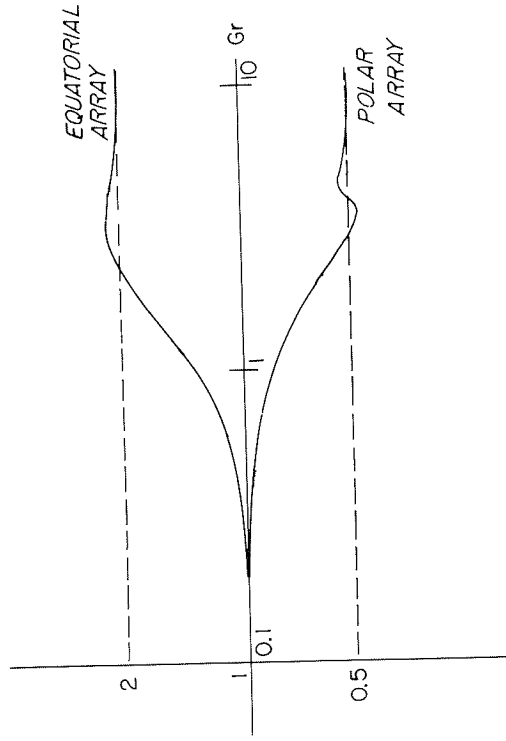


FIGURE 60. Variation of field strength with frequency for equatorial and polar dipoles over a uniform earth in which the real part of the wave number is G .

$$E_x \approx \frac{I dl \rho_0}{2 \pi r^3} \quad (\text{Polar dipole array}) \quad (221)$$

and

$$E_x \approx -\frac{I dl \rho_0}{\pi r^3} \quad (\text{Equatorial dipole array}) \quad (222)$$

It is interesting to note that in going from the DC behavior to the high frequency behavior, the electric field for the polar array halves and the electric field for the equatorial array doubles, after the inverse r^3 behavior is taken into consideration.

As in the other cases, apparent resistivity can be defined with either the high-frequency or the low-frequency approximations. Here, however, the low-frequency definitions are used more widely than the high-frequency definitions, being the basis for the direct-current resistivity methods.

It is also important to note that the low-frequency approximation is expressed as a function of the quadratic average resistivity of an anisotropic medium, $\lambda \rho_l = \rho_l / \lambda = \rho_Q$, while the high-frequency approximation is expressed in terms of the longitudinal resistivity of the medium. It appears that of the methods we have considered, only the electric-dipole/electric-dipole method provides this wealth of information.

Evaluation of other source-receiver combinations is straight forward, inasmuch as the forms of the Bessel integrals involved are all the same as the types already considered. We will not at this point continue with the evaluation for the case of a uniform earth, but results are summarized in table 12.

Range A, with $\gamma r > 6$: At large distances or high frequencies, the behavior of any of the electromagnetic field components simplifies to an inverse r^n behavior, with the value of the exponent n varying from 3 to 5 depending on the specific source and receiver being considered. The field components depend only on the longitudinal resistivity in a vertically anisotropic earth.

Range C, $\gamma r < 0.6$: At short distances or at low frequencies, the behavior of any of the field components also simplifies. Except for the electric field about an electric dipole, the field components become insensitive to the electrical properties of the earth. With the electric field about an electric dipole source, the method reduces to the DC resistivity sounding method. Generally, the effect of the earth properties at this end of the spectrum is contained in the term in quadrature to the principle term of the approximation, whether this be the inphase or the out-of-phase component. It is possible to define a simple expression for apparent resistivity in this range, based on the expectation that the quadrature signal can be separated from the main part of the field.

Range B, $0.6 < \gamma r < 6$: At moderate distances or frequencies, the behavior of any of the field components about any of the sources becomes very complicated, inasmuch as there are contributions to the electromagnetic field both by energy traveling through the earth and by energy traveling through the halfspace above the earth. While an apparent resistivity may be defined using various graphical techniques in this range, the definition is restricted in application, and is not normally used.

The relationship between earth resistivity separation and critical frequency separating each of these ranges is shown graphically in figure 61.

BEHAVIOR OF THE \tilde{R} AND R^* FUNCTIONS

There is a wide variety of electromagnetic field techniques which might be used in measuring the resistivity profile in a sequence of layers. From the point of view of operational ease, two types of field source are preferred to others—the source may be a grounded wire or coil of wire with a vertical axis. The first constitutes a current dipole source, if the length of the wire is small compared with the offset distance at which field components are observed, while the wire loop constitutes a vertical-axis magnetic dipole, if the diameter of the loop is small compared to the offset distance. With a current dipole source, one might measure the vertical magnetic field, or the horizontal magnetic field, or the horizontal electric field about the source. Depending on the

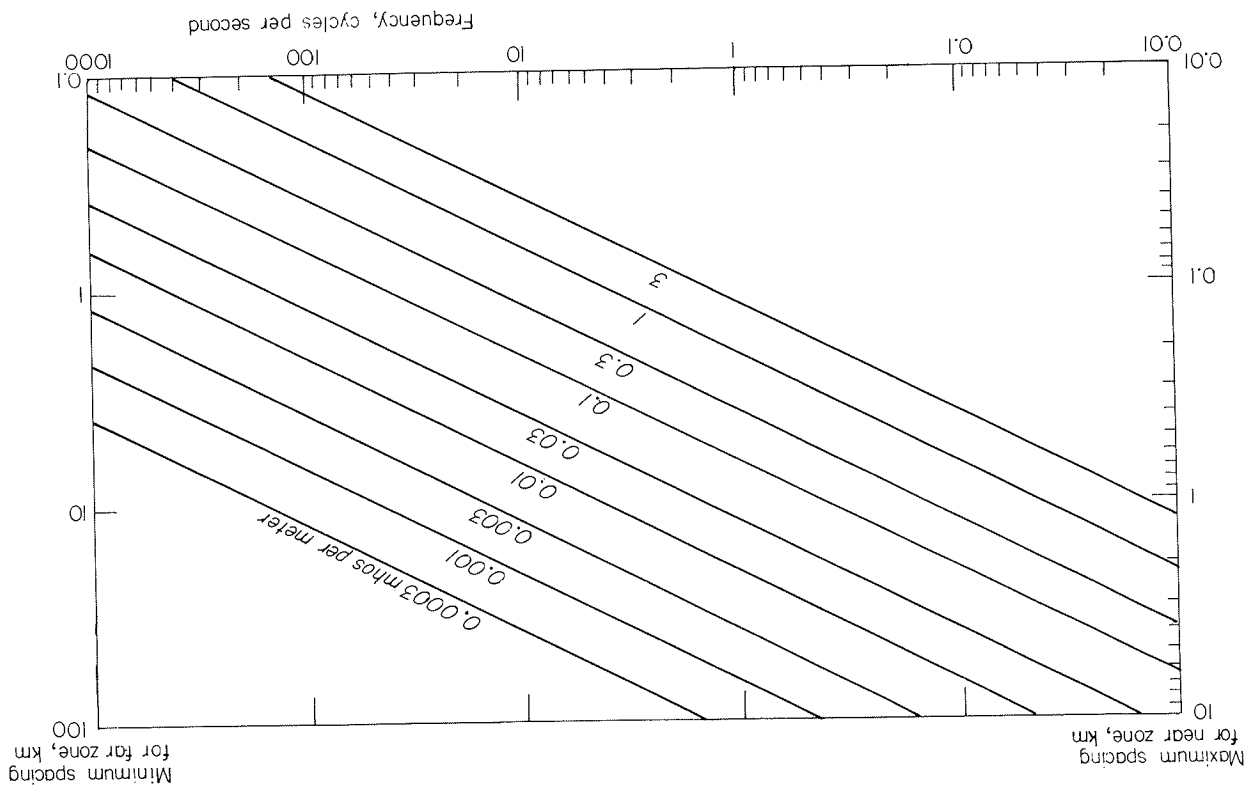


Figure 61.—Frequency-spacing boundaries between the near, intermediate and far zones of the induction field for the case of a uniform earth.

TABLE 12.—Expressions for apparent resistivity

Source	Receiver	Coupling system	
GR > 0.6	GR < 0.6	Apparent resistivity	Apparent resistivity
Vertical-axis magnetic dipole	Vertical-axis coil	$R_a = \frac{9! \omega^2 \mu_0^2 A_r M_s}{2 \pi r^5 V_r}$	$R_a = \frac{8 \pi^2 r^4 \text{Rad}^2 \{V_r\}}{\omega^5 \mu_0^3 A_r^2 M_s^2}$
Vertical-axis coil	Radial-axis coil	$R_a = \frac{16! \omega^3 \mu_0^3 A_r^2 M_s^2}{\pi^2 r^8 V_r^2}$	$R_a = \frac{9 \omega \mu_0 M_s^2 \text{Rad}^2 \{E_\phi\}}{32 \pi^2 r^4}$
Horizontal current dipole	Radial electric field	$R_a = \frac{2 \pi r^3}{3} E_r$	$R_a = \frac{I d l \cos \theta}{\pi r^3} E_r$
	Tangential electric field	$R_a = \frac{I d l \sin \theta}{\pi r^3} E_\phi$	$R_a = \frac{2 \pi r^3}{3} E_x$ ($\theta = \pi/2$)
Vertical-axis coil	Vertical-axis coil	$R_a = \frac{3 A_r I d l \sin \theta}{2 \pi r^4 V_r}$	$R_a = \frac{9 \omega^5 \mu_0^3 A_r^2 (I d l)^2}{32 \pi^2 r^4 + \text{Rad}^2 \{V_r\}}$
Vertical electric field	Vertical electric field	$R_a = \frac{2 \pi r^3 E_z}{\omega \mu_0 I d l \cos \theta}$	$R_a = \frac{2 \pi r^3 E_z}{\omega \mu_0 I d l \cos \theta}$

TABLE 12 continued—key to symbols

Radial-axis coil	$R_a = \frac{\pi^3 r^6 V_r}{A_r^2 \omega \mu_0 (I d l)^2 \sin^2 \theta}$
Tangential magnetic field	$R_a = \frac{4 \pi^2 r^6 V_r}{A_r^2 \omega \mu_0 (I d l)^2 \cos^2 \theta}$

- ω = frequency, rps
- $\mu_0 = 4\pi \times 10^{-7}$ H/M
- A_r = effective area of receiver induction coil
- M_s = moment of magnetic dipole source, current times effective area
- r = separation between source and receiver
- V_r = voltage output of an induction coil receiver
- R = real part of measured voltage
- E = tangential electric field; measured voltage divided by dipole length
- E_r = radial electric field; measured voltage divided by dipole length
- E_x = component of electric field parallel to current dipole axis
- $I d l$ = current dipole moment; product of current and electrode separation
- θ is the angle between the current dipole axis and the radius vector to the receiver location

geometry of the source and receiver combination, the variety of methods which might be used is almost limitless. With the magnetic source, the vertical magnetic field or the horizontal magnetic field or electric field can also be used to investigate the variation of resistivity with depth.

In spite of the variety of source-receiver geometries which might be used in the field, it is surprising how few independent estimates of the conductivity profile may be obtained. As a consequence of the use of the method of separation of variables in the solution of Maxwell's equations, each one of the expressions for a field component (as given by equations 131, 135, 136, 156, 157 and 158) consists of a Hankel transform of some combination of \tilde{R} and R^* functions. The \tilde{R} and R^* functions depend only on the electrical properties of the medium (and on the dummy, m , which was the separation constant), and not on the source-receiver geometry. The effect of source-receiver geometry enters only in the detailed nature of the integral transform. The problem of discussing various techniques is simplified because we can consider source-receiver geometry independently of the electrical structure of the earth, within the limits imposed by the fact that we have two functional representations of the resistivity structure of the earth. Let us now consider the properties of these two functions, \tilde{R} and R^* .

Asymptotic behavior for small m

The limiting behavior of the R functions as the separation parameter is made small is of particular concern. For the \tilde{R} function we have

$$\tilde{R} = \coth \left\{ \gamma_1 h_1 + \coth^{-1} \frac{\gamma_2}{\gamma_1} \left[\coth (\gamma_2 h_2 + \coth^{-1} \dots \coth^{-1} \frac{\gamma_N}{\gamma_{N-1}} \dots) \right] \right\} \quad (223)$$

which becomes in the limit

$$Q = \lim_{m \rightarrow 0} \tilde{R} = \coth \left\{ \gamma_1 h_1 + \coth^{-1} \frac{\gamma_2}{\gamma_1} \left[\coth (\gamma_2 h_2 + \coth^{-1} \dots \coth^{-1} \frac{\gamma_N}{\gamma_{N-1}} \dots) \right] \right\} \quad (224)$$

This limit provides a function which is relatively well-known in electrical prospecting. Wait (1962, p. 14) has designated this limit for the \tilde{R} function as a Q function, used in correcting the plane-wave impedance at the surface of a stratified earth for the effects of layering. Cagniard (1953) has used the Q function in defining apparent resistivity as measured with the magnetotelluric method. As a consequence of the interest in the use of the magnetotelluric method over the past decade, numerous computations of values for the Q function have appeared in the literature (Wait, 1962; Jackson, Wait and Walters, 1962; Yungul, 1961).

For the R^* function, we have

$$R^* = \coth \left\{ \lambda_1 \bar{r}_1 h_1 + \coth^{-1} \frac{\lambda_2 \bar{r}_2 \rho_2}{\lambda_1 \bar{r}_1 \rho_1} \left[\coth (\lambda_2 \bar{r}_2 h_2 + \coth^{-1} \dots \coth^{-1} \frac{\lambda_N \bar{r}_N \rho_N}{\lambda_{N-1} \bar{r}_{N-1} \rho_{N-1}} \dots) \right] \right\} \quad (225)$$

which becomes in the limit:

$$R_o^* = \coth \left\{ \lambda_1 \bar{r}_1 h_1 + \coth^{-1} \frac{\lambda_2 \bar{r}_2 \rho_2}{\lambda_1 \bar{r}_1 \rho_1} \left[\coth (\lambda_2 \bar{r}_2 h_2 + \coth^{-1} \dots \coth^{-1} \frac{\lambda_N \bar{r}_N \rho_N}{\lambda_{N-1} \bar{r}_{N-1} \rho_{N-1}} \dots) \right] \right\} \quad (226)$$

It is of interest to note that R_o^* and the Q function are very similar, the difference being solely in the ratio in the argument of each inverse hyperbolic cotangent. The terms of the form $\lambda_i \gamma_{i+1} h_i$ in 226 are exactly of the form $\gamma_{i+1} h_i$, which is identical with that of the corresponding terms in equation 224 for the Q function. Note that the ratios in equation 224 are:

$$\frac{\gamma_{i+1} h_i}{\gamma_{i+1}} = \left(\frac{\rho_{k,i}}{\rho_{k,i+1}} \right)^{1/2} \quad (227)$$

while the ratios in equation 226 are:

$$\frac{\lambda_i \gamma_{k,i} \rho_{k,i}}{\lambda_{i+1} \gamma_{k,i+1} \rho_{k,i+1}} = \frac{\lambda_{i+1}}{\lambda_i} \left(\frac{\rho_{k,i}}{\rho_{k,i+1}} \right)^{1/2} \quad (228)$$

Thus, if a sequence of layers is made up of isotropic rocks, there is no difference between the Q function and the R_o^* function. On the other hand, in a section of anisotropic rocks, the Q function depends only on the longitudinal resistivities, while the R_o^* function depends on the transverse resistivities. In principle, it should be possible to detect the effects of anisotropy in a layered medium with measurements which permit the evaluation of both the Q function and the R_o^* function.

Asymptotic behavior for small ω

It is also of considerable interest to consider the limiting behavior of the R functions for low frequency, rather than for small values of the separation variable, m . The \tilde{R} function in this limit becomes

$$\lim_{\omega \rightarrow 0} \tilde{R} = \coth \{ mh_1 + \coth^{-1} [\coth(mh_2 + \coth^{-1} \dots \coth^{-1}(1) \dots)] \} = 1 \tag{229}$$

(Note that the behavior of the hyperbolic and inverse hyperbolic functions which are of concern here was summarized graphically in figure 55). At zero frequency, the \tilde{R} function becomes independent of the electrical properties of the sequence.

The corresponding limit for the R^* function is:

$$K = \lim_{\omega \rightarrow 0} R^* = \coth \left\{ m \lambda_1 h_1 + \coth^{-1} \frac{\lambda_1 \rho_1}{\lambda_2 \rho_2} \left[\coth(m \lambda_2 h_2 + \coth^{-1} \dots \coth^{-1} \frac{\lambda_{N-1} \rho_{N-1}}{\lambda_N \rho_N} \dots) \right] \right\} \tag{230}$$

This function is one which is well known in electrical geophysics also, being the so-called kernel function for the direct-current resistivity problem, originally developed by Stefanescu and others (1930).

These considerations of asymptotic behavior for small m and small ω indicate the generality of the R functions—they include as special cases the theory for direct current methods as well as the theory for the magnetotelluric method.

The Q and K functions

Let us review the nature of the special Q and K functions, inasmuch as they have been discussed in considerable detail in the literature (Wait, 1962; Meinardus, 1967; Bödvarsson, 1965; Mooney and others, 1966; Flathe, 1955; Slichter, 1933; Onodera, 1960; Roman, 1963).

It is important to note that in taking a limit as frequency was made small the wave numbers dropped out of the R functions. This results in the $K(m)$ function being composed only of a real part, which considerably simplifies its evaluation. On the other hand, the Q function will normally consist of both real and imaginary parts, because it is a function of the wave numbers for the medium. Usual practice is to express the Q function in terms of a magnitude and phase, rather than in terms of real and imaginary sizes.

The behavior of the K and Q functions with changing m and ω , respectively, is shown in figures 62-66. In the first case, the independent variable is plotted in terms of the dimensionless product, mh . Inasmuch as m has the dimensions of inverse distance, and is related to the inverse spacing between source and receiver, the product mh may be viewed loosely as the ratio of layer thickness

KERNEL FUNCTION, $K(m)$

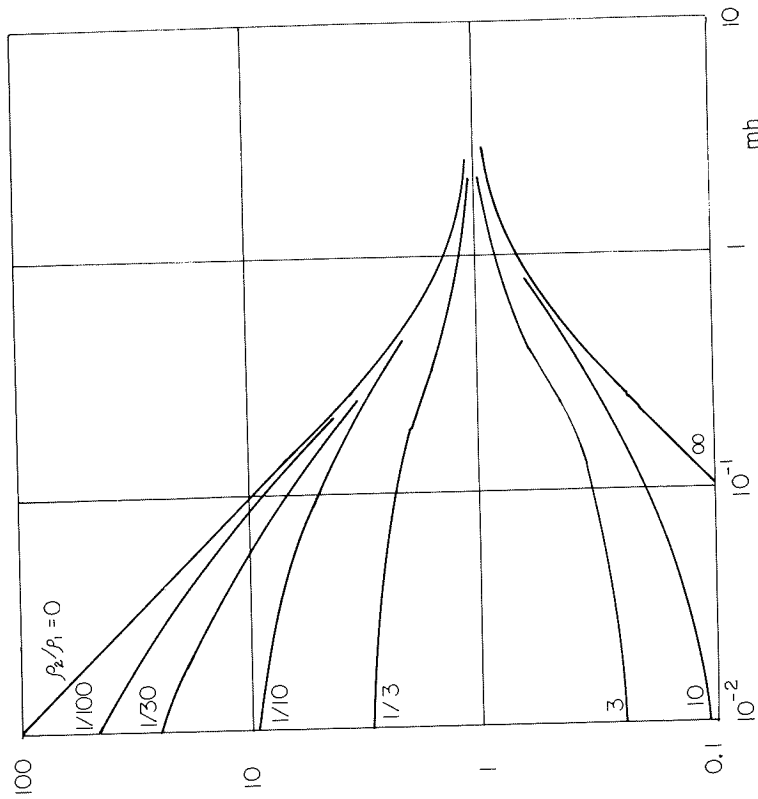


FIGURE 62. Numerical behavior of the K function for the case of two layers.

to source-receiver separation. The Q function is independent of m , but depends on frequency through the wave numbers, γ . The independent variable for the Q function plots is taken as $\lambda_1 h = (h^2 / \omega \mu \sigma)^{1/2}$, which is in effect the ratio of layer thickness to radian wave length in that layer. Thus, in the plots in figures 62-66, values for spacing or wave length increase to the left rather than to the right.

The expressions for the K and Q functions for the simple two-layer case with $\rho_2 / \rho_1 > 1$ are:

$$K_2(m) = \coth [m \lambda_1 h_1 + \coth^{-1} \frac{\lambda_1 \rho_1}{\lambda_2 \rho_2}] \tag{231}$$

$$Q_2(\omega) = \coth [\lambda_1 h_1 + \coth^{-1} \frac{\rho_1}{\rho_2}] \tag{232}$$

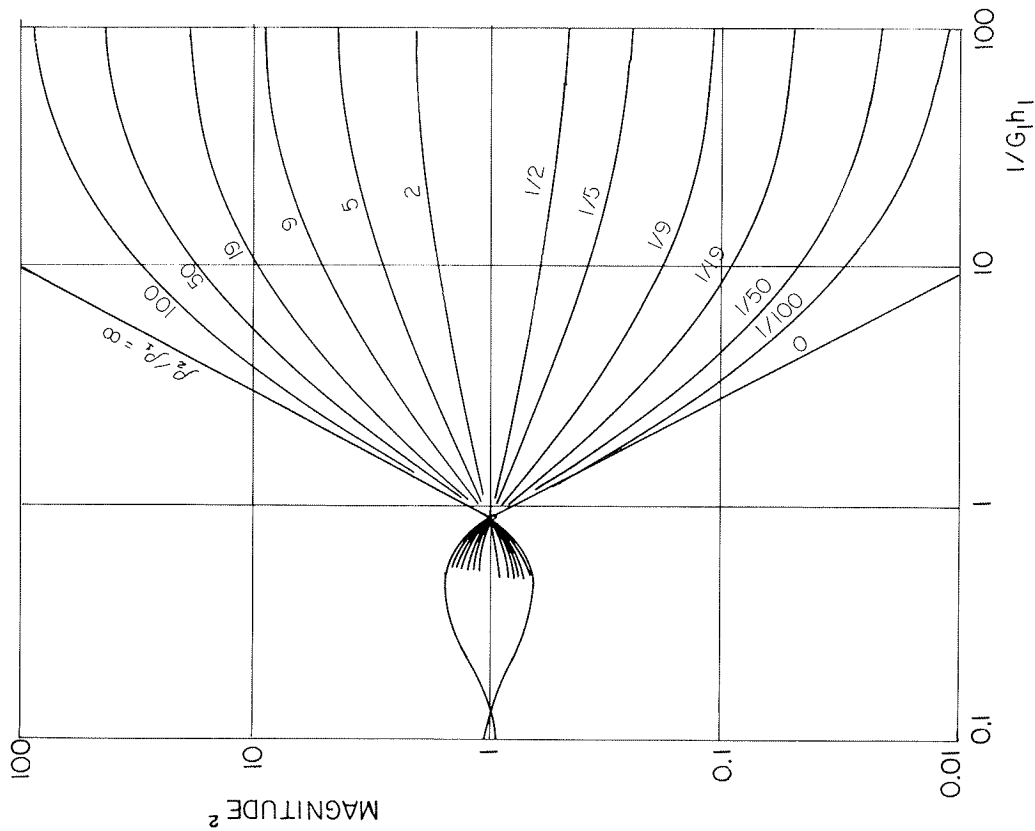


FIGURE 63. — Magnitude of the Q_2 function for the case of two layers, G_1 is the real part of the wave number in the surface layer, and h_1 is the thickness of that layer.

These two expressions are remarkably similar in form, but this similarity is distorted if we consider the complex nature of the wave number, γ_1 , in equation 232. If we write $\gamma_1 = G_1 + iG_1$, with $G_1 = (2/\omega\mu\sigma_1)^{1/2}$ equation 232 may be broken into real and imaginary parts:

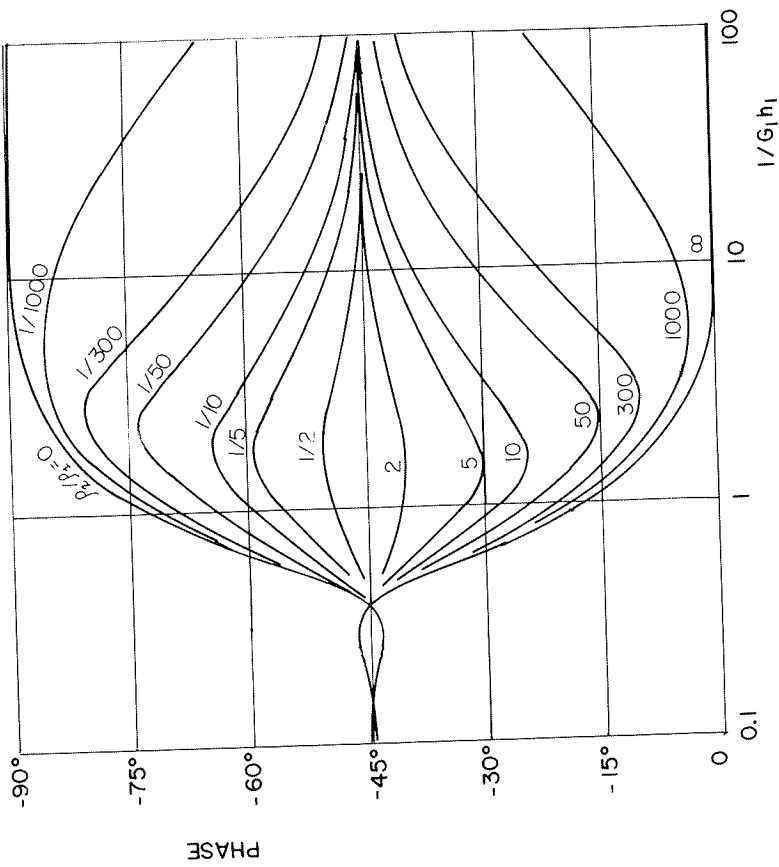


FIGURE 64. — Phase of the Q function for the case of two layers, G_1 is the real part of the wave number in the surface layer, and h_1 is the thickness of that layer.

$$Q_2(\omega) = \frac{\coth [G_1 h_1 + \coth^{-1} (\frac{\rho_1}{\rho_2})^{1/2}] \cdot (1 + \cot^2 G_1 h_1)}{\coth^2 [G_1 h_1 + \coth^{-1} (\frac{\rho_1}{\rho_2})^{1/2}] + \cot^2 G_1 h_1} + i \frac{\cot G_1 h_1 \{ \coth^2 [G_1 h_1 + \coth^{-1} (\frac{\rho_1}{\rho_2})^{1/2}] - 1 \}}{\coth^2 [G_1 h_1 + \coth^{-1} (\frac{\rho_1}{\rho_2})^{1/2}] + \cot^2 G_1 h_1} \quad (233)$$

It may be seen readily that as $m h_1$ is made large in equation 231 or $G_1 h_1$ in equation 232, the argument of the hyperbolic cotangent becomes large, and the K_2 or Q_2 functions approach an asymptotic value of unity to the right:

$$\lim_{m h_1 \rightarrow \infty} K_2 = 1 \quad (234)$$

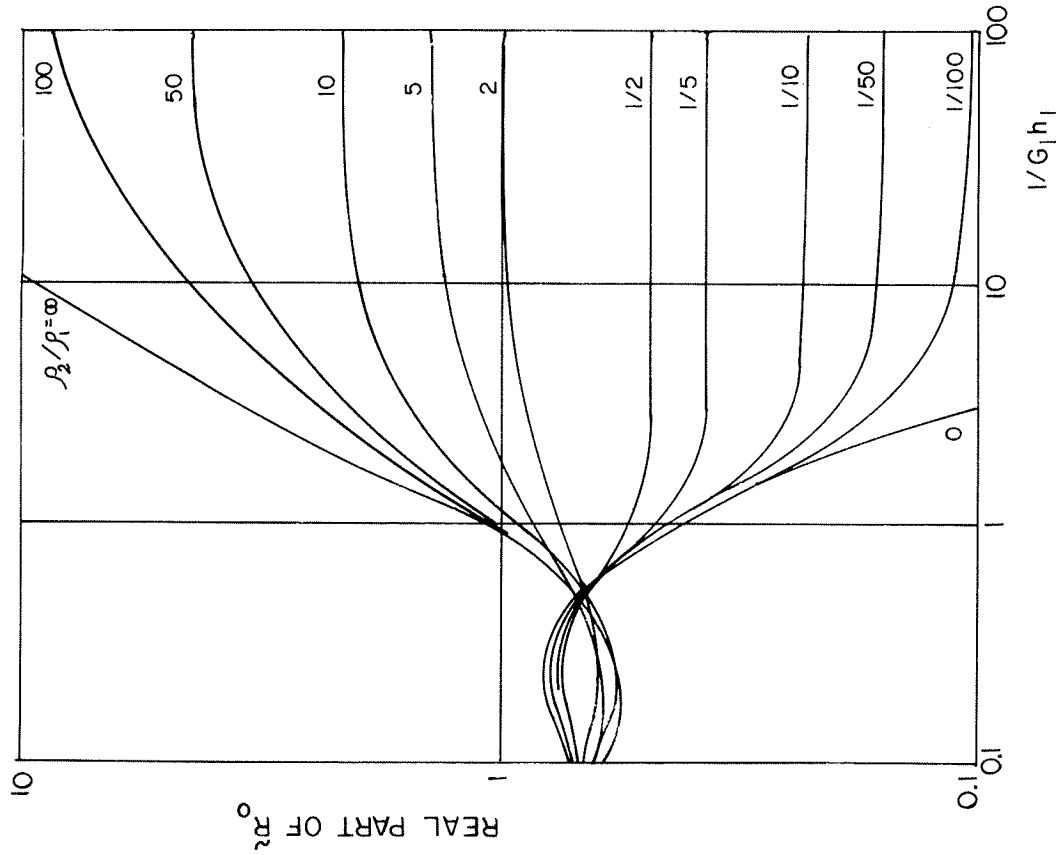


FIGURE 65.—Real part of the Q function for a single layer resting on a uniform substratum.

$$\lim_{G_1 h_1 \rightarrow \infty} Q_2 = 1 \quad (235)$$

The asymptotes for small mh_1 or $G_1 h_1$ are also easy to find if the argument of the inverse hyperbolic cotangent is greater than unity. The inverse hyperbolic cotangent is not defined for arguments less than unity, indicating that if such arguments arise, the expression for the R functions in terms of

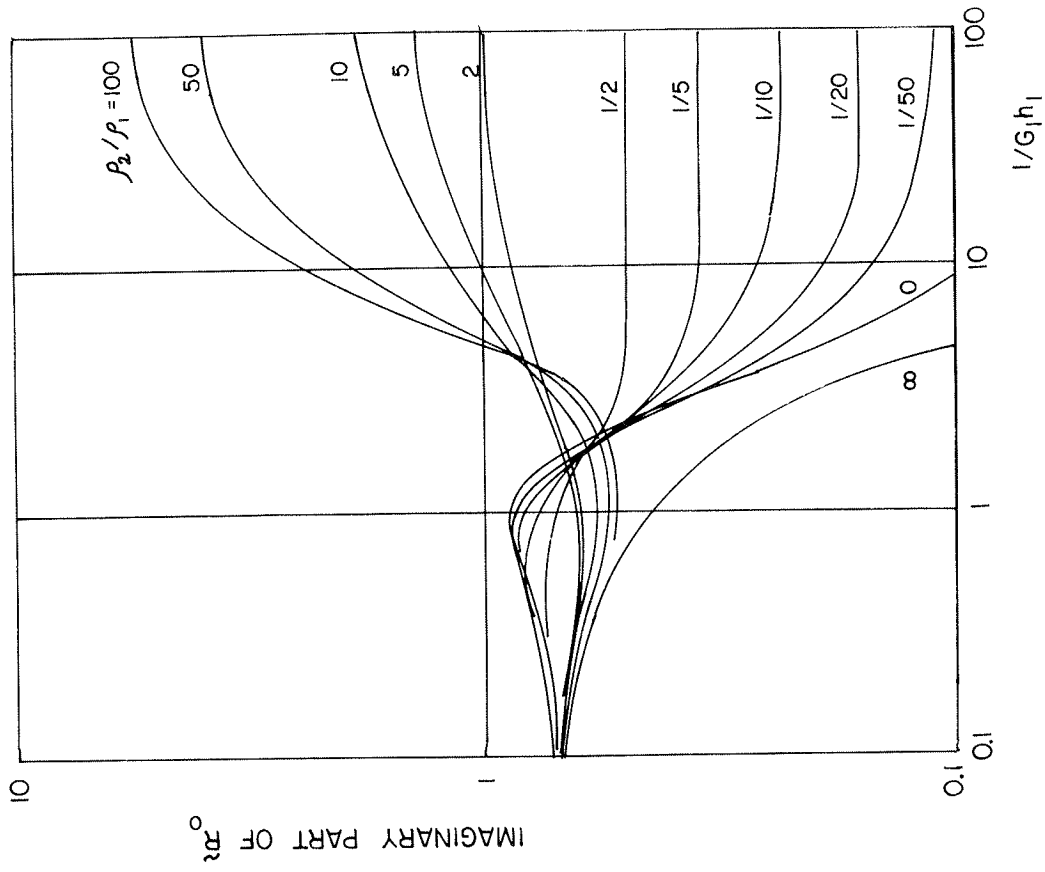


FIGURE 66.—Imaginary part of the Q function for a single layer resting on a uniform substratum.

hyperbolic tangents must be used. Thus the limits for small mh_1 or $G_1 h_1$ are:
 a. with $\rho_1 > \rho_2$

$$\lim_{mh_1 \rightarrow 0} K_2(m) = \lambda_1 \rho_1 / \lambda_2 \rho_2 \quad (236)$$

$$\lim_{G_1 h_1 \rightarrow 0} Q_2(\omega) = (\rho_1 / \rho_2)^{1/2} \quad (237)$$

b. with $\rho_1 < \rho_2$

$$\lim_{m h_1 \rightarrow 0} K_2(m) = \lambda_2 \rho_2 / \lambda_1 \rho_1 \quad (238)$$

$$\lim_{G h_1 \rightarrow 0} G_2(\omega) = (\rho_2 / \rho_1)^{1/2} \quad (239)$$

A different sequence must be used in taking limits if the contrast in resistivities between the layers is very large; that is, if ρ_1 / ρ_2 approaches either zero or infinity. In the first case, that of a buried insulator, the inverse hyperbolic cotangent in equations 231 and 232 is essentially zero and may be discarded in comparison with the first term, the one containing m or γ_1 :

$$\lim_{\lambda_2 / \rho_2 \rightarrow \infty} K_2(m) = \coth m \lambda_1 h_1 \quad (240)$$

$$\lim_{\rho_2 / \rho_1 \rightarrow \infty} G_2(\omega) = \coth \gamma_1 h_1 \quad (241)$$

These curves provide a limiting envelope for the two layer curves plotted as a function of the contrast in resistivity. For large m , or for large γ_1 , the curves approach the asymptote 1 as specified in equations 231 and 235. For small m , or for small γ_1 , the asymptotic form of 240 or 241 is:

$$\lim_{m \rightarrow \infty} \lim_{\lambda_2 / \rho_2 \rightarrow \infty} K_2(m) = \frac{1}{m \lambda_1 h_1} \quad (242)$$

$$\lim_{\omega \rightarrow 0} \lim_{\rho_2 / \rho_1 \rightarrow \infty} G_2(\omega) = \frac{1}{\gamma_1 h_1} \quad (243)$$

In both cases, the equation is that of a straight line on a logarithmic plot, with a slope of +1, intersecting the unity asymptote as $m h_1 = 1$ or $\gamma_1 h_1 = 1$.

With the case of a buried conductor, the inverse is found. The asymptotic behavior at small m or γ_1 is that of a straight line on a logarithmic plot, with a slope of -1, and with an intercept with the unity asymptote at unity. The two-layer enveloping kernel functions are shown graphically in figure 67. All two-layer Q and K functions must lie between these limiting curves and the unity axis. In fact, the K and Q functions can be shown to lie between two limiting curves, one passing through the point mH or $GH=1$ with a slope of +1, and the other passing through this point with a slope of -1, for any number of layers, with H being the total thickness of the layers, above the last one.

K and Q functions for thin layers

The problem of the sensitivity of an electrical sounding method to a thin layer with electrical properties different than the beds above it and below it is

MAGNITUDE OF K or Q FUNCTION

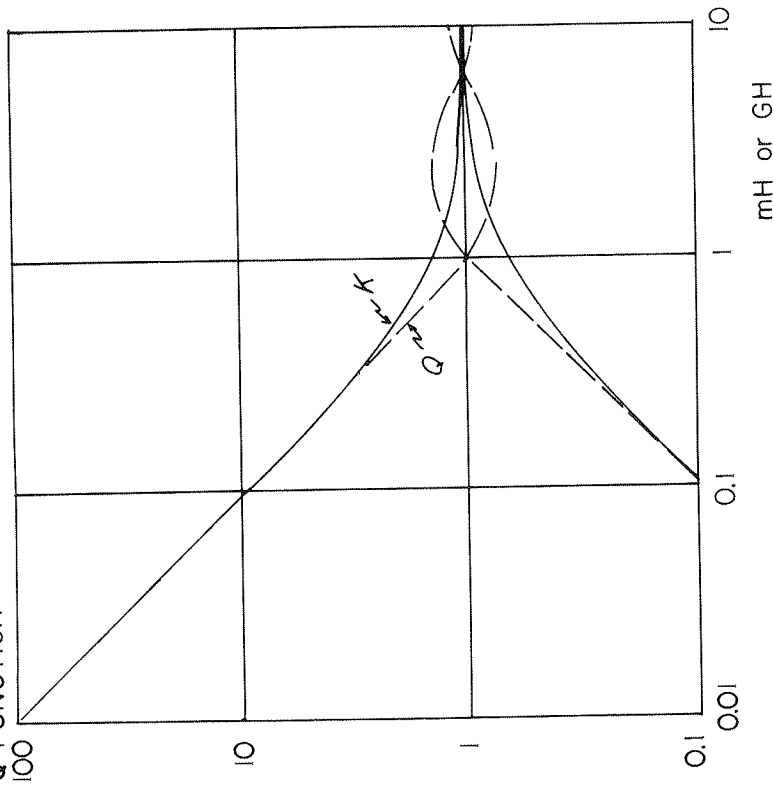


FIGURE 67.— Limiting values for the K or Q function for two layers. The actual value for the K or Q function must lie between these curves and the unity magnitude axis. H is the thickness of the top layer and G is the wave number in that layer.

of considerable interest in the petroleum prospecting applications, inasmuch as most oil fields are relatively thin compared to the depth of burial.

The problem may be formulated by assuming that a resistant layer is embedded in an otherwise uniform halfspace with a resistivity ρ_1 . The resistivity of the thin layer is taken as ρ_2 , with $\rho_2 \gg \rho_1$. The depth to the thin layer is taken as H , and the thickness as t . The definitions of these parameters describing the section are indicated on figure 63.

The K and Q functions for a three layer sequence are given by:

$$K_3(m) = \coth \left\{ m \lambda_1 H + \coth^{-1} \frac{\lambda_2 \rho_2}{\lambda_3 \rho_3} \left[\coth \left(m \lambda_2 t + \coth^{-1} \frac{\lambda_2 \rho_2}{\lambda_3 \rho_3} \right) \right] \right\} \quad (244)$$

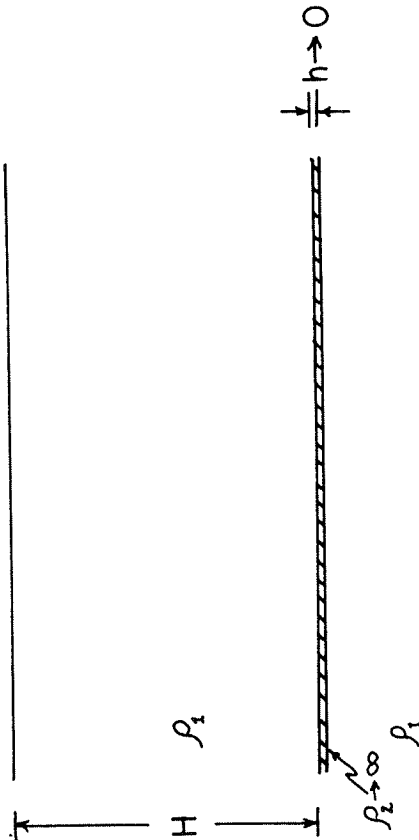


FIGURE 68. — Definition of the model used in computing the effect of a thin, resistant bed on electric and magnetic field behavior.

$$Q_3(\omega) = \tanh \left\{ \gamma_1 H + \tanh^{-1} \left(\frac{\rho_1}{\rho_2} \right)^{1/2} \left[\coth \left(\gamma_2 \frac{1}{2} + \coth^{-1} \left(\frac{\rho_2}{\rho_1} \right)^{1/2} \right) \right] \right\} \quad (215)$$

Let us now consider the limiting behavior of these two expressions as we let the ratio l/H become small. At the same time, we will let the ratio ρ_2/ρ_1 become large in such a way that the ratio $\rho_1 H/\rho_2 l$ remains constant (note that the product of the resistivity and the thickness of a layer, such as $\rho_1 H$ or $\rho_2 l$, is a parameter which might be used to characterize that layer, and which is called the transverse resistance, T). With the layer resistivity much greater than the resistivity of the underlying material, the inverse hyperbolic tangents in equations 214 and 215 become negligible in comparison with the term ml or $\gamma_2 l$, as the case may be, and the equations may be simplified to the forms:

$$K_3(m) \approx \tanh \left\{ m \lambda_1 H + \tanh^{-1} \left(\frac{\lambda_1 \rho_1}{\lambda_2^2 m T_2} \right) \right\} \quad (216)$$

$$Q_3(\omega) \approx \tanh \left\{ \gamma_1 H + \tanh^{-1} \left(\frac{\rho_1}{\rho_2} \right)^{1/2} \cdot \frac{1}{\gamma_2 l} \right\} = \tanh \left\{ \gamma_1 H + \tanh^{-1} \frac{1}{\gamma_2 l} \right\} \quad (217)$$

These equations may be rewritten using the formulas for the sums of arguments for hyperbolic tangents:

$$K_3(m) = \frac{\tanh mH + \frac{\lambda_1 \rho_1}{\lambda_2^2 m T_2}}{1 + \frac{\lambda_1 \rho_1}{\lambda_2^2 m T_2} \tanh mH} \quad (218)$$

$$Q_3(\omega) = \frac{\tanh \gamma_1 H + \frac{1}{\gamma_2 l}}{1 + \frac{1}{\gamma_2 l} \tanh \gamma_1 H} \quad (219)$$

Note that as $m \rightarrow \infty$, $K_3(m) \rightarrow 1$, and as $\omega \rightarrow \infty$, $Q_3(\omega) \rightarrow 1$, as is the proper behavior in the limit. However, the K and Q functions would be uniquely unity for the case in which the thin layer was not present, inasmuch as the earth would be a uniform halfspace in that case. Thus, in order to discuss the anomaly caused by the presence of the thin layer, we need to consider the difference $K_3(m) - 1$ or $Q_3(\omega) - 1$:

$$K_3(m) - 1 = \frac{\frac{\rho_1}{m T_2} + \left(1 - \frac{\rho_1}{m T_2}\right) \tanh mH - 1}{1 + \frac{\rho_1}{m T_2} \tanh mH} \quad (250)$$

$$Q_3(\omega) - 1 = \frac{\frac{1}{\gamma_2 l} + \left(1 - \frac{1}{\gamma_2 l}\right) \tanh \gamma_1 H - 1}{1 + \frac{1}{\gamma_2 l} \tanh \gamma_1 H} \quad (251)$$

Here, for convenience, the layers have been assumed to be isotropic. Let us now consider the behavior of these two functions—the kernel function differences which define the sensitivity of various electrical sounding methods to the presence of a thin, resistant layer. The asymptotic behavior for small m or ω is found by replacing the hyperbolic tangent by its argument:

$$K_3(m) - 1 \Big|_{m \rightarrow 0} \approx \frac{T_1/T_2}{1 + T_1/T_2} \cdot \frac{1}{mH} \quad (252)$$

$$Q_3(\omega) - 1 \Big|_{\omega \rightarrow 0} \approx \frac{H/l}{1 + H/l} \cdot \frac{1}{\gamma_1 H} \approx \frac{1}{\gamma_1 H} \left(1 - \frac{l}{H}\right) \quad (253)$$

It is interesting to note that for the K function, the values depend only on the transverse resistance, T_2 , of the thin layer, and on none of its other characteristics. For the Q function, the values depend only on the thickness of the thin layer, and not on the resistivity, so long as the resistivity contrast is high enough that the approximations used above are valid.

These last two equations show that the asymptotic behavior at small m or ω is such that on the usual bilogarithmic plot, the curves will approach straight lines with a slope of -1 to the left, with an intercept on the unity axis at

$$\frac{T_1/T_2}{1 + T_1/T_2} \text{ or on the unity axis for } \gamma_1 H \text{ at } (1 - t/H).$$

For a large m or high ω , the asymptotic behavior can be found by replacing the hyperbolic tangent in equations 250 and 251 by $1 - 2e^{-2m}$ or by $1 - 2e^{-2\gamma m}$, as the case may be:

$$K_3(m) - 1 \Big|_{m \rightarrow \infty} = -2e^{-2mH} \quad (251)$$

$$Q_3(\omega) - 1 \Big|_{\omega \rightarrow \infty} = -2e^{-2\gamma H} = -2e^{-2G_1 H} (\cos G_1 H - i \sin G_1 H) \quad (255)$$

The behavior of these three-layer K and Q functions is shown graphically in figures 69-71, for various resistivity and thickness parameters for the thin layer. The K function passes through a minimum which deepens as the ratio T_2/T_1 becomes larger, while the Q function has a magnitude which passes through a minimum which deepens as the ratio t/H becomes larger. The phase of the Q function differs from 45° only in the range of frequencies around $\gamma_1 H = 1$. It is interesting to note that the behavior of the two functions is so similar. One difference which is important is that the anomaly caused by the presence of the thin resistant layer is proportional to the transverse resistance for the K function, but to the relative thickness of the thin bed in the case of the Q function. Inasmuch as

$$T_2/T_1 = \frac{\rho_2 t}{\rho_1 H}$$

it is apparent that the anomaly in the K function caused by a thin resistant bed will always be much larger than the anomaly caused by the same bed in the Q function.

THE HANKEL TRANSFORM

The R^* , \tilde{R} , K and Q functions provide only a partial solution to the problem of describing electromagnetic field behavior, except for the one case of the magnetotelluric method (in which the earth resistivity is determined directly from measured Q functions). In all other cases, the R^* , \tilde{R} , K and Q functions must be incorporated in an integral transform before the field quantity actually measured can be determined. Conversely, in order to derive the electrical properties of the earth from measured field data, these data may

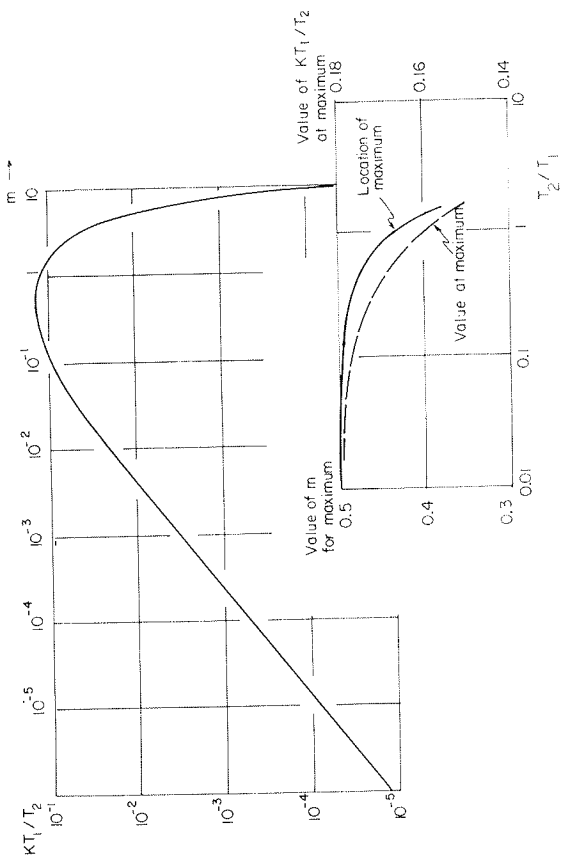


FIGURE 69.—Behavior of the K function for a resistant bed of limiting thickness. The upper curve is the contribution to the K function by a bed of zero thickness and infinite resistivity, characterized by a transverse resistance T_2 . The transverse resistance of the overlying bed is T_1 . The inset at the lower right shows how the maximum point on this curve departs from its position for $T_2 = 0$, as T_2 is made larger with respect to T_1 .

PERCENTAGE ANOMALY IN APPARENT RESISTIVITY, per $h/H = 1\%$

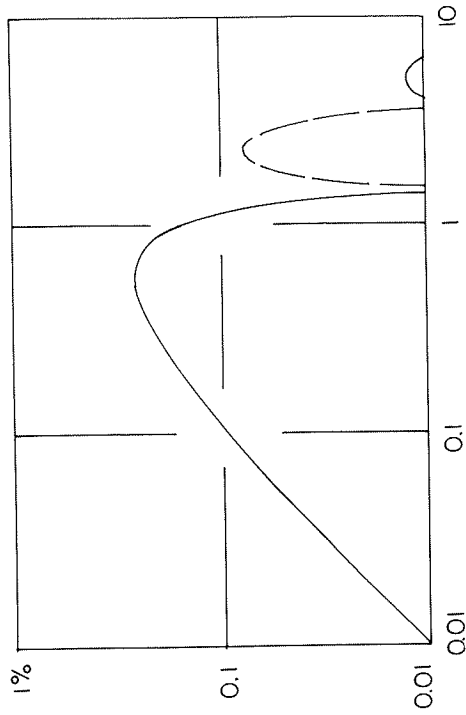


FIGURE 70.—Thin-bed anomaly in the Q function expressed as an apparent resistivity ($\rho_a = \rho_1 Q^2$). The dashed part of the curve is negative with respect to the solid part.

DEPTH TO WAVELENGTH RATIO

In equation 135:

$$I_3 = \int_0^\infty \frac{R^*}{m\lambda_1\bar{n}_1} \cdot \frac{1}{\frac{\gamma_2^2}{\gamma_1^2 n_0} + \frac{R^*}{\lambda_1\bar{n}}} J_0(mr) dm \quad (258)$$

In equation 136:

$$I_4 = \int_0^\infty \frac{\gamma_2^2}{\gamma_1^2 n_0} \frac{1}{R^* + \lambda_1\bar{n}} J_1(mr) dm \quad (259)$$

In equation 136:

$$I_5 = \int_0^\infty \frac{\gamma_2^2}{n_0 + \frac{n_1}{R}} \frac{n_1}{R} J_1(mr) dm \quad (260)$$

In equation 158:

$$I_6 = \int_0^\infty \frac{n_1}{R} \cdot \frac{m}{n_0 + \frac{n_1}{R}} J_0(mr) dm \quad (261)$$

There are a variety of approaches to evaluating such integral transforms, but let us first consider the case in which the spacing from source to receiver, r , is large. In this case, the object functions in the transforms can be approximated in such a way that the integrals may be evaluated in closed form.

Let us first consider the integral I_1 in equation 256. First note what happens if we consider spacings, r , which tend to be infinite. The Bessel function which is the kernel of the integral transform acts as a damped sinusoid for large values of its argument. Therefore, the integral is dominated by its behavior at $m \rightarrow 0$ when $r \rightarrow \infty$. In the limit for infinite spacing, the integral can be evaluated by taking $m=0+\epsilon$, defining the value for the ratio function \bar{R} under these circumstances as \bar{R}_0 :

$$\bar{R}_0 = \lim_{m \rightarrow 0} \bar{R} = \coth \left\{ \gamma_1 h_1 + \coth^{-1} \frac{\gamma_1}{\gamma_2} \left[\coth \left(\gamma_2 h_2 + \coth^{-1} \dots \coth^{-1} \frac{\gamma_{N-1}}{\gamma_N} \dots \right) \right] \right\} \quad (262)$$

If we expand the object function of the integral transform in equation 256, assuming small values for m , we have:

$$\frac{m}{n_0 + \bar{R}} \approx \frac{m}{m + \bar{R}_0} = \frac{m \bar{R}_0}{\gamma_1} - \frac{m^2 \bar{R}_0^2}{\gamma_1^2} + \dots \quad (263)$$

retaining only terms in m and m^2 as being significant. The following limiting values for the integral transforms have been shown to hold (Tikhonov, 1959):

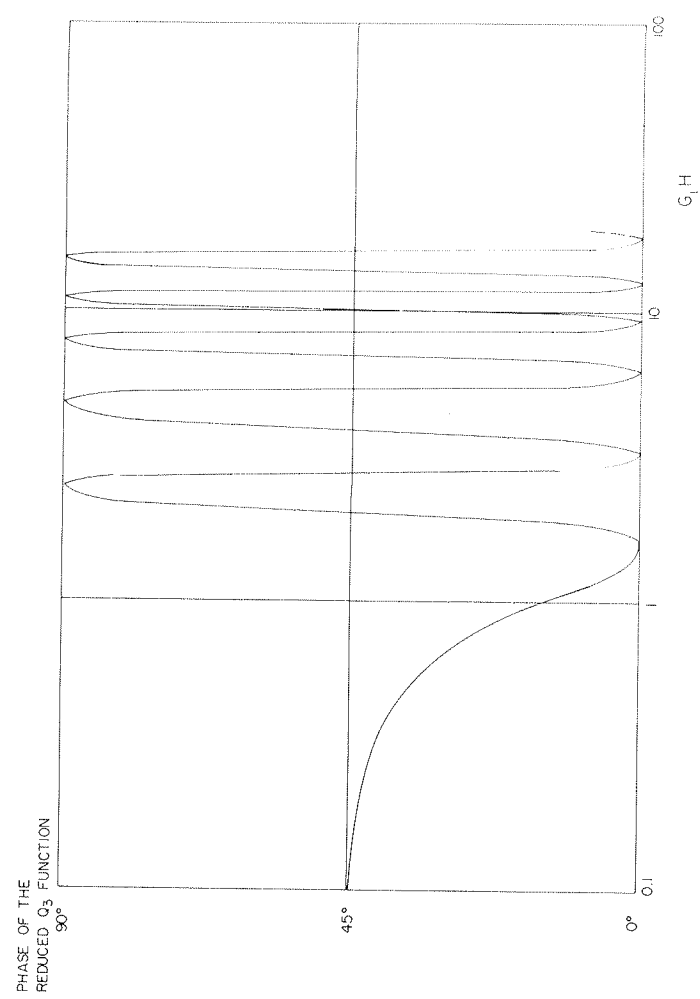


FIGURE 71.—Phase of the reduced impedance contribution, Q_3-1 for the case of a thin, resistant bed imbedded in an otherwise uniform medium in which the real part of the wave number is G_1 .

have to be inverse transformed to provide the R, K and Q functions for interpretation.

Examples of the integral transforms which must be made are contained in equations 134-136, for field components about a horizontal current dipole, and in equations 156-158, for field components about a vertical magnetic dipole. The particular forms of integral transforms which must be evaluated in these expressions are as follows:

In equations 134, 136, 156 and 157:

$$I_1 = \int_0^\infty \frac{m}{n_0 + \frac{n_1}{R}} J_0(mr) dm \quad (256)$$

In equation 135:

$$I_2 = \int_0^\infty \frac{n_1/\bar{R}}{m(n_0 + \frac{n_1}{R})} J_0(mr) dm \quad (257)$$

$$\lim_{r \rightarrow \infty} \int_0^{\infty} m J_0(mr) dm = 0 \tag{264}$$

$$\lim_{r \rightarrow \infty} \int_0^{\infty} m^2 J_0(mr) dm = \frac{1}{r^3} \tag{265}$$

$$\lim_{r \rightarrow \infty} \int_0^{\infty} m^{2n-1} J_0(mr) dm = 0, \quad n = 1, 2, \dots \tag{266}$$

$$\lim_{r \rightarrow \infty} \int_0^{\infty} m^{2n} J_0(mr) dm = \frac{1}{r^{2n+1}}, \quad n = 0, 1, 2, \dots \tag{267}$$

That is, when the zero-order Bessel kernel is multiplied by an odd power of m , the infinite integral has zero value.

The integral, I_1 , might be evaluated as follows:

$$\begin{aligned} -I_1 &= \frac{\tilde{R}_0^2}{\gamma_1^2} \cdot \frac{1}{r^3} + \frac{\tilde{R}_1^4}{\gamma_4^4} \cdot \frac{1}{r^5} + \frac{\tilde{R}_6^6}{\gamma_6^6} \cdot \frac{1}{r^7} + \dots \\ &= \frac{\tilde{R}_0^2}{\gamma_1^2} \cdot \frac{1}{r^3} \left[1 + \frac{\tilde{R}_1^2}{\gamma_1^2 r^2} \left(1 + \frac{\tilde{R}_2^2}{\gamma_2^2 r^2} \left(1 + \dots \right) \right) \right] \end{aligned} \tag{268}$$

Each of the integrals may be evaluated in the same way. For example, I_2 may be expanded for large r (or for small m) as:

$$\int_0^{\infty} \frac{\eta/\tilde{R}}{m(\eta_0 + \tilde{R})} J_0(mr) dm \approx \int_0^{\infty} \frac{1}{m} \left[1 - \frac{m\tilde{R}_0}{\gamma_1} + \frac{m^2\tilde{R}_2^2}{\gamma_2^2} - \frac{m^3\tilde{R}_3^3}{\gamma_3^3} + \dots \right] J_0(mr) dm \tag{269}$$

Evaluations of the other expressions may be found in several monographs by Vanyan (1966, 1967).

It is of considerable interest to note what happens if only the first order term in series expansions such as these is considered to be significant. The substitution of the first term from equation 268 in the expression for the tangential electric field about a vertical-axis magnetic dipole source (equation 156) provides the result:

$$E_{\theta}^* \Big|_{r \rightarrow \infty} = \frac{3MA}{2\pi r^3} \tilde{R}_0^2 \tag{270}$$

Multiplication of the tangential electric field strength by the geometric factor for a loop-to-wire coupling system, based on the field behavior over a homogeneous earth, leads to:

$$\mathcal{Q}_a = \rho_1 \tilde{R}_0^2 \tag{271}$$

Thus if the spacing from source to receiver is large enough, an induction sounding technique using a vertical-axis loop source and a grounded wire to detect the tangential electric field will provide the same curves for apparent resistivity as a function of frequency as the magnetotelluric method. The distance, r , is normalized in terms of radian wave lengths in the surface layer, γ_1 , and so the distance to which the approximation for large values of r is valid will depend on frequency. As the frequency is lowered, the higher-order terms in the series approximation for the integrals will become significant, and the apparent resistivity will depart from that for the magnetotelluric method.

Similar results may be found to each of the methods, and it is obvious that if only large spacings from source to receiver are considered, the apparent resistivity curves obtained will reduce to one of two forms: one specified by the \tilde{R}_0 function and the other by the \tilde{R}_n function. If the spacing is not as large in terms of wave lengths as is required for this approximation to be good, it is not apparent that all the many source-receiver combinations will behave similarly. There is considerable room for research on the relative merits of the various source-receiver combinations for moderate source-receiver separations.

General properties of the Hankel transforms

The expansion of the Hankel transform integrals for large source-receiver separations is useful in illustrating the nature of apparent resistivities measured with the various induction methods, but in fact, spacings large enough that this is a good approximation cannot always be used in the field. Therefore, it is essential that the integrals listed above be evaluated in a more general way. According to Erdelyi, the Hankel transform is generally written as:

$$g(r) = \int_0^{\infty} (mr)^{\gamma/2} f(m) J_{\nu}(mr) dm = \mathcal{H}_{\nu} \{ f(m), r \} \tag{272}$$

The Hankel transform has the useful characteristic of being self-reciprocal; that is:

$$f(m) = \int_0^{\infty} (mr)^{\gamma/2} g(r) J_{\nu}(mr) dm = \mathcal{H}_{\nu}^{-1} \{ f(m), r \} \tag{273}$$

For our purposes, only Hankel transforms of order zero and unity are needed:

$$\mathcal{H}_0 \{ f(m), r \} = \int_0^{\infty} (mr)^{1/2} f(m) J_0(mr) dm \tag{274}$$

$$\mathcal{H}_1 \{ f(m), r \} = \int_0^{\infty} (mr)^{3/2} f(m) J_1(mr) dm \tag{275}$$

A number of transform pairs of both types are listed and shown graphically in figures 72 and 73. The symmetry typical of transform pairs is readily evident here: right is exchanged for left and top is exchanged for bottom in going through a Hankel transformation, but in addition, a rotation of the transformed function takes place.

In determining the behavior of the actual field quantities from the Hankel transforms indicated in equations 256-261, computations are performed separately on the real and imaginary parts in the object function of the integrand. Typical sets of source functions and transformed functions are shown in figures 74-76.

Evaluation by series expansion

One approach to the evaluation of the transforms in equations 256-261 is the use of series expansions which will eliminate the need for evaluating the integral expressions. The case for small values of the separation, r , has been treated by Meinardus (1967) as follows. The Bessel function $J_\nu(mr)$ is replaced by an ascending power series (Abramowitz and Stegun, 1965, p. 360):

$$J_\nu(mr) = \left(\frac{mr}{2}\right)^\nu \sum_{k=0}^{\infty} \frac{(-\frac{m^2 r^2}{4})^k}{k! \Gamma(\nu+k+1)} \tag{276}$$

Replacing the Bessel functions in equations 256-261 leads to the forms:

$$I_1 = \int_0^{\infty} \Phi_1 \cdot \sum_{k=0}^{\infty} \frac{(-\frac{m^2 r^2}{4})^k}{k! \cdot k!} dm \tag{277}$$

where

$$\Phi_1 = \frac{m}{r_0 + \frac{r}{R}}$$

$$I_2 = \int_0^{\infty} \Phi_2 \sum_{k=0}^{\infty} \frac{(-\frac{m^2 r^2}{4})^k}{k! \cdot k!} dm \tag{278}$$

$$\Phi_2 = \frac{r_1/R}{m(r_0 + \frac{r}{R})}$$

where

$$I_3 = \int_0^{\infty} \Phi_3 \sum_{k=0}^{\infty} \frac{(-\frac{m^2 r^2}{4})^k}{k! \cdot k!} dm \tag{279}$$

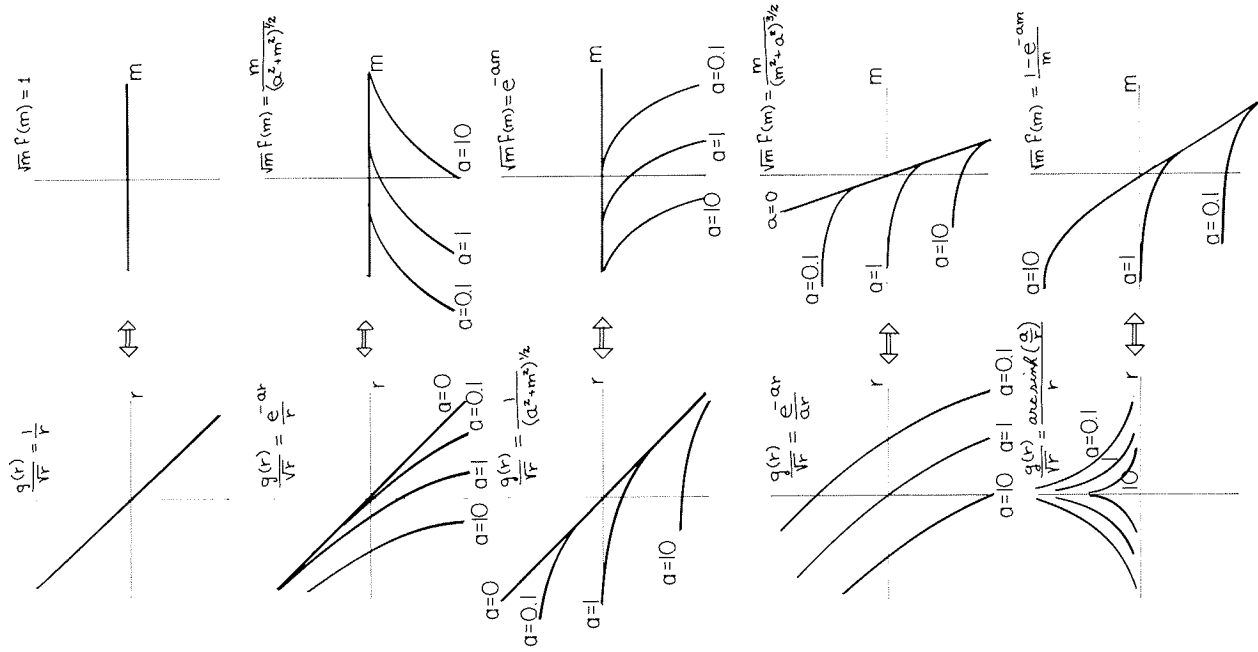


FIGURE 72.—Hankel transform pairs with the zero-order Bessel function as a kernel.

$$\Phi_3 = \frac{R^*}{m\lambda_1\eta_1} \frac{1}{\frac{\gamma_0^2}{\lambda_1^2\eta_0} + \frac{R^*}{\lambda_1\eta_1}}$$

where

$$I_4 = \int_0^\infty \frac{m^2 r}{2} \Phi_4 \sum_{k=0}^\infty \frac{(-\frac{m^2 r^2}{4})^k}{k!(k+1)!} dm \tag{280}$$

where

$$\Phi_4 = \frac{1}{\frac{\gamma_0^2}{\lambda_1^2\eta_0} + \frac{R^*}{\lambda_1\eta_1}}$$

(281)

$$I_5 = \int_0^\infty \frac{m^2 r}{2} \Phi_5 \sum_{k=0}^\infty \frac{(-\frac{m^2 r^2}{4})^k}{k!(k+1)!} dm$$

where

$$\Phi_5 = \frac{\gamma_{41}^2}{\eta_0 + \frac{\eta_1}{R}}$$

and

$$I_6 = \int_0^\infty \Phi_6 \sum_{k=0}^\infty \frac{(-\frac{m^2 r^2}{4})^k}{k!k!} dm \tag{282}$$

where

$$\Phi_6 = \frac{\eta_1}{R} \frac{m}{\eta_0 + \frac{m}{R}}$$

In order that these expressions be useful, it is essential that the series converge to an approximate value for the expression within a few terms. Writing out the series represented by one of the zero-order transforms, we have:

$$I_1 = \int_0^\infty \Phi_1 dm - \frac{r^2}{4} \int_0^\infty m^2 \Phi_1 dm + \frac{r^4}{8A} \int_0^\infty m^4 \Phi_1 dm - \dots \tag{283}$$

and one of the unity order transforms, we have:

$$I_4 = \frac{r}{2} \int_0^\infty m \Phi_4 dm - \frac{r^3}{8} \int_0^\infty m^3 \Phi_4 dm + \frac{r^5}{128} \int_0^\infty m^5 \Phi_4 dm - \dots \tag{284}$$

These series converge quickly only if the product γ_{1r} (the ratio of separation to skin depth in the surface layer) is considerably smaller than one.

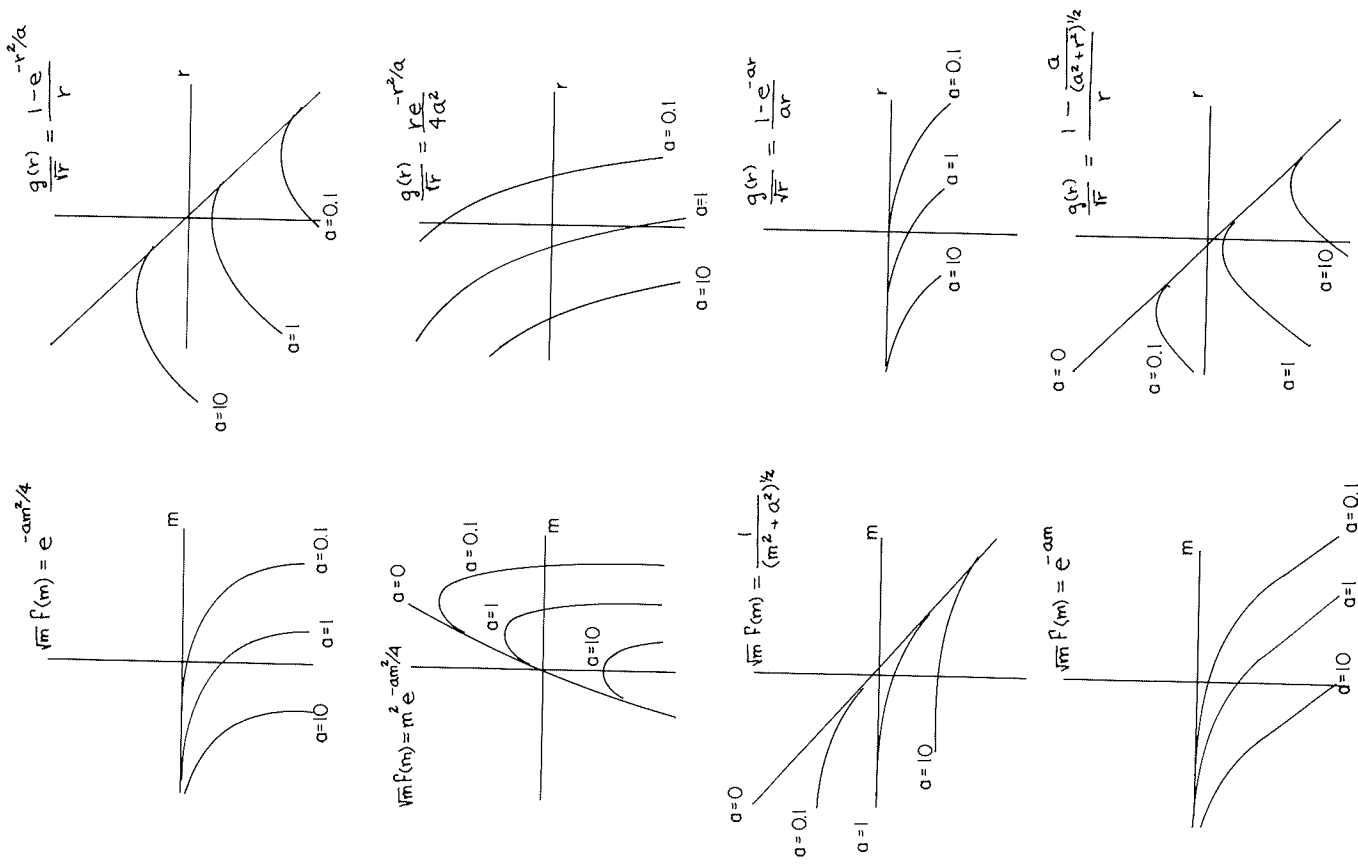


FIGURE 73. — Hankel transform pairs with the first-order Bessel function as a kernel.

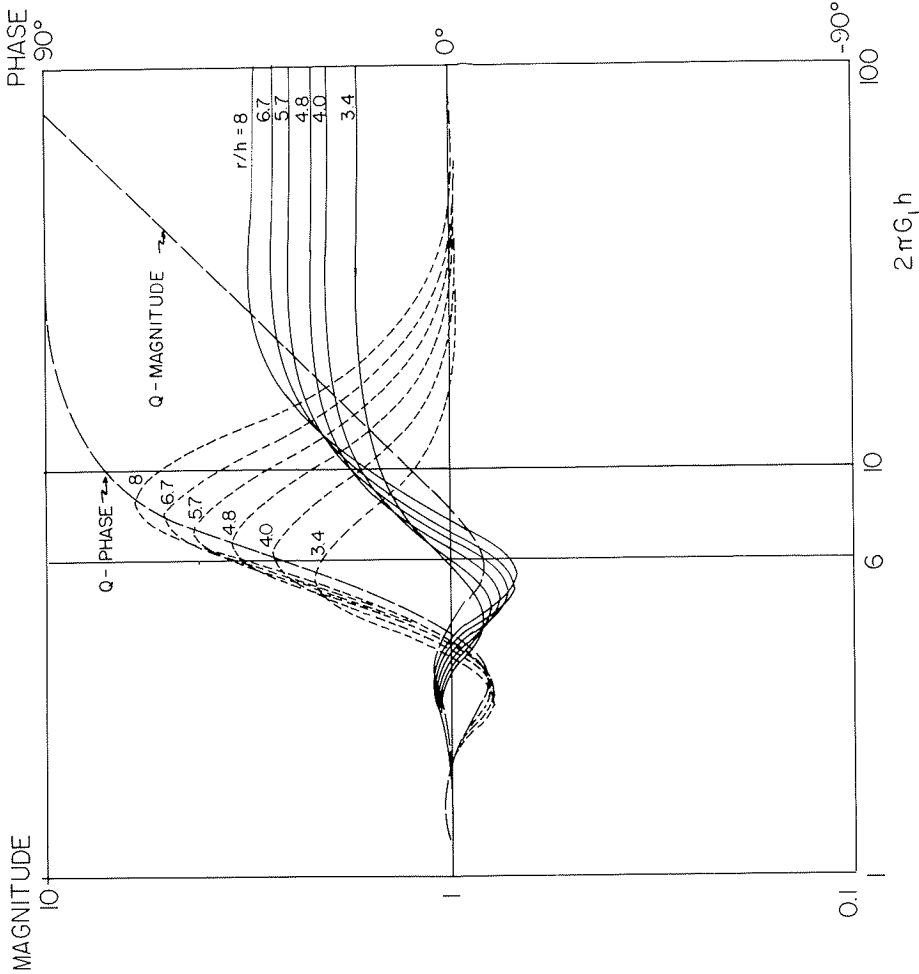


FIGURE 76. — Example of the transformation of a Q function to the apparent resistivity curves observed with electric dipole tangential electric dipole system. The case is that of a single uniform layer with a wave number G covering an insulating substratum.

These asymptotic expressions are useful only in evaluating the field components at very short spacings or low frequencies.

As pointed out by Baranov and Kunetz (1958), Bödvarsson (1966) and Meinardus (1967), an alternate approach to the series representation of the Hankel transform can be made which provides insight into the meaning of the transform process. Consider that any one of the object functions Φ_1 to Φ_6 , is the unilateral Laplace transform of some function, $q(z)$:

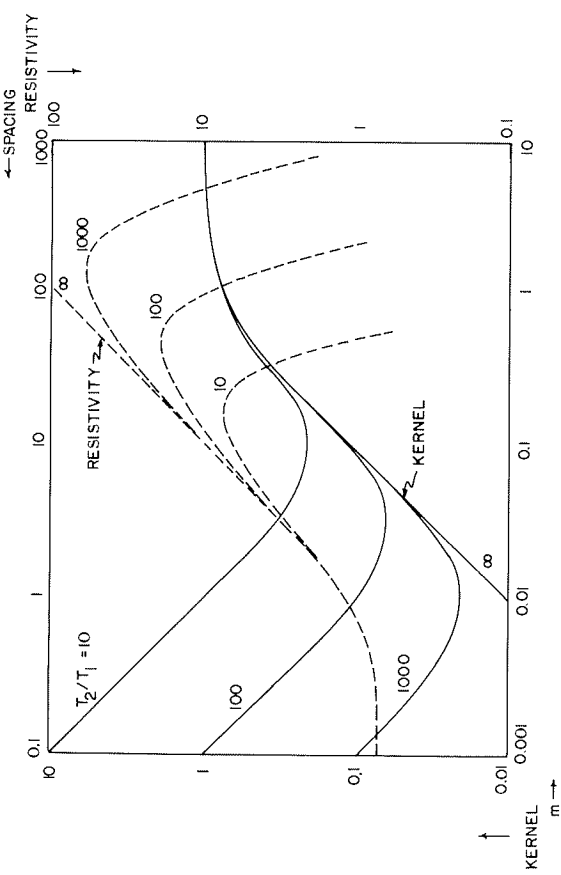


FIGURE 74. — Transformation of a K function to the resistivity function for a Schlumberger array. The case is that of three layers, with the middle one being thin and resistant, and the lowest one being perfectly conducting. T_2/T_1 is the ratio in transverse resistances between the surface layer and the middle layer.

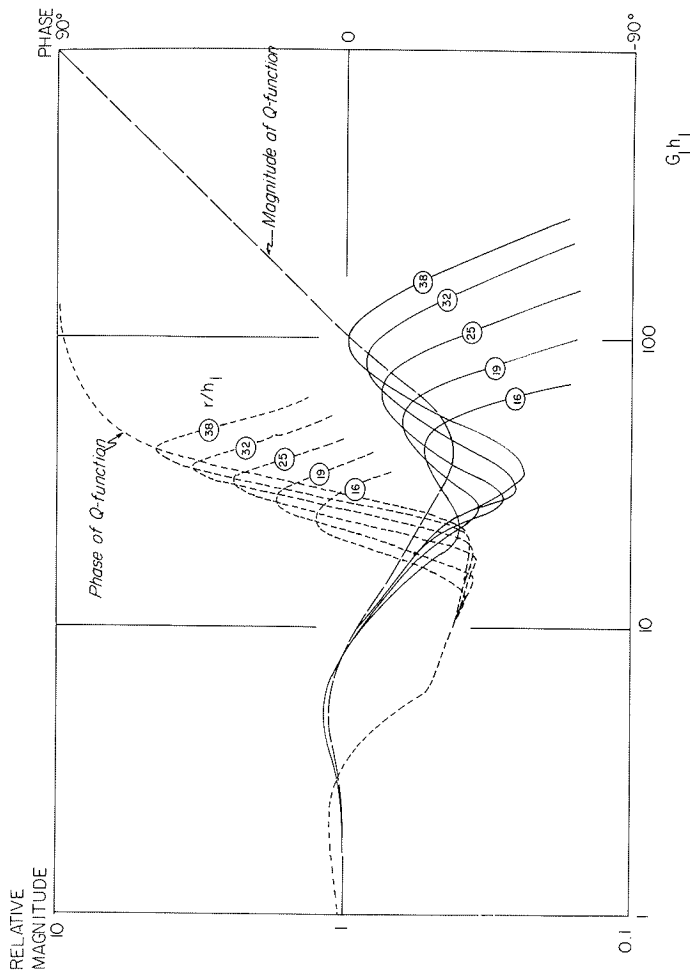


FIGURE 75. — Transformation of a Q function for three layers (resistivity sequence, 1; 1/4:∞, and thickness sequence 1:5) to an apparent resistivity curve for a vertical-axis coil source and tangential electric field receiver.

$$\Phi_1 = \int_0^\infty q(z) e^{-mz} dz \tag{285}$$

We substitute this integral expression in the transform integral (eq. 252 for example), with the result:

$$I_1 = \int_0^\infty \int_0^\infty q(z) e^{-mz} J_0(mr) dz dm \tag{286}$$

If the order of integration is changed, we have the Hankel transform of an exponential, which is well known (Erdelyi, 1953):

$$I_1 = \int_0^\infty \frac{q(z)}{(r^2+z^2)^{1/2}} dz \tag{287}$$

The quantity $(r^2+z^2)^{1/2}$ can be thought of as the distance from a point displaced up or down the z axis and a point located radially outward from the source at a distance r . The quantity $q(z)$ can be thought of as a Green's function, or a distribution of sources of field components along the z axis. The integral in equation 287 then represents the accumulation of effects at the observation point from a fictitious distribution of sources all along the z axis.

In the zero-frequency limit, the distribution along the z axis has the significance of images, as discussed by many authors in the development of the theory for direct-current flow (see Heiland, 1940; Roman, 1963; Meinardus, 1967; many others). For example, the object function to be transformed in the zero-frequency case for two layers is simply:

$$\Phi_0(m) = \frac{1 - ke^{-2mh_1}}{1 + ke^{-2mh_1}} \quad ; \quad k = \frac{\rho_1 - \rho_2}{\rho_1 + \rho_2} \tag{288}$$

Inasmuch as $|ke^{-2mh}| < 1$ (except for $\rho_2 = 0$ or ∞), the object function may be expanded in the series:

$$\Phi_0(m) = 1 + 2 \sum_{j=1}^\infty (-k)^j e^{-2jmh_1} \tag{289}$$

The inverse Laplace transform of this function is:

$$q(z) = \delta(z-o) + 2 \sum_{j=1}^\infty (-k)^j \delta(z \pm z_j h_1) \tag{290}$$

Thus, $q(z)$ consists of an infinite train of impulses along the z axis. These can be thought of as being optical images of the source reflected about the plane of separation between the layer.

The same approach may be used in evaluating the other Hankel transforms, though the image approach is used much less commonly for electromagnetic theory than for direct-current theory. Let us consider the same two-layer case, and evaluate the integral I_1 . The object function may be written as follows, if we assume the spacing, r , is relatively large:

$$\Phi_1 \Big|_{r \rightarrow \infty} = \frac{m}{\gamma_1} \tilde{\rho}_o = \frac{m}{\gamma_1} \frac{1 - ke^{-2\eta_1 h}}{1 + ke^{-2\eta_1 h}} \tag{291}$$

where

$$\frac{1 - ke^{-2\eta_1 h}}{1 + ke^{-2\eta_1 h}} = 1 + 2 \sum_{j=1}^\infty (-k)^j e^{-2j\eta_1 h}$$

and

$$k = \frac{\eta_2 - \eta_1}{\eta_2 + \eta_1}$$

The inverse Laplace transforms of the terms in the series also constitute a sequence of image strengths:

$$q(z) \approx e^{-2Qz} \left\{ \delta(z-o) + 2 \sum_{j=1}^\infty (-k)^j \delta(z \pm z_j h) \right\} \tag{292}$$

However, the intensity of the images decreases with distance along the z axis exponentially, representing the effects of attenuation, and there is a phase shift associated with each image.

Little has been done with the evaluation of the Hankel transforms using such an image analogy, but it may provide a useful approach in the future.

Evaluation using orthogonal polynomial approximation

It has been suggested by Onodera (1963) that the Hankel transform for the zero-frequency case may be evaluated by replacing the object function with a series of orthogonal polynomials of such a form that each term in the polynomial may be transformed easily. The simplest function which might be used in this way is an exponential, in view of the Lipschitz integral. The object function to be transformed is approximated with a series:

$$\Phi_\eta(m) \approx \sum_{\nu=0}^N A_\nu^{(\eta)} e^{-2\nu\eta m} \tag{293}$$

The coefficients in the series approximation are evaluated with simple techniques described by Onodera (1963) or Lee (1959). The transformation of the exponential series provides the result:

$$I_\eta(r) = \sum_{\nu=0}^\infty \frac{A_\nu^{(\eta)}}{(4\nu^2 + r^2)^{1/2}} \tag{294}$$

It is interesting to note that the coefficients A_n could be considered to be image sources located at points along the z axis determined by the values selected for v in matching the object function in the Hankel transform. These images are then an abbreviated approximation to the infinite series of optical images, an approach resembling that used by van Dam (1965, 1967) in evaluating the zero-frequency transform expression.

Evaluation using numerical quadrature

Meinardus (1967) has discussed in detail the evaluation of the Hankel transform for the zero-frequency case. He notes that there are two basic approaches to numerical quadrature: approximation of segments of the object function, such as ϕ_1 to ϕ_6 (taking their real and imaginary parts separately) with a polynomial which provides an integral which can be evaluated in closed form (the major difference between this and the preceding method is the fact that only segments of the object function are approximated at any one time, rather than the full function); and methods in which the complete integral, both object function and Bessel kernel, are approximated.

In the first approach, it is argued that the range of integration for the transform integrals need not actually be taken infinite as indicated in the defining equations 256-261, but may be terminated at some upper limit, m_c . The reason is that as m becomes large, any of the object functions approach unity as the value of their real portions, while the imaginary portions become small. For the real part, the contribution to the integral from the value m_c at which the object function becomes sensibly constant to $m = \infty$ can be written as the value of a Bessel integral, which has been tabulated (Chistova, 1958) or which may be computed using standard function subroutines (Abramowitz and Stegun, 1964). Thus, in practice, the integral transforms may be written as:

$$\text{Real} \{ I_1(r) \} = \int_0^{m_c} \text{Real} \{ \Phi_1(m) \} J_0(mr) dm + \frac{1}{r} - \beta_0(m_c) \quad (295)$$

where

$$\beta_0(m_c) = \int_0^\infty J_0(mr) dm$$

for the real part of the object function and as:

$$d \text{mag} \{ I_1(r) \} = \int_0^{m_c} d \text{mag} \{ \Phi_1(m) \} J_0(mr) dm \quad (296)$$

The finite range of integration is then divided into panels, so that equations 295 and 296 may be rewritten as:

$$\text{Real} \{ I_1(r) \} = \sum_{j=1}^p \int_{m_j}^{m_{j+1}} \text{Real} \{ \Phi_1(m) \} J_0(mr) dm + \frac{1}{r} - \beta_0(m_c) \quad (297)$$

$$d \text{mag} \{ I_1(r) \} = \sum_{j=1}^p \int_{m_j}^{m_{j+1}} d \text{mag} \{ \Phi_1(m) \} J_0(mr) dm \quad (298)$$

and

Over each individual panel, the object function is approximated with a polynomial of degree n , which passes precisely through $n+1$ points over the range of that panel:

$$\text{Real} \{ \Phi_1(m) \} \approx \sum_{i=0}^n a_i m^i \quad (299)$$

and

$$d \text{mag} \{ \Phi_1(m) \} \approx \sum_{i=0}^n b_i m^i \quad (300)$$

Combining these last two expressions, we obtain the quadrature formulas used in actual computations:

$$\text{Real} \{ I_1(r) \} = \sum_{j=1}^p \sum_{i=1}^{m_{j+1}} \sum_{i=1}^{m_j} a_i m^i J_0(mr) dm \quad (301)$$

and

$$d \text{mag} \{ I_1(r) \} = \sum_{j=1}^p \sum_{i=1}^{m_{j+1}} \sum_{i=1}^{m_j} b_i m^i J_0(mr) dm \quad (302)$$

These definite integrals may be evaluated by computational algorithms as given by Abramowitz and Stegun (1964), or may be looked up in tables such as those given by Chistova (1958). The first procedure is described in detail by Meinardus (1967).

This approach has been used by several authors in computing zero-frequency transforms, with good results (see Mooney and Wetzel, 1957, Galbraith and others, 1964).

Meinardus (1967) reports that even better results may be obtained in making a polynomial approximation for the entire integrand in the transform expressions. In numerical quadrature formulas, the integral as a whole is approximated by a finite sum of weighted ordinates of the function, with the weights being obtained from a polynomial which matches the function exactly at a series of sample points. There are a number of techniques for approximating the integrand, but Meinardus had most success with a Gaussian formula, where the samples are determined by the zeros of Legendre polynomials. The technique is described in detail in Meinardus (1967).

A number of compilations of values for the various integral transforms used in describing electromagnetic field components are available in the literature. The most extensive catalogs of such values for the non-zero-frequency cases are those by Vanyan (1967), Vanyan and others (1964), Zhogolev and

others (1962), and Frischknecht (1967). There are also numerous catalogs of curves and values for the more special case of the Q function, as given by Wait (1962), Jackson, Walters and Wait (1962) and Yungul (1961). The greatest number of curves and values have been published for the zero-frequency or direct-current application (CGG, 1957; Mooney and Wetzel, 1957; Alpin, 1966; Orellano and Mooney, 1967).

AN ALTERNATE APPROACH TO THE ZERO FREQUENCY CASE

If a direct-current method for measuring resistivity is to be used, one does not normally compute the current field behavior by starting with Maxwell's equations, as has been done so far in this approach. One usually considers only the divergence condition for current flow, and solves a differential equation based on conservation of current flowing from a single-pole source. Exact solutions for the single-pole potential function are restricted to those cases in which the boundaries between areas of different resistivities can be represented by simple geometric surfaces. Kraev (1951) has outlined a general solution for the single-pole potential function in the presence of a disturbing body of arbitrary shape, and this approach has been used by Alfano (1959) to compute the apparent resistivity for a variety of prismatic models in a single-pole current field. Vozoff (1960) has suggested a method of approximations for calculating apparent resistivities using Kraev's approach.

The method outlined by these authors requires extensive computations to obtain good results. A less exact form of Kraev's solution may be expressed in the form of a chart, similar to the dot-charts used in computing the field effects in gravity and magnetic methods. This chart permits a rapid, if not precise, graphical computation of the apparent resistivity anomaly due to an arbitrarily shaped body.

The physical statement of the problem to be solved is indicated in figure 77a. A boundary with arbitrary shape separates a volume with resistivity, ρ_2 , from a semi-infinite medium with resistivity, ρ_1 . A single current pole is located at point A on the surface of the semi-infinite medium. In order to eliminate the effect of the earth's surface on current flow, an image of the boundary is placed in the upper halfspace, and the earth's surface is removed. The problem is to determine the single-pole potential function, U, at a point M, on the plane $z=0$.

A scalar potential function can be defined using Ohm's law and the divergence condition. Ohm's law states that:

$$\vec{j} = \frac{1}{\rho} \vec{E} \tag{303}$$

where \vec{j} is the current density vector,

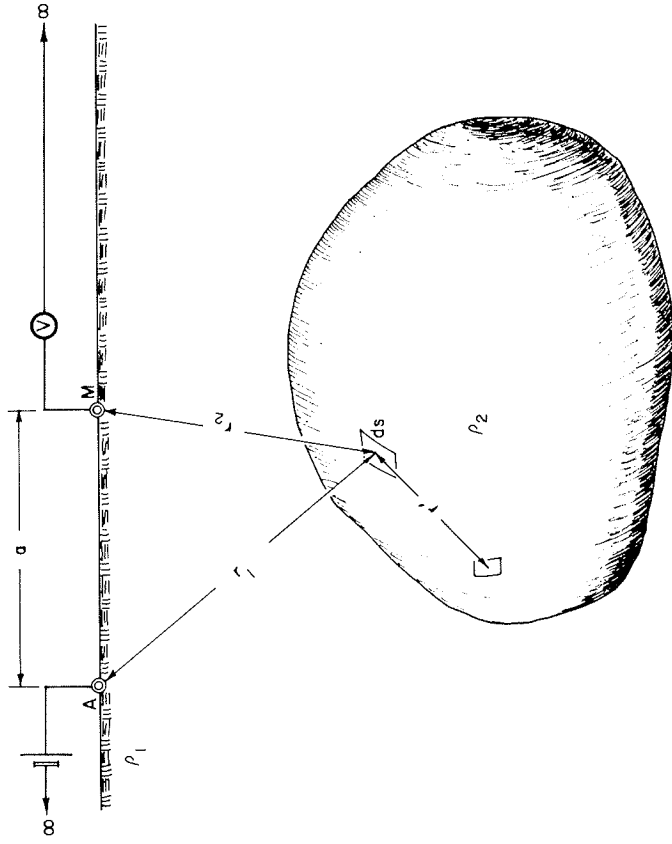


FIGURE 77. — Definition of the problem of measuring apparent resistivity over a body of arbitrary shape.

\vec{E} is the electric field vector, and

ρ is the resistivity of the medium, assumed to be scalar, but not necessarily constant.

The divergence of the current density vector must be zero every place except at the current source (point A). The divergence is:

$$\nabla \cdot \vec{j} = \frac{1}{\rho} \nabla \cdot \vec{E} + \vec{E} \cdot \nabla \left(\frac{1}{\rho} \right) \tag{304}$$

The potential function, by convention, is defined as a function whose gradient is the electric field, \vec{E}

$$\vec{E} = -\nabla U \tag{305}$$

Equation 304 expressed in terms of the potential function, U, is:

$$\nabla \cdot \vec{j} = -\frac{1}{\rho} \nabla \nabla U - \nabla U \cdot \nabla \left(\frac{1}{\rho} \right) \tag{306}$$

or

$$\Delta U = -\rho \left[\nabla \cdot \vec{j} + \nabla U \cdot \nabla \left(\frac{1}{\rho} \right) \right] \tag{307}$$

Equation 307 has the form of Poisson's equation, so that the terms to the right of the equality sign might be identified with current sources or charge accumulations in the medium. The solution to Poisson's equation is given by Poisson's integral:

$$\begin{aligned} u &= \frac{1}{4\pi} \int \frac{-\rho[\nabla^2 + \nabla u \cdot \nabla(\frac{1}{r_2})]}{r_2} dV \\ &= -\frac{1}{4\pi} \int \frac{\rho \nabla^2 \frac{1}{r_2}}{r_2} dV - \frac{1}{2\pi} \int \frac{\rho \nabla u \cdot \nabla(\frac{1}{r_2})}{r_2} dV \end{aligned} \quad (308)$$

where r_2 is the distance from a point in the medium to the point M at which the potential function is being evaluated.

Equation 308 can be viewed as expressing the total potential in terms of a normal potential, U_n , given by the first integral, and a disturbing potential, W , given by the second integral. The first integral is the potential due to a single-pole current source in a uniform halfspace with resistivity ρ_1 . The second integral can be thought of as representing the effect of a current-source distribution $\rho \nabla U \cdot \nabla(1/\rho)$ located on the surface of discontinuity in resistivity, inasmuch as these are the only places where the quantity $\nabla(1/\rho)$ is non-zero. The integral expression for the disturbing potential is:

$$W = \frac{1}{4\pi} \int \frac{\rho \nabla u \cdot \nabla(\frac{1}{r_2})}{r_2} dV \quad (309)$$

where the integration is carried out over all space. Inasmuch as the term $\nabla U \cdot \nabla(1/\rho)$ is non-zero only on surfaces where resistivity changes, the volume integral closely resembles a surface integral. Consider that the entire volume under consideration may be divided into two parts; one part consisting of thin shells which extend a distance, ϵ , which may be arbitrarily small, from each side of each surface of discontinuity in resistivity, and one part which includes all the rest of space, and which does not include any surface of discontinuity in resistivity. The integral in equation 309 for this second part will be zero. The integral for the first part may be rewritten:

$$W = \frac{1}{4\pi} \int_{-\epsilon}^{\epsilon} \frac{\rho \nabla u \cdot \nabla(\frac{1}{r_2})}{r_2} dn dS \quad (310)$$

where dn is the normal direction to the surface, S .

This integral may be evaluated by assuming the existence of an arbitrary current-source distribution $s(x,y,z)$ at the surface S . Designating the coordinates of the measuring point M as $(a,0,0)$, the integral for the disturbing potential becomes:

$$W = \frac{1}{4\pi} \int_{-\epsilon}^{\epsilon} \int \frac{s\phi(x,y,z)}{[(x-a)^2 + y^2 + z^2]^{3/2}} dn dS \quad (311)$$

The discussion may be simplified by considering elements of surface oriented normal to the x or z axes and extending infinitely far in both $+y$ and $-y$ directions. This limits us to considering structures elongate in a direction normal to the transverse along which potentials are being observed, but ordinarily, a resistivity contrast must be elongate in at least one dimension in order that the potential field will be modified sufficiently that the modification can be observed. The surface integral then has the form:

$$W_x = \frac{1}{4\pi} \iint \frac{s\phi(x,y)}{[(x-a)^2 + y^2 + z^2]^{3/2}} dy dz \quad (312)$$

for a surface element normal to the x axis, or:

$$W_z = \frac{1}{4\pi} \iint \frac{s\phi(x,y)}{[(x-a)^2 + y^2 + z^2]^{3/2}} dx dy \quad (313)$$

for a surface element normal to the z axis.

Alfano (1959) has shown how the charge density function, $s(x,y,z)$ or $s(x,y)$, may be evaluated by applying various boundary conditions. One of these conditions states the normal component of current density through a surface element must be continuous. For a surface element normal to the x axis, this is:

$$\frac{1}{\rho_1} \left(\frac{\partial u}{\partial x} \right)_{x \rightarrow x_0} = \frac{1}{\rho_2} \left(\frac{\partial u}{\partial x} \right)_{x \rightarrow x_0} \quad (314)$$

where ρ_1 and U_1 are the resistivity and the potential on one side, and ρ_2 and U_2 are the corresponding quantities on the other side of the element. For an element oriented normal to the z direction, the corresponding equation would be:

$$\frac{1}{\rho_1} \left(\frac{\partial u}{\partial z} \right)_{z \rightarrow z_0} = \frac{1}{\rho_2} \left(\frac{\partial u}{\partial z} \right)_{z \rightarrow z_0} \quad (315)$$

Consider the evaluation of this boundary condition at a plane, S_1 which separates regions with resistivities ρ_1 and ρ_2 . If the surface S_1 is oriented normal to the z direction, the current density normal to the surface is propor-

tional to a derivative of the potential taken in that direction. The component of current density in the z direction at points P_1 and P_2 located on opposite sides of a surface element are

$$\frac{1}{\rho_1} \frac{\partial u_1}{\partial z} \Big|_{P_1} = \frac{1}{\rho_1} \frac{\partial u_0}{\partial z} \Big|_{P_1} + \frac{1}{4\pi\rho_1} \iint_{P_1} s \frac{\partial}{\partial z} \left(\frac{1}{m_1} \right) dx dy \Big|_{P_1}$$

and

$$\frac{1}{\rho_2} \frac{\partial u_2}{\partial z} \Big|_{P_2} = \frac{1}{\rho_2} \frac{\partial u_0}{\partial z} \Big|_{P_2} + \frac{1}{4\pi\rho_2} \iint_{P_2} s \frac{\partial}{\partial z} \left(\frac{1}{m_2} \right) dx dy \Big|_{P_2} \tag{316}$$

where m_1 and m_2 are the distances from the points P_1 and P_2 to the charged surfaces, respectively.

As the points P_1 and P_2 are brought into the surface S_1 , these two expressions for current density become equal:

$$\begin{aligned} 0 &= \frac{1}{\rho_1} \frac{\partial u_1}{\partial z} \Big|_{P_1} - \frac{1}{\rho_2} \frac{\partial u_2}{\partial z} \Big|_{P_2} \\ &= \frac{1}{\rho_1} \frac{\partial u_0}{\partial z} \Big|_{P_1} - \frac{1}{\rho_2} \frac{\partial u_0}{\partial z} \Big|_{P_2} + \frac{1}{4\pi} \iint s \left[\frac{1}{\rho_1} \frac{\partial}{\partial z} \left(\frac{1}{m_1} \right) - \frac{1}{\rho_2} \frac{\partial}{\partial z} \left(\frac{1}{m_2} \right) \right] dx dy \end{aligned} \tag{317}$$

When the points P_1 and P_2 are very close to the surface, the term involving U_0 simplifies:

$$0 = \frac{\rho_2 - \rho_1}{\rho_1 \rho_2} \frac{\partial u_0}{\partial z} + \frac{1}{4\pi} \iint s \left[\frac{1}{\rho_1} \frac{\partial}{\partial z} \left(\frac{1}{m_1} \right) - \frac{1}{\rho_2} \frac{\partial}{\partial z} \left(\frac{1}{m_2} \right) \right] dx dy \tag{318}$$

The remaining integral term may be evaluated by considering two groups of m_1 and m_2 distances; namely, the distances from points P_1 and P_2 to all points on the same surface at which the charge density is being evaluated will be designated as m_1' and m_2' while distances from P_1 and P_2 to points on other charged surfaces will be designated as m_1'' and m_2'' . The remaining integral term is then broken into two integrals to separate these two types of distances:

$$\begin{aligned} 0 &= \frac{\rho_2 - \rho_1}{\rho_1 \rho_2} \frac{\partial u_0}{\partial z} + \frac{1}{4\pi} \iint s \left[\frac{1}{\rho_1} \frac{\partial}{\partial z} \left(\frac{1}{m_1'} \right) - \frac{1}{\rho_2} \frac{\partial}{\partial z} \left(\frac{1}{m_2'} \right) \right] dx dy \\ &\quad + \frac{1}{4\pi} \iint s \left[\frac{1}{\rho_1} \frac{\partial}{\partial z} \left(\frac{1}{m_1''} \right) - \frac{1}{\rho_2} \frac{\partial}{\partial z} \left(\frac{1}{m_2''} \right) \right] dx dy \end{aligned} \tag{319}$$

When the points P_1 and P_2 are close to the surface S_1 , the surface appears to be an infinite charged sheet, and the electric field outside such a sheet is:

$$\begin{aligned} \vec{E}_1 &= 2\pi s = \frac{\partial u_1}{\partial z} = \frac{\partial}{\partial z} \left[\frac{1}{4\pi} \iint \frac{s}{m_1'} dx dy \right] \\ \vec{E}_2 &= 2\pi s = \frac{\partial}{\partial z} \left[\frac{1}{4\pi} \iint \frac{s}{m_1'} dx dy \right] \end{aligned} \tag{320}$$

(In the equations for U_1 and U_2 , it is assumed the term representing the potential due to the charge on the surface near which the observation points are located is much larger than the terms representing the normal potential and the potential due to charges on other surfaces.) Beneath the charged sheet, the direction of the electric field vector is opposite to that above the sheet, so equation 319 becomes:

$$0 = 2\pi s \left(\frac{1}{\rho_1} + \frac{1}{\rho_2} \right) + \frac{1}{4\pi} \iint \left[\frac{1}{\rho_1} \frac{\partial}{\partial z} \left(\frac{1}{m_1''} \right) - \frac{1}{\rho_2} \frac{\partial}{\partial z} \left(\frac{1}{m_2''} \right) \right] dx dy + \frac{\rho_2 - \rho_1}{\rho_1 \rho_2} \frac{\partial u_0}{\partial z} \tag{321}$$

Inasmuch as points P_1 and P_2 are very close together, the distances m_1'' and m_2'' are nearly the same:

$$\frac{\partial}{\partial z} \left(\frac{1}{m_1''} \right) = \frac{\partial}{\partial z} \left(\frac{1}{m_2''} \right) = \frac{\partial}{\partial z} \left(\frac{1}{m''} \right) \tag{322}$$

Equation 321 becomes:

$$0 = 2\pi s \left(\frac{1}{\rho_1} + \frac{1}{\rho_2} \right) + \frac{1}{4\pi} \iint s \left(\frac{1}{\rho_1} - \frac{1}{\rho_2} \right) \frac{\partial}{\partial z} \left(\frac{1}{m''} \right) dx dy + \frac{\rho_2 - \rho_1}{\rho_1 \rho_2} \frac{\partial u_0}{\partial z}$$

Dividing this equation by $(\rho_1 + \rho_2)$ and multiplying by $\rho_1 \rho_2$, we have:

$$-2\pi s = \frac{\rho_2 - \rho_1}{\rho_2 + \rho_1} \left\{ \frac{\partial u_0}{\partial z} + \frac{1}{4\pi} \iint s \frac{\partial}{\partial z} \left(\frac{1}{m''} \right) dx dy \right\} \tag{323}$$

The quantity in front of the brackets is the reflection coefficient, K , for the resistivity contrast between ρ_1 and ρ_2 . Similar expressions can readily be obtained for surface elements oriented normal to the x and y directions.

Equations of the type in 323 may be used to calculate the potential about a single-pole current source for an arbitrary arrangement of boundaries between areas with different resistivities. The current-source density, s , on the various surfaces is found by numerical solution of equation 323. Once the charges are evaluated, the potential of any point, and at the measuring point, M , in particular, is found from Poisson's equation:

The quality of the approximation made in neglecting the integral term representing the interaction effect between charged surfaces may be demonstrated by applying the graphical method to a problem whose solution is well known. Such a problem is that of a uniform layer of one resistivity covering a uniform substratum of infinite extent having a different resistivity (Roman, 1960). The graphical method may be applied to this problem using the contour map shown in figure 78, integrating along a horizontal line at a depth equal to the thickness of the assumed layer. Performing this integration for thicknesses ranging from 1/2a to 2a, the results listed in table 13 are obtained.

TABLE 13. — Comparison of graphical and exact computations for the disturbing potential due to a single uniform layer of different thicknesses

h/a	W/K (graphical)	From Roman's tables (1960)		Average W/K
		W/K, K=0.1	W/K, K=-0.1	
0.5	0.176	0.149	0.143	0.146
1.0	0.108	0.107	0.104	0.106
1.4	0.081	0.079	0.077	0.078
2.0	0.056	0.060	0.058	0.059

For comparison, values for the ratio of disturbing potential to reflection coefficient, W/K, were taken from Roman's tables (1960) for reflection coefficients of 0.1 and -0.1, and averaged to determine the approximate value of this ratio for zero resistivity contrast. Except for the case in which the electrode spacing is twice the layer thickness, the disturbing potential determined with the graphical method is within about 5 percent of the correct value. A relatively large error, about 20 percent, was obtained for the case h = 0.5a.

The theory outlined in this paper predicts that the disturbing potential will be proportional to the reflection coefficient, while the exact solution indicates this is not true. Table 14 lists the disturbing potentials given by the graphical method as a function of reflection coefficient. The corresponding values for disturbing potential taken from Roman's tables are also listed for comparison. The disturbing potential determined by graphical means ranges from a value about 15 percent too large if the substratum is a perfect conductor to a value about 20 percent too small if the substratum is a perfect insulator. The percentage error increases with increasing resistivity contrast.

It appears that the graphical computation will provide values for disturbing potential due to an anomalous body buried at a depth comparable with or

TABLE 14.— Comparison of graphical and exact computations for the disturbing potential due to a single uniform layer of thickness, a, for various reflection coefficients

Reflection coefficient K	Disturbing potential (graphical) W	Disturbing potential (exact) W
-1.0	-0.108	-0.0939
-0.9	-0.097	-0.0854
-0.8	-0.086	-0.0766
-0.7	-0.075	-0.0678
-0.6	-0.065	-0.0588
-0.5	-0.054	-0.0495
-0.4	-0.043	-0.0401
-0.3	-0.032	-0.0304
-0.2	-0.022	-0.0205
-0.1	-0.011	-0.0104
0.1	0.011	0.0107
0.2	0.022	0.0217
0.3	0.032	0.0331
0.4	0.043	0.0450
0.5	0.054	0.0572
0.6	0.065	0.0701
0.7	0.075	0.0835
0.8	0.086	0.0978
0.9	0.097	0.1130
1.0	0.108	0.1300

somewhat greater than the electrode spacing which is accurate within a few percent for moderate resistivity contrasts, and within 20 percent for a very large resistivity contrast.

If, rather than considering a completely arbitrary structure, we assume a model of a thin layer with high resistivity embedded in an otherwise uniform earth, we obtain results of interest in petroleum prospecting. For this model, we can assume that the fictitious current sources on opposite faces of the layer are equal but opposite in sign. The resistive zone may be replaced by an assemblage of vertically oriented current dipoles, with intensities which we must still determine on the basis of boundary conditions.

The anomalous potential is

$$W = \frac{\rho_1}{4\pi} \int_S \frac{st \cos \theta}{r^2} dS \tag{327}$$

where s is the fictitious current density per unit of surface area, $dx dy$, on the resistant bed, and st is the current dipole moment per unit area. The fictitious current density is determined by applying a condition requiring continuity of the vertical component of current through the top and bottom surfaces of the layer (fig. 79). At the top boundary, this continuity condition is written as:

$$\frac{1}{\rho_1} \left[\frac{\partial u_0}{\partial z} + \frac{1}{4\pi} \int s \frac{\partial}{\partial z} \left(\frac{1}{m_1} \right) ds \right] = \frac{1}{\rho_2} \left[\frac{\partial u_0}{\partial z} + \frac{1}{4\pi} \int s \frac{\partial}{\partial z} \left(\frac{1}{m_2} \right) ds \right] \quad (328)$$

where m_1 and m_2 are the distances from two points, one above and one below the upper boundary, to any point on either surface which is contributing a fictitious current. In evaluating the boundary condition at the upper boundary, we let these two points approach that boundary, so that $m_1 \rightarrow m_2$:

$$\left[\frac{1}{\rho_1} - \frac{1}{\rho_2} \right] \frac{\partial u_0}{\partial z} + \frac{1}{4\pi} \int s \left[\frac{1}{\rho_1} \frac{\partial}{\partial z} \left(\frac{1}{m_1} \right) - \frac{1}{\rho_2} \frac{\partial}{\partial z} \left(\frac{1}{m_2} \right) \right] ds = 0 \quad (329)$$

Let us consider that the distances m are of two types: 1), from the test points to the close surface, designated as m' ; and 2), from the test points to the far surface, designated as m'' . Then equation 329 becomes

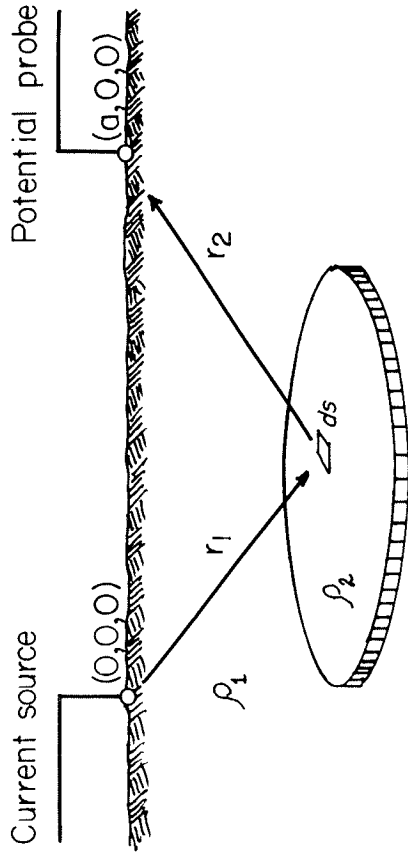


FIGURE 79. Definition of the geometry used in evaluating the resistivity anomaly caused by a thin resistant layer with limited areal extent.

$$\frac{\rho_2 - \rho_1}{\rho_1 \rho_2} \frac{\partial u_0}{\partial z} + \frac{1}{4\pi} \int s \left[\frac{1}{\rho_1} \frac{\partial}{\partial z} \left(\frac{1}{m_1} \right) - \frac{1}{\rho_2} \frac{\partial}{\partial z} \left(\frac{1}{m_2} \right) \right] ds + \frac{1}{4\pi} \int s \left[\frac{1}{\rho_1} \frac{\partial}{\partial z} \left(\frac{1}{m_1} \right) - \frac{1}{\rho_2} \frac{\partial}{\partial z} \left(\frac{1}{m_2} \right) \right] ds \quad (330)$$

Inasmuch as the test points are infinitely close to the upper boundary, any continuous distribution of fictitious current densities will appear as though they were uniform and infinite in extent. The electric field from such an infinite sheet of current density will be $E_1 = 0$ above the boundary and $E_2 = -17\pi s$ below the boundary (between the two sheets). Thus

$$E_1 = \frac{\partial}{\partial z} \left[\frac{1}{4\pi} \int \frac{s}{m_1} ds \right] = 0 \quad (331)$$

and

$$E_2 = \frac{\partial}{\partial z} \left[\frac{1}{4\pi} \int \frac{s}{m_2} ds \right] = -4\pi s \quad (332)$$

These conditions allow us to evaluate the first integral in equation 330:

$$\frac{\rho_2 - \rho_1}{\rho_1 \rho_2} \frac{\partial u_0}{\partial z} + \frac{4\pi s}{\rho_2} + \frac{1}{4\pi} \int s \left[\frac{1}{\rho_1} \frac{\partial}{\partial z} \left(\frac{1}{m_1} \right) - \frac{1}{\rho_2} \frac{\partial}{\partial z} \left(\frac{1}{m_2} \right) \right] ds \quad (333)$$

In evaluating the second integral, consider that $m_1'' \rightarrow m_2''$ when the test points are infinitely close to the upper surface. Then:

$$\frac{\partial}{\partial z} \left(\frac{1}{m_1} \right) = \frac{t}{(R^2 + t^2)^{3/2}} \quad (334)$$

and

$$\frac{1}{4\pi} \int_0^{2\pi} \int_0^{\infty} s \left(\frac{1}{\rho_1} - \frac{1}{\rho_2} \right) \cdot \frac{t}{(R^2 + t^2)^{3/2}} \cdot R d\theta dR = \frac{s}{2} \left(\frac{\rho_2 - \rho_1}{\rho_1 \rho_2} \right) \quad (335)$$

where R, θ is a circular coordinate system on the lower boundary with its origin at the point immediately below the point on the upper boundary where the fictitious current density is being evaluated. Thus

$$\frac{1}{\rho_2} \left\{ \frac{\rho_2 - \rho_1}{\rho_1} \frac{\partial u_0}{\partial z} + 4\pi s + \frac{\rho_2 - \rho_1}{\rho_1} \frac{s}{2} \right\} = 0 \quad (336)$$

The normal potential term is

$$\frac{\partial u_0}{\partial z} = \frac{\rho_1 I H}{4\pi (x^2 + y^2 + H^2)^{3/2}} \quad (337)$$

and so, the solution for the fictitious current density is

$$s = \frac{1}{4\pi} \cdot \frac{\rho_2}{\rho_1} \cdot \frac{I H}{4\pi H^3 \left(\frac{x^2}{H^2} + \frac{y^2}{H^2} + 1 \right)^{3/2}} \quad (338)$$

where an approximation has been made on the basis of the ratio ρ_2/ρ_1 being very large. Substituting this expression in the integral solution for Poisson's equation, we have for the anomalous potential:

$$W = \frac{\rho_1 I}{16\pi^2 H^5} \iint \frac{T_2/T_1}{\left[\left(\frac{x-a}{H}\right)^2 + \left(\frac{y}{H}\right)^2 + 1\right]^{3/2}} dxdy \quad (339)$$

This expression holds for oil fields of quite arbitrary shape, and in the general case, it must be evaluated numerically. It shows the same properties as the earlier, less general solution for a resistive bed of infinite extent: the anomaly in resistivity caused by the oil zone is proportional to the ratio T_2/T_1 .

If the area $dxdy$ over which the integration is performed is allowed to become infinite, this expression should reduce to that derived earlier for a layered medium. For a resistant zone of limited dimensions, the integration process may be thought of as determining the portion of the total anomaly for a bed of infinite extent which is applicable for a bed of finite extent. Then, the results obtained in integrating equation 339 may be used to form a point-by-point correction factor for converting the anomaly for a bed of infinite extent into the anomaly for a bed with specific finite dimensions. These correction curves will depend on the size and shape of the resistant zone, and on the array used in measuring resistivity, as well as on the position of the array relative to the resistant zone. As an example, the correction curve for a case in which the electrode array is centered symmetrically over an oil zone, with a circular shape, and subtending an angle of one steradian is shown in figure 80. For short spacings, the correction is quite large, but there is almost no anomaly to which the correction is to be applied. As the spacing is increased, the correction passes through a minimum at spacings shorter than that required to see the maximum anomaly for beds of infinite extent, and then increases again at large spacings.

REFERENCES

- Abramowitz, Milton and Stegun, Irene A. (Eds.), 1964. Handbook of mathematical functions: Natl. Bur. Standards, Applied Mathematics Series, no. 55. Washington, D. C.: U.S. Govt. Printing Office.
- Alfano, L., 1959. Introduction to the interpretation of resistivity measurements for complicated structural conditions: Geophys. Prospecting, v. 7, p. 311-366.
- Alpin, L. M., Berdichevskiy, M. N., Vedrintsev, G. A. and Zagarmistr, A. M., 1966. Dipole methods for measuring earth conductivity: New York, Consultants Bureau, 302 p.

PERCENTAGE RESISTIVITY ANOMALY per $T_2/T_1 = 1\%$

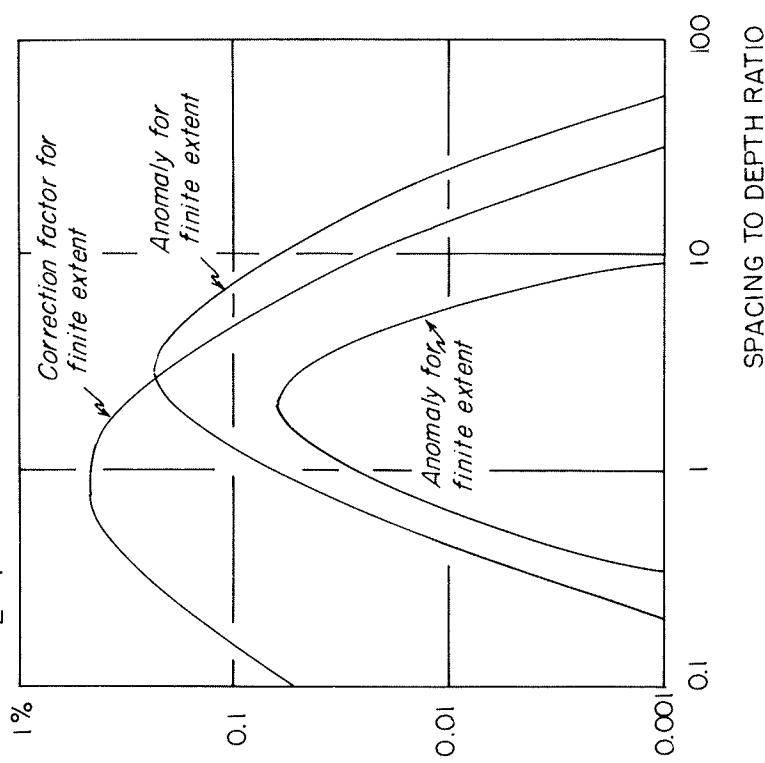


FIGURE 80.—Example of the correction which must be made for the limited extent of a thin, resistant layer, computed for a Schlumberger array centered over a circular resistant zone which subtends an angle of 1 steradian at the midpoint of the array.

- Baranov, Vladimir, and Kuntze, Geza, 1958. Distribution du potentiel dans un milieu stratifié: Acad. Sci. Paris, Comptes Rendus, v. 247, no. 23, p. 2170-2171.
- Berdichevskiy, M. N., 1965. Electrical prospecting with the telluric current method: Colorado School Mines Quart., v. 60, no. 1, 216 p.
- Bödvarsson, G., 1966. Direct methods in applied geophysics: Georexploration, v. 4, no. 3, p. 113-138.
- Cagniard, Louis, 1953. Basic theory of the magneto-telluric method of geophysical prospecting: Geophysics, v. 18, no. 3, p. 605-635.
- Chistova, E. A., 1958. Tables of Bessel functions of real arguments and their integrals: Moscow, Akad. Nauk SSSR, 523 p.
- Compagnie Generale de Geophysique (CGG), 1963. Master curves for electrical sounding, second edition: European Assoc. Exploration Geophysicists.

- Erdelyi, A. (Ed.), 1953, Higher transcendental functions, v. 2: New York, McGraw-Hill, 396 p.
- 1954, Tables of integral transforms, v. 2: New York, McGraw-Hill, 451 p.
- Flathe, H., 1955, A practical method of calculating geoelectrical model graphs for horizontally stratified media: *Geophys. Prospecting*, v. 3, no. 3, p. 268-294.
- Frischknecht, F. C., 1967, Fields about an oscillating magnetic dipole over a two-layer earth, and application to ground and airborne electromagnetic surveys: *Colorado School Mines Quart.*, v. 62, no. 1.
- Galbraith, J. N., Simpson, S. M., and Cantwell, T., 1964, Computer applications in geophysical modeling: *Colorado School Mines Quart.*, v. 59, no. 4, p. 67-80.
- Heiland, C. A., 1940, Geophysical exploration: New York, Prentice-Hall.
- Jackson, C. M., Wait, J. R., and Walters, L. C., 1962, Numerical results for the surface impedance for a stratified conductor: U.S. Nat. Bur. Standards, Tech. Note 143, Washington, D. C., Dept. of Commerce, Office Tech. Services.
- Kalenov, E. N., 1957, Interpretatsiya krivikh vertikal'nogo elektricheskogo zondirovaniya: Moscow, Gostoptekhizdat, 472 p.
- Karmazina, L. N., and Chistova, E. A., 1958, Tables of Bessel functions of complex arguments and their integrals: Moscow, Akad. Nauk SSSR, 328 p.
- Kraev, A. P., 1951, Osnovi Geoelektriki: Moscow, Gostoptekhizdat, 445 p.
- Kunetz, Geza, 1966, Principles of direct current resistivity prospecting: Berlin, Gebrüder Borntraeger, 103 p.
- Lastariges, P., 1957, Prospection par Courants Continus: Paris, Mason et Cie.
- Lee, Y. W., 1960, Statistical theory of communication: New York, John Wiley and Sons, 509 p.
- Luke, Yudell, L., 1962, Integrals of Bessel functions: New York, McGraw-Hill, 419 p.
- Meinardus, H. A., 1967, The kernel function in direct-current resistivity sounding: D.Sc. Thesis, Colorado School Mines.
- Mooney, H. M., Orellana, E., Pickett, H., and Tornheim, L., 1966, A resistivity computation method for layered earth models: *Geophysics*, v. 31, no. 1, p. 192-203.
- Mooney, H. M., and Wetzel, W. W., 1956, Potentials and resistivity curves for a layered earth: Minneapolis, Univ. Minnesota Press.
- Onodera, Seibe, 1960, The kernel function in the multiple-layer resistivity problem: *Jour. Geophys. Research*, v. 65, no. 11, p. 3787-3794.
- 1963, Numerical analysis of relative resistivity for a horizontally layered earth: *Geophysics*, v. 28, no. 2, p. 223-231.
- Orellana, Ernesto, and Mooney, M., 1966, Master tables and curves for vertical electrical sounding over layered structures: Madrid, Intercentia.
- Roman, Irwin, 1960, Apparent resistivity of a single uniform overburden: U.S. Geol. Survey Prof. Paper 365, Washington, D. C., U.S. Govt. Printing Office.
- 1963, The kernel function in the surface potential for a horizontally stratified earth: *Geophysics*, v. 28, no. 2, p. 232-249.
- Stiecher, L. B., 1933, The interpretation of the resistivity prospecting method for horizontal structures: *Physics*, v. 4, p. 307-322.
- Stefanescu, S., Schlumberger, C., and Schlumberger, M., 1930, Sur la distribution électrique potentielle autour d'une prise de terre ponctuelle dans un terrain à couches horizontales homogènes: *Jour. Physique et Radium*, ser. 7, v. 1, p. 132-140.
- Sunde, E. D., 1949, Earth conduction effects in transmission systems: New York, D. Van Nostrand Company, 373 p.

- Tagg, C. F., 1964, Earth resistances: New York, Pitman, 258 p.
- Tikhonov, A. N., 1950, On transient electric currents in an inhomogeneous layered medium (in Russian): *Izv. Akad. Nauk SSSR, ser. geofiz.*, no. 3.
- 1959, On the asymptotic behavior of integrals containing Bessel functions (in Russian): *Akad. Nauk, SSSR, Dokl.*, v. 125, no. 5.
- Tikhonov, A. N., and Shakhshvarov, D. N., 1956, Method of calculating the electromagnetic field generated by varying currents in a layered medium (in Russian): *Izv. Akad. Nauk SSSR, ser. geofiz.*, no. 3.
- van Dam, J. C., 1965, A simple method for the calculation of standard-graphs to be used in geo-electrical prospecting: *Geophys. Prospecting*, v. 13, no. 1, p. 37-65.
- 1967, Mathematical denotation of standard-graphs for resistivity prospecting in view of their calculation by means of a digital computer: *Geophys. Prospecting*, v. 15, no. 1, p. 57-70.
- Van Nostrand, R. G., and Cook, K. L., 1966, Interpretation of resistivity data: U. S. Geol. Survey Prof. Paper 499, Washington, D. C., U.S. Govt. Printing Office, 310 p.
- Vanyan, L. L., 1966, Electromagnetic fields and their use in solving problems in structural geology (in Russian): Nauka, Novosibirsk, 103 p.
- 1967, Electromagnetic depth soundings: New York, Consultants Bureau, 312 p.
- Vanyan, L. L., Shigul'skaya, T. A., and Omel'cheko, O. K., 1964, Tables for computing theoretical curves for frequency sounding in the far zone: *Geologii i Geofiziki*, no. 39, p. 76-175 (English trans., CSM RL-3, July 10, 1967).
- Vozoff, Keeva, 1960, Numerical resistivity interpretation, general inhomogeneity: *Geophysics*, v. 25, no. 6, p. 1184-1194.
- Wait, J. R., 1962, Electromagnetic waves in stratified media: New York, The Macmillan Company, 372 p.
- Watson, G. N., 1952, Theory of Bessel functions: Cambridge, University Press, 804 p.
- Yungul, Sulhi H., 1961, Magnetotelluric sounding three-layer interpretation curves: *Geophysics*, v. 26, no. 4, p. 465-473.
- Zhogolev, E. A., Trifonov, N. P., and Shakhshvarov, D. N., 1962, Computation of the electromagnetic field in a layered medium (in Russian) in Numerical methods and programming: Moscow State Univ., Pub., p. 203-231. (English trans., CSM RL-4, Aug. 10, 1967).

PART 3 — DESIGN CRITERIA FOR ELECTRICAL SURVEYING

So far we have considered the electrical characteristics of oil fields and the rocks in which they occur, along with a generalized theory for alternating current flow in the ground. The questions still remain: How might one use electrical probing methods in search for oil? What technique or techniques will provide the best chances for success? What spacing is required between source and receiver? What frequencies must be used? How much power is needed to achieve these spacings and frequencies, and still have signals at the receiver which may be recognized above the ambient electrical noise? What are the chances of recognizing the response one anticipates from an oil field in the presence of many other responses to extraneous resistivity contrasts, or "geologic noise"? We are now in a position to answer some of these questions, but in truth, complete answers to all of them cannot be obtained without more experience in electrical prospecting in potentially petroliferous regions.

COMPARISON OF ARRAYS USED IN DIRECT-CURRENT RESISTIVITY SURVEYS

A great many techniques have been used in measuring earth resistivity, variations being primarily in the way the various electrodes are placed relative to one another. Since high power, and accordingly, heavy equipment, is required in making deep resistivity surveys, both efficiency and safety are factors to be considered more seriously than in normal shallow penetration surveys. The first step, then, in planning a deep penetration survey using zero-frequency methods is an analysis of the advantages and disadvantages of the various electrode arrays.

Three basic arrays are considered: the Wenner, the Schlumberger, and the dipole array, (fig. 53). In comparing the various arrays, we must first establish comparable conditions for each. The lowest signal level which can be detected depends on recording equipment used. In practice, the lowest signal level which can be detected may be limited either by the sensitivity of the recording equipment or by the level of telluric noise between the measuring electrodes. Let us designate the threshold voltage which can be measured in the absence of noise as V_o . Similarly, let us designate the average telluric noise delivered from the measuring electrodes as V_T . The telluric noise level varies widely with time, location and local resistivity, but these factors will be common for all electrode arrays. However, telluric noise will also be proportional to the separation between measuring electrodes, so let us designate a primary telluric field strength, E_T , such that:

$$V_T = \overline{MN} E_T \quad (340)$$

where \overline{MN} is the spacing between the measuring electrodes. Berdichevskiy (1965) has shown that for a uniform earth with a resistivity, ρ , the electric field is proportional to the square root of resistivity, $E_T = k_T \rho^{1/2}$.

The voltage which we wish to compare with these limiting values is the signal voltage, V_s , developed between the measuring electrodes by the current supplied with the current electrodes. This voltage may be computed for any of the arrays for a uniform earth.

1. For the Wenner array, the measured voltage is:

$$V_{sw} = \frac{I\rho}{2\pi a_w} \quad (341)$$

where I is the current supplied to the ground, ρ is the resistivity of the ground, and a_w is the spacing between any two adjacent electrodes.

2. For the Schlumberger or reciprocal Schlumberger array, the measured voltage is:

$$V_{ss} = \frac{bI\rho}{\pi a_s^2} \quad (342)$$

where b is the spacing between measuring electrodes and a_s is half the spacing between the current electrodes.

3. For the equatorial dipole array, the measured voltage is:

$$V_{sDE} = \frac{bcI\rho}{2\pi a_{DE}^3} \quad (343)$$

where b and c are the dipole lengths, and a_{DE} is the distance between dipole centers.

4. For the polar dipole array, the measured voltage is:

$$V_{sDP} = \frac{bcI\rho}{\pi a_{DP}^3} \quad (344)$$

The amount of current supplied to the ground, I , can be considered to be limited by two factors: the weight of cable W_c , and batteries, W_b , which one wishes to transport, and the maximum safe voltage, V_B at which one chooses to operate. The weight, W_c , of the cable is proportional to its length, L , and cross sectional area, A :

$$W_c = \delta LA \quad (345)$$

where δ is the density of the material from which the cable is constructed. On the other hand, the cable resistance, R_c , is proportional to the cross-sectional area:

$$R_c = \rho_c L/A \quad (346)$$

where ρ_c is the resistivity of the material from which the cable is constructed.

The current which can be supplied to the ground is limited by the combined internal resistance of the batteries, R_b , the grounding resistance at the current electrodes, R_g , and the cable resistance:

$$I = \frac{V_B}{R_c + R_b + R_g} \quad (347)$$

The internal resistance of a lead storage battery, which is probably the most economical type battery to use in deep resistivity surveys, is approximately inversely proportional to the weight of batteries; and directly proportional to the battery voltage:

$$R_b = \frac{k_1 V_B}{W_b} \quad (348)$$

where k_1 is .025 to 0.75 ohm-pounds per volt.

Using equations 345, 346 and 348 to remove some of the inter-related parameters from equation 347, we have:

$$I = \frac{V_B}{\frac{\rho_c \delta L^2}{W_c} + \frac{k_1 V_B}{W_b} + R_g} \quad (349)$$

Generally, we will be concerned about the total weight limitation, $W = W_c + W_b$. Expressing the cable and battery weights as fractions of the total weight:

$$W_c = \alpha W$$

$$\text{and } W_b = (1-\alpha)W$$

we have from equation 349:

$$I = \frac{V_B}{\frac{\rho_c \delta L^2}{\alpha W} + \frac{k_1 V_B}{(1-\alpha)W} + R_g} \quad (350)$$

A maximum current can be provided to the ground when the denominator in equation 350 is a minimum. The extreme values for the denominator as

the parameter α is varied are given by the solutions to the equation:

$$\frac{k_1 V_B}{(1-\alpha_{ex})^2} = \frac{\rho \delta L^2}{\alpha_{ex}^2} \tag{351}$$

which are:

$$\alpha_{ex} = \frac{-1 \pm \left(\frac{k_1 V_B}{\rho \delta L^2} \right)^{1/2}}{\frac{k_1 V_B}{\rho \delta L^2} - 1} \tag{352}$$

We are now in a position to compare the maximum spacings which may be obtained with different electrode arrays under comparable conditions. This is done by solving equations 341 through 344 for the spacing, a , using the minimum detectable voltage generated by telluric noise, V_T , and the maximum possible current for maximized values of ρ , δ , V_B , and W common to all arrays.

1. For the Wenner array:

$$a_w = \frac{I \rho}{2\pi V_T} = \frac{V_B}{\left(\frac{\rho \delta L^2}{\alpha W} + \frac{k_1 V_B}{(1-\alpha)W} + R_g \right)} \cdot \frac{\rho^{1/2}}{2\pi MN k_T} \tag{353}$$

but $\overline{MN} = a_w$ and $L = 3a_w$, so

$$\alpha_w^2 = \frac{V_B}{\left(\frac{9\rho \delta \alpha_w^2}{\alpha W} + \frac{k_1 V_B}{(1-\alpha)W} + R_g \right)} \cdot \frac{\rho^{1/2}}{2\pi k_T} \tag{353}$$

2. For the Schlumberger array:

$$\alpha_s^2 = \frac{b I \rho}{\pi V_T} = \frac{V_B}{\left(\frac{\rho \delta L^2}{\alpha W} + \frac{k_1 V_B}{(1-\alpha)W} + R_g \right)} \cdot \frac{b \rho^{1/2}}{\pi \overline{MN} k_T} \tag{354}$$

but $\overline{MN} = b$ and $L = 2a_s$ so:

$$\alpha_s^2 = \frac{V_B}{\left(\frac{4\rho \delta \alpha_s^2}{\alpha W} + \frac{k_1 V_B}{(1-\alpha)W} + R_g \right)} \cdot \frac{\rho^{1/2}}{\pi k_T} \tag{354}$$

3. For the equatorial dipole array:

$$\alpha_{DE}^3 = \frac{bc I \rho}{2\pi V_T} = \frac{V_B}{\left(\frac{\rho \delta L^2}{\alpha W} + \frac{k_1 V_B}{(1-\alpha)W} + R_g \right)} \cdot \frac{bc \rho^{1/2}}{2\pi MN k_T} \tag{355}$$

but $\overline{MN} = b$ and we may write that:

$$\alpha_{DE}^3 = \frac{V_B}{\left(\frac{\rho \delta L^2}{\alpha W} + \frac{k_1 V_B}{(1-\alpha)W} + R_g \right)} \cdot \frac{c \rho^{1/2}}{2\pi k_T} \tag{355}$$

4. For the polar dipole array:

$$\alpha_{DP}^3 = \frac{V_B}{\left(\frac{\rho \delta L^2}{\alpha W} + \frac{k_1 V_B}{(1-\alpha)W} + R_g \right)} \cdot \frac{c \rho^{1/2}}{\pi k_T} \tag{356}$$

In comparing arrays, we might consider the ratios of maximum spacings attainable. For example, the ratio of maximum attainable Schlumberger spacing to the maximum attainable Wenner spacing can be obtained from the equation:

$$\frac{\alpha_s}{a_w} = \left\{ 2 \cdot \frac{\frac{9\rho \delta \alpha_w^2}{\alpha W} + \frac{k_1 V_B}{(1-\alpha)W} + R_g}{\frac{4\rho \delta \alpha_s^2}{\alpha W} + \frac{k_1 V_B}{(1-\alpha)W} + R_g} \right\}^{1/2} \tag{357}$$

The dipole arrays may also be compared readily with the Wenner array, providing we express the source dipole length as a fixed fraction of the maximum attainable spacing:

$$c = k_3 a$$

The ratio of maximum spacing attainable with an equatorial dipole array to the maximum spacing attainable with a Wenner array is then:

$$\frac{\alpha_{DE}}{\alpha_w} = \left\{ k_3 \cdot \frac{\frac{9\rho \delta \alpha_w^2}{\alpha W} + \frac{k_1 V_B}{(1-\alpha)W} + R_g}{\frac{k_3 \rho \delta \alpha_{DE}^2}{\alpha W} + \frac{k_1 V_B}{(1-\alpha)W} + R_g} \right\}^{1/2} \tag{358}$$

Similarly, the maximum spacing attainable with a polar dipole array, in proportion to the maximum spacing attainable with a Wenner array

$$\frac{\alpha_{DP}}{\alpha_w} = \left\{ 2k_3 \cdot \frac{\frac{9\rho \delta \alpha_w^2}{\alpha W} + \frac{k_1 V_B}{(1-\alpha)W} + R_g}{\frac{k_3 \rho \delta \alpha_{DP}^2}{\alpha W} + \frac{k_1 V_B}{(1-\alpha)W} + R_g} \right\}^{1/2} \tag{359}$$

At this point, it is desirable to assign numerical values to some of the fixed parameters in these equations:

$$\begin{aligned} V_B &= 500 \text{ volts} \\ k_1 &= 0.0001 \text{ ohm-pounds per volt} \\ \delta &= 550 \text{ pounds per cubic foot (copper)} \\ c &= 6 \times 10^{-8} \text{ ohm-feet} \\ k_1 V_B &= 1,600 \text{ square feet (used in equation 352)} \\ \rho_s \delta & \end{aligned}$$

The extreme values for α are:

$$\alpha_{\text{ex}} = \frac{-1 \pm 40/L}{L^2 - 1} \quad (360)$$

In deep electrical surveys, L will be much larger than 40 feet, so this expression can be approximated as:

$$\alpha_{\text{ex}} \approx 1 \mp \frac{40}{L} \quad (361)$$

This equation implies that best penetration is obtained through the use of a heavy cable, rather than through the use of high-capacity batteries.

Substituting numerical values for the fixed parameters in equations 357, 358 and 359, we have:

1. For the Schlumberger array in comparison with the Wenner array, and assuming that the maximum attainable spacing in either case is much greater than 40 feet, we have

$$\frac{\alpha_s}{\alpha_w} = \left\{ 2 \cdot \frac{9 \left(\frac{\rho_s \delta}{k_1 V_B} \right) \frac{c_w^2}{(1-40/3\alpha_w)} + \frac{3\alpha_w}{40}}{4 \left(\frac{\rho_s \delta}{k_1 V_B} \right) \frac{\alpha_s^2}{(1-20/\alpha_s)} + \frac{\alpha_s}{20}} \right\}^{1/2} \quad (362)$$

If the spacing α is sufficiently large (much larger than 40 feet), the second term in both the numerator and denominator is negligible in comparison with the first term:

$$\frac{\alpha_s}{\alpha_w} = \left(\frac{9}{2} \right)^{1/2} = 1.46 \quad (363)$$

2. For the equatorial dipole array in comparison with the Wenner array, we have:

$$\frac{\alpha_{DE}}{\alpha_w} = \left(\frac{9}{k_3} \right)^{1/4} \quad (364)$$

3. For the polar dipole array in comparison with the Wenner array, we have:

$$\frac{\alpha_{DP}}{\alpha_w} = \left(\frac{18}{k_3} \right)^{1/4} \quad (365)$$

In equations 364 and 365, k_3 must be much smaller than unity in order that the equations for dipole resistivity be correct.

The maximum spacing attainable for a given array is not the only factor to be considered in comparing the utility of arrays for deep soundings. The effective probing depth—the depth at which a boundary may be detected with a given array spacing—must also be considered. The probing depth in resistivity surveying cannot be specified. As an example, consider one case of a sequence of layers with alternating high and low resistivities resting upon an insulating basement in comparison and a second case of a uniform medium of the same total thickness covering the basement rock. The spacing between electrodes required to detect the presence of basement under the layered sequence is greater by the factor λ , than the spacing required to detect basement under the rock with uniform resistivity. The factor λ is the coefficient of pseudoanisotropy for the layered sequence, given by

$$\lambda = \frac{\int_0^H \rho dz \cdot \int_0^H \rho dz}{H} \quad (366)$$

where ρ is the resistivity in the layered sequence as a function of depth, z , and H are the total depth to the basement.

The coefficient has a maximum value when the layered medium is divided equally between two specific resistivities, and if the resistivity contrast is large, the maximum value is

$$\lambda_{\text{max}} = \frac{\rho_1 + \rho_2}{2(\rho_1 \rho_2)^{1/2}} \quad (367)$$

where ρ_1 and ρ_2 are the maximum and minimum resistivities which occur in the section above the contrast which is the target horizon in sounding. If the range in resistivities is very large, this is approximately:

$$\lambda_{\text{max}} \approx \frac{1}{2} \left(\frac{\rho_{\text{max}}}{\rho_{\text{min}}} \right) \quad (368)$$

For example, if we wish to detect the presence of a resistivity contrast beneath a series of layers in which the maximum resistivity contrast is 1000:1, under

the worst possible conditions, it may be necessary to use an array spacing about 16 times larger than that which would be required if the same target horizon were covered by a uniform medium.

It is possible to define a depth of probing for a given electrode array, providing the definition is given in terms of a specific set of conditions. Such a definition is useful in comparing arrays, but may not be used to estimate the actual spacing required in a field survey unless the correction for anisotropy given in equation 367 or 368 is applied. Probing depth (or array spacing factor) may be defined for measurements made at the surface of a single uniform layer with finite resistivity resting on a semi-infinite insulating medium.

Consider the apparent resistivity which is observed with a Schlumberger array under such circumstances. For array spacings considerably less than the thickness of the layer, the observed resistivity is nearly equal to the actual resistivity of the layer, while for spacings larger than several times the layer thickness, the observed resistivity is directly proportional to the array spacing. This proportionality may be shown as follows. Consider a point source of current at the surface of the layer. No current can leave the layer through either the upper or lower planes, and so the current must spread uniformly radially outward in two dimensions from the current source. The total current into the layer at the source can be used to calculate the current density at a distance from the source which is large compared to the layer thickness:

$$j = \frac{I}{2\pi r h} \quad (369)$$

where I is the total current, r is the distance from the source at which current density, j , is being calculated, and h is the thickness of the layer. The electric field intensity may be determined by applying Ohm's law:

$$E = j\rho = \frac{\rho I}{2\pi r h} = \frac{I}{2\pi r S} \quad (370)$$

where ρ is the resistivity of the layer and S is the longitudinal conductance, h/ρ .

The apparent resistivity measured with the Schlumberger array is defined in terms of the electric field intensity. With two current electrodes, as are actually used with the Schlumberger array, the observed electric field intensity will be twice the value given in equation 370 for a single-pole source. The apparent resistivity is:

$$\rho_s = \pi r^2 \frac{E}{I} \quad (371)$$

$$\rho_s = \frac{I}{S} \quad (372)$$

The observed resistivity is proportional to spacing and the constant of proportionality is $1/S$.

We may define the effective probing depth for the Schlumberger array as r , the halfspacing between current electrodes. This is the spacing at which the horizontal asymptote for resistivities measured with small spacings intersects a line representing the linear relation given in equation 372. The existence of the insulating basement is little apparent for measurements made with spacings r smaller than the layer thickness, h , while the insulating basement exerts a pronounced effect on measurements made with large spacings. The effective probing depths for other arrays may be defined similarly.

Of particular interest is the polar-dipole array in which the dipole lengths are not small compared to dipole separation. The parameters used in defining such an array are shown in figure 81.

In considering the effective array spacing for such an electrode arrangement, we assume the spacing between dipoles is large compared to the layer

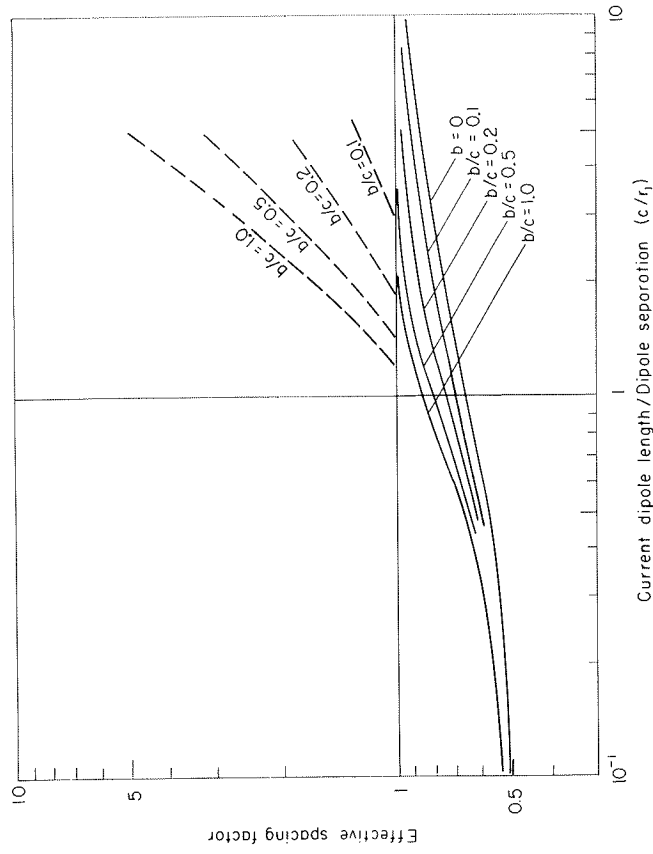


FIGURE 81.—Effective spacing factor as a function of dipole lengths (b and c) and separation r_1 for a polar dipole array (from Keller, 1966; reprinted by permission from the Society of Exploration Geophysicists).

thickness. The difference in potential observed between points M and N for a current I into the layer at point A is:

$$\begin{aligned} \Delta U_A &= \int_r^{r+b} E dr \\ &= \int_r^{r+b} \frac{I}{2\pi r S} dr \\ &= \frac{I}{2\pi S} \ln \left(\frac{r+b}{r} \right) \end{aligned} \quad (373)$$

The difference in potential observed between points M and N for a current -I into the layer at point B is:

$$\begin{aligned} \Delta U_B &= \int_{r+c}^{r+b+c} E dr \\ &= \frac{I}{2\pi S} \ln \left(\frac{r+c}{r+b+c} \right) \end{aligned} \quad (374)$$

The apparent resistivity computed for the arrangement of electrodes shown in figure 81 is:

$$\begin{aligned} \rho_a &= \frac{2\pi}{\frac{1}{r} - \frac{1}{r+c} - \frac{1}{r+b} + \frac{1}{r+b+c}} \cdot \left(\frac{\Delta U_A + \Delta U_B}{I} \right) \\ &= \frac{1}{S} \frac{1}{\frac{1}{r} - \frac{1}{r+c} - \frac{1}{r+b} + \frac{1}{r+b+c}} \ln \left[\left(\frac{r+b}{r} \right) \cdot \left(\frac{r+c}{r+b+c} \right) \right] \end{aligned} \quad (375)$$

In accordance with equation 372, the effective spacing factor, a' , is defined such that

$$\rho_a = \frac{\rho'}{S} \quad (376)$$

The effective spacing factor in equation 376 is then:

$$\rho' = \frac{\ln \left[\left(\frac{r+b}{r} \right) \cdot \left(\frac{r+c}{r+b+c} \right) \right]}{\frac{1}{r} - \frac{1}{r+c} - \frac{1}{r+b} + \frac{1}{r+b+c}} \quad (377)$$

For convenience, this equation may be expressed in terms of dimensionless ratios:

$$\frac{\rho'}{r_1} = \frac{\ln \left[\left(1 + \frac{b}{r_1} \right) \cdot \left(\frac{1 + \frac{c}{r_1}}{1 + \frac{b}{r_1} + \frac{c}{r_1}} \right) \right]}{1 - \frac{1}{1 + \frac{c}{r_1}} - \frac{1}{1 + \frac{b}{r_1}} + \frac{1}{1 + \frac{b}{r_1} + \frac{c}{r_1}}} \quad (378)$$

This equation must apply for an ideal dipole array in which dipole lengths are short, as well as for the non-ideal dipole array shown in figure 81. In an ideal dipole array, the spacing r is large in comparison with the spacings b and c , so that both the logarithm in the numerator and the fractions in the denominator may be replaced by short power series:

$$\begin{aligned} \frac{\rho'}{r_1} \Big|_{\frac{b}{r_1}, \frac{c}{r_1} \rightarrow 0} &= \frac{\frac{b}{r_1} - \frac{1}{2} \left(\frac{b}{r_1} \right)^2 + \frac{c}{r_1} - \frac{1}{2} \left(\frac{c}{r_1} \right)^2 - \left(\frac{b}{r_1} + \frac{c}{r_1} \right) + \frac{1}{2} \left(\frac{b}{r_1} + \frac{c}{r_1} \right)^2}{1 - \left[1 - \frac{c}{r_1} + \left(\frac{c}{r_1} \right)^2 \right] - \left[1 - \frac{b}{r_1} + \left(\frac{b}{r_1} \right)^2 \right] + \left[1 - \left(\frac{b}{r_1} + \frac{c}{r_1} \right) + \left(\frac{b}{r_1} + \frac{c}{r_1} \right)^2 \right]} \\ &\approx \frac{1}{2} \end{aligned} \quad (379)$$

This is the spacing factor for the polar dipole array given by Al'pin, (1966).

Unfortunately, we cannot examine the behavior of equation 378 for small values of r , ($r_1 \rightarrow 0$) because in the model, r_1 was required to remain large compared to the layer thickness.

A series of curves showing the effective spacing factor for various values of b/c and c/r_1 are given in figure 82. These curves provide reasonable spacing factors for those cases in which the dipole separation, r , is larger than the source dipole length, c . However, if the spacing, r , is small compared to the dipole length, c , the probing depth given by equation 378 is larger than we intuitively expect. This is a consequence of the way the definition was set up, inasmuch as it was required that the electrode separations be large in comparison with the thickness of the surface layer. The probing depths given by equation 378 are valid if the substratum is truly an insulator, but not when the resistivity of the substratum is finite. When the resistivity of the substratum is finite and the spacing, r , is much less than the dipole length, c , the array behaves approximately as a three-terminal array with the contribution from the distant current electrode being insignificant. The potential ΔU_B in equation 375 is arbitrarily set equal to zero, with the result:

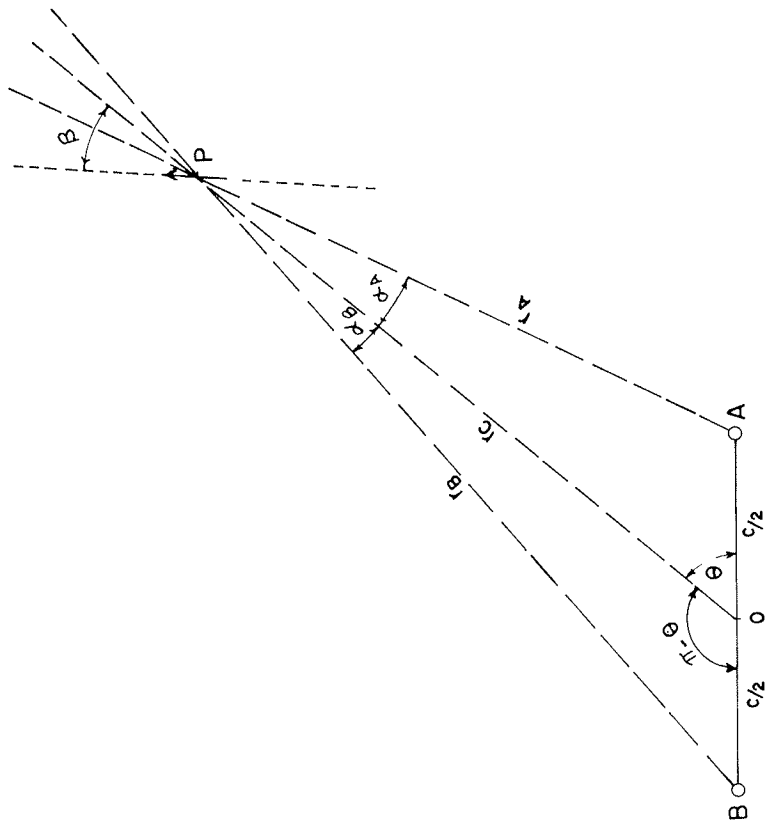


FIG. 82. — Definition of parameters used in discussing a general dipole array. A and B are current electrodes, P is the center of a measuring dipole, θ is the azimuth angle between the AB dipole axis and the radius vector to the point P, and β is the bearing angle between the direction of the receiving dipole and the radius vector from the midpoint of the source dipole. (from Keller, 1966; reprinted by permission from the Society of Exploration Geophysicists).

$$\rho_a = \frac{2\pi}{\frac{1}{r_1} - \frac{1}{r_1+b}} \frac{\Delta U_A}{I}$$

$$= \frac{1}{S} \frac{1}{\frac{1}{r_1} - \frac{1}{r_1+b}} \ln \left(\frac{r_1+b}{r_1} \right)$$
(380)

Defining the effective spacing factor in accordance with equation 376, we have:

$$\alpha' = \frac{\ln \left(\frac{r_1+b}{r_1} \right)}{\frac{1}{r_1} - \frac{1}{r_1+b}}$$
(381)

or, using dimensionless ratios:

$$\frac{\alpha'}{r} = \frac{\ln \left(1 + \frac{b}{r_1} \right)}{1 - \frac{1}{1 + \frac{b}{r_1}}}$$
(382)

Normally, the ratio b/r_1 is quite small so that both the numerator and denominator in equation 382 may be expanded in series:

$$\lim_{b \rightarrow 0} \left(\frac{\alpha'}{r} \right) = \lim_{b \rightarrow 0} \frac{\frac{b}{r_1} - \frac{1}{2} \left(\frac{b}{r_1} \right)^2 + \dots}{1 - \left[1 - \frac{b}{r_1} + \left(\frac{b}{r_1} \right)^2 - \dots \right]}$$

$$= 1$$
(383)

The probing depth curves in figure 82 should approach a limit of 1.0 as r_1 becomes small, rather than become large without limit. Curves which behave properly for a four-electrode array at large separations, and properly for a three-electrode array at small separations are shown as dashed lines on figure 82. The curves in figure 82 are valid when all electrodes lie along a common line. In practice, this requirement is not usually met for the larger separations. With spacings over a few miles, topography and road patterns may dictate the use of a nonlinear array. The effective probing depth of such an array may be defined in the same way as that for a colinear array. The array is considered to be located on the surface of a layer with resistivity, ρ_1 , with a thickness much smaller than the dipole separation, r_1 , and resting on an insulating substratum. The source dipole is considered to have an appreciable length, c , while the measuring dipole is considered to be so short that it can be treated as an idealized dipole. The line from the midpoint of the source dipole to the measuring point makes an angle θ with the polar axis of the source dipole, while the receiving dipole axis forms an angle β with the line connecting the dipole centers (fig. 83).

The magnitude of the electric field at the receiving dipole due to a current I driven into the ground at point A is:

$$E_A = J\rho = \frac{\rho I}{2\pi r_A H}$$
(384)

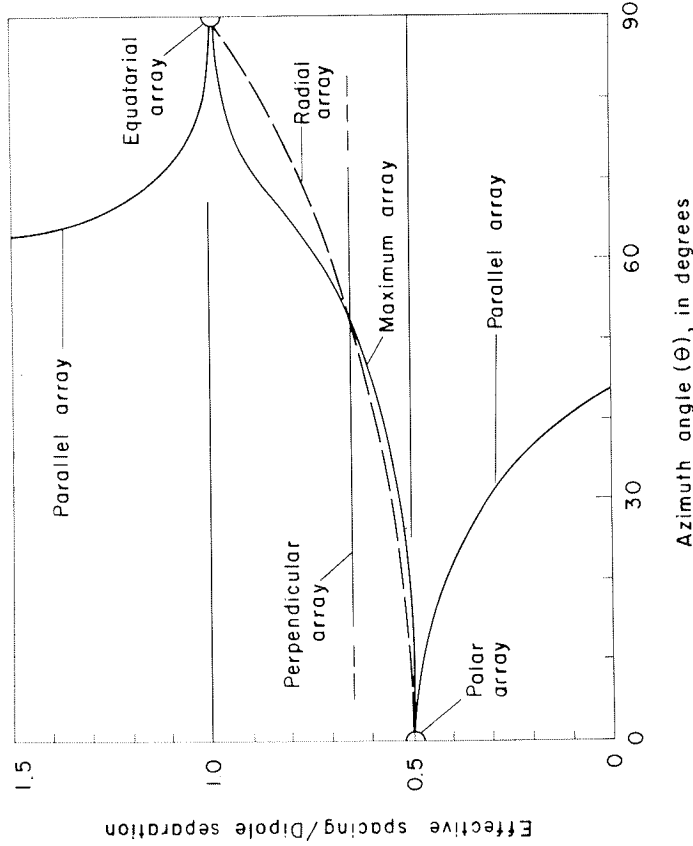


FIGURE 83.—Effective spacing factor as a function of azimuth angle for various dipole arrays (from Keller, 1966; reprinted by permission from the Society of Exploration Geophysicists).

The component of this vector directed along the receiving dipole is:

$$E_{A,\beta} = \frac{\rho I}{2\pi r_A h} \cos(\beta - \alpha_A) \tag{385}$$

Similarly, the component of the electric field vector developed by the current $-I$ entering the earth at point B, projected along the receiving dipole, is:

$$E_{B,\beta} = -\frac{\rho I}{2\pi r_B h} \cos(\beta - \alpha_B) \tag{386}$$

The total electric field observed along the receiving dipole is:

$$E_{A+B,\beta} = \frac{\rho I}{2\pi h} \left[\frac{\cos(\beta - \alpha_A)}{r_A} - \frac{\cos(\beta - \alpha_B)}{r_B} \right] \tag{387}$$

The angles α_A and α_B are very nearly equal, so equation 387 may be written as:

$$E_\beta = \frac{\rho I}{2\pi r_A h} \cos(\beta - \alpha) - \frac{\rho I}{2\pi r_B h} \cos(\beta + \alpha) \tag{388}$$

The two distances r_A and r_B from the receiving dipole to each of the current electrodes may be expressed in terms of the central distance, r , if the length of the current dipole is small compared to the distance r :

$$r_A = r - \frac{c}{2} \cos \theta$$

$$r_B = r + \frac{c}{2} \cos \theta$$

where c is the separation between the two current electrodes and θ is the angle between the axis of the current dipole and the radius vector r . Equation 388 becomes:

$$E_\beta = \frac{\rho I}{2\pi h} \left[\frac{\cos(\beta - \alpha)}{r - \frac{c}{2} \cos \theta} - \frac{\cos(\beta + \alpha)}{r + \frac{c}{2} \cos \theta} \right] \tag{389}$$

or, making a single fraction:

$$E_\beta = \frac{\rho I}{2\pi r h} \left[\frac{\cos(\beta - \alpha) + \frac{c}{2r} \cos \theta \cos(\beta - \alpha) - \cos(\beta + \alpha) - \frac{c}{2r} \cos \theta \cos(\beta + \alpha)}{1 - \frac{1}{4} \left(\frac{c}{r}\right)^2 \cos^2 \theta} \right] \tag{390}$$

The second term in the denominator is small compared with the first and may be neglected. Let us now expand the trigonometric functions:

$$\cos(\beta + \alpha) = \cos \beta \cos \alpha - \sin \beta \sin \alpha$$

$$\cos(\beta - \alpha) = \cos \beta \cos \alpha + \sin \beta \sin \alpha$$

$$E_\beta = \frac{\rho I}{2\pi r h} \left[\cos \beta \cos \alpha + \sin \beta \sin \alpha + \frac{c}{2r} \cos \theta (\cos \beta \cos \alpha + \sin \beta \sin \alpha) - \cos \beta \cos \alpha + \sin \beta \sin \alpha + \frac{c}{2r} \cos \theta (\cos \beta \cos \alpha - \sin \beta \sin \alpha) \right] \tag{391}$$

This reduces to:

$$E_\beta = \frac{\rho I}{2\pi r h} \left[2 \sin \beta \sin \alpha + \frac{c}{r} \cos \theta \cos \beta \cos \alpha \right] \tag{392}$$

We may simplify this further if we recognize that the angle α is very small, and the sine and cosine may be approximated as:

$$\sin \alpha = \alpha$$

$$\cos \alpha = 1 - \frac{1}{2} \alpha^2$$

Moreover, since α is a small angle, the product of the angle with a radius, such as r , should be approximately equal to the length of the chord at the radius, $c \sin \theta$

$$2\alpha r = c \sin \theta$$

Thus, equation 392 may be rewritten approximately as:

$$E_{\beta} = \frac{\rho I}{2\pi h} \left[\frac{c}{r} \sin \beta \sin \theta + \frac{c}{r} \cos \beta \cos \alpha - \frac{1}{8} \left(\frac{c}{r} \right)^3 \sin \theta \cos \theta \cos \beta \right] \quad (393)$$

The last term is very small and may be neglected:

$$E_{\beta} \approx \frac{\rho I c}{2\pi h r^2} [\sin \beta \sin \theta + \cos \beta \cos \theta] \quad (394)$$

Remembering that the observed voltage is $\Delta U = bE$, and using the defining equation for apparent resistivity measured with a dipole array:

$$\rho_a = \frac{\pi r^3}{bc (\cos \theta \cos \beta + \frac{1}{2} \sin \theta \sin \beta)} \frac{\Delta U}{I}$$

we have:

$$\rho_a = \frac{\pi r^3}{I bc (\cos \theta \cos \beta + \frac{1}{2} \sin \theta \sin \beta)} \cdot \frac{\rho I bc}{2\pi h r^2} [\sin \theta \sin \beta + \cos \theta \cos \beta] \quad (395)$$

$$\text{or, simply: } \rho_a = \frac{\rho r}{2h} \left[\frac{\cos \theta \cos \beta + \sin \theta \sin \beta}{\cos \theta \cos \beta + \frac{1}{2} \sin \theta \sin \beta} \right] \quad (396)$$

Alternate ways of writing the same equation are:

$$\rho_a = \frac{\rho r}{2h} \left[\frac{\tan \theta \tan \beta + 1}{\frac{1}{2} \tan \theta \tan \beta + 1} \right] \quad (397)$$

$$\text{and: } \rho_a = \frac{r}{S} \left[\frac{\tan \theta \tan \beta + 1}{\tan \theta \tan \beta + 2} \right] \quad (398)$$

These last equations indicate that the effective spacing factor for a dipole array is not only a function of the separation between dipole centers, but also of the azimuth angle from the current dipole to the receiving dipole, and the bearing angle of the receiving dipole. Let us now consider a few special cases.

With the polar dipole array, we have:

$$\beta = 0$$

$$\theta = 0$$

and the effective spacing factor is

$$\alpha'_{DP} = \frac{r}{2} \quad (399)$$

for the equatorial dipole array, both angles are $\pi/2$, and the effective spacing factor is:

$$\alpha'_{DE} = r \quad (400)$$

For the parallel dipole array:

$$\beta = \pi - \theta$$

θ is arbitrary

and the effective spacing factors:

$$\alpha'_D = \frac{-\tan^2 \theta + 1}{-\tan^2 \theta - 1} r \quad (401)$$

It is interesting to note that when the angle θ has a tangent² equal to $+2$ ($\theta = 53^\circ 44'$), the effective spacing for a parallel dipole array becomes large without limit. This is the same value for θ for which the normal electric field (that observed over a homogeneous earth), has a zero component in the direction parallel to a source dipole. Accordingly, the geometric factor for the parallel dipole array when $\tan^2 \theta = 2$ is infinitely large. The presence of a layer in the otherwise homogeneous earth will distort the dipole field so that where previously no parallel component of electric field was observed for $\theta = 53^\circ 44'$, some very slight electric field component is observed. Since this small anomalous field value is multiplied by an infinitely large geometric factor, the measurement becomes infinitely sensitive to the presence of layers at depth, at least theoretically.

The effective spacing factor goes to zero when the azimuth angle is such that $\tan^2 \theta = 1$, or $\theta = 45^\circ$. With this azimuth angle the observed resistivity becomes completely independent of the presence of a resistive layer at depth. For the perpendicular array:

$$\beta = \frac{\pi}{2} - \theta$$

θ is arbitrary,

and the effective spacing factor is:

$$\alpha'_D = \frac{2r}{3} \quad (402)$$

For the perpendicular array, the effective spacing factor is independent of the azimuth angle.

For the radial array:

$$\beta = 0$$

θ is arbitrary.

and the effective spacing factor is:

$$\alpha'_{DR} = \frac{\Sigma}{2} \quad (403)$$

In view of the symmetry of the electric field about a dipole source, we are concerned only with definitions applying to a single quadrant. Thus, while $\tan \theta$ could have a value of -2 , generating a singularity in the expression for the effective spacing factor for the radial dipole array, we have restricted our considerations to a range of values for the azimuth angle running from 0 to $\pi/2$.

The wide range over which the effective spacing factor for the various dipole arrays can vary suggests that care should be taken in orienting the two dipoles. Arbitrary orientations can lead to widely scattered data. Therefore, if electric field observations are to be made over the full range of azimuth angles, the measuring dipole should preferably be oriented perpendicular to the current dipole, or in the direction of greatest electric field strength (or the direction which would be that of greatest field strength in a homogeneous medium). A perpendicular array provides a fairly simple surveying problem, but has the disadvantage that the amplitude of the electric field component becomes quite small for bearing or azimuth angles near 0 or $\pi/2$. Maximum-field orientation is a more difficult surveying problem, but provides a much larger signal to be measured in many cases, and signal level is frequently a critical problem in surveys made with the dipole methods.

The bearing angle for the direction of maximum field strength for a dipole over a homogeneous earth may be found by taking the ratio of radial and tangential components of electric field strength:

$$E_{\text{rad}}/E_{\text{tang}} = 2 \cot \theta \quad (404)$$

This ratio of field components is the cotangent of the angle:

$$\cot \beta = 2 \cot \theta \quad (405)$$

The effective spacing factor for such an array is:

$$\alpha_{D, \text{max}} = \frac{\frac{1}{2} \tan^2 \theta + 1}{\frac{1}{2} \tan^2 \theta + 2} r \quad (406)$$

Values for the ratio a'/r for various azimuth angles are as follows:

TABLE 15.

Azimuth angle, θ	Maximum array a'/r	Polar array a'/r	Equatorial array a'/r	Radial array a'/r	Parallel array a'/r	Perpendicular array a'/r
0°	.500	.500	—	.500	.500	—
10°	.503	—	—	.538	.497	.667
15°	.507	—	—	.553	.493	.667
30°	.534	—	—	.609	.400	.667
45°	.600	—	—	.667	0	.667
60°	.710	—	—	.727	2.00	.667
75°	.930	—	—	.830	1.08	.667
80°	.968	—	—	.865	1.02	.667
90°	1.000	—	1.000	—	1.00	—

These relationships are shown graphically in figure 84.

For any given azimuth angle, θ , there is some bearing angle, β , which will lead to an apparently infinite sampling depth. This infinite sampling depth is of no practical interest, since it is associated with the direction of zero electric field strength. The variation of sampling depth with bearing angle indicates only that it is preferable to have the receiving dipole directed in the direction of maximum electric field strength.

The effective spacing factor for the standard type electrode arrays may be used in conjunction with equations 363, 364 and 365 to determine the maximum depths at which resistivity contrasts may be detected for a given limitation to the weight of equipment and safe operating voltage. In equations 363 to 365, the Schlumberger and dipole arrays were compared with the Wenner array. The effective spacing factor for a Wenner array may be found by integrating the expression for electric field intensity given in equation 370 over the limits $2a$ to a , a being the Wenner spacing:

$$\begin{aligned} \Delta U &= -2 \int_{2a}^a E \, dr = 2 \int_a^{2a} \frac{I}{2\pi r S} \, dr \\ &= \frac{1}{\pi S} \ln 2 \end{aligned} \quad (407)$$

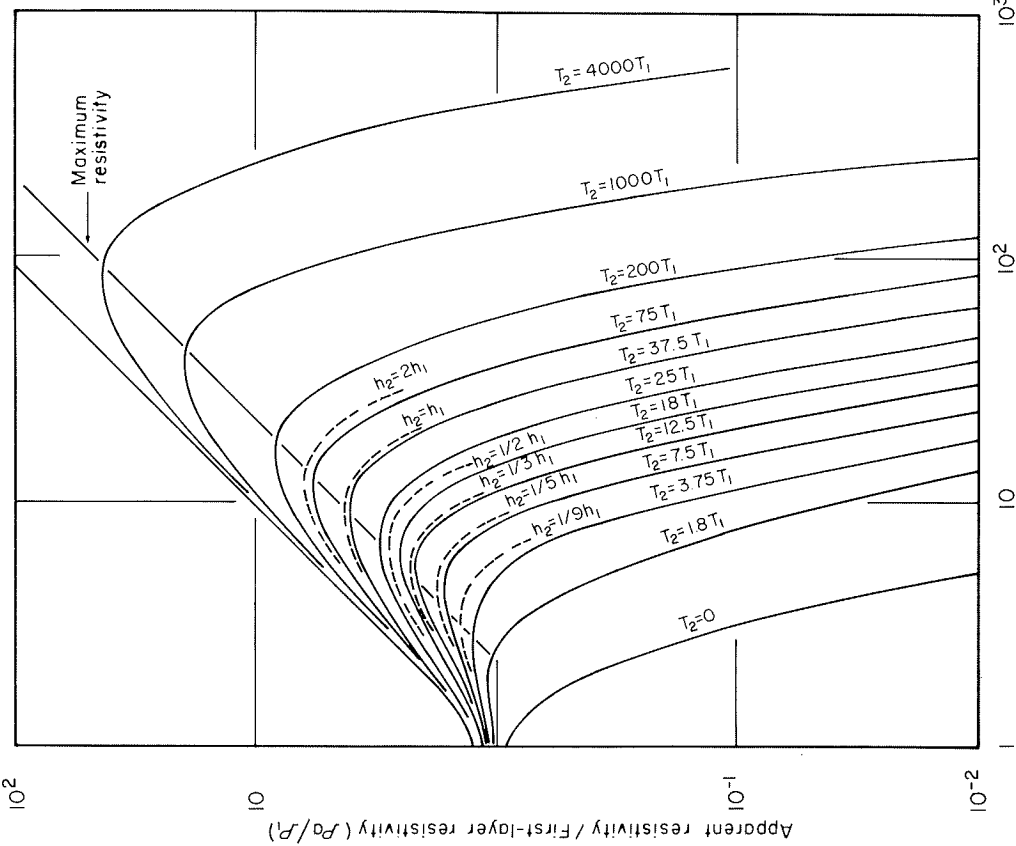


FIGURE 84.— Apparent resistivity curves obtained with a Schlumberger array over a sequence of three layers in which the transverse resistance of the middle layer is large. Curves are taken from sets computed by Compagnie Generale de Geophysique (CGG). The dashed curves are taken from a set for a resistivity contrast of 39:1 between the second and first layers (from Keller, 1966; reprinted by permission from the Society of Exploration Geophysicists).

The equation defining apparent resistivity for the Wenner array is:

$$\rho_w = 2\pi a_w \frac{\Delta U}{I} \tag{408}$$

or, substituting from equation 407:

$$\rho_w = \frac{2a_w}{5} \epsilon_{12} \tag{409}$$

Defining the effective spacing factor as in equation 376:

$$a'_w = 2a_w \epsilon_{12} \tag{410}$$

The ratio of effective spacing factors for the Schlumberger and Wenner arrays is:

$$\frac{a'_s}{a'_w} = \frac{a_s}{2a_w \epsilon_{12}} \tag{411}$$

where $a_{s, \max} / a_{w, \max}$ is the ratio of maximum attainable spacings arrived at in equation 357, having the value $(\frac{9}{2})^{1/4} = 1.16$

$$\frac{a'_s}{a'_w} = \frac{1.46}{1.38} = 1.05 \tag{412}$$

Thus, for a given total weight limitation, resistivity contrasts may be found at 5 percent greater depths with the Schlumberger array than with the Wenner array.

Similarly, for the equatorial dipole array:

$$\frac{a'_{DE}}{a'_w} = \frac{1}{1.38} \left(\frac{9}{k_3}\right)^{1/4} = 1.05 k_3^{-1/4} \tag{413}$$

and for the polar dipole array

$$\frac{a'_{DP}}{a'_w} = \frac{0.50}{1.38} \left(\frac{9}{2k_3}\right)^{1/4} = 0.625 k_3^{-1/4}$$

The parameter, k_3 , which is the ratio of receiving dipole length to dipole separation, is quite small. If it is assigned a value of 0.1, the maximum attainable "reach" with a dipole array is somewhat better than half the reach for a Schlumberger array, with the same weight limitations.

The relative capacities of various arrays for detecting boundaries at depth may perhaps be better seen by comparing theoretical sounding curves over simple layer sequences. Curves for the very simple case of a single layer with resistivity ρ_1 covering an insulating substratum are shown in figure 85. All the curves are plotted with the total distance between outermost electrodes as the characteristic distance, rather than the more commonly defined spacings.

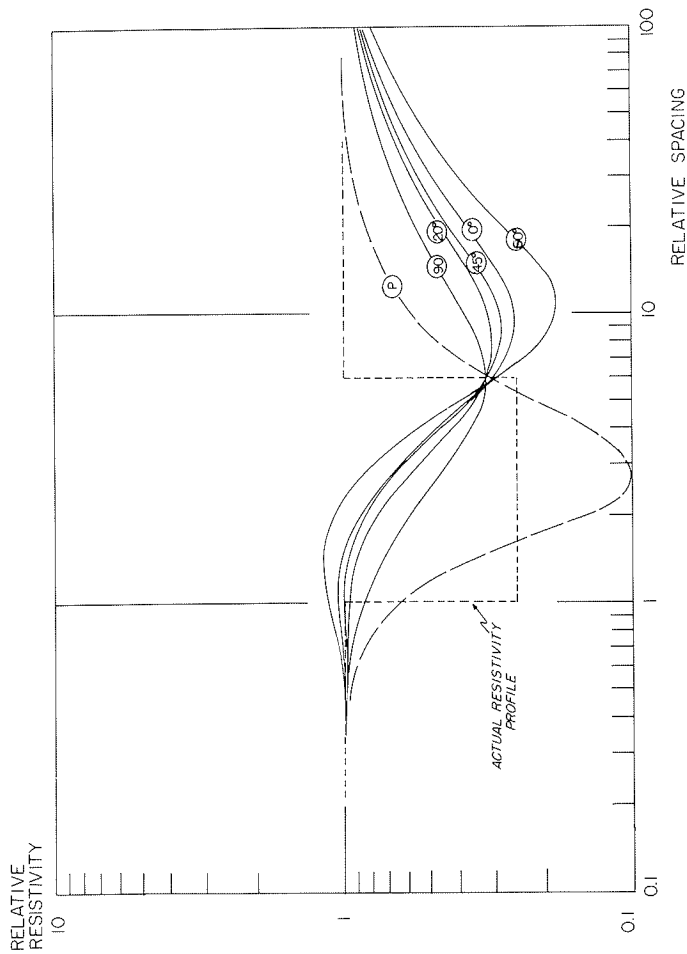


FIGURE 86.—Various dipole resistivity curves for a common set of layers with a sequence of resistivities of 1:1/4:1 and a sequence of thickness of 1:5. The dashed curve is valid for the perpendicular dipole array, while the solid curves are valid for parallel dipole arrangements with the azimuth angles as indicated.

DEPTH OF PROBING WITH ELECTROMAGNETIC METHODS

We will now consider the requirements for frequencies and source-receiver separations in order that a layered earth may be investigated to a desired depth. Such requirements must be considered in determining how much power is required with the various source and receiver sensor configurations to reach a given depth, if the relative merits of the methods are to be investigated.

We must first agree on how the "depth of probing" or the "depth of penetration" of a method is to be measured. No simple definition of depth of penetration is available for any of the electrical geophysical methods because the ability to detect a bed at a given depth depends on the electrical properties of all the beds lying above that depth, and no single, universal measure of depth of penetration can be specified. Rather, since we are interested only in comparative measures of depth of penetration, we will postulate a simple model, and compare requirements to see through such a simple model with each of the techniques. The simplest model which has meaning is a two-layer model,

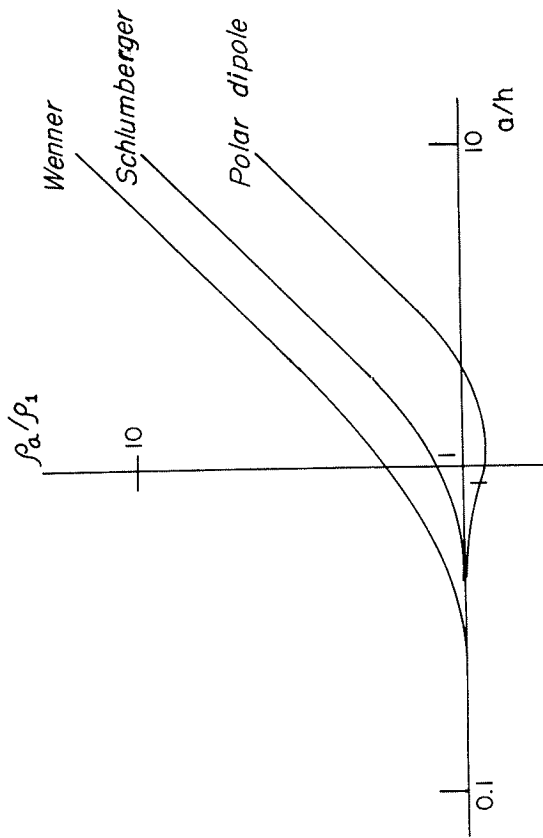


FIGURE 85. Apparent resistivity curves for several electrode arrays for the case of a single uniform layer covering an insulating substratum.

It is interesting to note, that with one exception, all curves approach a rising asymptote for long spacings, with the position of the asymptote depending on the array considered. The one exception consists of an array of parallel dipoles arranged so that the receiving dipole lies almost at the position where no electric field would be detected for a uniform earth. In this one case, a buried insulator looks like a buried conductor.

Three-layer sequences are considered in figures 86 and 87, the first being a sandwich of layers with the middle one being relatively more conductive than the outer layers, and the second being a sandwich of layers with the middle one being relatively more resistive than the outer layers. It should be noted that the introduction of the third layer does not affect the relative positions of the rising asymptote for the various arrays. However, the capacity for an array to see through a resistive layer into an underlying conductive layer does not vary in the same way as does the capacity to see through a conductive layer into a resistive layer. For example, it is necessary to use spacings twice as great with polar dipole array as with an equatorial dipole array to see a buried insulator. However, the polar dipole spacing required to see a buried conductor is only slightly greater than the spacing required with the equatorial dipole array.

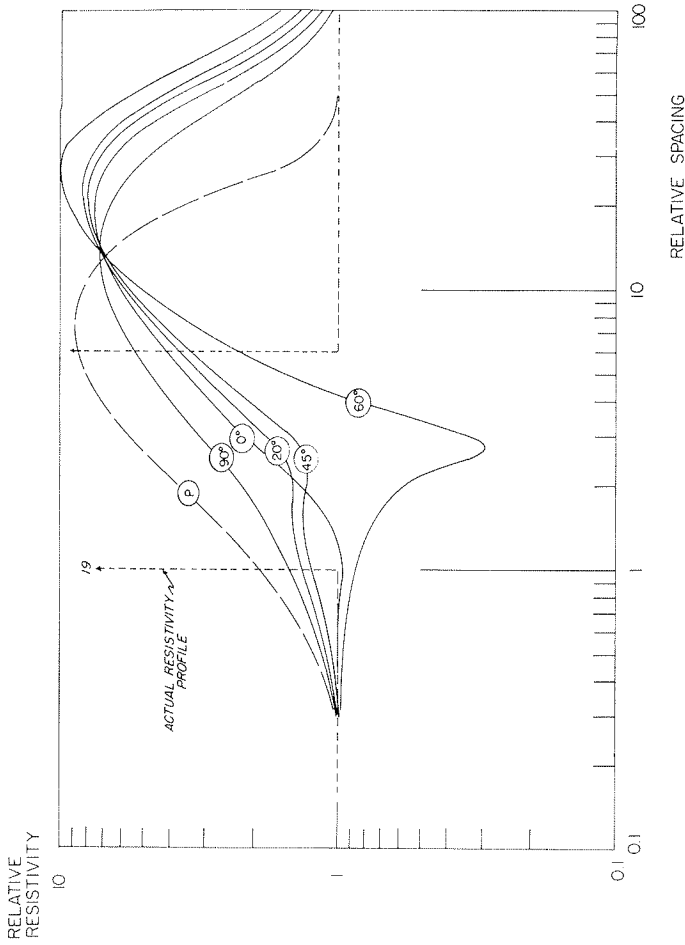


FIGURE 87. — Various dipole resistivity curves for a common set of layers with a sequence of resistivities of 1:19:1, and a sequence of thicknesses of 1:5. The dashed curve is valid for the perpendicular dipole arrangement, while the solid curves are valid for parallel dipole arrangements with the azimuth angles as indicated.

characterized by a single overburden layer with a resistivity, ρ_1 , and a thickness, h , resting on a halfspace with a resistivity, ρ_2 , (fig. 88).

The model could be investigated for an arbitrary contrast in resistivities, ρ_2/ρ_1 , but in view of the complexity of the expressions for coupling between various sources and receivers, this would have to be done numerically, so that generalizations would be difficult to make. Fortunately, the various expressions can be simplified by considering extreme contrasts in resistivity; that is, $\rho_2/\rho_1 \rightarrow 0$ or $\rho_2/\rho_1 \rightarrow \infty$.

We will first consider the expression for tangential electric field about a vertical-axis coil source.

For the two-layer case, \tilde{R}_o is:

$$\tilde{R}_o = \coth(\chi_1 h + \coth^{-1} \frac{\chi_1}{\chi_2}) = \frac{\frac{\chi_1}{\chi_2} \coth \chi_1 h + 1}{\frac{\chi_1}{\chi_2} + \coth \chi_1 h} \quad (414)$$

Assuming either that $\rho_2/\rho_1 \rightarrow 0$ or ∞ , we have two asymptotic expressions:

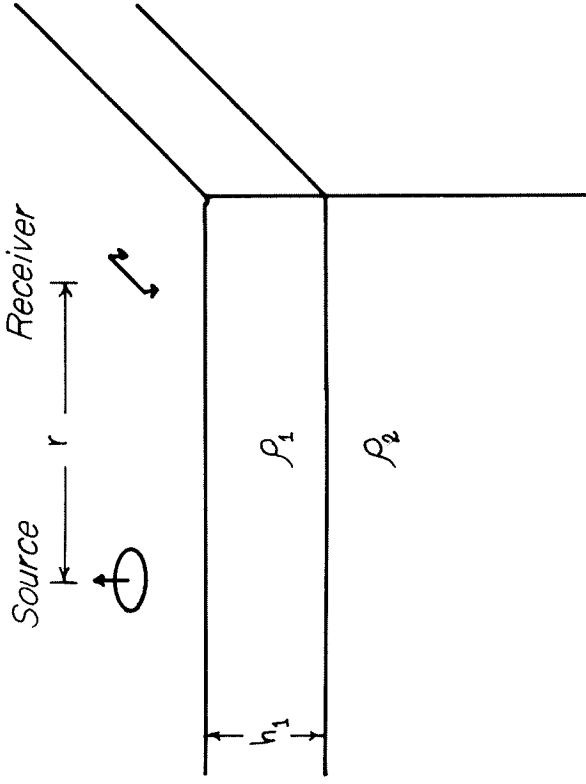


FIGURE 88. — Formulation of the two-layer problem for determining the depth of investigation of various electromagnetic coupling techniques.

a. For $\rho_2/\rho_1 \rightarrow 0$:

$$\tilde{R}_o \Big|_{\rho_2 \rightarrow 0} = \frac{1}{\coth \chi_1 h} \quad (415)$$

b. For $\rho_2/\rho_1 \rightarrow \infty$:

$$\tilde{R}_o \Big|_{\rho_2 \rightarrow \infty} = \coth \chi_1 h \quad (416)$$

Let us now examine the low-frequency and high-frequency asymptotes for these two expressions. For small arguments, the hyperbolic cotangent can be replaced with the reciprocal for its argument, while for large arguments, its value approaches 1:

a1. For $\omega \rightarrow 0$ $\tilde{R}_o \Big|_{\rho_2 \rightarrow 0} = \chi_1 h$ (417)

a2. For $\omega \rightarrow \infty$ $\tilde{R}_o \Big|_{\rho_2 \rightarrow 0} = 1$ (418)

b1. For $\omega \rightarrow 0$ $\tilde{R}_o \Big|_{\rho_2 \rightarrow \infty} = \frac{1}{\chi_1 h}$ (419)

b2. For $\omega \rightarrow \infty$

$$\tilde{R}_o \Big|_{\rho_2 \rightarrow \infty} = 1 \tag{420}$$

These asymptotic conditions have simple forms which plot as straight lines on the usual logarithmic coordinates (fig. 89). Using the appropriate definition for apparent resistivity, we find that the ratio ρ_a/ρ_1 is constant at unity for the two low-frequency asymptotes. At high frequencies, the apparent resistivity increases directly as $\gamma_1^2 h$ if the lower medium is a perfect insulator, and decreased directly as $1/\gamma_1^2 h$, if the lower medium is a perfect conductor.

These two asymptotic conditions provide a fairly simple definition for depth of penetration: the depth of penetration is the intersection of the low-frequency and high-frequency asymptotes. For frequencies higher than that intersection frequency, the lower medium has little effect on the field components, while for frequencies lower than the intersection frequency, the lower medium has a progressively larger effect on the field components. Therefore, we have a frequency requirement:

Radian wave lengths somewhat longer than the wave length in the surface layer (or layers) must be used to see through a sequence to a given depth; or:

$$\omega < \frac{1}{\mu_0 \sigma_1 h^2} \tag{421}$$

We are also concerned with the requirement for the spacing necessary to see to a given depth, inasmuch as the amount of power required will vary rapidly with spacing. We may forecast the nature of the results we are after by considering some coupling curves which have already been computed by Vanyan (1967). The curves shown in figure 90a are for the case of a two-layer sequence with the lower medium a perfect conductor. With progressively shorter spacings in comparison with the thickness of the overburden, the curves for finite separation depart from the curve for infinite separation at higher and higher frequencies, until at very short spacings, the presence of the lower halfspace cannot be detected easily.

A similar situation is seen if the lower medium is an insulator (fig. 90b) though the curves differ in detail. If the separation is too short in comparison with the thickness of the surface layer, the effect of the lower halfspace becomes difficult to see.

In the various integral expressions, distance from source to receiver is contained only in the argument of the Bessel function, and so these integrals must be evaluated in order to determine for what spacings the curve for \tilde{R}^2 first departs a given amount from the curve for \tilde{R}_o^2 . The separation parameter

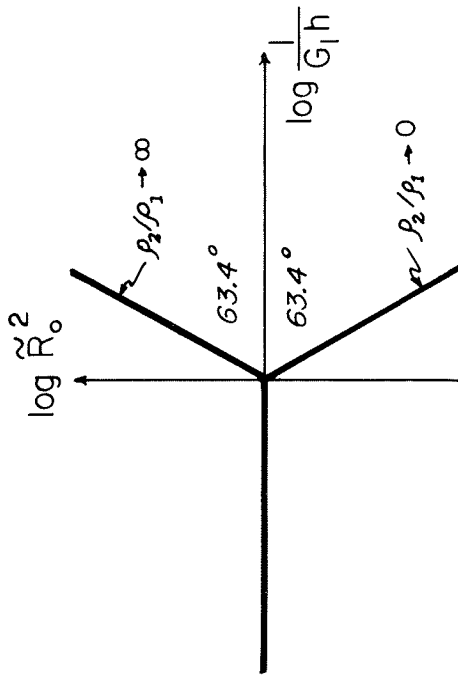


FIGURE 89. — Use of asymptotes for asymptotic coupling function to define depth of investigation as a function of frequency.

m has roughly the significance in the integrals of the inverse of the separation. Thus, if we are concerned with relaxing our limit condition on r from infinity to merely large, it is equivalent to relaxing the condition on m from zero to merely small. In place of \tilde{R}_o , we can use a better approximation:

$$\tilde{R} \Big|_{m \ll 1} = \tilde{R}_o + \Delta \tilde{R} \tag{422}$$

Because the case is somewhat simpler, let us first consider the requirement for spacing when $\rho_2 = 0$. The ratio function is

$$\tilde{R} = \coth \lambda (\eta_1 h + \coth \lambda^{-1} \frac{\eta_1}{\eta_2}) \tag{423}$$

For small values of m , we may make the following approximations:

$$\eta_1 = (m^2 + \gamma_1^2)^{1/2} \approx \gamma_1 (1 + \frac{1}{2} \frac{m^2}{\gamma_1^2}) \tag{424}$$

$$\eta_2 = (m^2 + \gamma_2^2)^{1/2} \approx \gamma_2 (1 + \frac{1}{2} \frac{m^2}{\gamma_2^2}) \tag{425}$$

$$\frac{\eta_1}{\eta_2} \approx \frac{\gamma_1}{\gamma_2} [1 + \frac{m^2}{2} (\frac{1}{\gamma_2^2} - \frac{1}{\gamma_1^2})] \tag{426}$$

$$\coth \lambda \eta_1 h \approx \coth \lambda \delta_1 h + \frac{m^2 h}{2 \delta_1} (1 - \coth^2 \lambda^2 \delta_1 h) \tag{427}$$

Substituting these approximations in equation 423, we have for small m :

$$\tilde{R} \Big|_{m \ll \epsilon} \approx \frac{\gamma_1}{\gamma_2} \left[1 + \frac{m^2}{2} \left(\frac{1}{\gamma_2^2} - \frac{1}{\gamma_1^2} \right) \right] \cdot \left[\coth \delta_1 h + \frac{m^2 h}{2 \delta_1} (1 - \coth \delta_1 h) \right] + 1 + \frac{m^2 h}{2 \delta_1} \left[1 + \frac{m^2}{2} \left(\frac{1}{\gamma_2^2} - \frac{1}{\gamma_1^2} \right) \right] + \left[\coth \delta_1 h + \frac{m^2 h}{2 \delta_1} (1 - \coth \delta_1 h) \right] \quad (428)$$

The terms in the denominator can be rearranged so that all which are multiplied by m^2 can be treated as a small quantity when compared with the rest of the terms in the denominator:

$$\tilde{R} \Big|_{m \ll \epsilon} \approx \frac{\frac{\gamma_1}{\gamma_2} \left\{ \coth \delta_1 h + \frac{m^2 h}{2 \delta_1} (1 - \coth \delta_1 h) + \frac{m^2}{2} \left(\frac{1}{\gamma_2^2} - \frac{1}{\gamma_1^2} \right) \coth \delta_1 h \right\} + 1}{\left[\coth \delta_1 h + \frac{\gamma_1}{\gamma_2} \right] + \frac{m^2}{2} \left[\left(\frac{1}{\gamma_2^2} - \frac{1}{\gamma_1^2} \right) + \frac{\gamma_1}{\gamma_2} (1 - \coth \delta_1 h) \right]} \quad (429)$$

The terms which represent the ratio for $m=0$ can be divided out of this last equation, with the result:

$$\tilde{R} \Big|_{m \ll \epsilon} = \left\{ \frac{1 + \frac{\gamma_1}{\gamma_2} \coth \delta_1 h}{\coth \delta_1 h + \frac{\gamma_1}{\gamma_2}} \right\} \cdot \left\{ \left[1 + \frac{\gamma_1 m^2}{2 \delta_1} \left(\frac{1}{\gamma_2^2} - \frac{1}{\gamma_1^2} \right) \coth \delta_1 h + \frac{\gamma_1}{2} \frac{m^2 h}{2 \delta_1} (1 - \coth \delta_1 h) \right] \right. \\ \left. \cdot \left[1 - \frac{m^2 \left[\frac{\gamma_1}{\gamma_2} (1 - \coth \delta_1 h) + \frac{\gamma_1}{\gamma_2} \left(\frac{1}{\gamma_2^2} - \frac{1}{\gamma_1^2} \right) \right]}{\frac{\gamma_1}{\gamma_2} + \coth \delta_1 h} \right] \right\} \quad (430)$$

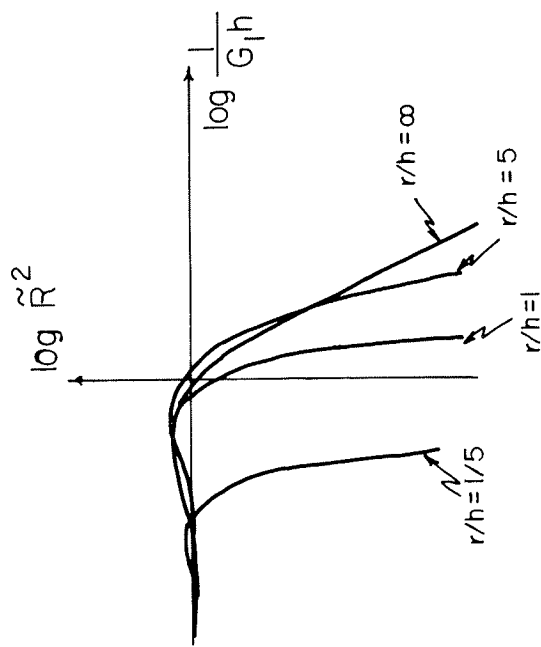
Keeping terms only of order m^2 and taking $\gamma_1/\gamma_2=0$, we have:

$$\tilde{R} \Big|_{m \ll \epsilon} = \tilde{R}_0 \left\{ 1 - \frac{m^2 \left[\frac{\gamma_1}{\gamma_2} (1 - \coth \delta_1 h) \right]}{\coth \delta_1 h} \right\} \\ = \tilde{R}_0 + \Delta \tilde{R} \quad (431)$$

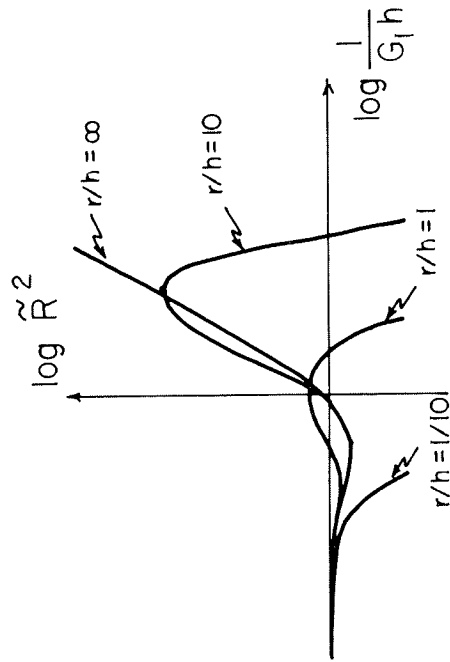
We have achieved our goal—that of expressing the behavior for m not quite zero as an additive correction to \tilde{R}_0 . Remember that the term containing \tilde{R} in the integrand of the Sommerfeld integral can be expanded as follows for small values of m :

$$\frac{m}{m + \tilde{R}} \approx \frac{m \tilde{R}}{\tilde{R}} - \frac{m^2 \tilde{R}^2}{\tilde{R}^2}$$

Considering equation 431, it is obvious that the first term will contribute nothing on integration because it leads to an m^3 weight in integration. So, we need only consider integration of the terms:



A. Coupling over a buried conductor



B. Coupling over a buried insulator

FIGURE 90. — Coupling between a vertical-axis loop and a tangential wire as a function of source-receiver separation for the case of a single layer covering a perfect conductor or a perfect insulator.

$$\bar{R}^2 = (\bar{R}_0 + \Delta\bar{R})^2 = \bar{R}_0^2 + 2\bar{R}_0\Delta\bar{R} + \Delta\bar{R}^2 \quad (432)$$

The first of these three terms provides the answer obtained previously for infinite source-receiver separation. The last term leads to an integral with weight m^6 , which we will neglect. With the first two terms:

$$E_{\phi}^* = -\frac{i\mu_0 M \omega}{2\pi} \frac{\partial}{\partial r} \left\{ -\frac{\bar{R}_0^2}{\gamma^2} \int_0^{\infty} m^2 J_0(mr) dm + \frac{2}{\gamma^2} \frac{h(1 - \coth^2 \gamma_1 h)}{\coth \gamma_1 h} \int_0^{\infty} \frac{m^4}{2} J_0(mr) dm \right\} \quad (433)$$

Performing the indicated integrations and differentiation:

$$E_{\phi}^* = -\frac{3M\rho_1}{2\pi r^4} \left[1 - \left(\frac{h}{r}\right) \cdot \frac{1}{\gamma r} \cdot \frac{(1 - \coth^2 \gamma_1 h)}{\coth \gamma_1 h} \right] \quad (434)$$

The second term in the brackets represents the fractional correction to the value of tangential electric field arising from finite separation:

$$\left(\frac{h}{r}\right) \cdot \frac{1}{\gamma r} \cdot \frac{(1 - \coth^2 \gamma_1 h)}{\coth \gamma_1 h} < Q \quad (435)$$

where Q is the fractional accuracy required, presumably of the order of unity for realistic requirements. Because $\gamma_1 h < 1$, we might make the approximation:

$$\left(\frac{h}{\gamma r}\right)^2 - \left(\frac{h}{r}\right)^2 < Q \quad (436)$$

Our result indicates that the spacing must be comparable to the thickness, and be greater than the thickness by the same ratio as the spacing is greater than a wave length in the surface layer (by 2π).

Similar analyses should be made of the spacing requirements for other combinations of sources and receivers, but on the basis of this analysis, we may infer that the spacing between source and receiver must probably be at least five times the depth to be explored.

NOISE CONSIDERATIONS AND POWER REQUIREMENTS

We are now in a position to ask the question: Having chosen a spacing and frequency, and knowing the approximate conductivity of the earth we wish to measure, what source strength do we need and what receiver sensitivity is required? If we examine the expressions for any of the source and receiver types listed in the first section, we note an extremely important fact:

For any source-receiver combination, the apparent resistivity is a function of the ratio of measured field strength to source strength.

As a result, there is a direct trade-off between source strength and receiver

sensitivity, so long as we do not encounter any nonlinear constraints not given in these expressions. The two most important nonlinear constraints we will be concerned with are:

1. The maximum source strength is almost always limited by the amount of weight which is allowed in the source. For all except small source strengths, the weight of a source is very nearly proportional to the source strength.
2. The maximum receiver sensitivity is almost always limited by the ambient noise field. Generally, weight is not a factor in determining receiver sensitivity.

With both an upper limit on source power and an upper limit on receiver sensitivity, there is an ultimate capability for electromagnetic sounding methods within a given set of constraints. This ultimate capability is not the same for all combinations of source and receiver, and so, it will appear that for measurements which strain the constraints of a given problem, some systems will be better than others.

Electric field components are measured quite simply, using a pair of electrodes in contact with the ground. Various considerations enter into the choice of electrodes: if very low frequencies (less than 10 cycles per second) are being used, the old non-polarizing type of electrodes consisting of a metal rod immersed in a saturated solution of one of its salts, all carried in a porous cup, must be used to avoid difficulties with electrode drift after it is placed in the ground. At higher frequencies, the choice of electrodes is less important, and the only thing which must be considered is the development of a resistant surface corrosion layer on many metals. Oxidized lead electrodes and cast iron electrodes are generally recommended; stainless steel electrodes or copper-clad steel electrodes should be avoided.

Electric field is not measured directly. Rather, the voltage drop is measured between electrodes with an appreciable separation, and the electric field is assumed to be about equal to the ratio of voltage drop to electrode separation. However, the electric field is usually determined more precisely, the longer the electrode separation is made. Near-surface rocks nearly always have inhomogeneities in resistivity which distort the current flow locally. With a long electrode separation, these irregularities in current flow tend to average out. Also, with longer separations, the bearing of the electrode pair can be established with more precision and less trouble. Usually, it is wise to use as large an electrode separation as is compatible with the assumption of dipole sources and receivers; that is, receiver dipole lengths of approximately one-fifth the spacing. At very large spacings, in excess of 10 kilometers, this is no longer so important because the precision with which the electric field is measured becomes limited by the ambient noise-field.

The ambient noise field is contributed largely by three sources:

1. Rapid variations of the earth's magnetic field (micropulsations)
2. Induction from power distribution systems, primarily at 60 cps and harmonics.
3. Energy from atmospheric electric discharges.

Noise above 1 cps

Which of the three noise sources is most important depends on the frequency range under consideration. Micropulsations of the earth's magnetic field are important only below frequencies of about 1 cps. Power distribution noise is a problem whenever measurements are made within several miles of a power line or transformer. The worst difficulties are presented by low-voltage high-current distribution systems, and particularly from 1100/220 volt transformers which are common on poles near homes, irrigation wells and so on.

Where noise from AC distribution systems is a problem, the problem may be minimized with filtering. At the higher frequencies, noise from atmospheric electric discharges contributes to the received electric field at all frequencies, and normally constitutes the background against which a signal must be recognized at frequencies above 1 cps.

During local summer seasons, spherics noise from nearby showers may be so intense as to make electrical prospecting infeasible, not only because of high noise levels, but also because of high lightning hazards. Even during non-storm periods, spherics noise is contributed by lightning discharges around the world, which excite a cavity resonance between the earth and the ionosphere at low frequencies, or which propagate as a trapped wave in the earth-ionosphere wave guide at higher frequencies. The lowest resonance frequency, the so-called Schumann resonance, is observed at about 8-1/2 cps, with other resonances at intervals of about 4 cps going upward in frequency. Above about 20 cps, noise contributed by spherics forms a smooth spectrum up to frequencies in excess of 10 kilocycles per second, the highest frequency we are likely to be concerned with in electromagnetic sounding.

Most of the distant spherics noise originates in the tropical areas where electrical storms are common. During the course of a day, the center of storm activity shifts westward with the sun, providing a surprisingly consistent level of spherics activity. The least active period of the day corresponds to midafternoon in the mid-Pacific where the storm activity is least, but the diurnal pattern to noise level is difficult to recognize.

There is a moderate seasonal variation in distant spherics noise level at a given station, as the center of storm activity shifts north and south with the climate. In northern latitudes, the spherics noise level is lower during the winter months than during the summer months. There is also a pronounced

latitude dependence to the amplitude of spherics noise, with noise levels dropping off markedly at auroral latitudes.

Maxwell (1967) has summarized observations of the noise environment above 20 cps for a variety of locations in the northern and southern hemispheres. Data are primarily for the vertical electric field intensity above the surface of the earth. These spectra provide a basis for rough estimates of noise field intensities over the world.

Average spectra for the vertical electric field for summer in Colorado are shown in figure 91 (from Maxwell, 1967). These spectra, as are most spectra, are expressed as power density spectra. A scale for power density in the horizontal magnetic field is included on figure 91, although the field quantity measured was the vertical electric field. In free space, and assuming large distances from the source, orthogonal electric and magnetic fields are related to one another by the freespace impedance:

$$\frac{|E|}{|H|} = 377 \quad (437)$$

The scale to the right of figure 91 was obtained using this relationship.

These noise spectra show some characteristics which are common to noise spectra observed the world over. The noise power density decreases gradually with increasing frequency, except that a minimum power density is observed at frequencies of 1 to 5 keps, and a local maximum power density is observed

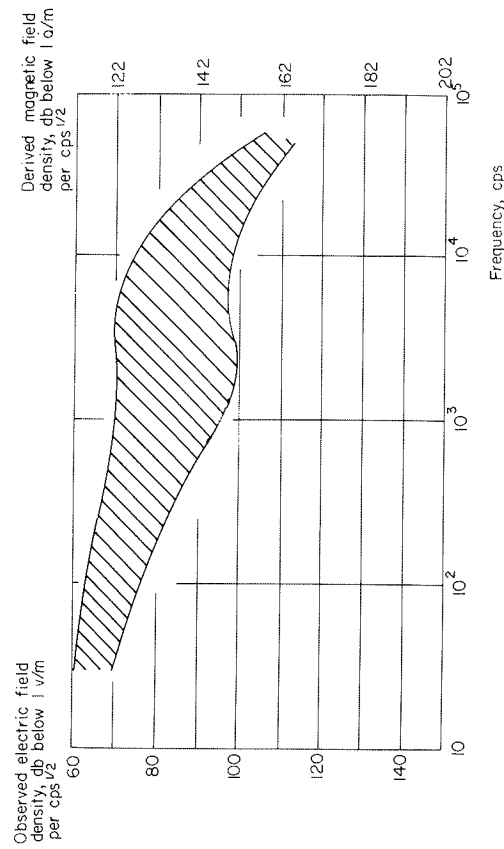


FIGURE 91. Observed spectral density of the vertical electric field during the summer season in Colorado. Horizontal magnetic field density is derived by assuming plane-wave impedance. (From Maxwell, 1967).

in the neighborhood of 5 to 10 keps. As one goes further from the source of the noise, the rate of decrease of power density with frequency increases, and the minimum at 1 to 5 keps gets deeper. This feature is illustrated by noise spectra for the summer season in Alaska, shown in figure 92 (from Maxwell, 1967).

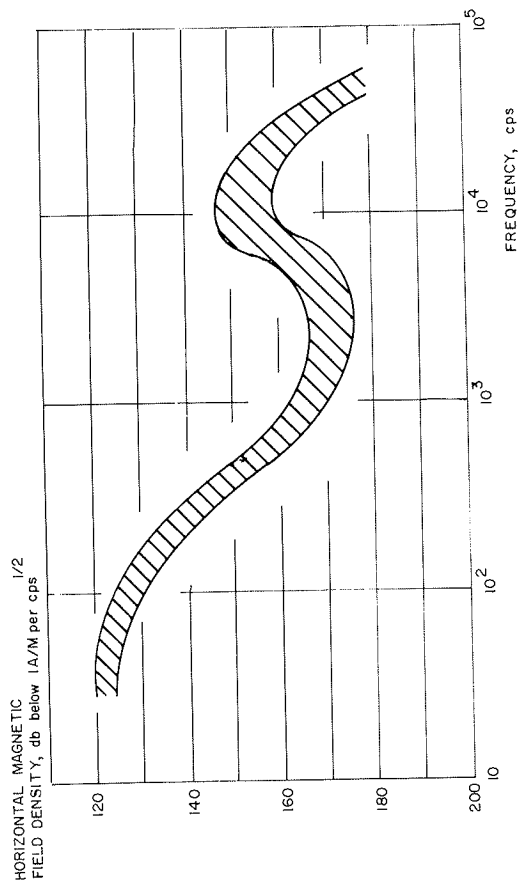


FIGURE 92. — Power density spectrum for the horizontal component of magnetic intensity, summarized for the summer season of 1963, Alaska region (from Maxwell, 1967).

As a crude estimate of noise density suitable for use in estimating the best receiver sensitivity which may be used, we can approximate these spectra between frequencies of 50 to 5,000 cps with a straight line on the logarithmic plot, which has an equation:

$$\frac{\partial H_h^2}{\partial f} = 1.42 \frac{\partial E_z^2}{\partial f} \times 10^5 = k_0 f^{-n} \quad (438)$$

where the parameters k_0 and n will depend on season and latitude.

In methods in which the horizontal component of electric field intensity is measured, the horizontal magnetic noise density can be used to estimate the amount of noise detected with the receiver. We may make use of the relationship between the horizontal component of the magnetic field above the earth and the orthogonal component of electric field in the earth given by Cagniard:

$$|E_x| = (\omega \mu \rho)^{1/2} |H_y| \quad (439)$$

Noise below 1 cps

Frequencies above 1 cps provide relatively shallow penetrations and require relatively small separations between source and receiver, so that obtaining sufficient signal strength to provide recognizable signals in the presence of noise is usually not a serious problem. During the periods of local thunder shower activity, the noise environment may make measurements infeasible because of high-frequency impulsive noise, but generally, the largest problem is with noise at frequencies below 1 cps. For deep soundings in conductive sedimentary basins, the required frequencies may be as low as 10^{-1} cps, and the source-receiver spacing as large as 20 miles.

Noise in the frequency range below 1 cps has been described in a large number of scientific papers published in recent years in journals such as the *Journal of Geophysical Research*. For our purposes, useful descriptions of low-frequency noise have been given by Santirocco and Parker (1963), Davidson (1964), Troitskaya (1964), Heitzler (1964), Lokken (1964), Pritchard (1964), Herron (1967), Hoffman and Horton (1966), Balachandran (1967) and Welch (1968).

At frequencies below 1 cps, the natural noise environment at the earth's surface is dominated by small-amplitude fluctuations in the magnetic field, having amplitudes up to tens of gammas and a wide range of periods, known as *micropulsations*. The micropulsations observed at the earth's surface are the consequence of electromagnetic wave disturbances propagating to the surface of the earth from the outer atmosphere. The frequency content of these waves above 1 cps is strongly attenuated in the ionosphere before reaching the surface of the earth, accounting for the separation in frequency as well as in origin between micropulsations and sub-audio frequency noise (Nawrocki and Papa, 1963; fig. 1). The ultimate source of the electromagnetic waves called micropulsations is the interaction of solar particles with the boundary of the earth's magnetic field.

The low-frequency natural electromagnetic field is varied in character, but it does show characteristic structures which have led to the classification of numerous types of micropulsation activity. Classification may be on the basis of the frequency content or the duration in time of the micropulsation activity.

Micropulsation activity which consists of oscillations in magnetic field intensity lasting only a few cycles is termed *transient micropulsation activity*, sometimes designated by the symbol Pt. Pt pulsations consist of several series of oscillations, each series being a set of heavily damped oscillations persisting for a few minutes, with 1-1/2 to 3 cycles. The period of pulsations lies in the range from 20 seconds to several minutes.

Micro pulsation activity which lasts for long periods with fairly constant frequency of oscillation of the magnetic field is termed *continuous micropulsation activity*, sometimes designated by the symbol Pc. Pc pulsations have a number of characteristic frequencies, and are divided into three types, depending on the characteristic frequency: Pc I, Pc II, and Pc III, having periods in the ranges 10-50, 60-150 and 150-600 seconds, respectively.

Pearl-type pulsations are regular amplitude-modulated sinusoidal oscillations with periods in the range 0.3 to 1 seconds. They occur in the form of separate bursts, gradually developing into a series of pulsations persisting from tens of minutes to tens of hours. Pearl pulsations may have quite large amplitudes in the auroral latitudes, but in the mid-latitudes, they rarely are of sufficient amplitude to be observable.

The amplitude of micropulsation noise is by no means completely random, but shows many consistencies which may be used in predicting noise amplitudes. Many types of micropulsation noise show a diurnal pattern of intensity. The Pc-I and Pc-II types of continuous micropulsation activity are normally most intense during the daytime hours and least intense during the night hours. Pc-III pulsations show the opposite behavior, having the largest amplitudes during the night hours.

The structure of the pulsation noise field also shows an approximately monthly pattern related to the period of rotation of the sun, and the occurrence of magnetic storms. Magnetic storms are periods when increased amounts of solar plasma are emitted by the sun, leading to turbulent and chaotic interactions with the earth's magnetic field. Some types of micropulsation activity are enhanced during magnetic storms (Pt, Pc-I), while other types of micropulsation activity are inhibited (Pc-III). The periods of Pc-I activity are shortened during magnetic storms: during the peak of storm activity, Pc-I periods may be as short as 15 seconds, lengthening gradually to about 50 seconds after the storm is over.

Long-period cycles in magnetic storm activity are also observed, with the 11-year cycle being the best known. During the peaks of these cycles, the essentially monthly occurrence of magnetic storms continues, but the probability of a particular storm being intense increases. Inasmuch as magnetic storms appear to be closely associated with sun spots, it is common to measure solar activity in terms of the number of sunspots which occur. Data on sunspot numbers are available over about the past two and a half centuries, as indicated in figure 93. It is readily apparent that the 11-year cycles of activity show marked long-period variations in intensity, and the current cycle of activity, which should reach a peak during 1969, may be one of the most intense in the past two and a half centuries. A more detailed comparison of the past three cycles of sunspot activity is given in figure 94.

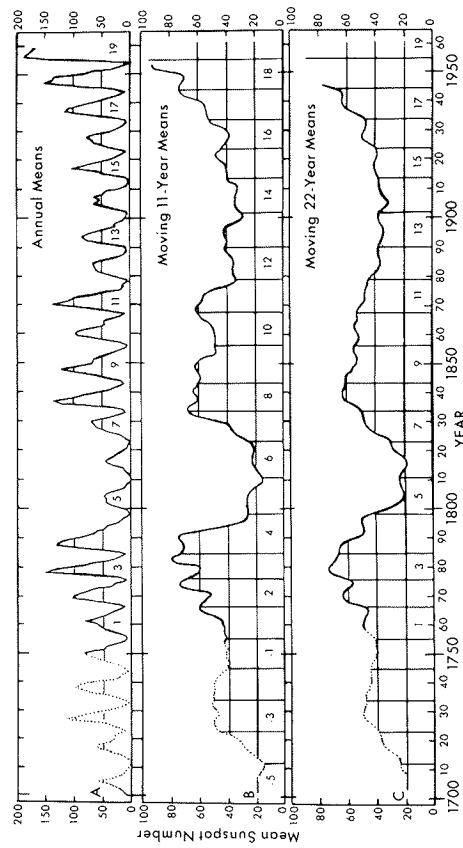
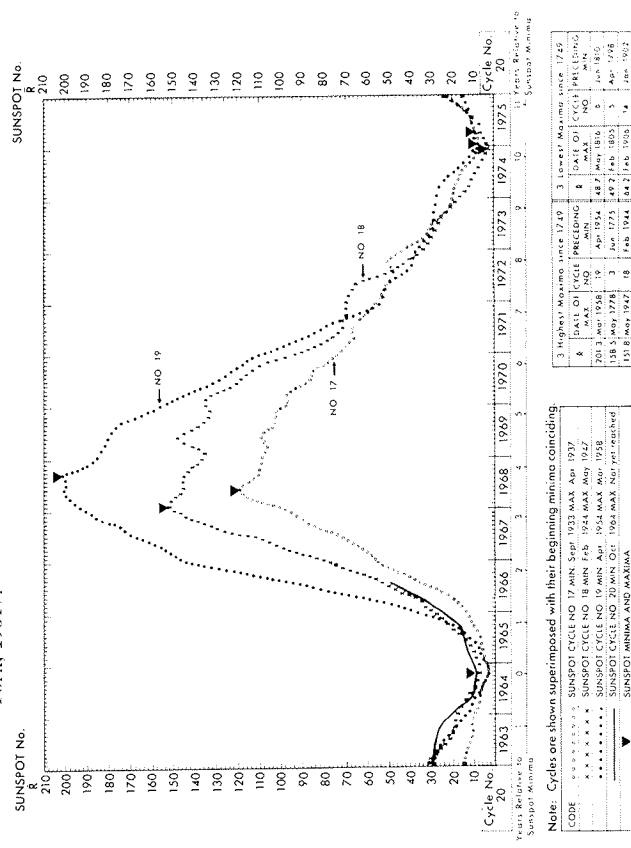


FIGURE 93. --- Various measures of sunspot activity over the period from 1700 to 1968 (from *Handbook of Geophysics*, The MacMillan Company, New York, 1961).



Sunspot Cycles No's. 17, 18, 19 and 20. Zurich Smoothed Relative Sunspot Numbers (R)

FIGURE 94. --- Comparison of activity patterns for sunspots over recent cycles (from "The current trend in solar activity," in IQSY Notes No. 20, April, 1967, p. 2).

Micro-pulsation activity is usually considered to be variation in magnetic field intensity, but such variations also induce current flow in the earth, giving rise to electric-field noise which is essentially identical in character, and so, no separate terminology is needed to describe the electric component of the natural noise field.

Let us now examine the typical character of natural electromagnetic noise below 1 cps by examining records obtained at the Cecil Green Geophysical Observatory, operated by the Colorado School of Mines. The Observatory is located near Bergen Park, Colorado, at $39^{\circ} 42'$ North, $105^{\circ} 22'$ West. The site is on metamorphic rocks with a resistivity of about 1000 ohm-meters, in the Front Range west of Denver. Electric field effects are detected with orthogonal electrode arrays, with electrode separations of approximately 0.3 kilometer. Electrodes are lead plates buried at a depth of six feet to minimize the effect of diurnal temperature ranges on electrode potential.

A record showing electric-field variations over a twenty-four hour period fairly typical of a non-storm period is shown in figure 95. On this record, each scan line represents three hours of time. The large-amplitude rapid fluctuations apparent on every scan line except the ones starting at 2200 and 0100 hours (Mountain Standard Time) are Pc-I oscillations having about a twenty-five second apparent period. Excellent examples of Pt oscillations are apparent about 2100 hours MST.

The record in figure 95 shows the fairly typical increase in the level of Pc-I activity during the daylight hours. The increase in this activity is not uniform from day to day, but highly irregular. This is shown by a typical set of records for a period of 9 days, shown in figure 96 (covering the period from the morning of July 21, 1964, to the morning of August 2, 1964). Each scan line on this illustration represents a duration of approximately 48 hours (note that the length of each trace is from the time on one morning when the magnetic tape on a recorder was changed to the time on the morning two days later when the tape was changed, and not necessarily exactly 48 hours). On this time scale, the Pc-I activity is observable only as a fuzzing of the trace; individual oscillations cannot be discerned on the reproduction of these records. However, the relative amplitudes of the Pc-I noise can be recognized from the amplitude of fuzzing of the trace. It is apparent that in almost all cases, the Pc-I oscillations are much larger during the daylight hours than during the night hours. However, the amplitude is much less for the days of July 26 and 27 than on the days of July 29 and 30. The sudden increase in level is associated with the occurrence of a small magnetic storm which started just after midnight of July 28/29.

On records of electric field recorded with a wide-band recorder (flat frequency response up to a frequency of 1 cps or so), the Pc-I oscillations are

usually the most obvious of the micropulsation types. The inefficiency of induction at lower frequency discriminates against the recognition of Pc-II and Pc-III oscillations, as well as long-period events on records made in this way. The existence of Pc-III oscillations may better be recognized on records where the higher-frequency contributions have been rejected by filtering. Typical 24-hour records of electric field made at Bergen Park using a recording system which had a decrease in response of -1.81 db/octave above .01 cps are shown in figures 97-99. These records have a scan duration of one hour. The three records are typical of periods of low magnetic activity (fig. 97), moderate activity (fig. 98) and high activity (fig. 99). It is of interest to note that the Pc-III oscillations are best developed at night during periods of low magnetic activity.

For design of a recording system to detect signals in the presence of low-frequency noise, it is desirable to summarize information on the noise in the form of power density spectra, as has been done by Pritchard (1964), Welch (1968) and others. Spectra for electric field intensity recorded at three locations (Hawaiian Volcano Observatory, China Lake Naval Ordnance Test Station and Bergen Park) are shown in figure 100 for a magnetically quiet 24-hour period, and figure 101 for a magnetically active period. These spectra show characteristics which are typical of many which have been published:

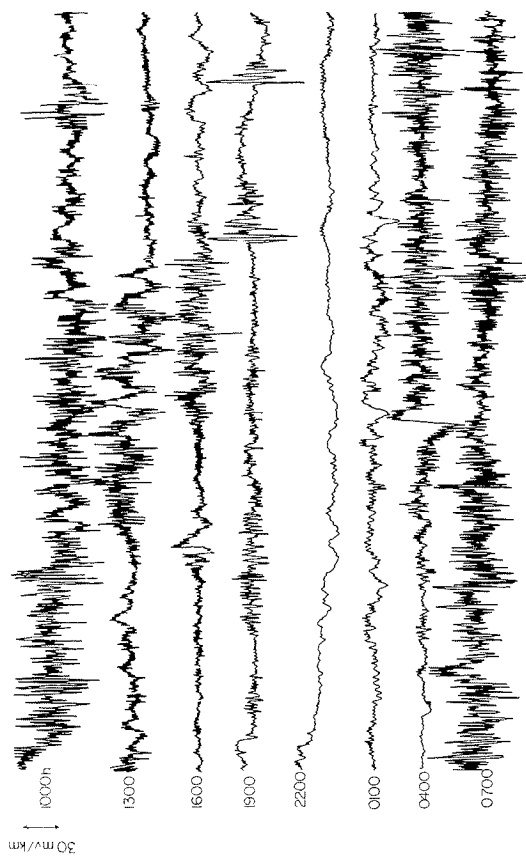


FIGURE 95.—Electric field variations recorded over a 24-hour period at the Green Geophysical Observatory at Bergen Park, Colorado. Each scan line represents three hours of recording.

1. The spectral density increases nearly linearly with increasing period, if the spectral peaks are not considered;
2. The spectrum consists of sharp peaks (almost lines) corresponding to the named varieties of micropulsations (Pc-I, Pc-II, Pc-III) superimposed on the linear background spectrum;
3. The effect of a magnetic storm is to "fill in" the spectral density between the peaks or lines, indicating that the increased activity during magnetic storms is much more random than the activity associated with the normal quiet-period pulsations.

Summaries of spectra reported by Parker (1963), Davidson (1964), Hoffman and Horton (1966) and Herron (1967) are given in figure 102. Each shows the linear increase in power density with increasing period, though levels of noise differ because of the differing earth resistivity at the various recording sites. If we ignore the spectral lines, the noise density may be expressed as a function of frequency as:

$$\frac{\partial P_N}{\partial F} = K_N f^{-b} \tag{440}$$

where $\partial P_N / \partial F$ is the power density, f is the frequency cycle per second, b is a constant with a value of 1.5 to 2, and K_N represents the control of source and local geology on noise power. Values of b and K_N taken from published spectra are listed in table 16.

TABLE 16. — Parameters describing power density spectra

Periods	K_N	b	Source
1—2,000 sec	-82db/ $1\gamma^2$ /cps	2.5	Santirocco and Parker, 1963
10—1,000 sec	-53db/ $1\gamma^2$ /cps	2.6	Davidson, 1964
100—10,000 sec	-35db/ $1\gamma^2$ /cps	2.7	Hoffman and Horton, 1966
10—10,000 sec	-50db/ $1\gamma^2$ /cps	2.4	Herron, 1967

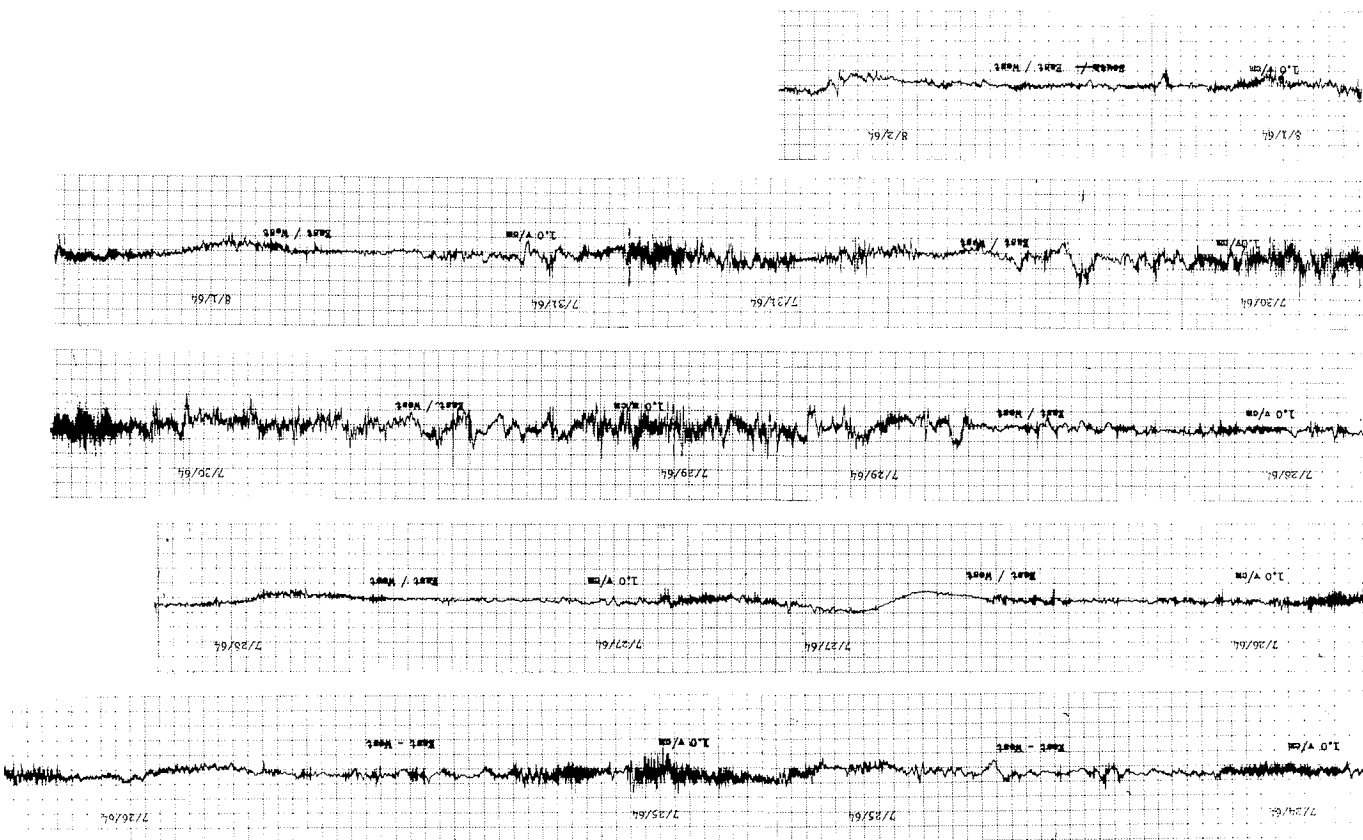
The amplitude of the noise spectrum computed from electric field observations is proportional to the effective resistivity of the earth, measured at the frequency under consideration:

$$K_N = K_N \rho$$

where the new constant k_N is now a function only of the source strength of the noise field, and not of the electrical properties of the earth.

Twenty-four hour averages of power density spectra do not provide insight into the hour-by-hour variation in noise levels which we know is present.

Figure 96. — Recorded electric field intensity at Bergen Park for the interval from July 24 to August 2, 1964. The scale on the record is 50 millivolts per kilometer for a full-scale deflection.



For example, "running" spectra for electric field data averaged over one-hour time intervals are shown in figure 103 for the time interval from 0500 hours to 1700 hours, December 7, 1966. These spectra show the shift between dominant frequencies from hour to hour which may take place.

An effective approach to description of noise density is a presentation as a contour map in which the independent variables are frequency and clock time. Two examples of such noise density maps are shown in figures 104 and 105. The map in figure 104 is representative of a quiet interval during the times from noon on December 24, 1966, to noon on December 25. The consistency of the Pe-III pulsations is apparent from the smooth contours of noise density at frequencies of about .005 cps through the night hours of Christmas Eve, 1966.

The noise density map in figure 105 is representative of a disturbed magnetic interval on December 14, 1966. The record from which this noise density map was taken was characterized by the occurrence of numerous Pt pulsations. As a consequence, the noise density map is less structured than during the quiet period of December 24-25, and shows a more uniform noise density as a function both of time and frequency.

Current requirements for zero-frequency methods

Having specified the frequencies which must be used for direct-current of zero-frequency behavior, and having specified the noise density as a function of frequency, if not of time, we are in a position to estimate the current required in making surveys over sedimentary basins of specified depth. In the exploration of sedimentary basins, the lowermost layer is usually very much more resistant than any of the overlying rocks, and can be considered to be an insulator. When this is the case, the extreme right-hand portion of the resistivity-spacing curve will approach asymptotically a line rising with a slope of 1 on logarithmic coordinates, no matter which of the basic arrays is used. The ratio of spacing to apparent resistivity for any point along this line will be some constant multiplied times S , the longitudinal conductance for

FIGURE 97.—Electric fields recorded at the Green Geophysical Observatory, during a relatively quiet period from 17:02, Jan. 28 to 18:32 GMT, Feb. 3, 1967. The daily sums of the three-hour range indices of magnetic activity, Kp^2 , for these days were:

Jan. 28:	19+
Jan. 29:	9
Jan. 30:	5
Jan. 31:	4
Feb. 1:	9—
Feb. 2:	4
Feb. 3:	4

the rocks above the insulator.

$$\sigma/\rho_a = CS \quad (441)$$

where the value for the constant, C depends only on the type of array used. It has a value of unity for the Schlumberger array, a value of $2 \ln 2$ for the Wenner array and of $1/2$ for the polar dipole array.

If the rocks above the insulating zone are perfectly uniform and isotropic, the left-hand asymptote is a horizontal line with $\rho_a = \rho_1$. The intercept of the two asymptotes defines the least electrode spacing required to first detect the presence of insulating basement rock, and so, is of considerable importance in designing the requirements for electrical resistivity surveys to see through a column of sedimentary rocks.

The problem is not so simple if the conducting layers are anisotropic or have variable resistivities. To a first approximation, a layered medium in which the layers have different resistivities may be treated as an anisotropic medium, provided the basement resistivity is large compared to the layer resistivities. Dakhnov (1960) has given an analysis of the measurement of resistivity in an anisotropic medium which is uniformly anisotropic—that is, the whole medium can be characterized by a single value for the coefficient of anisotropy. This mathematical treatment indicates that in the case of an anisotropic medium resting on an insulator, the interpreted thickness of the conductive beds will be too large by the ratio of anisotropy, and the interpreted resistivity for the anisotropic medium will be:

$$\rho_Q = (\rho_{tr} \cdot \rho)^{1/2} = \lambda \rho \quad (442)$$

where ρ_Q is the geometric average of the transverse and longitudinal resistivities. Therefore, the maximum spacing required to probe through a uniformly anisotropic series of layers and establish the right-hand asymptote for the resistivity sounding curve is:

$$Q_{max} > \lambda CH \quad (443)$$

FIGURE 98. — Electric fields recorded at the Green Geophysical Observatory during a period of moderate activity from 17:12 GMT, Dec. 28, 1966 to 17:24 GMT, Jan. 2, 1967. The daily sums of the three-hour range indices of magnetic activity, Kp^2 , for these days were:

Dec. 28: 22
 Dec. 29: 15—
 Dec. 30: 11—
 Dec. 31: 6—
 Jan. 1: 24—
 Jan. 2: 14—

The anisotropy coefficient for a sedimentary column may range from 1.2 for a sandstone-shale sequence to 1.5 for a section with many limestone layers, and larger if the section contains a high fraction of evaporites. In order to penetrate a column of sediments 6 kilometers thick with an anisotropy coefficient of 1.3, a maximum spacing of nearly 16 kilometers would be required with the Schlumberger array, or of nearly 32 kilometers with the polar dipole array.

Resistivity soundings made to spacings of tens of kilometers require a large amount of effort, but are quite commonly done at the present time. Surveys made with array dimensions as large as 100 kilometers have been reported in crustal-scale soundings by Keller (1966), Anderson and Keller (1966), Jackson (1966), Watt, Mathews and Maxwell (1963), and by Cantwell, Galbraith and Nelson (1964).

The sensitivity requirements for a zero-frequency resistivity survey are best expressed in terms of *mutual resistance* between the current electrodes and the measuring electrodes. The mutual resistance is defined as the ratio of the voltage detected at the measuring electrodes to the current supplied to the current electrodes:

$$R_m = \frac{V}{I} = \frac{\rho_0}{K_g} \quad (444)$$

The mutual resistance is a function of both the resistivity of the material in which the array is located and the array geometry. Curves showing the relationship between array geometry, spacing and mutual resistance are given in figure 106 for two extreme values of apparent resistivity likely to be encountered in petroleum exploration, 1 ohm-meter and 100 ohm-meters. In calculating these curves it was assumed arbitrarily that for the dipole arrays, the dipole lengths are one-tenth the dipole separation. It must be recognized, however, that these spacings are not usually increased each time the array spacing is increased, and that mutual resistance is less when the dipole lengths are shorter in proportion to the spacing. Considering the curves in figure 106, it is apparent that mutual resistances as small as 10^{-8} ohms must be measured if the dipole arrays are to be used, and as large as 10^{-1} ohms, if

FIGURE 99.— Electric fields recorded at the Green Geophysical Observatory during a period of higher than average activity from 16:14 GMT, Dec. 12 to 17:08, Dec. 16, 1966. The daily sums of the three-hour range indices of magnetic activity, K_p^2 , for these days were:
 Dec. 12: 3—
 Dec. 13: 26
 Dec. 14: 35
 Dec. 15: 25—
 Dec. 16: 17

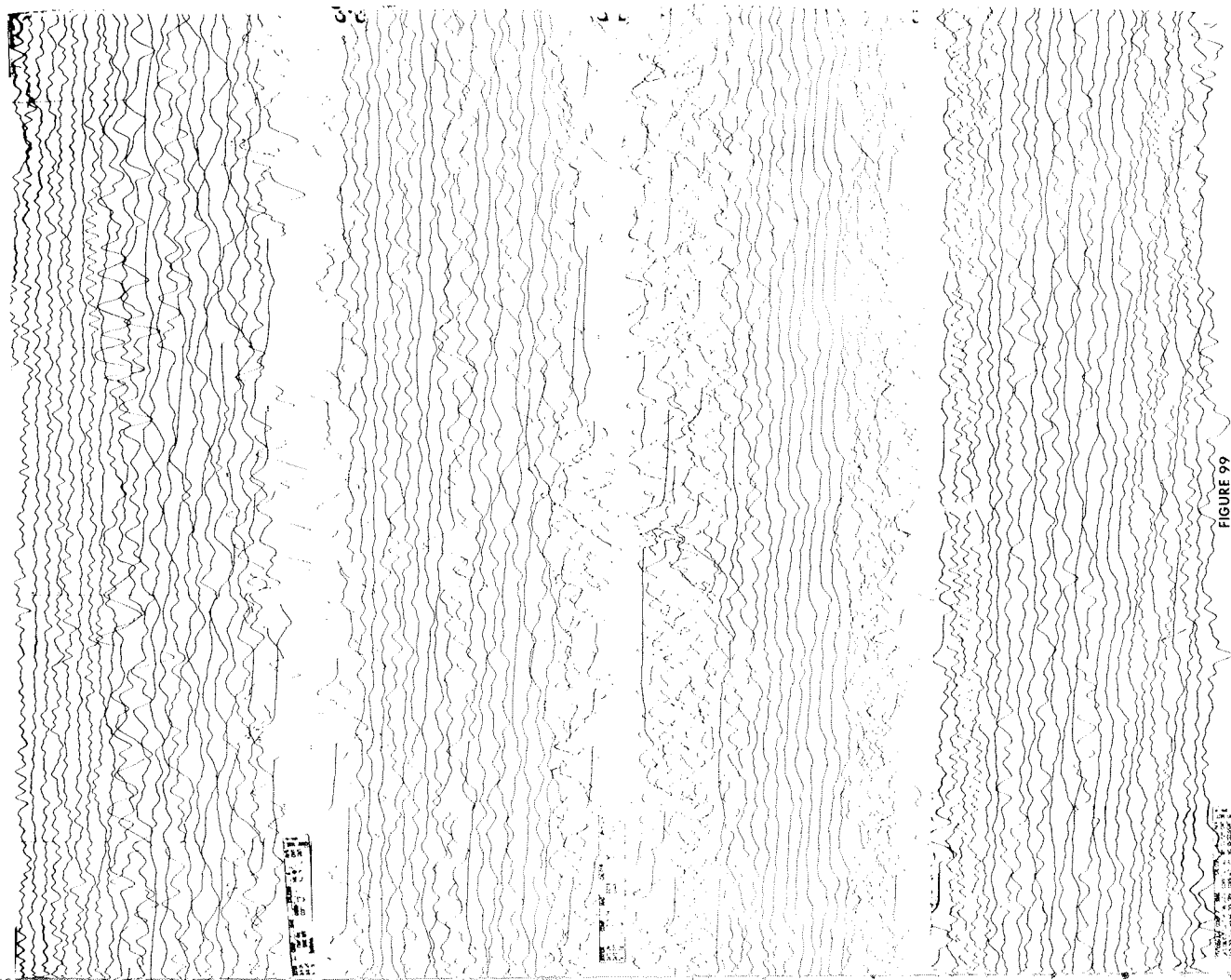


FIGURE 99

Amplitude Density,
mv/km/cps

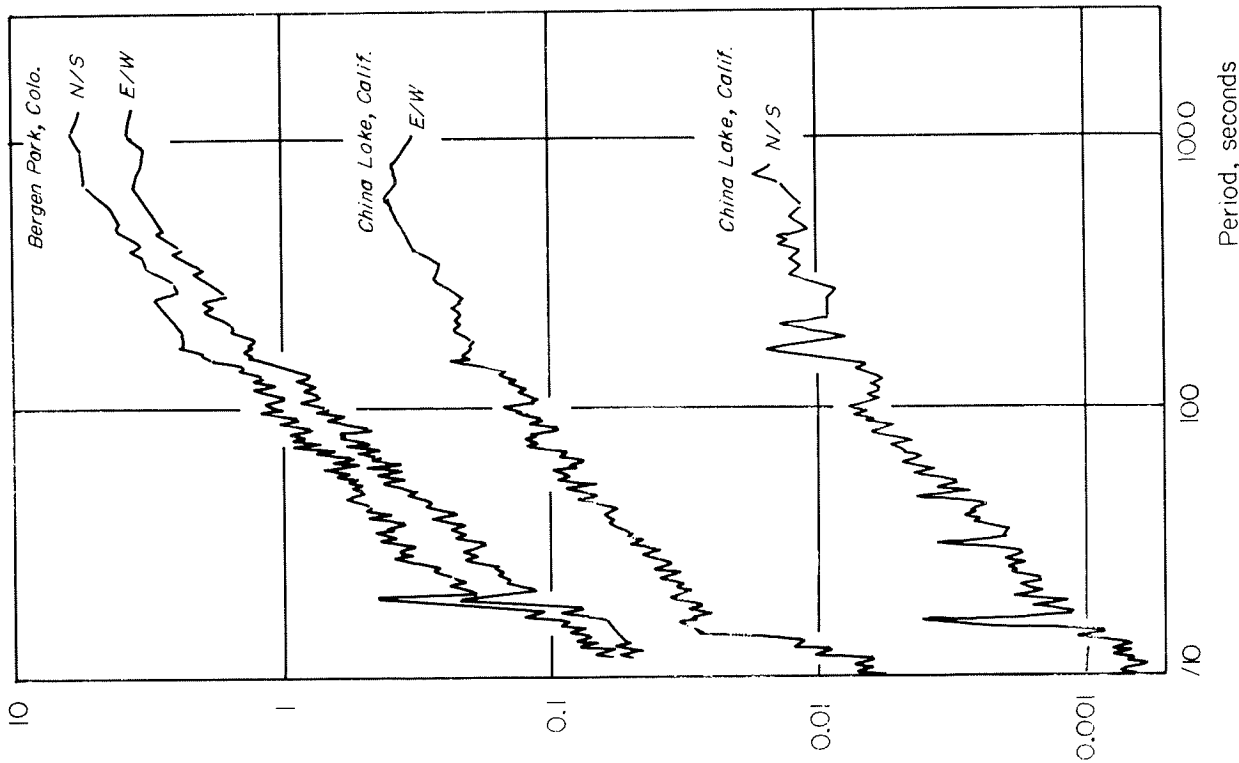
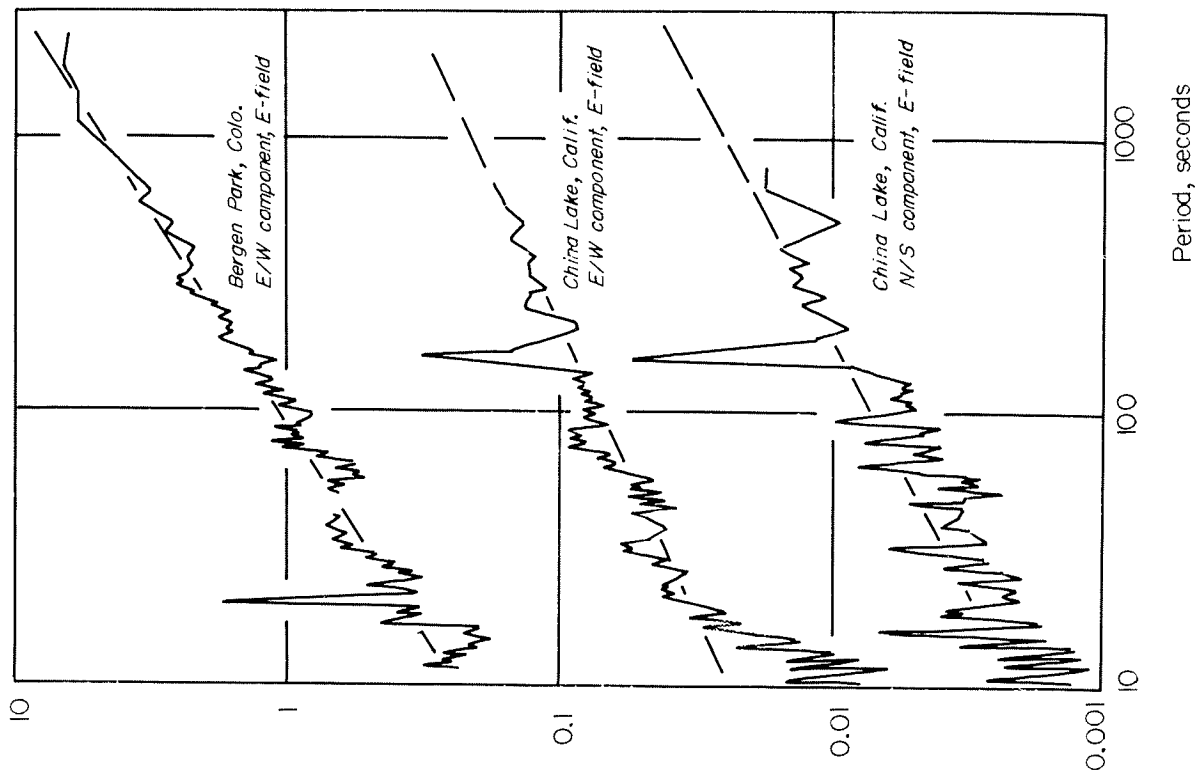


FIGURE 100.—Amplitude spectral density curves for natural electric fields averaged over a common 24-hour period at several recording stations for a relatively quiet period (from Pritchard, 1964).

Amplitude Density,
mv/km/cps



Period, seconds

FIGURE 101.—Amplitude spectral density curves for natural electric fields averaged over a common 24-hour period at several recording locations for a magnetically active period (from Pritchard, 1964).

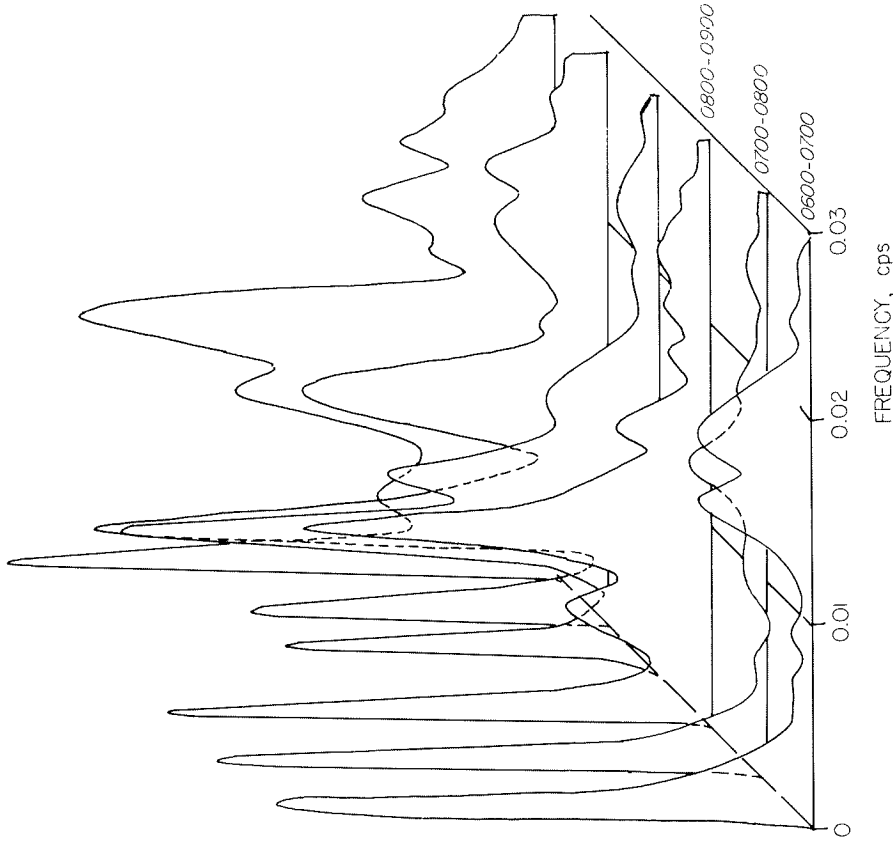


Figure 103.—Running spectral density curves for electric field observed at the Green Geophysical Observatory, Bergen Park, Colorado, for the interval 0600-1300 MST, December 7, 1966. Each spectral density curve represents one hour of recording.

Achieving a sensitivity approaching 10^{-8} volts per ampere requires the use of as large currents as can be obtained, and advanced signal-processing procedures to lower the detectable voltage level to as low a value as possible. The minimum detectable voltage level is determined primarily by natural noise in the frequency range at which measurements must be made, and is itself a function of the frequency. The frequency must be made sufficiently low that the resistivity measured is strictly a static-field value, as indicated by the curves in figure 61.

NORTHWEST MISSOURI
STATE COLLEGE LIBRARY
MARYVILLE, MISSOURI

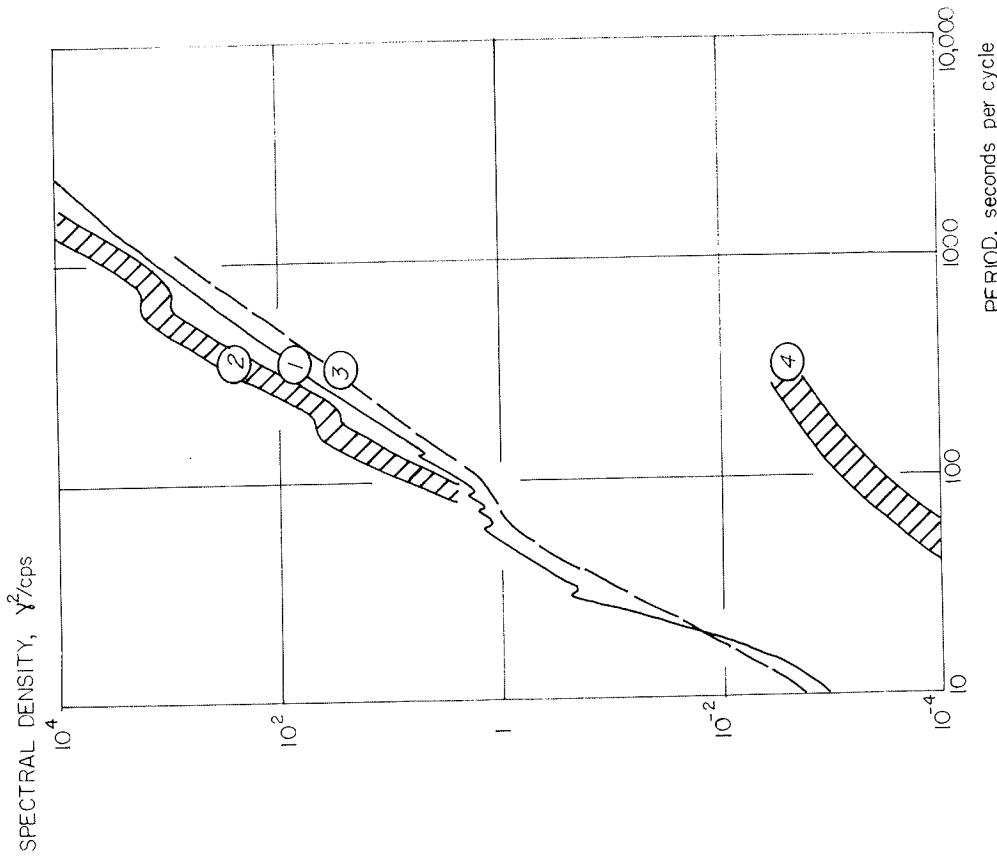
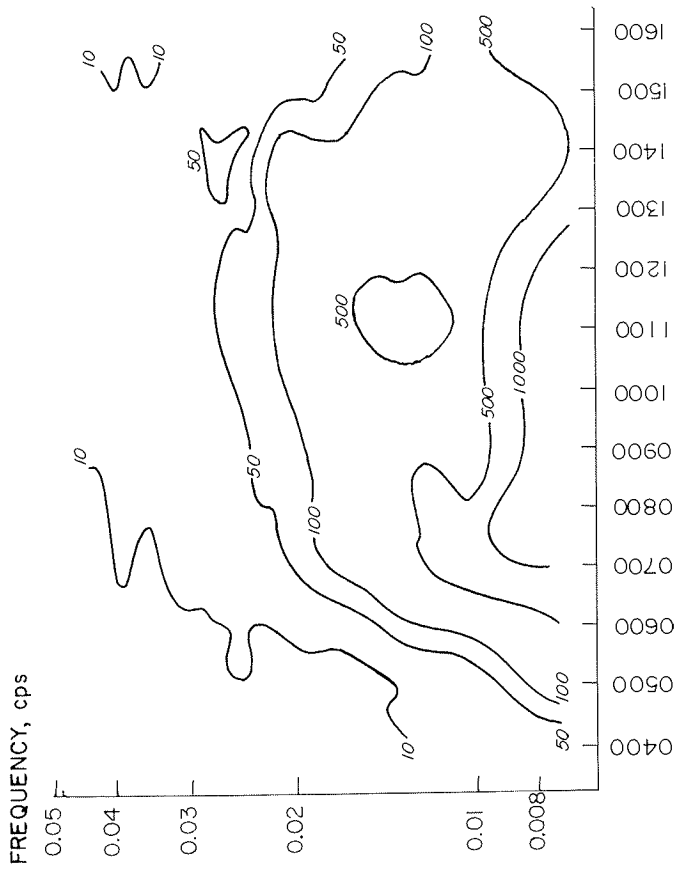


Figure 102.—Typical spectral density curves for magnetic variations from the literature.
Curve 1: Herron, 1967.
Curve 2: Hoffman and Horton, 1966.
Curve 3: Davidson, 1964.
Curve 4: Santirocco and Parker, 1963.

the Schlumberger array is to be used. The upper limit for mutual resistance presents no special problems in instrumentation, but a requirement for measuring 10 millimicrovolts with an absolute precision of a few percent or better for each ampere of current provided to the ground does provide a challenge.

MISSOURI STATE COLLEGE LIBRARY
MARYVILLE, MISSOURI

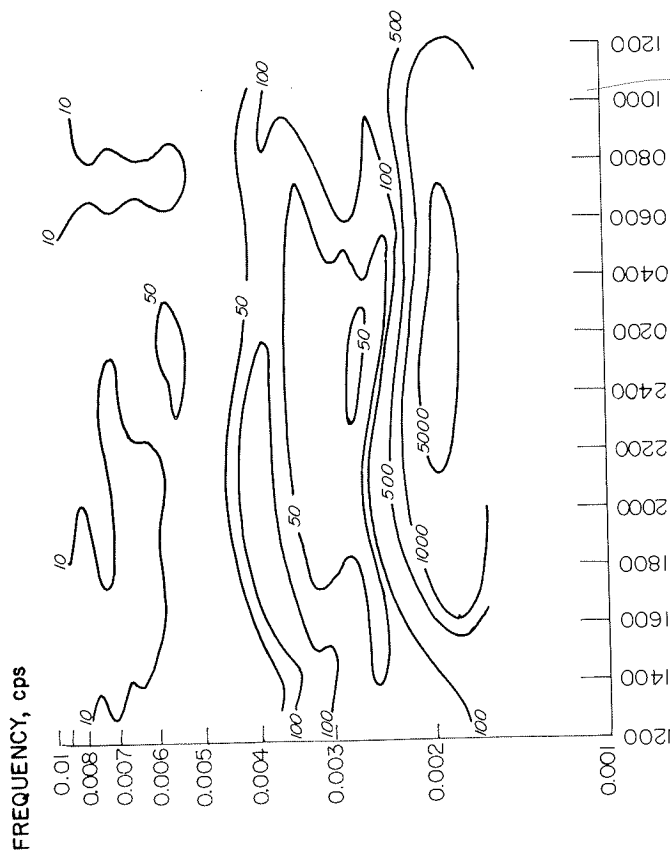


DECEMBER 14, 1966

FIGURE 105. — Contour map of spectral density for electric field intensity recorded at the Green Geophysical Observatory between 0400 and 1600, MST, December 14, 1966. Spectra are computed for one hour intervals (from Welch, 1968).

in figure 108. The curves are straight lines rising with a slope +2 for spacings over which the apparent resistivity is constant, and change to straight lines rising with a slope of +1 at spacings over which the apparent resistivity increases linearly with spacing. As one might expect, longer periods are required at the larger dipole separations and with the lower resistivity models. If an upper practical limit of one hour is placed on the wave period which is to be used, a separation of 10 kilometers may be obtained in a medium with a resistivity of one ohm-meter.

Evaluation of the noise detected at the receiver is most simple if the output of the detector (the electrode pair in this case) is first filtered sharply, as is advantageous when measurements are being made at single frequencies. With a narrow-band filter, which is one with a bandwidth, Δf , considerably less than the mid-frequency, f_c , the energy which persists after filtering is very nearly the product of bandwidth and the noise density at the frequency f_c .



DECEMBER 25, 1966

DECEMBER 24

FIGURE 104. — Contour map of spectral density for electric field intensity recorded at the Green Geophysical Observatory between noon, December 24 and noon, December 25, 1966. Spectra are computed for one hour intervals (from Welch, 1968).

While the estimate of frequency obtained from these curves is strictly valid only for a uniform earth, it is a reasonable approximation. A simple set of working models for sedimentary basins is illustrated in figure 107. Apparent resistivity curves for three models are shown; each model is assumed to represent a sedimentary thickness of 10 kilometers. Three resistivity values are considered; 1 ohm-meter, 10 ohm-meters, and 100 ohm-meters, with corresponding values for the longitudinal conductance being 10^4 mhos, 10^3 mhos, and 10^2 mhos. The basement is assumed to be a perfect insulator, so that the right-hand asymptote for the apparent resistivity curve can be assumed to rise with a slope of +1. An approximation to the highest frequency which may be used can be obtained by using the apparent resistivity from such a model in place of the resistivity for a uniform medium.

The period corresponding to the maximum permissible frequency for these three working models is shown as a function of dipole spacing by the curves

APPARENT RESISTIVITY,
Ohm-meters

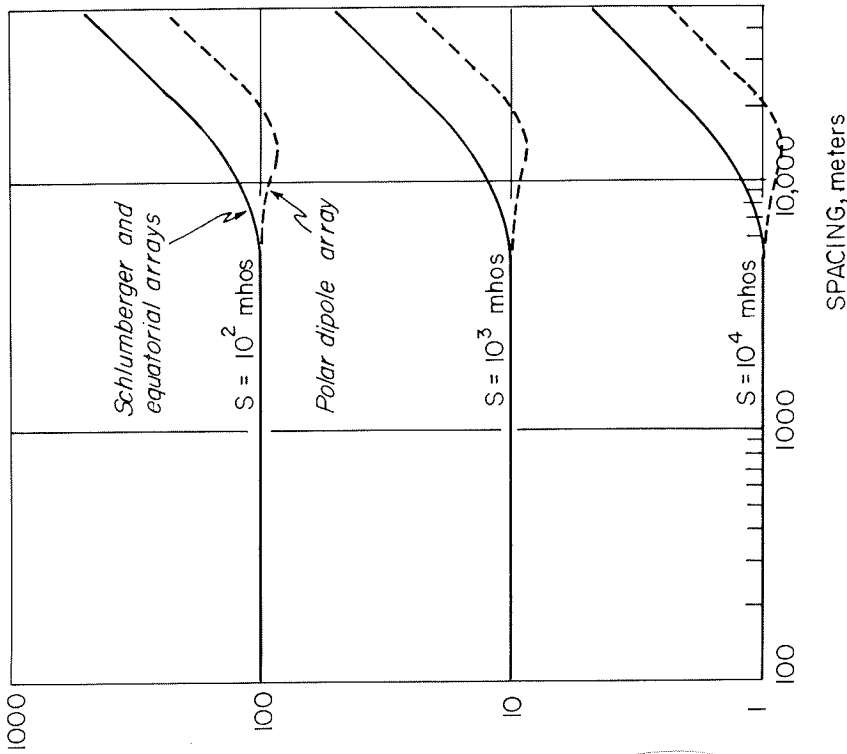


Figure 107. — Idealized apparent resistivity sounding curves which would be obtained over a sedimentary sequence 10 kilometers thick resting on insulating basement, with assumed resistivities of 1, 10 and 100 ohm-meters.

$$E^2 \approx \Delta F \frac{\partial E^2}{\partial F} \quad (445)$$

The signal power for a transmitted sinusoid depends on the number of cycles transmitted. According to Kharkevich (1960), the running spectral density for n cycles of a sinusoidal signal is:

$$\frac{\partial E^2}{\partial F} = \left[\frac{2}{F} \frac{1}{1 - \left(\frac{F}{F_0}\right)^2} \sin^2 \left(\frac{F}{F_0}\right) \cdot \frac{F}{2} \right]^2 \quad (446)$$

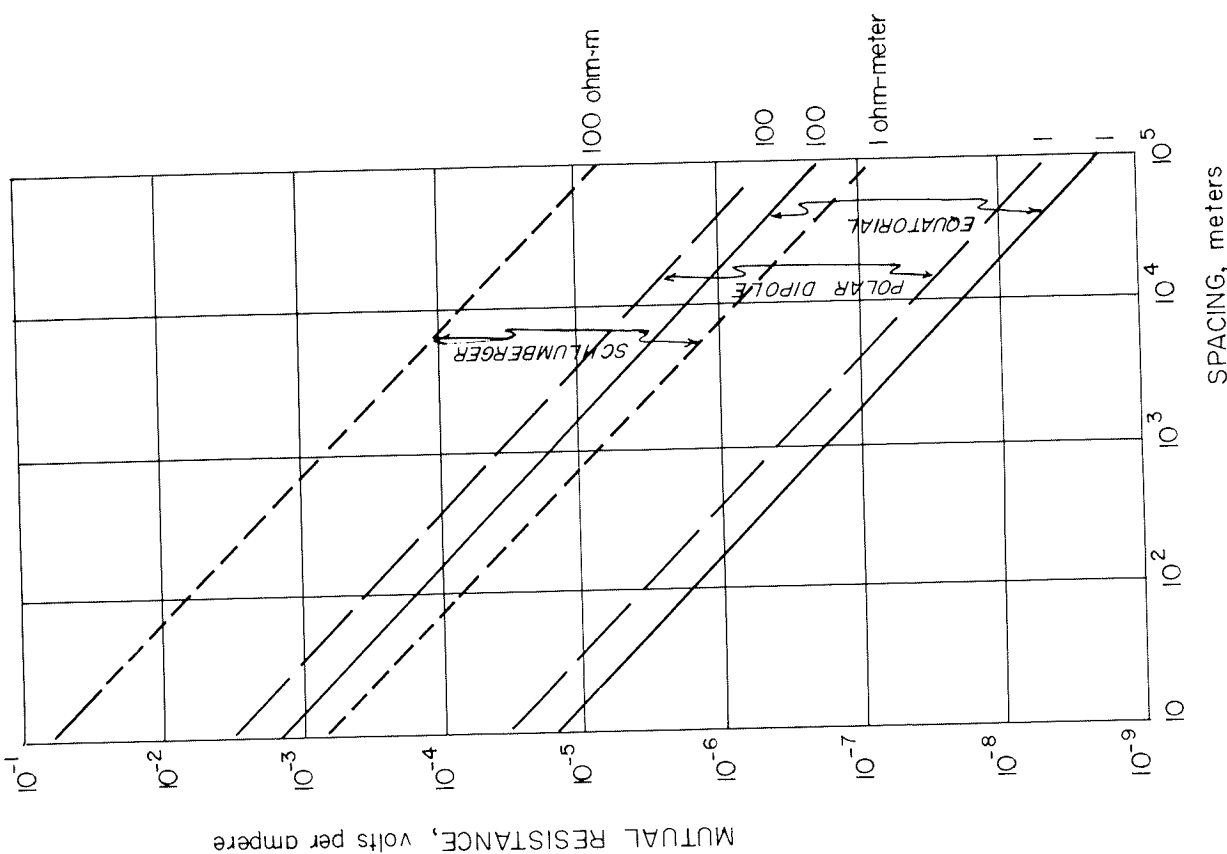


Figure 106. — Mutual resistance values which must be measured in investigating sequences of rocks with resistivities in the range 1 to 100 ohm-meters. Dipole lengths are assumed to be one-tenth the spacing, while the MN separation for the Schlumberger array is assumed to be one-fifth the spacing.

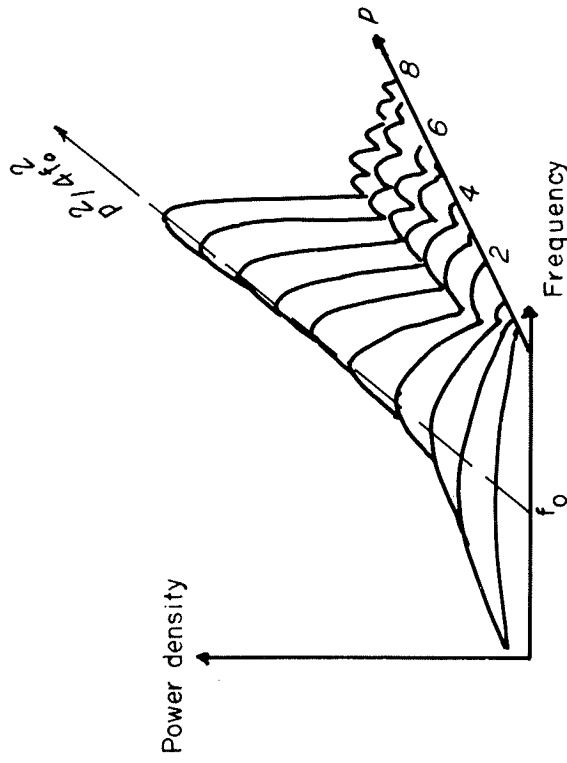


FIGURE 109. — Running spectra for p cycles of a sinusoid (from Kharkevich, 1960).

where p is the number of cycles transmitted, and A is the amplitude of the signal at the receiver computed for the noise-free condition, before filtering. If the bandwidth of the filter is less than the width of the spectral peak associated with the transmitted signal, the noise power transferred through the filter is merely the product of the spectral density given by equation 447 and the filter bandwidth. This condition will hold so long as the number of cycles transmitted is less than the ratio of the center frequency to the bandwidth:

$$P < \frac{f_0}{\Delta F} \quad (448)$$

If a greater number of cycles is transmitted, the width of the spectral peak diminishes as the height increases, and the amount of power transferred through the filter remains nearly constant, for any greater number of cycles.

In view of the low frequencies required in deep electrical prospecting, efficient field operations require that as few cycles as possible be used. Let us assume that the number of cycles of signal transmitted will be the inverse of the bandwidth-frequency ratio:

$$n = \frac{f_0}{\Delta F}$$

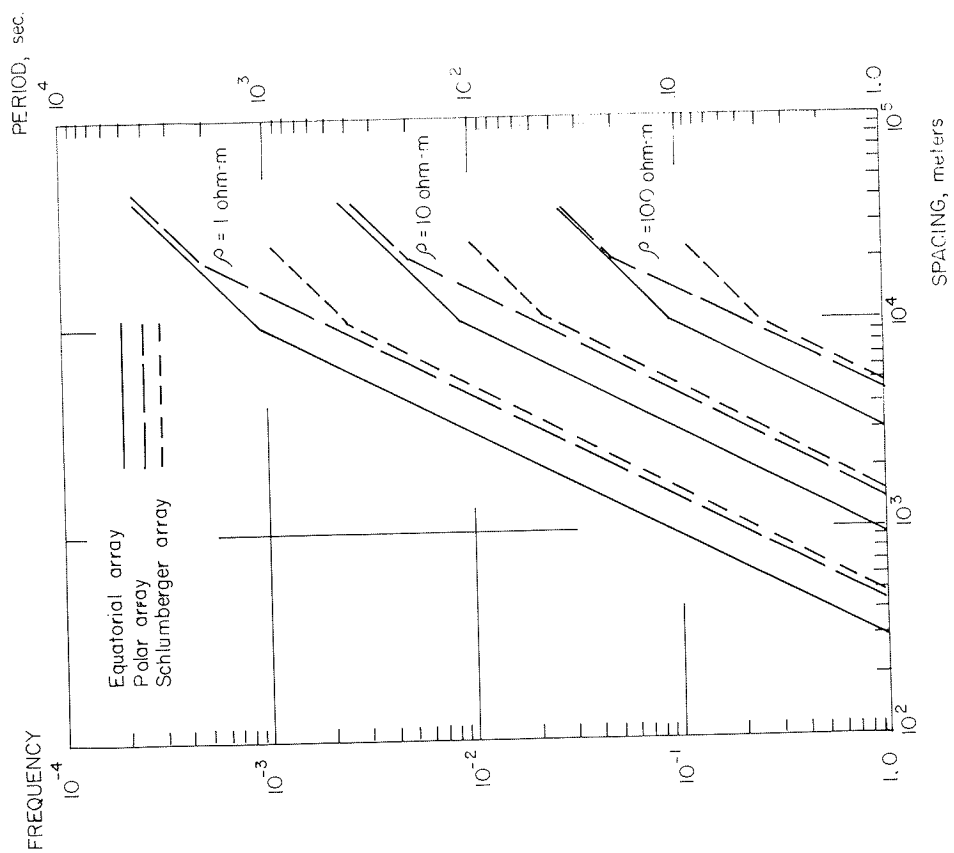


FIGURE 108. — Frequencies which are required for direct-current soundings for the model cases given in figure 107.

A three-dimensional sketch of this spectrum is shown in figure 109. It should be noted that the height of the spectrum at the frequency of the transmitted signal grows with the number of cycles. Ultimately, for an infinite number of cycles, the spectral density becomes infinitely large at the frequency f_0 . At the frequency, f_0 , the amplitude of the spectral density is related to the number of cycles as:

$$\frac{\partial E_s^2}{\partial F} = A^2 p^2 / 4f_0^2 \quad (447)$$

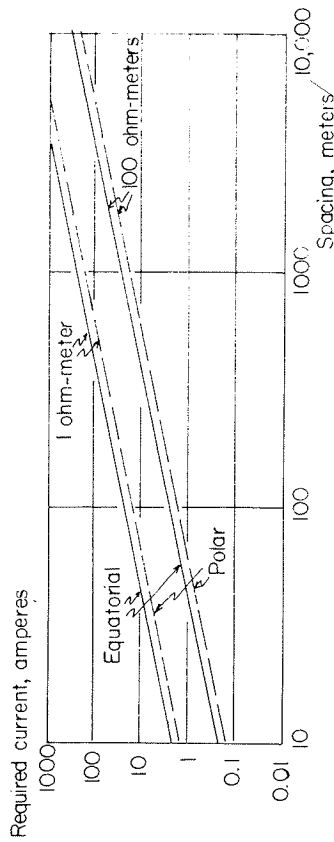


FIGURE 110.—Current required to provide a 20-decibel signal to noise ratio through a filter with a relative bandwidth of 0.1, when the direct-current method is considered.

Currents in excess of 1,000 amperes may be required for spacings of tens of kilometers. Current requirements can be reduced in several ways: the length of the source dipole may be increased with a proportionate decrease in the required current, or the bandwidth-frequency ratio may be reduced, with a reduction in required current in proportion to the square root of the reduction in fractional bandwidth. These factors, combined with operation during quiet periods at large spacings can reduce the required current to several hundreds of amperes, which is well within reason. Jackson (1966) reports the use of currents up to 300 amperes in crustal resistivity surveys, where all the power was provided by batteries.

Current requirements in AC methods

With AC methods, the signal power incident to a filter at the receiver is a function of the source strength, the distance from the source to the receiver, and in some cases, the frequency and the resistivity of the earth. The source strength is a specified parameter, which can be changed almost at will to obtain additional sensitivity, and so, is not of primary concern in considering design criteria in terms of earth properties.

For simplicity in comparison of various source-receiver combinations, let us consider only a uniform earth. We have no real requirement on the separation between source and receiver, except that imposed by the need to have a spacing comparable to a wave length in the earth:

$$\alpha = \frac{2\pi}{\lambda} \tag{454}$$

Let us use this as the spacing for which the power requirements for various receiver-source combinations are to be compared.

The amplitude of the peak in the signal spectrum for a terminated sinusoid with an amplitude E_s , volts per meter for n cycles after filtering is:

$$P_s = \frac{E_s^2}{4F_0} \tag{449}$$

The signal-to-noise ratio is:

$$\frac{P_s}{P_n} = \frac{E_s^2}{4kF_0\rho} \cdot \frac{f_0}{\Delta f} \tag{450}$$

The signal level, E_s , can be evaluated from the appropriate expression for apparent resistivity for the electrode array being used. For the equatorial and polar dipole arrays, assuming the source dipole length is one-tenth the spacing between dipole centers, the signal level is:

$$E_s = \frac{\rho I}{10c\pi a^2} \tag{451}$$

where a is the spacing between dipole centers, and c is a parameter depending on the array used, being 1 for the polar arrangement and 2 for the equatorial arrangement.

The highest frequency which may be used is also the most efficient one. At the maximum required spacing, the frequency required to penetrate a section with uniform resistivity, ρ , is

$$f_0 = \frac{\rho}{2\pi\mu_0 H^2 Q} = \frac{\rho Q}{2\pi\mu_0 \left(\frac{c\rho a^2}{\lambda c}\right)^2} \tag{452}$$

where f_0 is the operating frequency at maximum spacing, μ_0 is $4\pi \times 10^{-7}$ H/M and Q is a quality factor, determined by the precision with which the direct-current behavior must be approximated. For an approach within 5 percent of the static behavior, Q should be approximately 1. Combining equations 451 and 452 with equation 450, we have:

$$I^2 = \frac{200c^2 k \pi Q^2}{\mu_0} \left(\frac{\alpha^2}{\rho}\right) \left(\frac{\Delta f}{f_0}\right) \left(\frac{P_s}{P_n}\right) \tag{453}$$

The quantities which are contained in the first term to the right of the equality sign are of the order of 0.001 for the equatorial array and 0.002 for the polar array, based on noise power density surveys at the Bergen Park Observatory of the Colorado School of Mines.

Assuming a desired signal/noise ratio of 100 (20 decibels) and a bandwidth-frequency ratio of 0.1, the currents required for a given spacing, a , for resistivities of 1 and 100 ohm-meters are shown graphically in figure 110.

fact that as the conductivity varies, the spacing varies and the amplitude of the signal varies as the inverse fifth power of the spacing. A slight decrease in conductivity, which causes a slight increase in the required spacing, will require a large increase in the required current. This is offset in part by the fact that the requirements on frequency, f_0 , are inverse to the requirements on spacing.

Let us next consider the tangential electric field from a vertical-axis magnetic dipole source so that we may compare the effectiveness of the two types of receiver for a common source. The signal strength is:

$$E_{\phi} = \frac{3M}{2\pi a^3 \sigma} \tag{462}$$

Using condition 454 to find the electric field component at the least spacing for which equation 462 is valid, we have:

$$E_{\phi, \alpha_{\min}} = \frac{3M f_0^2 \mu_0 \sigma}{8\pi^3} \tag{463}$$

The electric field is usually detected by measuring the voltage drop between a pair of electrodes whose separation is a small fraction of the spacing, the fraction being C:

$$V(E_{\phi, \alpha_{\min}}) = C \alpha_{\min} E_{\phi, \alpha_{\min}} = \frac{3CM f_0^2 \mu_0 \sigma}{(2\pi)^{5/2}} \tag{464}$$

The signal power density which passes the filter is:

$$P_s = \frac{QC^2 M^2 f_0 \mu_0 \sigma}{128 \pi^5} \left(\frac{f_0}{\Delta f} \right) \tag{465}$$

The voltage detected with a pair of electrodes is proportional to the spacing between the electrodes, and to the square root of the resistivity of the earth. Therefore, the noise power which penetrates a narrow-band filter will be:

$$P_N = \frac{\Delta f}{f_0} \frac{\partial}{\partial f} \left\{ V^2 \right\} = \frac{2\pi C^2 K_E}{f_0 \mu_0 \sigma^2} \left(\frac{\Delta f}{f_0} \right) \tag{466}$$

The ratio of signal power to noise power is:

$$\frac{P_s}{P_N} = \frac{9M^2 \sigma^3 f_0^2 \mu_0}{256 \pi^6 K_E} \left(\frac{f_0}{\Delta f} \right)^2 \tag{467}$$

Considering that the source moment is still IA_s , the required current is:

Vertical magnetic dipole source: Consider first the signal strength from a vertical-axis magnetic dipole source. The vertical magnetic field component at a receiver will be:

$$H_z = \frac{9i\omega\sigma\mu_0 M}{2\pi a^5} \tag{455}$$

Using condition 454 to find the magnetic field component at the least spacing for which equation 455 is valid, we have:

$$H_{z, \alpha_{\min}} = \frac{-9i(\omega\mu_0)^{7/2} M}{64\pi^6} \tag{456}$$

If the magnetic field at the receiver is detected with an induction coil, the voltage output of the induction coil will be:

$$V(H_{z, \alpha_{\min}}) = \frac{-9iA_r\omega\mu_0(\omega\mu_0)^{7/2} M}{64\pi^6} \tag{457}$$

where A_r is the effective area of the receiver, the product of area and the number of turns.

If we take as a standard that the number of cycles of signal transmitted is the inverse of the bandwidth-center frequency ratio of the filter, then using equation 447 to determine the signal power density transferred through the filter, we have:

$$P_s = \frac{\Delta f}{f_0} \frac{\partial}{\partial f} \left\{ V^2(H_{z, \alpha_{\min}}) \right\} = \left(\frac{f_0}{\Delta f} \right)^2 \frac{81A_r^2 f_0^7 \mu_0^7 \sigma^7 M^2}{32\pi^3} \tag{458}$$

The noise density which penetrates the filter will be:

$$P_N = \frac{\Delta f}{f_0} \frac{\partial}{\partial f} \left\{ V_N^2 \right\} = 4\pi^2 f_0^2 A_r^2 K_{Bz} \left(\frac{\Delta f}{f_0} \right) \tag{459}$$

where K_{Bz} is the spectral density of the vertical magnetic induction noise at the frequency under consideration.

The ratio of signal power to noise power at the output of the filter is:

$$\frac{P_s}{P_N} = \frac{81 f_0^2 \mu_0^7 \sigma^7 M^2}{128 \pi^2 K_{Bz}} \left(\frac{f_0}{\Delta f} \right)^2 \tag{460}$$

Or, conversely, the current required to operate at the lower limit of the asymptotic frequency range is:

$$I^2 = \frac{128 \pi^5 K_{Bz}}{81 A_s^2 f_0^5 \mu_0^7 \sigma^7} \left(\frac{\Delta f}{f_0} \right)^2 \left(\frac{P_s}{P_N} \right) \tag{461}$$

where A_s is the effective area of the source coil. The current required depends very greatly on the conductivity, reflecting the

$$I^2 = \frac{256 \pi^6 K_E}{9 A_5^2 \sigma^3 f_0^2 \mu_0} \left(\frac{\Delta f}{f_0} \right)^2 \frac{P_S}{P_N} \quad (468)$$

We are now in a position to compare the relative merits of induction and E-field receivers for a magnetic dipole source. The ratio of the current required for an induction coil receiver to the current required with an electric field detector is the ratio of the expressions in 461 and 468 with the square root taken:

$$\frac{I_{\text{vertical axis induction coil}}}{I_{\text{electric field detector}}} = \frac{1}{3 f_0 \sigma^2 (2 \pi \mu_0^3)^{1/2}} \left(\frac{K_{Bz}}{K_E} \right)^{1/2} \quad (469)$$

As an example, consider a case in which the earth has a conductivity of 0.1 mhos per meter, as in eastern Colorado. Referring to figure 61, for the minimum conditions for far-field behavior, the frequency f_0 would be 100 cps for a 1220 meter spacing. The ratio of currents in this example would be:

$$10^7 \left(\frac{K_{Bz}}{K_E} \right)^{1/2}$$

The ratio of currents required depends on the statistics of the noise for vertical induction receivers and E-field receivers. Little information is available on such statistics, but at Bergen Park, Colorado, the ratio K_{Bz}/K_E is probably of the order of 10^{-4} . In this case, the E-field detector is much more efficient than the induction coil receiver. However, the noise ratio could be much lower in other areas. As conductivity increases or as the transition frequency increases, the advantage of the E-field detector decreases in comparison with the induction coil receiver. The induction receiver will be preferable at short spacings over a highly conductive earth, with the transition being a spacing of a few hundred meters over an earth with a conductivity of 1 mho per meter.

We might also consider the relative merits of a coil source and an electric dipole source. Consider the electric field seen with an equatorial dipole array (an electric dipole source with a parallel electric dipole receiver displaced along the equatorial axis of the source).

The signal strength at a distance a from a current-dipole source with a moment $I ds$ is:

$$E_{\phi} = \frac{I ds}{\pi \sigma a^3} \quad (470)$$

Using condition 454 to find the electric field component at the least spacing for which equation 470 is valid, we have:

$$E_{\phi} = \frac{I ds f_0^{3/2} \mu_0 \sigma^{1/2}}{\pi (2 \pi)^{3/2}} \quad (471)$$

If the length of the receiver electrode spread is $C_{a,max}$, the voltage sensed at the receiver is:

$$V_S = \frac{C f_0 \mu_0 I ds}{2 \pi^2} \quad (472)$$

The signal power which passes through the filter, from equation 447, is:

$$P_S = \frac{C^2 \mu_0^2 (I ds)^2}{16 \pi^4} \left(\frac{f_0}{\Delta f} \right) \quad (473)$$

The noise power is the same as that given by equation 466 for an E-field receiver from a magnetic source. The ratio of signal power to noise power is:

$$\frac{P_S}{P_N} = \frac{f_0 \mu_0^3 \sigma^2 (I ds)^2}{32 \pi^5 K_E} \left(\frac{f_0}{\Delta f} \right)^2 \quad (474)$$

and the current required is:

$$I^2 = \frac{32 \pi^5 K_E}{f_0 \mu_0^3 \sigma^2 (ds)^2} \left(\frac{\Delta f}{f_0} \right)^2 \frac{P_S}{P_N} \quad (475)$$

Now, let us compare a magnetic source and an electric source, using an electric receiver with both. The ratio of current required with a magnetic source to that required with an electric source is:

$$\frac{I_{\text{vertical axis magnetic source}}}{I_{\text{electric dipole source}}} = \left(\frac{8 \pi}{9 \sigma f \mu_0} \right)^{1/2} \frac{ds}{A_s} \quad (476)$$

However, consider that the maximum dimension of a coil source is the same as the length of an electric dipole source, limited by the size $C_{a,min}$. Then:

$$\frac{ds}{A_s} = \frac{ds}{n ds^2} = \frac{1}{n C_{a,min}} = \frac{(2 \pi f_0 \mu_0 \sigma)^{1/2}}{2 \pi n C} \quad (477)$$

and equation 476 becomes:

$$\frac{I}{I} = \frac{2}{3 n C} \quad (478)$$

where n is the number of turns in the source coil. It is interesting to note that the electrical properties of the earth do not enter, and that a multi-turn coil is always preferable to an electric dipole source. This result is deceptive, however, because the amount of current which can be driven into the ground depends to a very great degree on the resistivity of that ground, particularly near the surface where the electrode contacts must be made. Although it will not be shown here, it is reasonable to expect that the coil source will be preferable to the current dipole source in regions where the surficial resistance is high.

Correlation filter techniques appear to provide a means for measuring resistivity with relatively low power requirements, but at the expense of measurement time. Pulse filter techniques also appear to provide a means for obtaining measurements, but probably with higher-power sources being required than for correlation filter methods. The choice between the two approaches must be based on economic considerations for a given problem: which is more expensive, time or source power?

GEOLOGIC NOISE AND PRECISION OF MEASUREMENTS

Other factors to be considered in designing a galvanic resistivity surveying program are those involved in the precision of measurement. Usually we may assume that instrumental errors will be insignificant, in terms of accuracies of a few percent. However, even with the observed quantities being measured quite precisely, commonly a plot of resistivity values will show considerable scatter, as in the example in figure 111. The example is one of a crustal-scale resistivity soundings, but it illustrates the problem of *geologic noise* quite well. Geologic noise is the variation in apparent resistivity caused by small-dimensioned variations in resistivity in the surface layer and near the various electrode locations. Large dimensioned lateral variations lead to distinctive sounding-curve character and may be interpreted using theoretical curves which have been given in the literature (see Kalenov, 1957; Keller and Frischknecht, 1966; Al'pin, 1966; Van Nostrand and Cook, 1966). We shall not be concerned with these in a discussion of electrical soundings in sedimentary basins, where usually, lateral uniformity can be assumed. However, if major lateral changes are to be located, interpretation methods are available.

Small-dimensioned resistivity variations in the surface layer can be quite arbitrary in shape, and thus, a detailed, quantitative discussion of the effect they have on observed resistivity is tedious. However, for our purposes we need only a semi-quantitative discussion, and for this, a consideration of the effect that hemispherical pods may have on measured resistivity is useful. If the pods are small compared with the spacing in a dipole array, the behavior of the current from the source dipole in the vicinity of the pod will be approximately that of a planar current sheet. Many curves have been computed for the distortion of planar current sheets by various resistivity structures (see Kurnetz and Chastenet de Gery, 1956; Berdichevskiy, 1965), including the hemispherical pod embedded in a surface layer resting on a subsurface layer resting with different resistivity. Typical electric field curves over resistant pods and conductive pods are shown in figure 112. The important feature of these curves is that the electric field inside a resistive pod is never more than about twice the electric field which would be observed if the pod were not there, while the electric field inside a conductive pod is decreased by

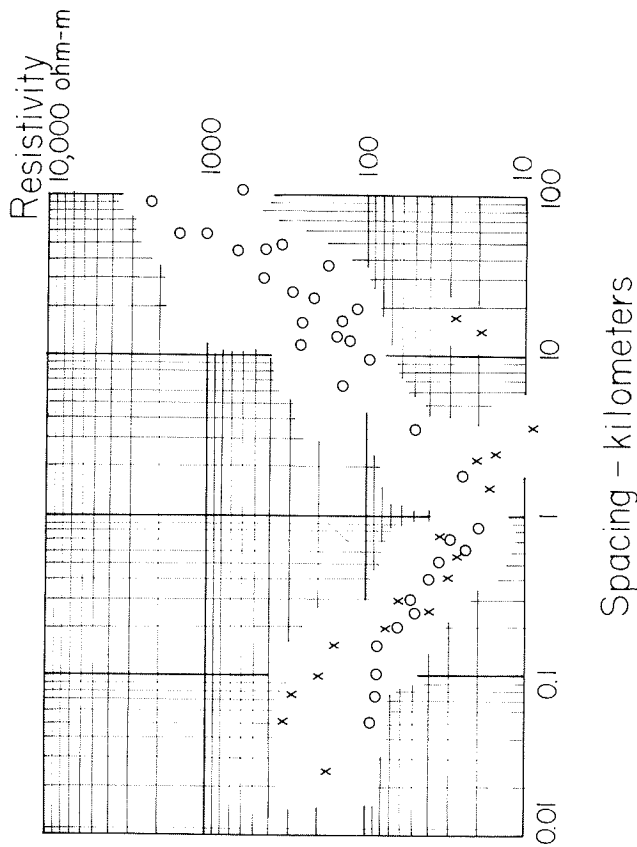


FIGURE 111.—Example of typical scatter of DC resistivity determinations caused by lateral inhomogeneities in resistivity. The surveys were made using two source dipole locations, with electric field measurements about each being differentiated by the symbol used in plotting the apparent resistivity value. The surveys were made on the Columbia River Plateau in the state of Washington.

the ratio of the resistivity contrast between the pod and the surrounding medium. The effect is diminished by about 10 percent if the resistivity decreases with depth, and is enhanced by about 10 percent if the resistivity increases with depth below the surface layer.

These results pertain only to hemispherical pods, and the results may be expected to be much more complicated for less symmetrical pods. However, it is a meaningful generality to say that conductive inclusions in a surface layer will lead to greater amplitude geologic noise than will resistive inclusions. If we were to assume a uniform distribution density of pods with resistivity both greater than and less than the gross resistivity of a surface layer, the errors in observed electric field intensities caused by these pods would be skewed towards the low side as indicated in figure 113a. The probability density for errors on the low side will be the same as the probability density for the occurrence of pods with low resistivity, while the density of errors on the high side will show a peak for error ratios of about 2. Since we have assumed an

OBSERVED ELECTRIC FIELD
FIELD WITH NO POD

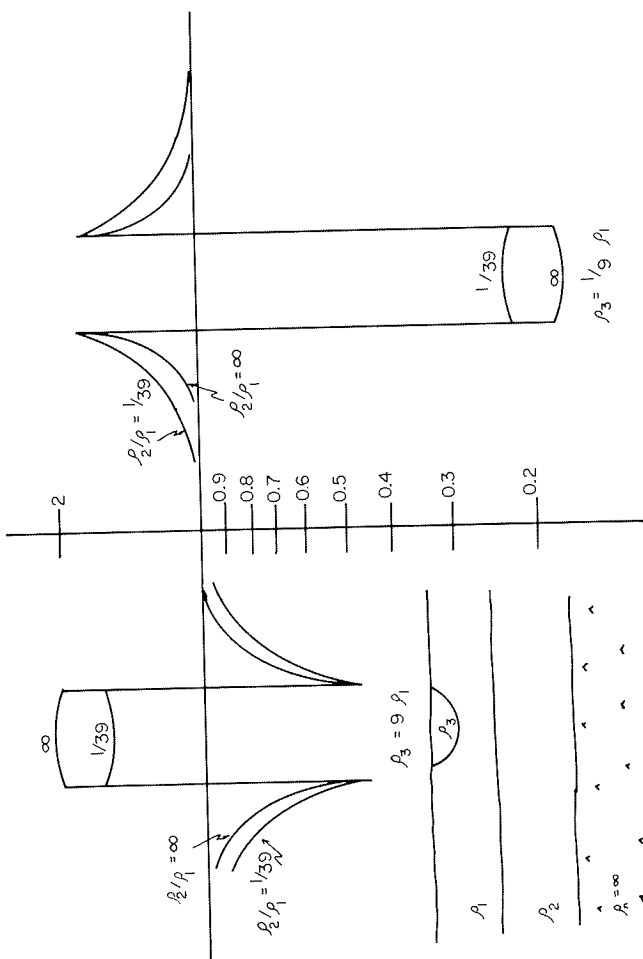
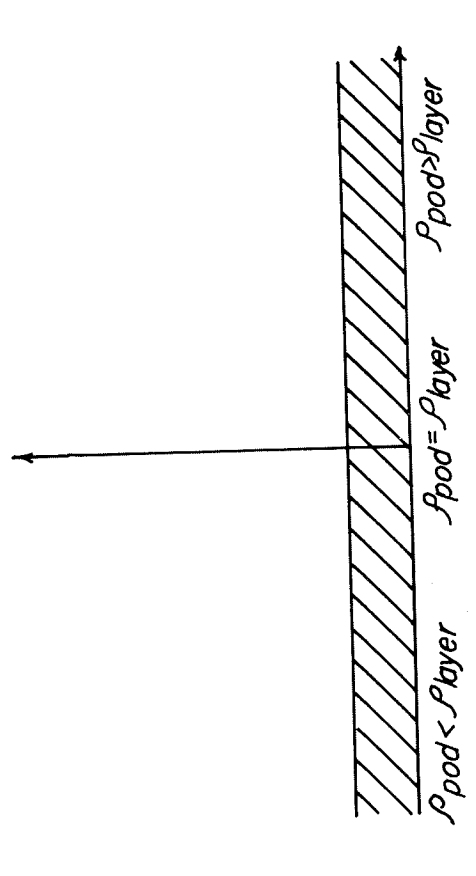


FIGURE 112.—Anomalies in electric field caused by a hemispherical pod at the surface of a layered earth, for the case of a planar current sheet.

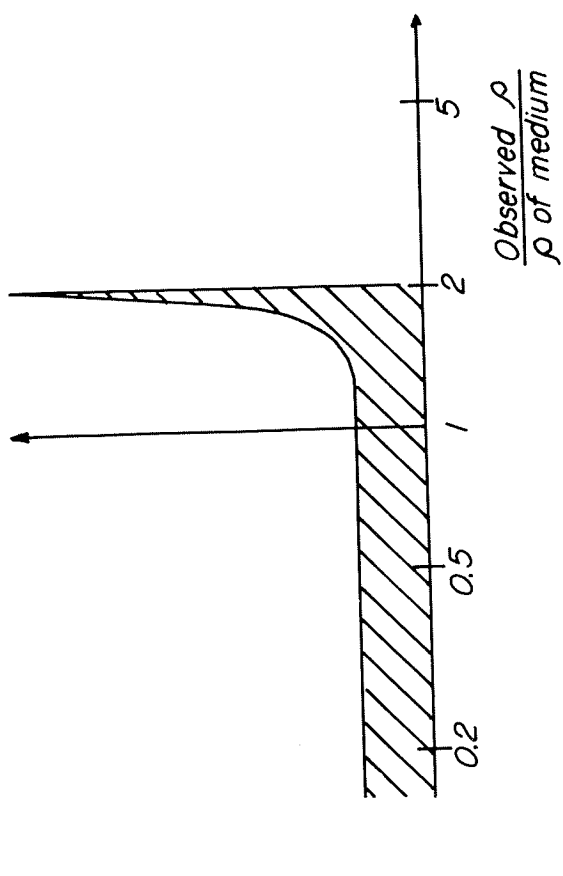
equal probability for resistive pods as for conductive pods, the errors in the low direction will be much more important than errors in the high direction.

In the general case we do not expect there to be a uniform distribution of pod resistivities. Some idea of the occurrence of resistivities in a surface layer may be obtained from the compilation of earth resistivities determined from radio-wave intensity measurements about standard broadcast stations (Part I, Section 2).

If the resistivity of the surface layer is relatively large, higher than the median resistivity indicated in these distribution density curves, there is a greater probability that pods will be more conductive than the layer than that they will be more resistive. This in turn shifts the average error further from zero than in the case of an equal distribution of pod resistivities above and below the layer resistivity. If the resistivity of the surface layer is relatively low, lower than the median resistivity indicated in these distribution density curves, there is a greater probability that pods will be more resistive



A. Uniform distribution of pod resistivities.



B. Distribution of errors caused by pods.

FIGURE 113.—Distribution of errors in measured electric field intensity which might be caused by pods of different resistivities embedded in a uniform surface layer.

than the layer, than that they will be more conductive than the layer. This shifts the average error towards zero, or in extreme cases, slightly above zero. This non-uniform occurrence of errors is demonstrated by the hypothetical probability curves in figure 114. Although this discussion is not quantitative, two things should be noted:

1. Geologic noise does not necessarily contribute random errors in resistivity, so simple averaging will not always reduce errors. However, if the surface layer is relatively conductive, geologic noise is more likely to have zero average than if the surface layer is relatively resistive.
2. Geologic noise should provide lower variance (average of squared errors) when the surface layer resistivity is low than when it is high.

Since the surface layer covering a sedimentary basin is usually less resistive than the average surface layer, it appears that electrical exploration in such basins is favored over exploration in other areas. In fact, from the noise point of view, it appears that the optimum surface layer for electrical exploration would be a thin sheet of sea water. Because of its uniformity in electrical character, the scatter to observed resistivities would be virtually zero.

The variance contributed by geologic noise is of concern in specifying the number of resistivity observations which must be made to determine the shape of a resistivity sounding curve within a required precision. If the variance is zero, or at least less than the precision required for a resistivity sounding curve, the number of points needed to specify a sounding curve may be estimated using the Nyquist sampling theorem. The sharpest curvature and thus the highest required sampling density, is observed for the case of a thin resistive layer embedded in an otherwise homogeneous medium (Keller, 1966). The sounding curves for the various arrays which would be obtained for such a sequence of layers are shown in figure 115. The horizontal scale shown in figure 115 as $\log a/h_1$ is equated with a time scale in sampling theory, while the vertical scale shown in figure 115 as $\log \rho_a/\rho_{a-\max}$ is equated with the amplitude scale in sampling theory. In this manner, resistivity sounding curves may be thought of as time functions. The power density spectrum may be obtained from the Fourier transform of the equivalent time function. The power density spectra for the two curves in figure 115 are shown in figure 116. Most of the power density is found at frequencies under 0.8 cycles per decade. According to the Nyquist sampling theorem, we must have at least two samples per cycle to determine the presence of these frequencies in a resistivity sounding curve. This requirement corresponds to sampling rates of at least 1.1/2 points per decade.

In the absence of noise, a single sample can be assumed to be a single measurement. However, if there are random measurement errors such that a group of measurements within a Nyquist sampling interval has a standard

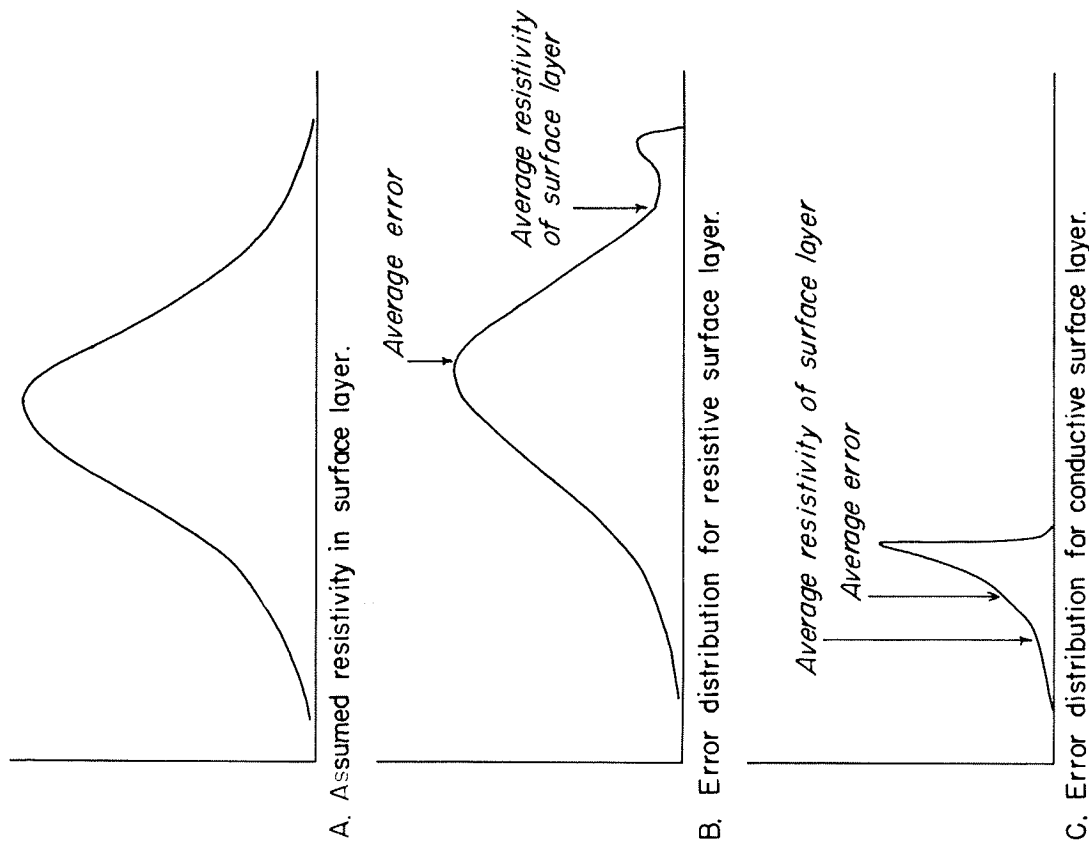


FIGURE 114.—Distributions of errors in electric field intensity which might be caused by a distribution of pods with different resistivities in a surface layer which is either more conductive than the average pod resistivity or more resistive.

deviation (square root of variance) of p percent, and if we wish to have our sample accurate within q percent (assumed to be smaller than p percent): then, for a normal distribution of errors with zero average, the number of measurements required per sample is $(p/q)^2 + 1$. Thus, if the standard

deviation of measurements is 10 percent, and the desired precision for each Nyquist sample is 2 percent. 26 measurements must be made in each sampling interval. Some caution in the use of such estimates must be exercised unless one is quite sure that the errors can be assumed to be normally distributed with zero average. This is a more reasonable assumption for exploration problems in which the surface layer is relatively conductive than in exploration problems in which the surface layer is relatively resistive.

A related consideration is the matter of resolution—how small a change in resistivity or how thin a layer can be resolved at depth. It seems reasonable to require sampling to provide a precision of two percent on the average. Much higher precision might be obtained in marine exploration, perhaps with average errors of the order of 0.2 percent. However, if the average sampling error is two percent, we may expect to obtain reliable interpretations for layers which contribute a change in observed resistivity of five times as much, or of 10 percent.

In view of the nature of a typical oil field as given in Part I, we should consider the resolution with which a thin layer can be detected. Lack of thickness is offset by the larger contrast in resistivity. If a thin layer is embedded in a homogeneous medium, the resistivity curve shows a bump or a depression, as indicated in figure 117. The amplitude of the bump is a function only of the contrast in transverse resistance of the layer to that of the overlying medium (T_2/T_1) if the layer is more resistant than the rest of the medium, or only of the contrast in longitudinal conductance of the layer to that of the overlying medium, if the layer is less resistant than the rest of the medium. For small contrasts in T_2/T_1 or S_2/S_1 , the amplitude of the anomaly on the sounding curve is the same as the contrast in the layer parameters. If the contrast in layer parameters is 10 percent, the amplitude of the anomaly on the sounding curve is about 5 percent. Slightly larger anomalies are obtained with the polar dipole array than with the Schlumberger or equatorial dipole arrays.

The precision with which a contrast in transverse resistance or a contrast in longitudinal conductance can be determined is:

$$\epsilon_1 = [\epsilon_p / (N-1)^{1/2}]^{1/2} \quad (179)$$

where ϵ_1 is the error in interpretation and N is the number of samples per decade range in spacing, or the range over which the shape of the anomaly is determined.

It is perhaps important to point out here that the scatter caused by random inhomogeneities of the surface layer is most important in the applications of

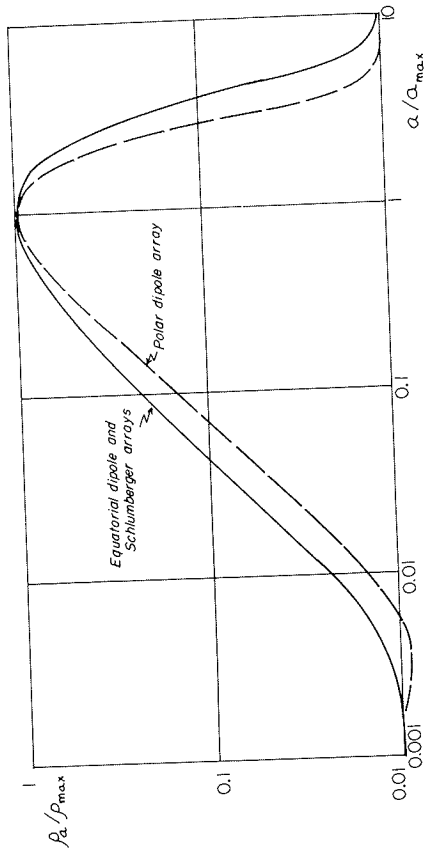


FIGURE 115.— Direct-current resistivity curves which exhibit maximum curvature, and therefore, high "frequency" content, for several arrays. The curves have been normalized to the maximum observed apparent resistivity and the spacing at which that maximum is recorded.

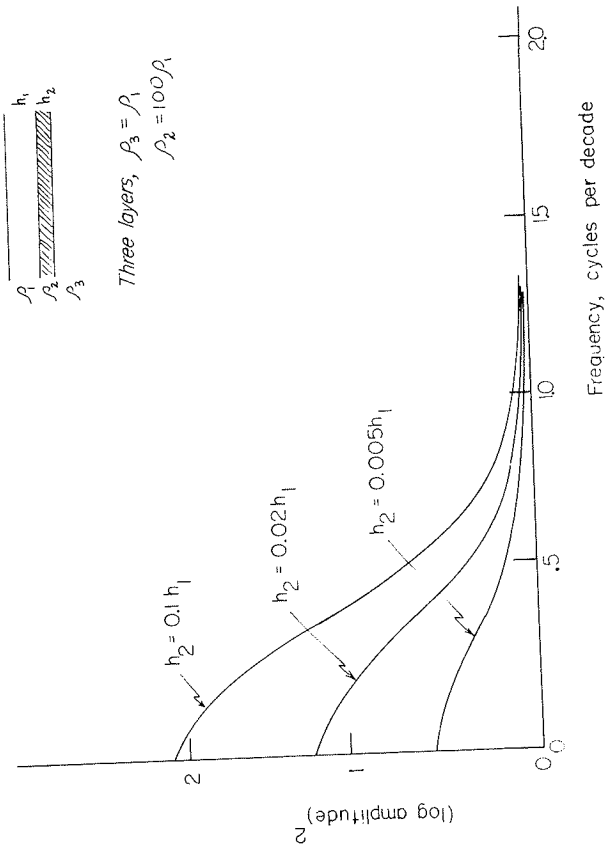


FIGURE 116.— "Power density spectra" calculated for resistivity curves for thin resistant layers embedded in an otherwise uniform earth.

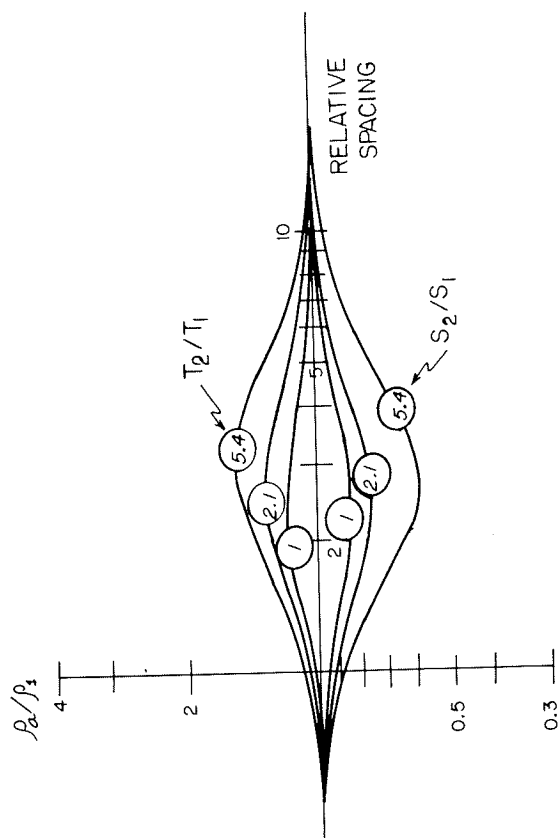


FIGURE 117.— Anomaly in resistivity measured with a Schlumberger array by a thin resistant or conductive layer embedded in an otherwise uniform earth. The relative spacing is the ratio of the Schlumberger spacing to the depth to the thin layer.

dipole resistivity surveys, where one or the other of the dipoles must be moved about over the surface of the earth. In a system where the source and the receiver are fixed, and frequency is varied to obtain a range of penetrations, the effect of surface inhomogeneities is to distort the shape of the observed data smoothly, rather than randomly. However, virtually nothing has been done in the analysis of errors which may arise with such systems when the surface-layer resistivity varies.

REFERENCES

Al'pin, I. M., Berdichevskiy, M. N., Vedritsev, G. A., and Zagarmistr, A. M., 1966, Dipole methods for measuring earth conductivity: New York, Consultants Bureau, 302 p.
 Anderson, L. A., and Keller, G. V., 1966, Experimental deep resistivity probes in the central and eastern United States: Geophysics, v. 31, no. 6, p. 1105-1122.
 Balachandran, K., 1967, A theory of the solar wind interaction with the geomagnetic fields: D.Sc. Thesis, Colorado School Mines, 69 p.
 Berdichevskiy, M. N., 1965, Electrical prospecting with the telluric current method: Colorado School Mines Quart., v. 60, no. 1.
 Cantwell, T., Galbraith, J. N., Jr., and Nelson, P., 1964, Deep resistivity results from New York and Virginia: Jour. Geophys. Research, v. 69, no. 20, p. 4367-4376.

DESIGN CRITERIA FOR ELECTRICAL SURVEYING

Dakhnov, V. N., 1962, Geophysical well logging: Colorado School Mines Quart., v. 57, no. 2.
 Davidson, M. J., 1964, Average diurnal characteristics of geomagnetic power spectrums in the period range 4.5 to 1000 seconds: Jour. Geophys. Research, v. 69, no. 23, p. 5116-5119.
 Jacobs, J. A., 1964, Micropulsations of the earth's electromagnetic field in the frequency range 0.1 to 10 cps in National electromagnetic phenomena below 30 KC/S: New York, Plenum Press, p. 319-350.
 Heirtzler, J., 1964, A summary of the observed characteristics of geomagnetic micropulsations in Natural electromagnetic phenomena below 30 KC/S: New York, Plenum Press, p. 351-372.
 Herron, T. J., 1967, An average geomagnetic power spectrum for the period range 4.5 to 12,900 seconds: Jour. Geophys. Research, v. 72, no. 2, p. 759-761.
 Hoffman, A. A. J., and Horton, C. W., 1966, An analysis of some magnetotelluric records from Takhaya Bay, U.S.S.R.: Jour. Geophys. Research, v. 71, no. 16, p. 4047-4051.
 Jackson, D. B., 1965, Deep resistivity probes in the southwestern United States: Geophysics, v. 31, no. 6, p. 1123-1144.
 Kalenov, E. N., 1957, Interpretatsii krivikh vertikalnoye elektricheskovo zondirovaniya: Moscow, Gostoptekizdat, 473, p.
 Keller, G. V., 1966, Dipole methods for deep resistivity studies: Geophysics, v. 31, no. 6, p. 1088-1104.
 Keller, G. V., and Frischknecht, F. C., 1966, Electrical methods in geophysical prospecting: Oxford, Pergamon Press, 527 p.
 Kharkevich, A. A., 1960, Spectra and analysis: New York, Consultants Bureau, 222 p.
 Kunetz, C., and Chastenet de Gery, J., 1956, La representation conforme et divers problems de potentiel dans les milieux de "permeabilite" differente: Revue de Inst. Tech. Francais Pet., Octobre, p. 1179, 1192.
 Lokken, J. E., 1964, Instrumentation for receiving electromagnetic noise below 3000 cps in Natural electromagnetic phenomena below 30 KC/S: New York, Plenum Press, p. 373-428.
 Maxwell, E. L., 1967, Atmospheric noise from 20 Hz to 30kHz: Radio Science, v. 2, no. 6.
 Naidu, Prabakar, 1967, Random telluric field and signal extraction: Jour. Geophys. Research, v. 72, no. 20, p. 5059-5064.
 Nawrocki, P. J., and Papa, Robert, 1963, Atmospheric processes: Englewood Cliffs, New Jersey, Prentice-Hall.
 Pritchard, J. L., 1964, Spectral analysis of twenty-four-hour time intervals of micropulsations observed at stations in mid latitudes: M.Sc. Thesis, Colorado School Mines, 125 p.
 Santirocco, R. A., and Parker, D. C., 1963, The polarization and power spectrums of Pc micropulsations in Bermuda: Jour. Geophys. Research, v. 68, no. 19, p. 5545-5558.
 Tarkhov, A. G., (Ed.), 1963, Spravochnik Geofizika: Tom 3, Elektrozavodka: Moscow, Gostoptekizdat, 582 p.
 Troitskaya, V. A., 1964, Rapid variations of the electromagnetic field of the earth in Research in Geophysics, v. 1, Cambridge, Mass. Inst. Tech. Press, p. 485-532.
 Vanyan, L. L., 1967, Electromagnetic depth soundings: New York, Consultants Bureau, 312 p.
 Watt, A. D., Mathews, F. S., and Maxwell, E. L., 1963, Some electrical characteristics of the earth's crust: Inst. Elec. & Electronic Engineers Trans., v. 51, no. 6, p. 897-910.
 Welch, T. M., 1968, Variations in telluric current power spectrums with local time and magnetic activity: M.Sc. Thesis, Colorado School Mines, 113 p.

SUMMARY AND CONCLUSIONS — STRATEGY

Considering the material presented in the preceding three sections, one might use a variety of approaches to exploring for oil with electrical prospecting methods. Let us now consider what still needs to be done in defining the capabilities of the electrical prospecting methods, as well as their limitations, and the strategies which might be employed in applying the methods in exploration.

We might first summarize the factors which would be involved in the choice of an AC method or a DC method.

1. AC and DC methods:

With AC sounding methods, theory is based on the solution of Maxwell's equations, usually with propagation effects and displacement currents being neglected. Such a solution is difficult for any but simple geometries.

With DC sounding methods, theory is based on the solution of Laplace's equation. Such solutions are much simpler than solutions to Maxwell's equations for comparable conditions. Thus, more extensive catalogs of reference curves are available for the DC methods.

With AC methods, field observations can be converted to values of "apparent" resistivity using simple formulas only for a restricted range of frequencies, and the particular range for which computations may be made depends on the resistivity, or a priori knowledge of it.

With DC sounding methods, a value for "apparent" resistivity which has some significance can always be computed from field data using simple formulas.

With AC sounding methods, the depth of investigation may be controlled either by varying the spacing between source and receiver or by changing the frequencies used. In the latter case, scatter caused by surface irregularities in resistivity can be minimized.

With DC sounding methods, the depth of investigation can be controlled only by changing the positions of the electrodes on the surface of the earth. Surface irregularities in resistivity can cause large scatter in the measurements known as "geologic noise."

With AC sounding methods the response caused at the surface by a resistivity contrast ρ_2/ρ_1 at depth is a function of the square root of the contrast in

resistivity. Thus, the AC methods are relatively insensitive to small contrasts, but do not saturate as rapidly with large contrasts as do the DC methods.

With DC sounding methods, the response caused at the surface by a resistivity contrast ρ_2/ρ_1 at depth is a function of the ratio directly. Thus, DC methods are quite sensitive to small changes in resistivity, but this sensitivity saturates quickly as the contrast increases.

With AC methods, relatively little effect is seen at the surface from a thin, insulating layer at depth. Such a layer is difficult to detect, but its presence does not interfere with detection of deeper layers.

With DC sounding methods, a thin insulating layer effectively prohibits the penetration of current further into the earth, and completely screens the deeper layers from detection.

With AC sounding methods, a thin, perfectly conducting layer completely reflects the incident electromagnetic field, so that no information can be obtained about deeper layers.

With DC sounding methods, a thin, perfectly conducting layer will trap all current, and none will penetrate to deeper layers. Thus, neither the AC methods nor the DC methods can see through a conductive screening layer.

Measurements may be made relatively rapidly with AC methods in comparison with DC methods, inasmuch as only one or a few source-receiver separations need be used, and the frequencies of interest are at least an order of magnitude higher than those used in the DC methods.

Field work is cumbersome with the DC sounding methods, inasmuch as many source-receiver separations must be used. In deep sounding, very low frequencies must be used to avoid induction effects, and measurements are time consuming.

There is considerable flexibility in the design of AC sounding methods, in that either inductive or conductive receivers may be used, depending on operating conditions, allowing the choice of a technique which detects minimum electrical or geologic noise.

With DC methods, one has to use a conductive receiver, and there is no flexibility in discriminating against electrical or geologic noise.

With some of the AC methods, only the longitudinal resistivity of the earth is detected and the depths which are interpreted are true depths to boundaries between layers with different resistivities. With other AC methods, the re-

sponse will depend on both vertical and longitudinal resistivity, and depths will be distorted by anisotropy. In theory at least, it is possible to use a combination of AC methods to find both longitudinal resistivities, and the effect of anisotropy.

With DC methods, the results are always distorted by anisotropy. The measured resistivity is the quadratic average of the longitudinal and transverse values, and interpreted depths are always scaled up by the coefficient of anisotropy. Auxiliary data of some type must be provided to find true depths.

The considerations relating to the ease of field operations with AC methods, their rapidity, lack of sensitivity to geologic noise, and flexibility would appear to make AC methods preferable to DC methods in most cases. An exception would be the case of marine operations, where DC measurements may be made easily by trailing the measurement electrodes from a moving vessel. This reduces the work involved in getting a number of source-receiver separations, and in addition, the uniformity of a sea water layer will reduce the problems with geologic noise to the point where they need not be considered seriously. Having eliminated the principal advantages of the AC methods in this case, the advantage of the DC method in being more sensitive to small-dimensional anomalies in the subsurface resistivity becomes dominant. However, if DC methods are used at sea, some auxiliary information must be provided to correct depths for the effect of anisotropy.

2. The target

The target of exploration is also a matter to consider in designing an approach to oil exploration using electrical methods. The target might be the anomaly in resistivity caused by oil saturation directly, or a change in resistivity in areas favorable for oil accumulation. As was pointed out in the section on detection of the resistivity contrast associated directly with oil saturation, the least of oil fields which is of economic interest would cause the field components measured at the earth's surface to change by about one-quarter to one-half percent, if DC sounding methods are used, or by about a tenth as much, if AC sounding methods are used. Thus, it is not entirely unreasonable to base exploration on the detection of a direct anomaly from oil saturation. Conventional DC surveys are commonly made with precisions of the order of a few percent, and detection of an anomaly of a fraction of a percent would require only a moderate improvement in the precision of DC sounding methods. In the past decade, airborne electromagnetic surveys have been developed to the point of detecting anomalies with a resolution of a few hundred parts per million, which is the precision which would be needed in oil exploration. It should be noted, of course, that the scale of the airborne

electromagnetic surveys is much smaller than that needed for oil exploration. In the application of electrical methods for the direct location of oil fields, the question is not so much whether the accuracy of the measurements may be improved to the point where the direct anomaly can be detected, but rather, whether an anomaly of one-half percent in DC resistivity or 500 parts per million in AC coupling can be recognized as representing oil saturation. It is readily apparent that other changes in a section will cause measured field quantities to vary by more than these minimum amounts even when oil is not present. Direct location of oil with electrical methods would seem to be feasible only in cases where the approximate location of an oil field was known beforehand, both in plan and in depth. For example, it may be known that oil pools occur in a given reservoir horizon, along a trend line, and that otherwise, the character of the section varies in a logical manner. One would then prospect for small differences in resistivity associated with that specific depth. In such cases, an anomaly of a half percent in DC resistivity or 500 parts per million in AC coupling might be recognized as representing oil saturation, even though changes in other parts of the section would cause considerably larger changes in observed resistivity.

Another approach to the use of electrical methods in oil exploration is in the study of lithologic variations in the stratigraphic column which affect the electrical properties. Hopefully, an understanding of lithologic variations will assist indirectly in the location of oil. However, detection of large-dimensional changes in resistivity associated with lithologic transitions is a much simpler problem than detection of the contrast in resistivity associated directly with oil saturation. Mapping of changes in average resistivity of a sedimentary column, such as those apparent from the electric log studies in the first part of this monograph, are well within the capabilities of any of the varieties of electrical prospecting methods described here. Average resistivity of a formation or group of similar formations appears to vary by factors of 2 to 5 over a sedimentary basin, as a consequence of the change in lithology of the section, or of changes in the salinity of the connate water. It is even within reason to recognize which change is taking place, if electrical surveys are run with methods which allow the recognition of the effect of anisotropy. A combination of induction methods which gives both the longitudinal resistivity and a resistivity value distorted by the effect of anisotropy (for example, the use of an electric dipole source, with electric field detectors and magnetic field detectors) would permit this. A change in longitudinal resistivity without an associated change in the coefficient of anisotropy would indicate changes in connate water salinity, while changes in the coefficient of anisotropy would indicate changes in the lithology of the sedimentary sequence. Considering that such measurements may be made with standard methods with adequate pre-

cision to accomplish this, the study of lithology through combined measurements of resistivity and anisotropy may well be the most powerful application of electrical methods in oil prospecting.

A third approach to the use of electrical methods in oil prospecting is in the mapping of electrical marker horizons. With electrical methods as they are used today, it is feasible to map the relief of a marker horizon with a much higher or lower resistivity than the overlying sequence with a precision of the order of one or two percent. This resolution is comparable to that obtainable with the seismic refraction method, but is less than can be obtained with a seismic reflection survey. Deep electrical surveying methods are not inexpensive, though they may cost less than seismic surveys with a similar coverage by a factor of 5 to 10. The application of electrical surveys to mapping relief of a marker horizon is probably of value only in cases where the marker cannot be easily mapped by seismic methods for one reason or another.

3. Problems to be solved

Before electrical methods can find a place in a petroleum exploration program, there are a number of problems that remain to be solved. The least of these is the problem of developing equipment with the power capacity and accuracy required in oil exploration.

A very important problem which may be evaluated without the expense of undertaking field operations with large scale electrical surveys is the problem as to the size and detectability of anomalies associated with oil occurrence. The size of the anomaly caused directly by oil saturation can be estimated by analyzing the electric logs which have been obtained in oil fields. The magnitude of changes in resistivity associated with lithologic changes within a basin may be studied by compiling average resistivities from logs as was done in the first section of this monograph. Perhaps even more important, synthetic electrical surveys may be run by using resistivities from electric logs to compute the response to various electrical sounding methods. This approach would allow the accumulation of considerable experience in evaluating electrical surveys without the cost involved in field surveys.

A second problem to be solved is that of interpretation. Present techniques used in interpreting electrical survey data are archaic, consisting usually of eyeball comparison of field data with albums of curves computed for various earth models. Such a procedure works well enough for field data in which the precision is five percent or less, but with more precise field data, one cannot discriminate visually among curve shapes which vary by the small amounts which are significant differences in the data. Several approaches may be available in such a case, one of which is the trial and error fitting of observed

data with theoretically calculated curves in order to get a best fit. A more exciting possibility is the concept of direct decomposition of the observed data into a resistivity vs. depth function. It is certain, however, that a major improvement must be made in interpretation capability before the full capacity of electrical prospecting methods can be recognized in oil exploration.

A third problem to be solved is that of geologic noise. The precision of electrical surveying techniques appears to be limited primarily by the scatter contributed by surficial variations in resistivity. Some survey methods are less sensitive to geologic noise than others; methods in which induction coils are used as sources and receivers are much less sensitive to local inhomogeneities in resistivity than are methods in which electrode contacts are used; and methods in which frequency is varied rather than source-receiver separation exhibit less scatter caused by surface inhomogeneities. Also, there are applications in which geologic noise is of less concern than is generally the case; surveys made over a sea-water layer are essentially immune to problems caused by geologic noise, and there are on-shore areas where the surface soil is sufficiently uniform that the problem is minor. However, working only in areas where noise is not a problem, or only with techniques which are least subject to noise may be an unnecessary limitation on the applicability of electrical prospecting methods. Consideration of field survey methods which will minimize the errors caused by geologic noise, and of data processing techniques which will allow the separation of deep-seated signals from surficial noise may provide a solution to this problem.

In summary, considering the difficulty of finding oil with present techniques, and the apparent applicability of electrical surveying methods to the problem, it is surprising that electrical methods have not been used more widely in exploration for oil.